NASA CONTRACTOR REPORT

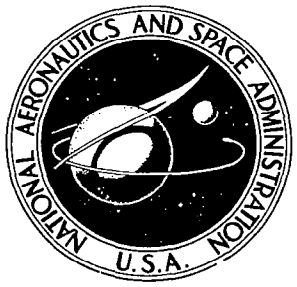

NASA CR-8

NASA CR-802

RESEARCH AND DEVELOPMENT OF HIGH-PERFORMANCE AXIAL-FLOW TURBOMACHINERY

Volume 3 - Design of Backup Gas Bearings

by J. T. McCabe, W. Shapiro, and T. Y. Chu

Prepared by
PRATT & WHITNEY AIRCRAFT
Philadelphia, Pa.
for Lewis Research Center

NATIONAL AERONAUTICS AND SPACE ADMINISTRATION • WASHINGTON, D. C. • MAY 1968

RESEARCH AND DEVELOPMENT OF HIGH-PERFORMANCE AXIAL-FLOW TURBOMACHINERY

Volume 3 — Design of Backup Gas Bearings

By J. T. McCabe, W. Shapiro, and T. Y. Chu

Prepared under Contract No. NAS 3-4179 by
PRATT & WHITNEY AIRCRAFT
Philadelphia, Pa.

for Lewis Research Center

NATIONAL AERONAUTICS AND SPACE ADMINISTRATION

For sale by the Clearinghouse for Federal Scientific and Technical Information
Springfield, Virginia 22151 – CFSTI price $3.00

FOREWORD

This report was prepared in accordance with Contract NAS3-4179 under the technical management of Jack A. Heller of the Space Power System Division, and in consultation with Harold E. Rohlik, Calvin L. Ball, William J. Anderson, and George K. Fischer of the Fluid System Components Division, NASA Lewis Research Center, Cleveland, Ohio. It is published in three volumes, as follows:

Volume 1 CR-800 - - Design of Turbine-Compressor (Pratt & Whitney Aircraft)

Volume 2 CR-801 - - Design of Gas Bearings (Mechanical Technology Incorporated)

Volume 3 CR-802 - - Design of Backup Gas Bearings (The Franklin Institute Research Laboratories)

ABSTRACT

The National Aeronautics and Space Administration is conducting an evaluation of candidate Brayton-cycle turbomachinery configurations. As part of this program, Pratt & Whitney Aircraft has designed a turbine-compressor incorporating a single-stage axial-flow turbine driving a six-stage axial-flow compressor supported on gas bearings. A backup gas bearing system was designed by The Franklin Institute Research Laboratories. The design activities included steady-state analysis and time transient rotor support system studies. A satisfactory backup gas bearing system was designed.

TABLE OF CONTENTS

TABLE OF CONTENTS (continued)

TABLE OF CONTENTS (continued)

LIST OF FIGURES

LIST OF FIGURES (continued)

LIST OF FIGURES (continued)

LIST OF FIGURES (continued)

FIGURES IN APPENDICES (continued)

FIGURES IN APPENDICES (continued)

FIGURES IN APPENDICES (continued)

1. INTRODUCTION

The NASA/Lewis Research Center is engaged in development technology and components for dynamic space power systems. The Brayton cycle, utilizing solar or nuclear energy as a heat source and an inert gas as the working fluid, has been selected as a candidate for evaluation. Turbine-compressors and turbine-alternators, supported by gas lubricated bearings (i.e. the working fluid) are currently being designed and developed to meet the requirements for space power.

In this Brayton cycle concept, the turbine driven compressor and the turbine driven alternator are mounted on separate shafts, rotating in opposite directions about the same centerline to reduce gyroscopic effects on the space vehicle. The working fluid, argon, enters the turbine-compressor inlet duct at approximately 75°F and is conducted to a six-stage axial flow compressor around a housing containing gas lubricated thrust and journal bearings. The argon leaves the compressor and radial diffuser through exhaust scroll ducting and flows through a regenerator to a heat source where the gas temperature is elevated to 1490°F. The argon then enters the turbine inlet scroll and expands through a single stage axial flow turbine which drives the compressor at 50,000 rpm. Housed between the compressor exit and turbine inlet is the second gas lubricated journal bearing. The argon exhausts from the turbine-compressor discharge ducting to a two-stage axial flow turbine driving an alternator at 12,000 rpm. Before being returned to the turbine-compressor inlet to close the cycle, the argon is cooled in a regenerator and heat rejection systems.

The subject of this report is the design of an alternate gas bearing system for the turbine-compressor. (See Volumes I and II for primary system).

The Brayton cycle machinery must be able to operate on the ground in various orientations and in space with nominally zero gravity forces. The bearing system must survive ground storage, handling and the

launch environment. The 10.7 pound rotor, the 15 pound aerodynamic design thrust and the start-up reverse thrust impose loads on the bearing system in a variety of combinations.

The reliability and high efficiency requirements of Brayton cycle space power plants have initiated intensive analytical and experimental studies of gas bearings applied to high speed rotating equipment. Although gas bearings have been successfully developed for other types of rotating equipment, they are by no means an "off-the-shelf" item. A gas bearing system was selected for this application because it provides low bearing power loss, eliminates the need for seals to prevent cycle fluid contamination, and offers promise for long, dependable bearing life.

The results obtained from this project will prove useful not only in advancing the state of the understanding of gas bearings - especially with respect to the dynamics of tilting-pad journal bearings - but also in providing sufficient data for undertaking the design of similar bearing systems.

2. SUMMARY

This report contains a detailed analysis and the subsequent design of a gas-lubricated bearing system consisting of two tilting-pad journal bearings with a spiral groove main thrust bearing for a 50,000 rpm Brayton cycle turbine-compressor.

Using the working fluid argon as the bearing lubricant, the principal objective was to provide a low friction bearing system of high reliability potential. To accomplish this purpose, extensive steady-state data was generated so that sufficient information was available for system optimization. Having established a preliminary design based on steady-state consideration, a dynamical analysis was undertaken to examine the response of the rotor/bearing system to the specified loading. In this connection, a non-linear rotor/journal bearing analysis was formulated, validated and applied to finalize the preliminary design. Concurrently, the stability of the double acting thrust bearing was investigated. The proposed final design of the bearing system, shown incorporated in the turbine-compressor on Figure A, is predicted to meet all the required design specifications.

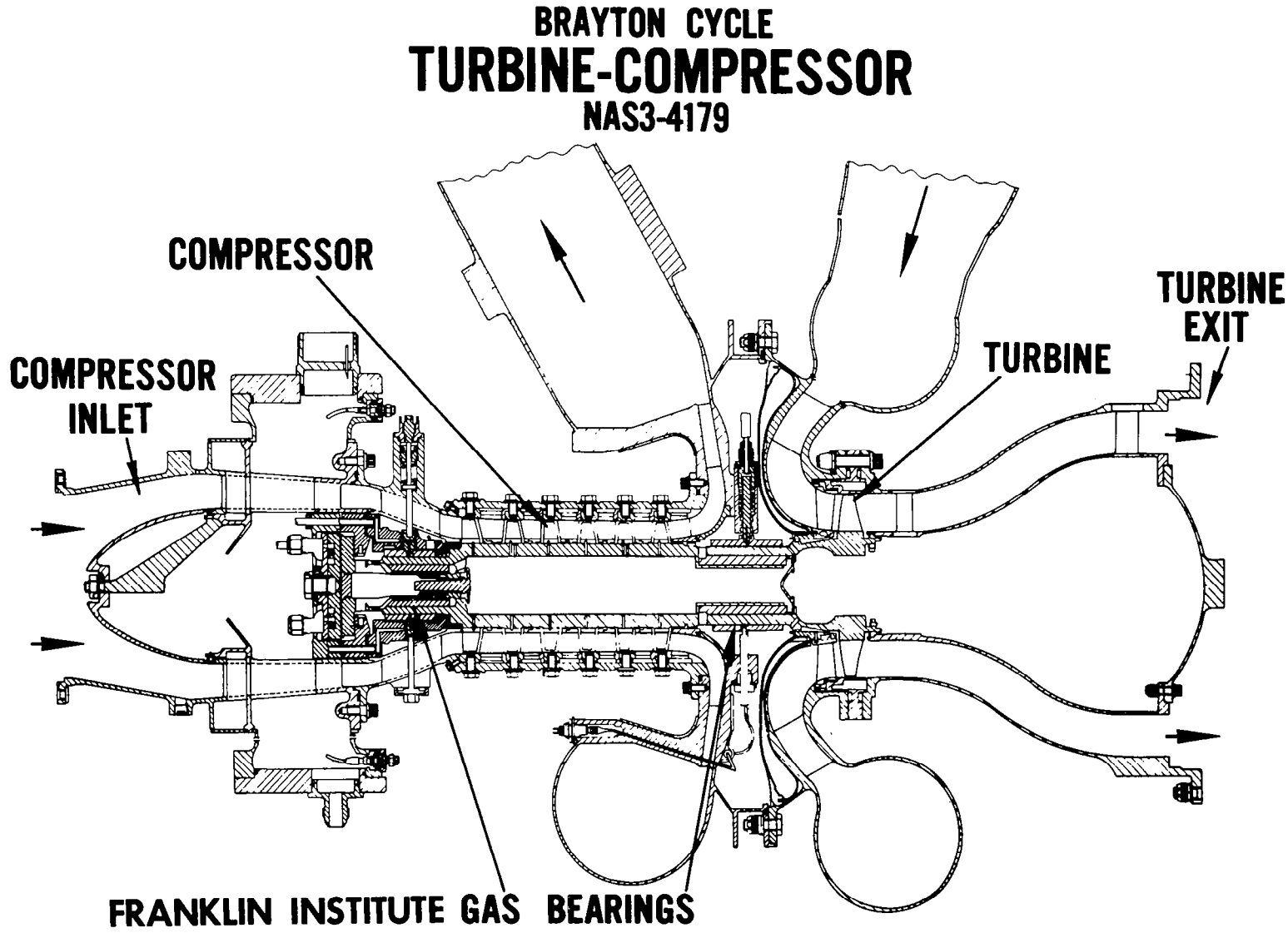

Fig. A - Sectional View of Turbine-Compressor

3. CONCLUSIONS AND RECOMMENDATIONS

3.1 Conclusions

3.1.1 A gas bearing system consisting of two-three shoe tilting pad bearings, a spiral groove main thrust bearing and a step sector reverse thrust bearing has been produced which has the potential of satisfying all of the design specifications. Some of the features of this system are:

- Low power loss
- Stable operation
- Moderate clearances
- High reliability potential
- Positive protection during start-up using jacking gas
- Reverse thrust protection against loss of cycle flow
- Stable operation at design speed even with a large increase in pivot friction
- Potential for operation during launch (using jacking gas)
- Mounting of one shoe on a preloaded soft spring maintains constant pivot film thickness for safe guard against loss of clearance due to shaft growth.

3.1.2 The non-linear orbit concept which was established in Reference 7 has been extended to investigate the response of a rotor supported on gas lubricated tilting pad journal bearings.

3.2 Recommendations

3.2.1 Use the Non-linear Orbit analysis to examine various off-design and potential failure modes of operation, especially those that are difficult to test.

3.2.2 Extend the basis for the design of gas lubricated bearings in the following areas:

- Steady-state data for tilting pad journal bearings. The available data should be extended to cover a wide range of Λ, R/L and α
- Steady-state data for various types of spiral groove thrust bearings with a compressible lubricant. Emphasis should be placed on the effects of misalignment and surface distortion
- Develop design data for the selection of mass and inertia properties of tilting pad journal bearings
- Develop design data for estimating the effects of surface distortion on load capacity and stiffness for tilting pad journal bearings

4. SELECTION OF BEARING CONFIGURATIONS

4.1 Journal Bearings

4.1.1 General Considerations

The following specifications were to be staisfied by the journal bearing design:

a. Rotor speed - 50,000 rpm design, 60,000 rpm overspeed
b. Rotor weight - 10.7 pounds
c. Bearing lubricant - argon gas
d. Rotor unbalance - 0.002 ounce - inch in plane of turbine
e. Ambient gas pressure - 12 psia all bearings (6 psia also desired)
f. Bearing No. 1 (forward of compressor)
   Static load (horizontal rotor) - 3.4 pounds
   Ambient temperature - 150°F
g. Bearing No. 2
   Static load (horizontal rotor) - 7.3 pounds
   Ambient temperature - 260°F
h. Rotor polar moment of inertia - 0.0294 inch-ounces-sec^2
i. Rotor transverse moment of inertia (at c.g.) - 0.554 inch-ounces-sec^2
j. Rotor must operate horizontally, vertically and in nominal zero g environment.

The space, both axially and radially, forward of the compressor and between the compressor exit and turbine inlet scrolls was considered adequate to install either a 360 degree cylindrical or a tilting pad journal bearing.

The object of the bearing system was to carry the loads reliably with low friction power loss. Consideration was to be given to providing the bearings with an environment that would reduce difficulties such as crowning, coning etc., associated with the thermal ambient.

4.1.2 Selection of Bearing Type

The first choice to be made in selecting a bearing type is between those that are externally pressurized and those that are self-acting. Externally pressurized bearings were eliminated because the loads were small enough and the shaft speed high enough so that the complication of a continuous gas supply system, together with the compressor power required, could not be justified.

The choice for self-acting hournal bearings is basically between tilting-pad and 360 degree cylindrical types. Influencing this choice are considerations of past experience, available design data, ease of generating new data, relative load capacity, ease of manufacture and stability potential.

4.1.2.1 Cylindrical Journals

There are a variety of cylindrical journal types, e.g. plain sleeve, axial groove, displaced center, pocket, etc. The plain cylindrical bearing has excellent load capacity and is relatively simple to manufacture and install. But this type of bearing is very susceptable to fractional frequency whirl - especially in the nominal zero g environment. In addition, this type of bearing is sensitive to changes in clearance and sensitive to jamming by dirt or other foreign particles. In order to enhance stability, grooves, lobes and vented pockets are often used. Loss of load capacity and increased difficulty in manufacturing are compromises that usually accompany these geometric alterations.

4.1.2.2 Tilting Pad Journal

With one adjustable and spring loaded pad, the three shoe tilting pad journal is virtually free from serious gas film instabilities. The pivots provide adjustment to misaligned loads and particles are less likely to be trapped within the clearance space. Among the disadvantages associated with tilting pad journals are the dynamic problems related to

the additional degrees of freedom, lower load capacity, pivot material problems, lack of design information and the complication of providing mechanical preload.

The self-acting, three-shoe, tilting-pad journal bearing was selected for the turbine-compressor principally because of its stability potential.

4.1.3 Bearing Cooling Scheme

After preliminary examination, the task of controlling the bearing ambient temperature for minimum pad distortion was identified as a system integration problem. Given the predicted bearing friction power losses, Pratt and Whitney Aircraft studied the problem in depth.* The method selected as the journal bearing cooling scheme consisted of introducing cooling gas at 12.8 psia and 100°F into the number one bearing compartment (the compressor end). The gas flows behind the thrust bearing into a hollow shaft, which is provided with an internal heat exchanger under the number one bearing, through the shaft to a heat exchanger under the number two bearing and then into the number two bearing compartment. The number one bearing (generating 40 watts) was expected to operate with an average pad temperature of about 140°F and about a 1.5°F/in. pad gradient in the axial direction. The number two bearing (generating about 117 watts) was expected to operate with an average pad temperature of 264°F, an average shaft temperature of 248°F and an axial pad gradient of 3.8°F/in. Using the cooling scheme described above, the resulting pad distortions were not expected to detract significantly from the idealized performance of the journal bearings.

---

*The Requirements of Gas Bearings in Brayton Cycle Axial Flow Machinery by P. Bolan, W. B. Spencer and E. E. Striebel, Pratt and Whitney Aircraft.

4.2 Thrust Bearings

4.2.1 General Considerations

The thrust bearing for the turbine-compressor was located on the compressor inlet end of the rotor. For space operation and in a horizontal attitude in a gravitational field, the primary thrust load is from the aerodynamic unbalance between the turbine and compressor. The turbine-compressor will also operate on the ground in a vertical attitude with the compressor inlet facing up. For this condition a reverse or reaction thrust bearing was required to support the rotor weight during start-up. In addition to the normal steady bearing loads, start-up and shut-down may produce high transient loading in either direction and the bearings must be designed to withstand these loads. External pressurization of both the main and reaction bearings was provided during start-up and shut-down to insure shaft support in the absence of sufficient hydrodynamic load generation. The reverse thrust bearing was designed to support some load hydrodynamically.

The thrust bearing selection and performance analyses were based on the following specifications:

a. Lubricant-argon gas
b. Operating temperature - 250°F
c. Gas viscosity - 3.6×10^{-9} lb-sec/in^2
d. Shaft speed - 50,000 rpm
e. Supply pressure for liftoff-100 psia max.
f. Ambient pressure - 12 psia.
g. Aerodynamic load - 15 lbs.
h. Rotor weight 10.7 lbs.
i. Transient load-forward - 100 lbs. max.
j. Transient load - rearward - 50 lbs. max.
k. Bearing max. diameter - 2.67 in.
l. Maximum total clearance of both main thrust and reaction bearing - 10 mils.

4.2.2 Selection of Bearing Type

Prior to selection of a bearing, a review to determine performance characteristics of a number of bearing types was conducted so that an optimum configuration could be selected. The following paragraphs describe the various bearings analyzed and the results obtained. During the period the review was in process preliminary design conditions were employed, not the final design condition. However comparisons were made using consistent data so that fundamental differences could be clearly evaluated.

4.2.2.1 Equalized Tilting Pad Bearing

This type bearing has been eminently successful for incompressible applications and is probably the most common type thrust bearing in contemporary use. Thus it was a natural configuration for initial investigations. A cylindrically curved slider was analyzed with the information described in Reference (1)*. Curved sliders are used for gas bearings to insure hydrodynamic start-up. The following requirements were used for design purposes:

Gravity Load = 9.541 lbs.
Aerodynamic Load = 25 lbs.
Ambient Pressure = 11.6 psia
Operating Speed = 50,000 rpm
Maximum O. D. = 3.125 in.
Minimum I. D. = 0.80 in.

Proceeding with the calculations the following minimum clearances resulted:

Minimum Clearance = 0.281 mils (Gravity + Aerodynamic Load)
Minimum Clearance = 0.392 mils (Aerodynamic Load Only)

These clearances were considered unacceptable. To provide a minimum clearance of 0.5 mils, the bearing O.D. would have to be 3.84 inches. This was excessive.

*Numbers in parenthesis refer to references listed in Section 8.

4.2.2.2 Stepped Bearing

A stepped thrust bearing configuration was analyzed, using procedures and information as described in Reference (2). The analysis was based on optimizing the configuration for load capacity. Design requirements were the same as for the tilting pad bearings. The results of the analysis were as follows:

Optimum Sector Ratio (step angle/pad angle)	= 0.217
Optimum no. of pads	= 3
Step Height	= 0.677 mils
Minimum clearance (34.54 lbs)	= 0.677 mils
Power Loss	= 0.195 hp

This bearing was also analyzed using References (1) and (3) but the above data was considered the most reliable. Reference (3) was developed strictly for incompressible lubricants. The results of all analysis are contained in the comparative tabulation at the end of this section. This concept appears to be a suitable candidate.

4.2.2.3 Tapered Land Bearing

Tapered land configurations were analyzed using References (1) and (3). Reference (1) was limited to L/D ratio's of 1 and Reference (3) was developed for incompressible lubricants. For design conditions specified above the following performance was calculated:

Minimum clearance	= 0.628 mils
No. of pads	= 4
Land height	= 1.013 mils
Power Loss	= 0.125 hp

This concept also appears to be a suitable candidate.

4.2.2.4 Pocket Bearing

The pocket bearing has demonstrated a high load capacity and low friction loss for incompressible lubricants. Unfortunately there

was no information concerning its behavior with compressible lubricants. An investigation was performed using the incompressible theory as established in Reference (4) and elaborated upon in Reference (3). The following performance resulted.

Minimum clearance	= 0.695 mils
No. of pads	= 3
Depth of land	= 1.390 mils
Power loss	= 0.089 hp

This bearing appeared especially attractive for the turbine-compressor application because of its low power loss. However, with a compressible lubricant, the stability potential of this type bearing was considered questionable and therefore no further consideration was given to this configuration.

4.2.2.5 Spiral Groove Bearing

The spiral groove type thrust bearing has found wide acceptance in gas bearing applications. Theoretically, for a given area it has superior load carrying ability over all the other types considered — so long as it remains reasonably well aligned. Several variations of this bearing were investigated. Those included the outward pumping type, the inward pumping type with central hole, the dead-ended type and the herringbone groove type. The various configurations are described in Reference (5). Two references sources were used in the initial investigation, namely References (5) and (6). Reference (6) was limited to inward pumping types only, while Reference (5) covered the entire spectrum of types although its discussions and information were limited to incompressible lubricants. The outward pumping bearing was not given serious consideration, since the inlet flow area was less than the outlet flow area and if pumping rates are high, the tendency was to pump more fluid than could be supplied, with subsequent net reduction in load capacity and possible stability problems. The inward pumping and dead

ended bearings were particularly attractive in regards to load capacity. This, combined with their previous history of satisfactory performance, dictated their selection as the thrust bearing type to be employed in the turbine compressor. Since these were the ultimate bearing selected, the spiral groove bearings were investigated more thoroughly than any of the other types.

A summary of the various spiral groove types considered throughout the analytical and design phase progression are shown on Table 1. During one stage of the design evolution a bearing machined into the shaft was being considered in order to eliminate some of the problems of a separate mount. These are referred to as the integral collar in Table 1.

Table I

SPIRAL GROOVE BEARING SUMMARY

	Bearing Dimensions	Bearing Type	Gas	Load (lbs)	$h_m \times 10^3$ (in)	Power Loss Watts
Integral Collar	O.D. = 2.25" I.D. = 0.625"	SGI	Compressor Inlet	13	0.625	46
			Compressor Inlet	35	0.385	74
			Compressor Discharge	13	0.733	49
			Compressor Discharge	35	0.430	83
		SGDE	Compressor Inlet	13	0.965	24
			Compressor Inlet	35	0.589	36
Separate Collar	O.D. = 3.125" I.D. = 0.80"	SGI	Compressor Discharge	35	0.876	151
	* O.D. = 2.66" I.D. = 1.60"	SGDE	Compressor Inlet	50	0.680	95

SGI = Spiral Groove Inward Pumping
SGDE = Spiral Groove Dead Ended
*Final Design Size

4.2.3 Comparative Performance

Comparative performance of the various type thrust bearings investigated during the initial review stage and the references used are presented in Table 2. The temperature rise, was calculated assuming all the heat was absorbed by the cooling fluid which was taken to be 1% of the compressor flow.

Table 2.

COMPARISON OF CHARACTERISTICS OF VARIOUS TYPES OF THRUST BEARINGS

Brg. Type	Ref.	Min. Clear. (in. x 10^3)	Design Stiffness (lb/in x 10^{-4})	System Nat. Freq. (CPM x 10^{-3})	Gas Flow (lb/sec x 10^4)	Power Loss (Watts)	Temp. Rise (°F)	No of Pads
TP	(4)	0.281						5
S	(5)	0.677	9.0	18.24		145	184	3
S	(4)	0.565						5
S	(6)	0.580			4.97	160	200	6
TL	(4)	0.636						5
TL	(3)	0.628	11.20	20.0	5.47	93	117	4
P	(6)	0.695	9.25	18.5	2.91	66	84	3
SGI	(8)	0.876	7.14	16.2				
SGI	(9)	1.000	6.50	15.5		101	128	
SGI	(10)	0.804			.392			
SGO	(9)	0.700						
HB	(9)	0.538						

Operating Conditions
O.D. = 3.125 in.
I.D. = 0.800 in.
N = 50,000 RPM
μ = 4.6×10^{-9} lb-sec/in^2 (argon at 390° F)
P_a = 11.6 psia
W_T = 34.54 lbs

Key
TP = Tilting Pad
S = Stepped
TL = Tapered Land
P = Pocket
SGI = Spiral Groove Inflow
SGO = Spiral Groove Outflow
HB = Herringbone

4.2.4 Bearing Cooling Scheme

The general construction features associated with the stationary thrust collar allowed the introduction of a liquid coolant directly into a spiral cavity inside the thrust stator. This provided an extremely efficient means for cooling the stator and maintaining a uniform temperature distribution across the stator face. The thrust rotor was cooled both by the heat transfer across the fluid film to the stator, and by compressor discharge bleed-off that was externally cooled by a liquid flowing through a heat exchanger. An analytical thermal map, generated by Pratt and Whitney Aircraft, predicted that the runner and stator would operate at metal temperatures of 145°F and 115°F respectively.

5. DESIGN SUMMARY

5.1 Journal Bearings

1. Type - self-acting tilting pad
2. Number of pads - 3
3. Pad wrap angle - 100°
4. Radius to length ratio - 0.5
5. Shaft diameter - 1.500 inches at Brg. 1; 2.125 inches at Brg. 2
6. Pivot location - 65% from leading edge
7. Design Λ - 1.5
8. Preload - 8 pounds Brg. 1; 9 pounds Brg. 2
9. Preload spring constant - 91 lb/in.
10. Machined in clearance - 0.0020 inches Brg. 1; 0.0029 inches Brg. 2
11. Pivot - 0.6 inch radius sphere on 3/16 inch pin against flat surface
12. Pad weight - 0.118 pounds (each shoe of Brg. 1)
    0.236 pounds (each shoe of Brg. 2)
13. Pad inertias (in-lb/sec^2)

	Brg. 1	Brg. 2
Pitch	0.66×10^{-4}	2.39×10^{-4}
Roll	0.67×10^{-4}	2.58×10^{-4}

14. Pad radius tolerances and finish
    Brg. 1 - 0.0018 to .0029 inches larger than mean shaft radius*; 4 micro-inch RMS roughness
    Brg. 2 - 0.0027 to 0.0029 inches larger than mean shaft radius*; 4 microinch RMS roughness.
15. Materials
    a) Pads - hardened AMS 6440 steel; face flame sprayed with 0.002 to 0.003 inches of chrome oxide (finished)
    b) Pivot pin - hardened AMS 5616
    c) Preload spring - Inconel X

*Refers to shaft and shoes at design in operating conditions

16. Jacking gas
    a) Supply pressure - 100 psia
    b) Pivot pin passage - 0.031 inch diameter
    c) Recess - 0.28 inch diameter by 0.0002 inches deep Brg. 1; 0.3 inch diameter by 0.0002 inches deep Brg. 2

17. Film Stiffness (lb/inch)

	Brg. 1	Brg. 2
x	13,700	7500
y	4,600	2500

18. Rigid Body Critical Speeds - 7000 to 15,500 Brg. 1; 3000 to 8500 Brg. 2

19. Operating Conditions (vertical rotor)

	Brg. 1	Brg. 2
Min. Clearance	0.63×10^{-3} inches	1.20×10^{-3} inches
Shoe Load	8 pounds	9 pounds
Power loss	48 watts	102 watts

5.2 Thrust Bearing

5.2.1 Main Thrust Bearing

1. Type - dead ended inward pumping spiral groove with a row of feeding orifices for jacking gas
2. Spiral groove specifications
    a) Number of grooves - 15
    b) Nominal groove depth - 0.0037 inches
    c) Land surface material - chrome oxide
    d) Groove angle - 11.7°
    e) Ridge/groove ratio - 1.19
    f) Radius ratio - 0.6
    g) Outside diameter - 2.666 inches
    h) Inside diameter - 1.600 inches
    i) Substrate material - aluminum
    j) Land flatness - 2 sodium light bands
    k) Land roughness - 20 micro inches RMS

3. Operating Conditions - self-acting with 15 pound thrust load at 50,000 rpm
   a) Minimum clearance - 0.0011 inches
   b) Power loss - 41 watts
   c) Axial film stiffness - 28,000 pounds/inch
   d) Torsional film stiffness 15,550 inch-pound/radian
   e) Maximum relative swash between plates - .18 times initial angular misalignment.
4. Hydrostatic main thrust specifications
   a) Number of holes - 20
   b) Diameter of holes - 0.032 inches
   c) Hole circle diameter - 1.23 inches

5.2.2 Reverse Thrust Bearing

1. Type - Rayleigh step with orifices in lands for start-up.
2. Rayleigh step specifications
   a) Number of sectors - 7
   b) Recess arc length - 8.23°
   c) Step height - 0.0006 inches
   d) Coating - chrome oxide
   e) Outside diameter - 2.666 inches
   f) Inside diameter - 1.520 inches
   g) Number of feed hole per sector - 4
   h) Diameter of feed holes - 0.032 inches
   i) Land flatness - 2 sodium light bands
   j) Roughness - 20 micro inches RMS

5.2.3 Hydrodynamic Start-up Operating Conditions

5.2.3.1 Forward Load - 50 lbs.

Reaction bearing clearance = 0.0085 inches
Main bearing clearance = 0.0015 inches
Supply pressure = 100 psia
Reaction bearing flow = 0.052 lbs/sec
Main bearing flow = 0.006 lbs/sec
Critical load = 132 lbs.

5.2.3.2 Reverse Load - 100 lbs

Reaction bearing clearance = 0.0008 inches

Main bearing clearance = 0.0092 inches

Supply pressure = 100 psia

Reaction bearing flow = 0.005 lbs/sec.

Main bearing flow = 0.040 lbs/sec.

NOTE: Reverse loads stability is not critical because reverse bearings do not have any significant recessed areas.

6. JOURNAL BEARING ANALYSIS

The basic approach to the bearing system design consists of treating the journal bearings independent of the thrust bearings. The assumption is that the radial force induced by misalignment and swashing of the thrust bearing and the axial force induced by the journal bearings are negligible. Therefore, the thrust bearing is essentially isolated from the journal bearings.

The method used in reaching an optimized journal bearing design consists of first obtaining steady-state characteristics over a range of bearing parameters, concluding a basic design and then examining this design by means of a comprehensive dynamical analysis.

The dynamics analysis undertaken for this project is based on Reference (7) and constitutes a major step forward in the analysis of tilting-pad/rotor systems. The steady-state and stability analysis applied to the thrust bearings are modifications of various analytical techniques that are currently available in the literature.

The journal bearing analyses phase consist of obtaining the appropriate differential equations, recognizing their assumptions and limitations, developing a technique to solve these equations and using this information to obtain load capacity, clearance and friction loss. Enough data is collected to access the effects of Λ, pivot location, ect. on the load capacity and friction loss. A bearing design that carries the load, has an exceptable minimum film thickness and an exceptable friction loss is then formulated. A system preliminary design is established in which values are assigned to the masses and inertias of the system. Natural frequencies and system critical speeds are examined for compatibility. The question of system stability at the design speed is then answered by a dynamics analysis that solves the exact equations of motion of the entire system together with the Reynolds equation for

the film pressures. The amplitudes and frequencis of all the degrees of freedom, and an understanding of how, and hopefully why, the rotors respond to the presence of the journal bearings is obtained from this analysis.

6.1 Steady-State Analysis

6.1.1 The Reynolds Equation

The differential equation governing the pressure distribution in a bearing clearance, generally referred to as the "Reynolds" equation, is well known in the field of lubrication; its derivation can be found, for example, in Reference (1). Since the Reynolds equation forms the theoretical basis for the bearing design, it is appropriate that the restriction imposed on the use of this equation due to its derivation, should be reviewed. A review of the derivation is outlined in Appendix I. The essential results are that, for the compressible case considered, the flow in the bearing clearance is laminar, the inertia forces of the gas lubricant are small, the "no-slip" boundary condition at the bearing surface applies and the fluid flow may be considered isothermal. In its non-dimensional form, the steady-state Reynolds equation is written

$$\frac{\partial}{\partial\theta}\left[H^3\ P\ \frac{\partial P}{\partial\theta}\right] + \left(\frac{R}{L}\right)^2 \frac{\partial}{\partial\zeta}\left[H^3\ P\ \frac{\partial P}{\partial\zeta}\right] = \Lambda\frac{\partial}{\partial\theta}\quad (PH) \tag{1}$$

where the clearance H is given by

$$H = 1 + (X + A_1\zeta)\ \sin\theta + (Y + A_2\zeta)\ \cos\theta \tag{2}$$

The dimensional coordinates are shown in Figure 1.

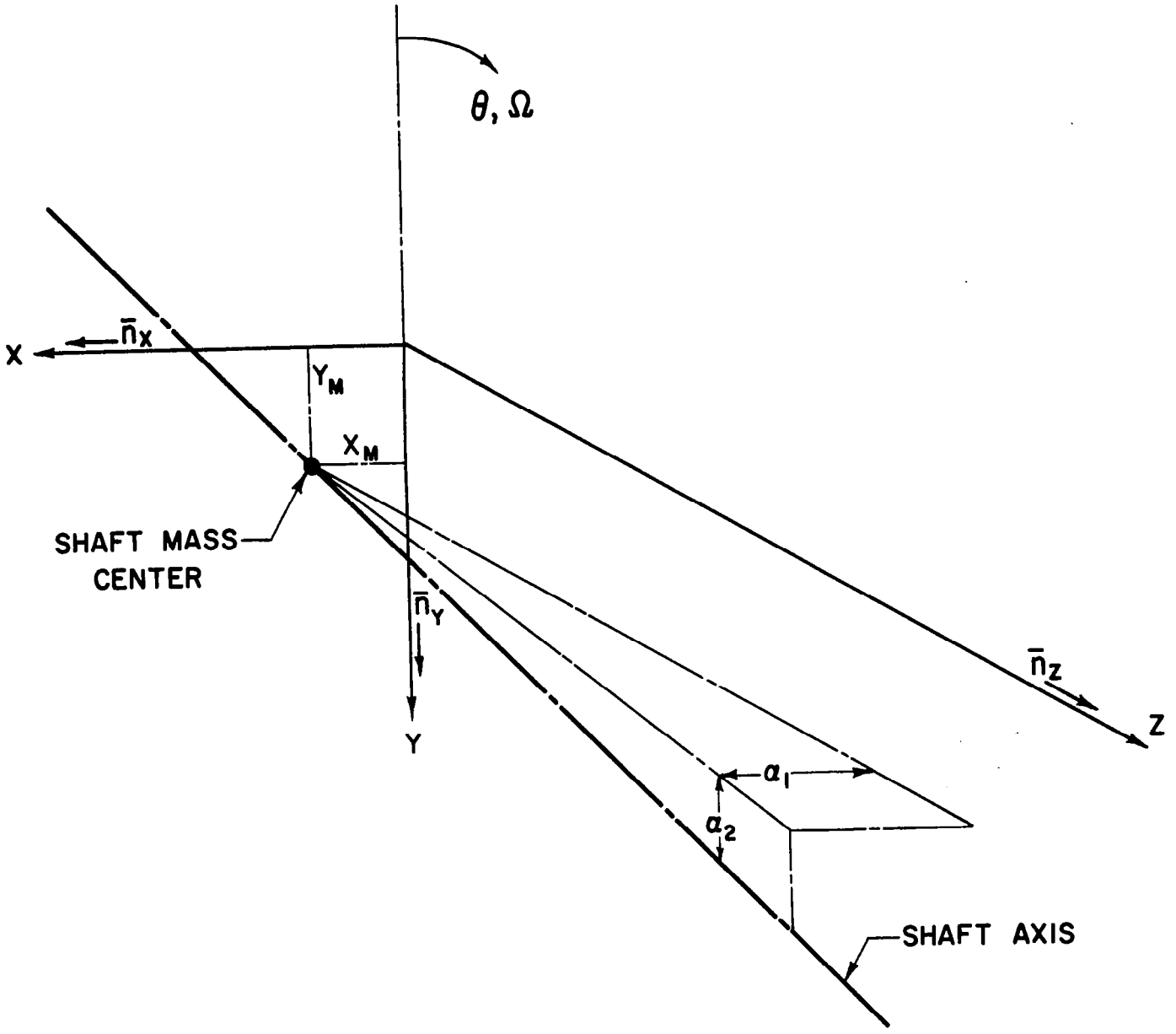

Fig. 1 - Journal Coordinate System

6.1.2 Solution of the Reynolds Equation

Equation 1 is a non-linear (in the pressure P), second order, partial differential equation with non-constant coefficients H (x,y,θ). Except for certain limiting solutions [8], Equation 1 must be solved approximately. The method chosen is to express the Reynolds equation in finite difference form and to solve the equation by an explicitly overrelaxation numerical procedure.

Refering to Figure 2 the load coefficients parallel C_{Ly} and normal C_{Lx} to the line of centers are determined by integrating the pressure against cos θ and sin θ.

$$C_{Ly} = \frac{W_y}{P_a RL} = - \int_{-1/2}^{1/2} \int_{\xi}^{\xi+\alpha} (P-1) \cos \theta d\theta d\zeta \qquad (3)$$

$$C_{Lx} = \frac{W_x}{P_a RL} = - \int_{-1/2}^{1/2} \int_{\xi}^{\xi+\alpha} (P-1) \sin \theta d\theta d\zeta \qquad (4)$$

The total load coefficient is given by

$$C_L = \frac{W_t}{P_a RL} = - (C^2_{Ly} + C^2_{Lx})^{1/2} \qquad (5)$$

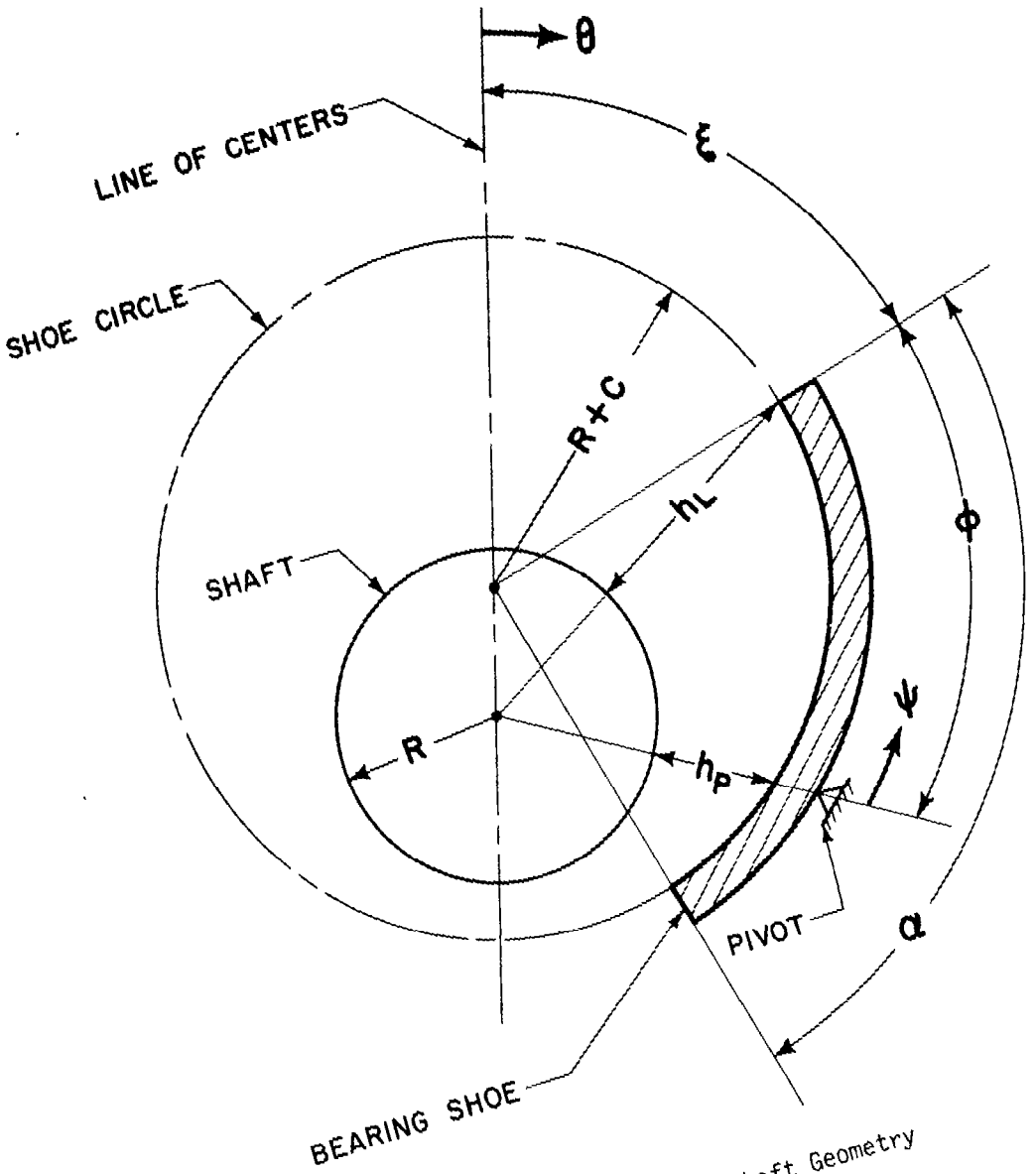

Fig. 2 - Shoe-Shaft Geometry

The friction moment F_m that arises from the shear of the bearing film due to the shaft rotation is determined by integrating the momentum equation in the circumferential direction to obtain the film velocity "u" and then integrating the moment due to the shear stress τ where

$$\tau = \mu \frac{du}{dy} \tag{6}$$

$$f_m = \int_0^L \int_\xi^{\xi+d} \tau R^2 d\theta dz \tag{7}$$

In non-dimensional form (see Appendix I)

$$F_m = \frac{f_m}{P_a RCL} = \int_{-1/2}^{1/2} \int_\xi^{\xi+d} \left[\frac{\partial p}{\partial \theta} H + \frac{\Lambda}{3H}\right] d\theta d\zeta \tag{8}$$

6.2 Steady-State Design

6.2.1 Steady-State Field Maps

Given Λ, R/L, α and a set of geometrical coordinates ξ and $\varepsilon = e/C$ (Figure 2), the steady-state analysis is used to determine the shoe load coefficient C_L, the non-dimensional pivot (H_p) and trailing edge (H_T) film thicknesses, the friction loss coefficient μ_F and the center of pressure (pivot location ϕ/α). The above four parameters are plotted against ϕ/α and referred to as "field maps". These maps provide the basis for the steady-state characteristics. Note that if the angle

$\xi + \alpha$ is equal to or less than 180° the field map H_T vs. ϕ/α gives the minimum film thickness directly. If $\xi + \alpha$ is greater than 180°, the minimum film thickness is inside the shoe at an angle 180° from the line of centers. Figures 3 to 6 are examples of field maps for $\Lambda = 1.5$. Other field maps are presented in Appendix II.

6.2.2 Selection of Pivot Location (ϕ/α)

Figure 3 shows that the line $\xi = 90°$ is practically the line of optimum pivot location from a load carrying point of view. For $\xi = 90°$ the bearing film thickness would converge for 90° and diverge for 10° over the 100° pad arc length. The optimum ϕ/α is seen to depend on the required load coefficient C_L. For load coefficients between 0.5 and 1.0 the pivot whould be located between $\phi/\alpha = 0.594$ and $\phi/\alpha = 0.666$. In this range ε goes from 0.55 to 0.78. Referring to Figure 6 in the same range for ξ and ε, the optimum pivot location for minimum friction varies from $\phi/\alpha = 0.610$ to $\phi/\alpha = 0.682$. Therefore, to optimize from a friction standpoint requires that the pivot be located closer to the trailing edge than for optimization of load capacity. For higher Λ's the pivot should be moved even closer to the trailing edge. As a compromise, ϕ/α has been taken as 0.65.

6.2.3 Selection of the Bearing Number (Λ).

The solid lines on Figure 7 show how the non-dimensional clearance varies with Λ for constant load. The broken lines show how the dimensional clearance varies when Λ is changed by varying the ground-in clearance only. The broken curves have been normalized by using the conditions $C_0, \frac{6\mu\Omega R^2}{P_a}$ at $\Lambda = 10$. From these curves it is seen that the greatest minimum film thickness is obtained between $\Lambda = 0.05$ and $\Lambda = 1.2$. Figure 8 shows the relation between Λ and the friction coefficient $\bar{\mu}_F$ for constant load. Figure 9, normalized at $\Lambda = 1.5$, is similar to Figure 7 in that it shows the effect on the friction horsepower loss when Λ is changed by varying the ground in clearance only. Figure 9 shows that for a narrow range of Λ around 1.0 friction is constant.

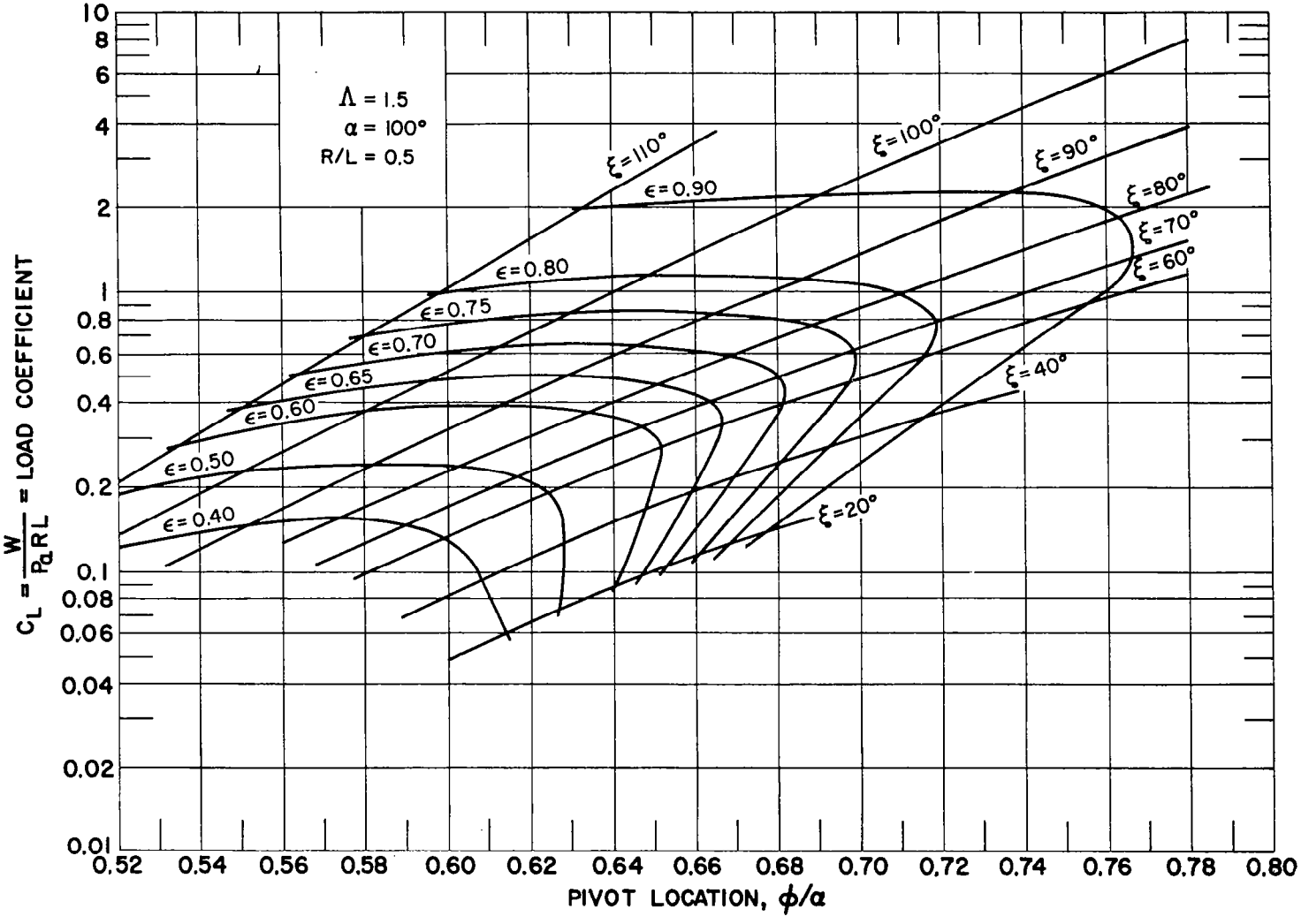

Fig. 3 - Load Coefficient vs. Pivot Location for R/L = 0.5, α = 100°, Λ = 1.5

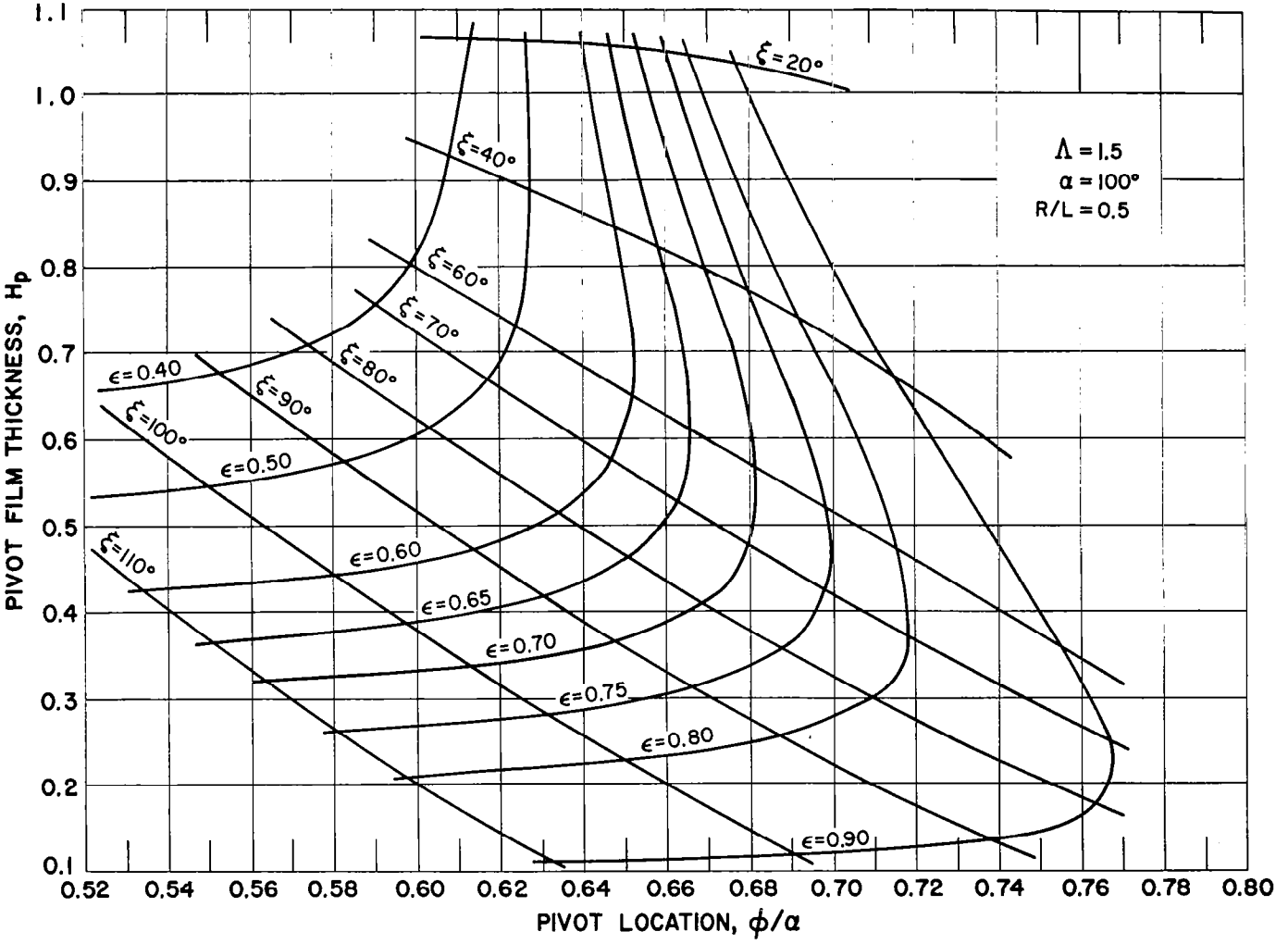

Fig. 4 - Pivot Film Thickness vs. Pivot Location for R/L = 0.5, $\alpha = 100°$, $\Lambda = 1.5$

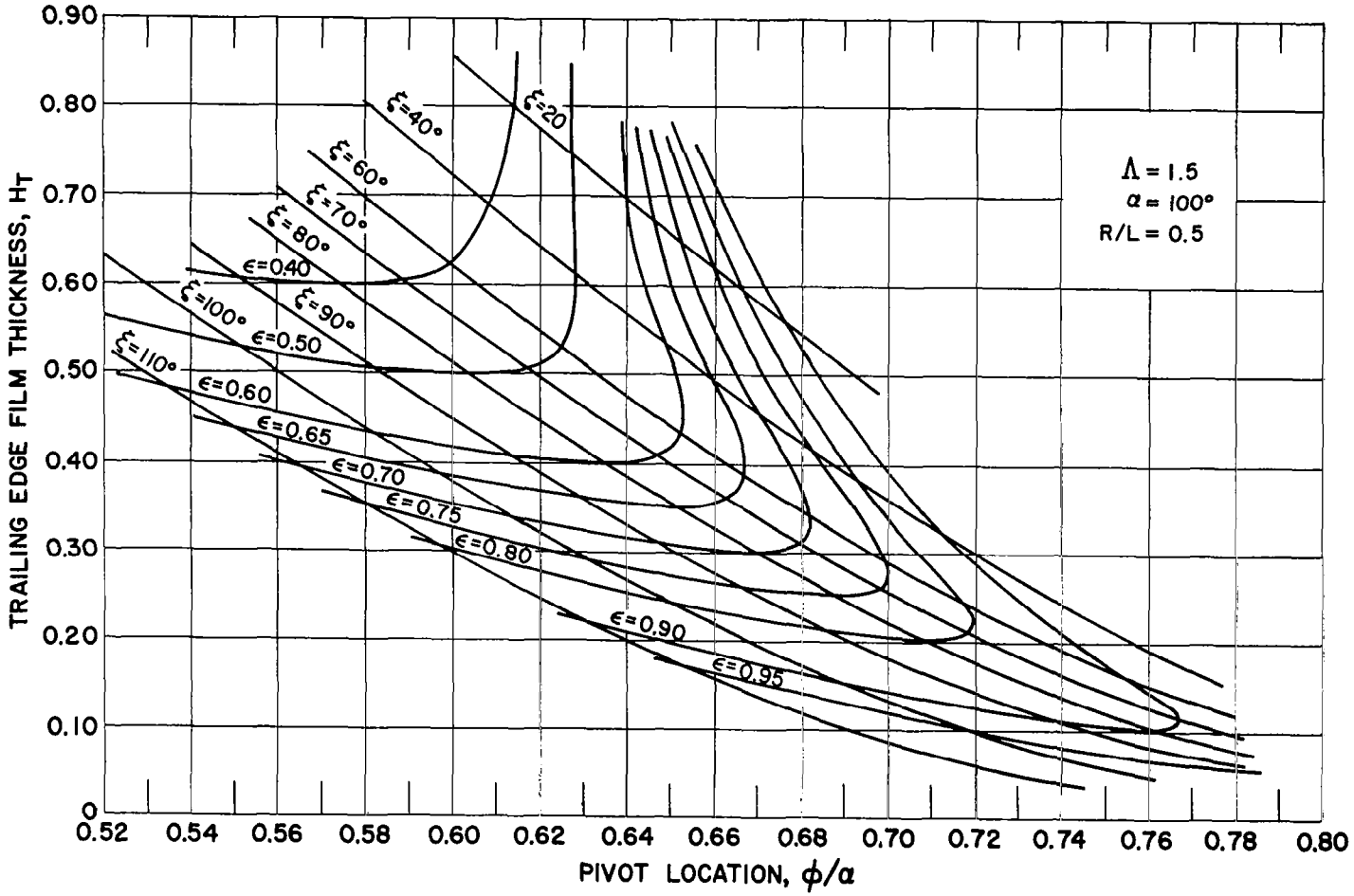

Fig. 5 - Tailing Edge Film Thickness vs. Pivot Location for R/L = 0.5, α = 100°, Λ = 1.5

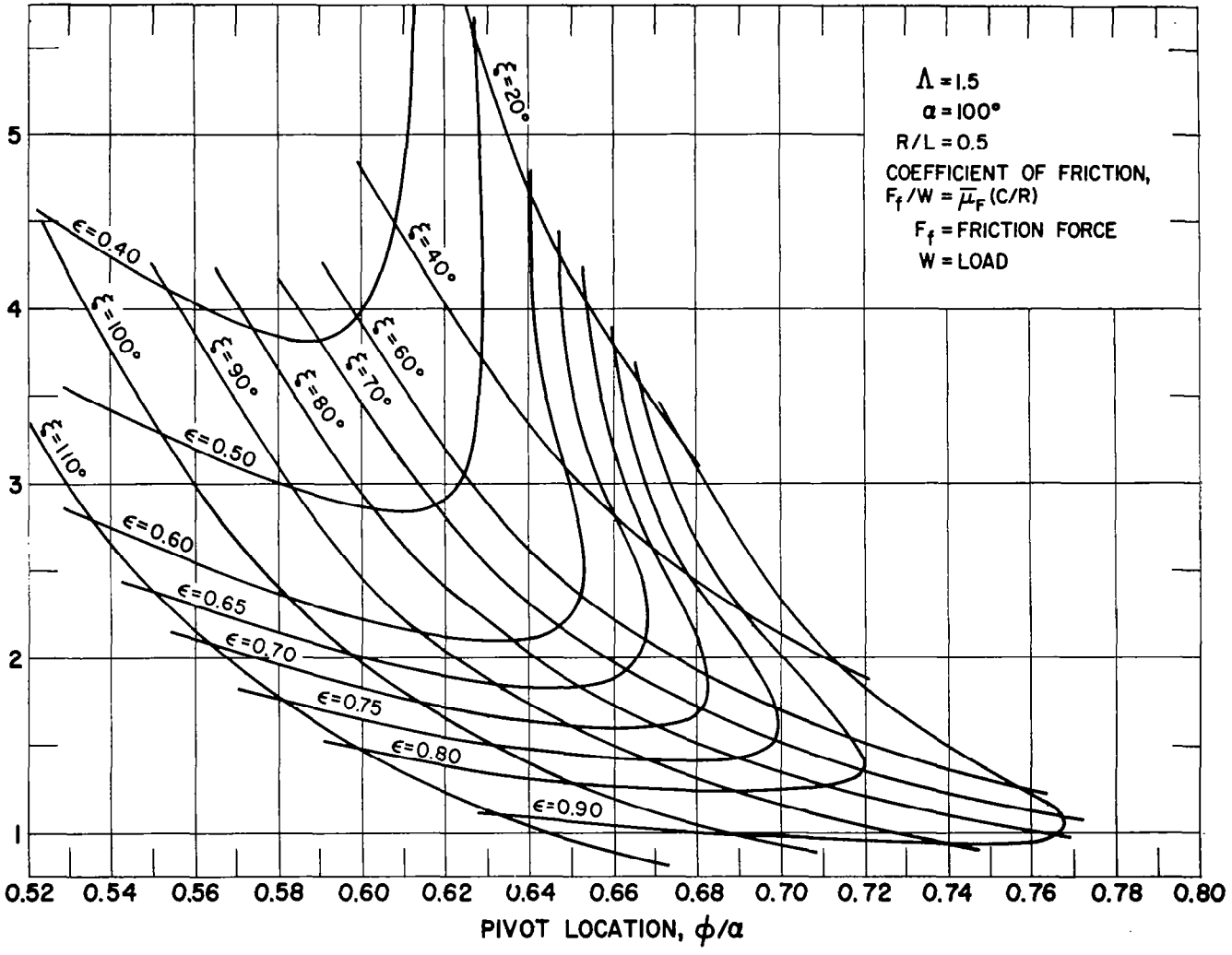

Fig. 6 - Friction Factor vs. Pivot Location for R/L = 0.5, α = 100°, Λ = 1.5

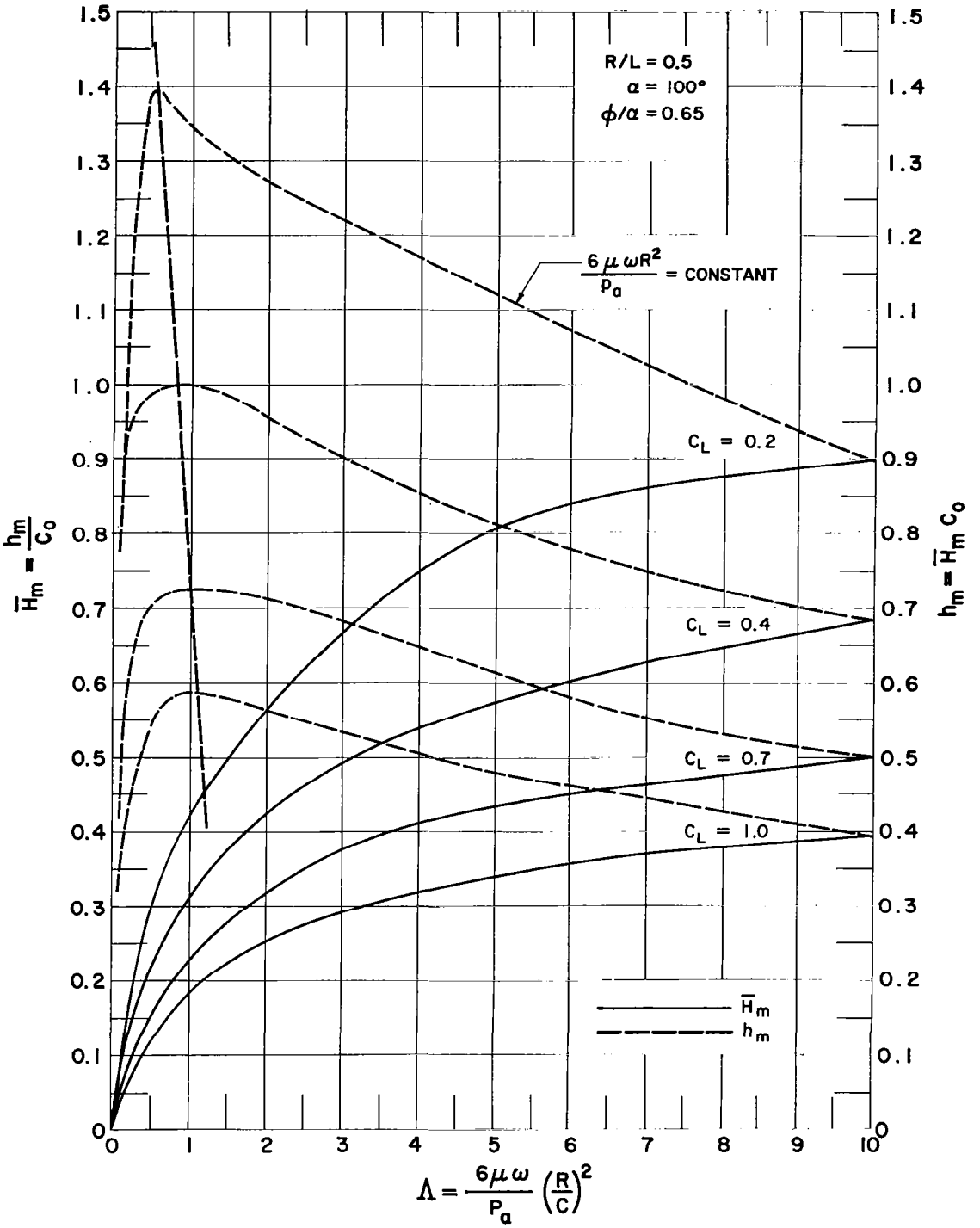

Fig. 7 - Minimum Film Thickness vs. Λ for R/L = 0.5, α = 100°, ϕ/α = 0.65

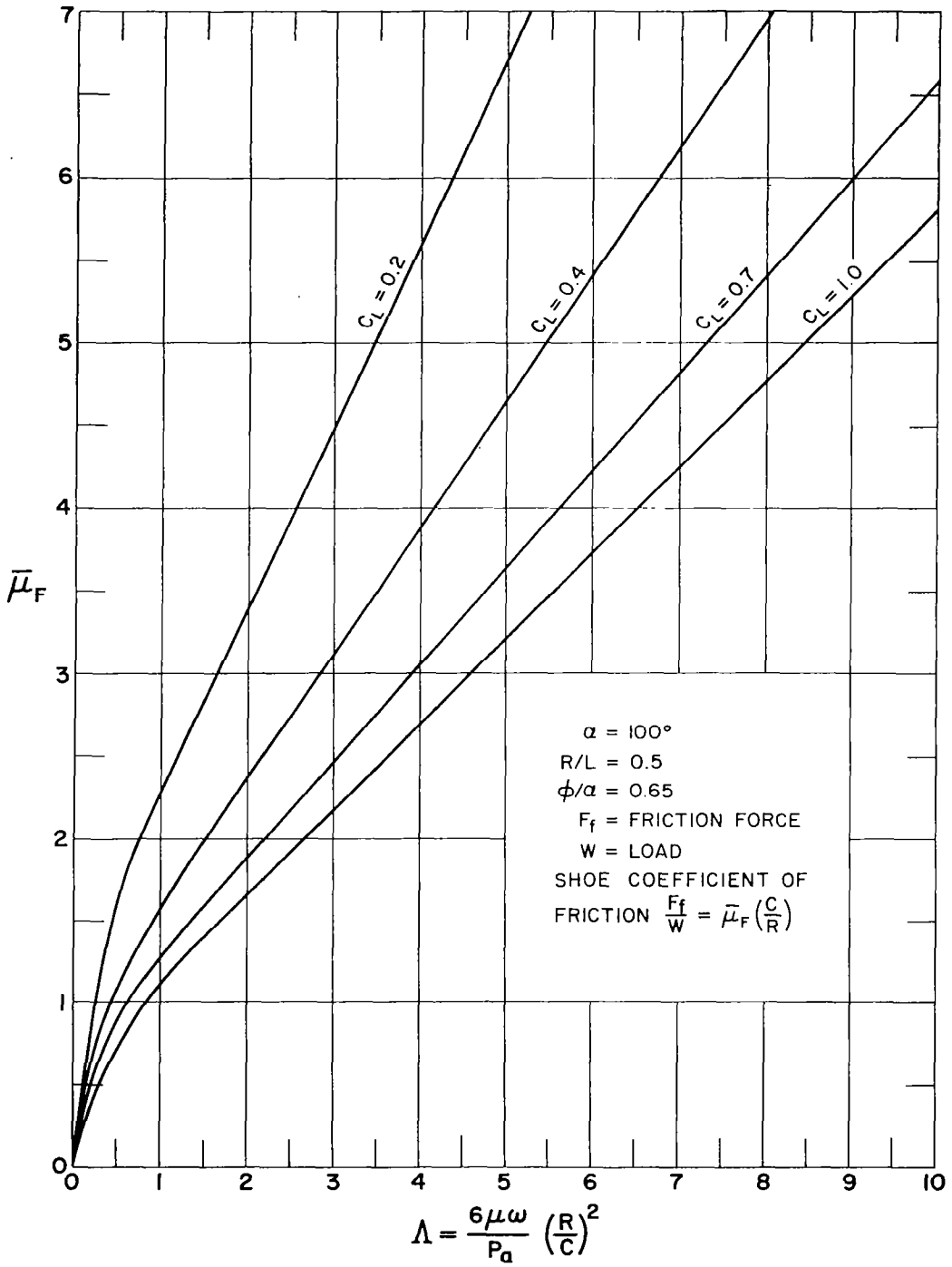

Fig. 8 - Friction Factor vs. Λ for R/L = 0.5, α = 100°, ϕ/α = 0.65

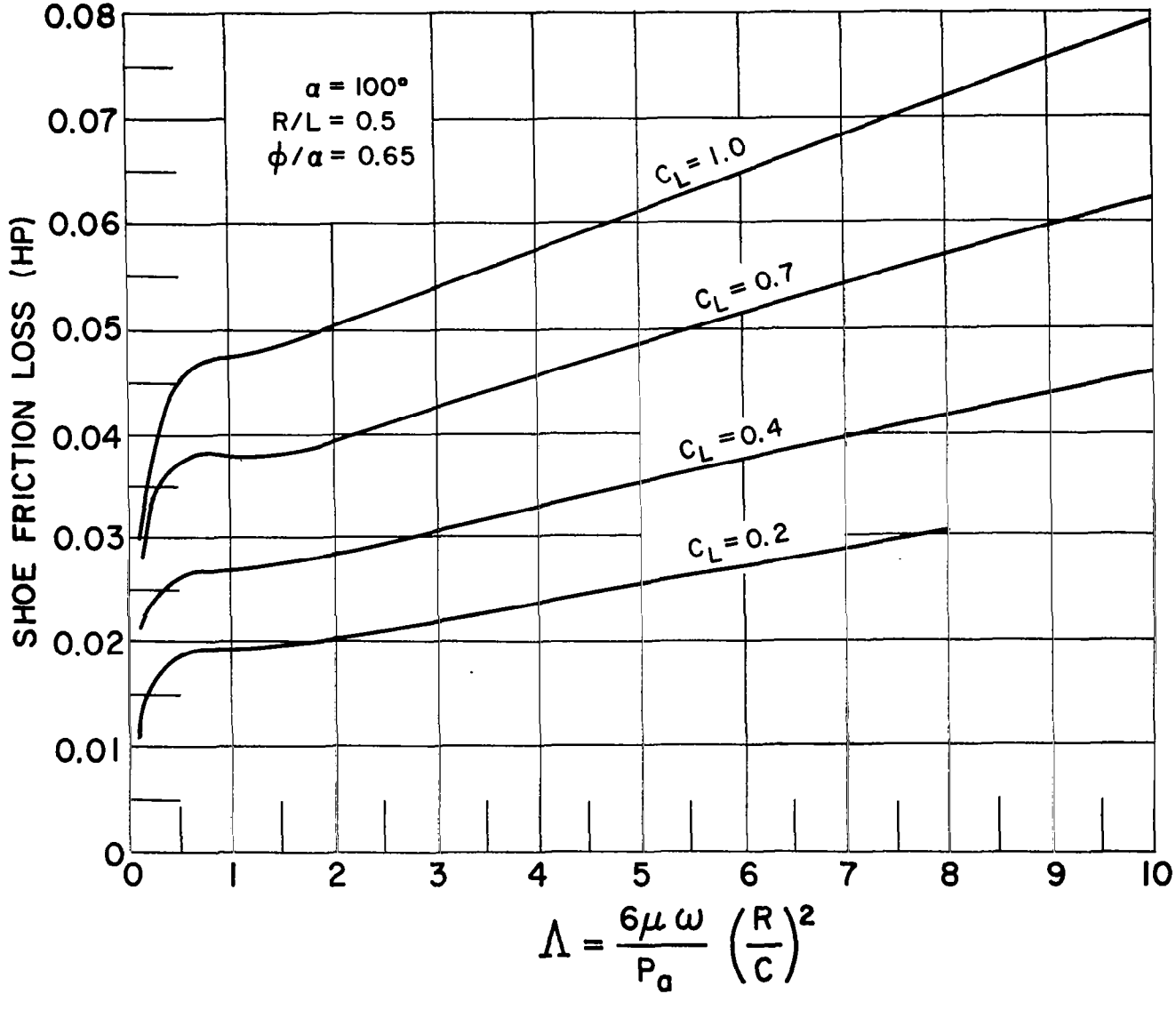

Fig. 9 - Shoe Friction Horsepower Loss vs. Λ for R/L = 0.5, $\alpha = 100°$, $\phi/\alpha = 0.65$

$\Lambda = 1.5$ was selected for the design of both journal bearings because it is close to the optimum for both load and friction loss and also because as the speed of the unit is reduced from the design point the minimum film thickness will grow before beginning to decline. This will provide a degree of safety during shut-down and low speed operation.

6.2.4 Selection of the Bearing Radius to Axial Width Ratio (R/L)

Short bearings have larger axial leakage and poor load capacity. Long bearings have good load capacity but poor roll dynamic characteristic because of large roll inertia. A bearing with an R/L of 0.5 seems to provide an acceptable compromise between load and inertia.

6.2.5 Selection of the Number of Shoes

A two-shoe system has poor stiffness in the direction normal to the line joining the two pivots.

The number of shoes selected for the design is limited to three for each bearing for the following reasons:

1. It is desirable to have a minimum number of parts.
2. The shoe load capacity varies approximately with the square of the wrap angle. More than three shoes causes a reduction in the effective load-carrying capacity.
3. Three pivot points always define a unique pivot circle. One point can be preloaded with a soft spring to maintain constant pivot film thickness to compensate for geometric changes due to thermal growth and centrifugal strain.
4. Control of rigid body critical through preload setting.
5. Yaw restoring moment increases with wrap angle

6.2.6 Selection of the Wrap Angle (α)

As a compromise among load capacity, pitch inertia, yaw righting moment and clearance between adjacent shoes, the wrap angle is taken as 100°.

6.2.7 Design of Preload Spring

The philosophy of the preload spring is to provide a device that produces a preload force but will, at the same time, be soft enough to allow the pivot circle to "breathe" without substantially changing the film pressure. In this manner, the pivot film thicknesses will remain constant even though the shaft may experience some growth. If a 100 lb/in. spring is given a preload of 10 pounds and if the spring is moved 1×10^{-3} inches, the net change in the film force would be 1%. Therefore, since the film force is not substantially changed, neither will the clearance. If the shaft grows but the pivot circle does not, the bearing friction will increase thus aggravating the distortion situation.

The material chosen for the spring wire is "Inconel X" because it is good to 1000°F for prolonged periods and resists corrosion and oxidation. The properties of Inconel X are:

	Tensile (psi)	Torsional (psi)
Ultimate Strength	130,000 to 220,000	90,000 to 155,000
Elastic Limit	90,000 to 150,000	50,000 to 90,000
Modulus of Elasticity	31×10^6	11.5×10^6

The total deflection, δ, of the spring is given by:

$$\delta = \frac{8\ W\ D^3 N}{G\ d^4} \tag{9}$$

where W = load = 8 lb. Brg. 1; 9 lb. Brg. 2

D = coil diameter = 0.36 inches

N = number of active coils = 5

G = shear modulus = 11.5×10^6 psi

d = wire diameter = 0.062 inches

Therefore

$$\delta^{(1)} = \frac{8 \times 8 \times (.36)^3 \times 5}{11.5 \times 10^6 \times (.062)^4}$$

$\delta^{(1)}$ = 0.0879 inches deflection for Brg. 1
$\delta^{(2)}$ = 0.0982 inches deflection for Brg. 2

The spring constants for both bearings are:

$$K^{(1)} = \frac{W^{(1)}}{\delta^{(1)}} = \frac{8}{0.0879} = 91 \text{ pounds per inch}$$

$$K^{(2)} = 91 \text{ pounds per inch}$$

The natural frequency (using Ricardo's formula) is given by:

$$N = \frac{761{,}500\ d}{ND^2} \qquad (10)$$

$$= \frac{761{,}500 \times .062}{5 \times (0.36)^2}$$

$$N = 72{,}859 \text{ cpm}$$

The torsion stress is given by:

$$S = \frac{8\ W\ D}{\pi\ d^3} \qquad (11)$$

$$S^{(1)} = \frac{8 \times 8 \times .36}{\pi\ (0.062)^3}$$

$$S^{(1)} = 30{,}759 \text{ psi}$$

$$S^{(2)} = 34{,}374 \text{ psi}$$

For tolerancing, the wire size of 0.062 inches should be considered a lower limit; the coil diameter of 0.36 inches should be considered an upper limit. The total number of coils should be 7.5 for a free length of 0.68 inches with the ends closed and ground.

6.2.8 Pivot Design

The pivot design is considered an important part of the bearing system since an incorrectly designed pivot can induce shaft whirl. Increasing the pivot friction moment can cause the shoes to stick in a position where load capacity and stability would suffer. Further increase in the pivot friction will cause the bearing to act as a "fixed" partial arc bearing. If the shaft is well balanced, the shaft operating orbit will be small and therefore the shoe pitch motions will be small. Should the pivot friction moment increase during operation (due to, for instance, fretting and corrosion) the friction moment may eventually become larger than the film force pitching moment generated due to the shaft orbital motion. When the friction moment is equal to or larger than the pitching moment the shoe will remain stationary. Under these conditions stability is in doubt.

If the speed of the rotor is changed the shoes will try to adjust to a new mean pitch position and should the pivot friction moment be too high, an unstable situation could arise. Because pivot friction always exists to some degree the shoes would take a different position depending on whether a particular speed is approached from below or above.

From the above comments it can be seen that excessive pivot friction moments should be avoided. It appears that there are two ways at present to determine the limiting pivot friction. These are:

(1) Experimentally

(2) With the orbit program discussed in the dynamics analysis.

In the orbit program the pivot friction could be slowly increased with time until the shoe locks. If the rotor remains stable the speed could be changed with the shoes (or shoe) locked in position to determine where (or if) whirl onset occurs. This can be done experimentally, but it is difficult to control and to know the amount of pivot friction moment that is being applied.

On the other hand, if pivot friction is low, then the shoe resonance motion could be high. A certain amount of pivot damping seems to be desirable.

The roll motion of the shoes appears to be desirable only insofar as adjustment to gross case distortions are required. Because of the approximately uniform clearance in the axial direction, the shoes have no initial roll stiffness. Therefore small roll moments create relatively large roll motions (compared to the pitch direction). Also, since the shoe has a non-zero roll inertia, the shoe roll motion will always be out of phase with the shaft motion to some degree. Therefore, it appears that the minimum film thickness along the axial edges of the shoe would be larger if the shoe was restrained from motion in the roll direction. At this time, relatively little work has been done in investigating pivot types that would restrain the roll mode. This is an area that requires more detailed study.

From our past experimental experience with pivot designs we recommend at this time, a Ball with a 0.6 inch spherical radius at the tip of a 3/16 inch hardened pin and a recessed hardened flat on the shoe. There may be better possible pivot designs, but they could not be recommended until these designs have been experimentally studied.

The pivot pin is made of AMS 5616 steel hardened to Rockwell "C" 45-50. The pivot pin has a tip spherical radius of 0.60 inches and sits in a 0.094 inch recess with a 0.002 to 0.003 inch radial clearance. The pivot seat has a roughness of 4 micro inches RMS and is flat to within two sodium light bands. The pin and the shoe are drilled for a 0.031 inch diameter jacking gas passage.

6.2.9 Lift - Off Design

If the average static pad pressure exceeds 2 to 3 psi and many stops and starts are to be performed, then externally-pressurized gas should be used to produce a bearing film during the transient periods. In any case, the shoes and the shaft should be coated with a suitable material for rubbing purposes. If the shoe wears in with the shaft, the ground in clearance will go to zero. This will increase Λ which would raise the friction heat generated in the bearing and could also lower the speed at which whirl can occur.

For horizontal operation, the load on one of fixed shoes of the number 2 bearing is

$$W = \text{preload} \times \cos 60^\circ + \text{shaft load} \times \cos 60^\circ$$

$$= (9 + 7.5) \times .5$$

$$W = 8.25 \text{ pounds}$$

The area of the shoe is approximately 4.5 inches. Therefore, the average static pressure on the shoe is

$$\bar{P}^{(2)} = \frac{8.25}{4.5} = 1.84 \text{ psi}$$

On the number 1 bearing

$$\bar{P}^{(1)} = \frac{12.3}{2.25} = 5.48 \text{ psi}$$

The 8 pound preload on the number 1 bearing requires that lift-off facilities be provided.

Experimental experience has shown that if a hole is drilled through the shoe, the shaft will blank off the hole and will not lift off unless the shaft is backed off from the hole. This situation is

avoided by providing a recess around the hole with enough area so that the area times the recess pressure is greater than the shoe load. The recess should be very shallow so that pneumatic hammer is avoided. The depth should be on the order of .0002 inches. This can be done by making a templet of the required area and polishing this region with lapping compound. The depth of the recess can be checked by a light fringe method. The recess area could be circular and should be centered slightly forward (towards the shoe leading edge) of the feed hole. This will cause the shoe to cock open forming a converging film when the pressurized gas is fed to the shoe.

The number 1 bearing has a jacking gas recess at the pivot 0.28 inches in diameter and .0002 inches deep. The diameter of the recess is 0.33 inches for the number 2 bearing.

The gas line supplying the lift-off recess should contain a Bourdon tube pressure gage for monitoring the pressure at the pivot point. This pressure is directly related to the shoe-shaft relative geometry. By experimentally establishing the relation between the pivot pressure and the pivot film thickness the shoe operating point can be readily observed. The safe operating range for the shoe can be established in terms of an upper and lower pressure limits.

The gas line feeding the shoe should also contain valves for throttling the flow. Once the flows have been experimentally established for lifting the rotor without cocking, the values can be replaced with the appropriate orifices.

6.2.10 Shoe Material, Finishes and Tolerances

The shoe is made of hardened AMS 6440 steel with the face of the shoe flame sprayed with chrome oxide to a finished depth of between 0.002 and 0.003 inches. The face of the shoe is within 4 micro inches RMS roughness. The radius of the number 1 bearing* is to be between 0.0018 and 0.0020 inches larger than the mean shaft radius at the number 1

*Given dimensions refer to conditions at design operating shaft speed and temperature.

bearing. The radius of the number 2 bearing is to be between 0.0027 and 0.0029 inches larger than the mean shaft radius at the number 2 bearing. The shoe thickness is 3/16 inches for both bearings.

Probes mounted in the shoe and leads to the probes should be done in such a manner as to minimize the roll moment applied to the shoe. Cut-outs in the shoe edges for shaft monitoring probes should be made symmetric about the pivot circle plane.

6.2.11 Operating Conditions with Shaft Vertical

The prime orientation for design is with the shaft vertical. In order to insure a small shaft orbit resulting from transient, unbalance and other dynamical loadings, the preload on the number one (compressor end) bearing is taken as 8 pounds. The shaft radius at the number 1 end is given as 0.750 inches; the radius at the number 2 (turbine end) bearing is given as 1.0625 inches. For both bearings to have the same Λ, the clearances must be different. The shaft mass center is located at about 70% of the bearing span from the number 1 bearing. Because the bearings will have different stiffnesses and because of the location of the shaft mass center, the shaft will tend to run inclined as well as in a conical mode. To limit this motion the preload on the number 2 bearing must be carefully chosen. If the selection were left to the bearing designer, the shaft would have the same bearing diameters on either end and the shaft mass center would be midway between the two bearings.

The spring loaded shoe will have a load coefficient C_{L_3} (shoe no. 3, bearing no. 1) that is determined by the preload

$$C_{L_3} = \frac{W_3}{P_a RL} = \frac{8}{12 \times .75 \times 1.5} = .592 \qquad (12)$$

From Figure 3 for $\phi/\alpha = .65$

$$\varepsilon = 0.68, \quad \xi = 86°$$

From Figure 4:

$$H_{P_3} = .398$$

Let Y be the displacement of the shaft in the reference circle of radius R + C. For vertical operation assume that the pivot circle eccentricity is zero, therefore all shoes have the same pivot film thickness. Shoe 1 has a pivot film thickness given by

$$H_{P_1} = 1 + Y^{(1)} \cos \theta_{P_1} \tag{13}$$

Or

$$.398 = 1 + Y^{(1)} \cos 120°$$

Then

$$Y^{(1)} = \frac{y}{C^{(1)}} = 1.204$$

where $C^{(1)}$ is the ground-in clearance for bearing 1.

At bearing 1:

$$\Lambda = 1.5$$
$$\Omega = 5236 \text{ rad/sec}$$
$$R = 0.75$$
$$P_a = 12 \text{ psig}$$
$$\mu = 4.1 \times 10^{-9} \text{ lb. - sec/in.}^2$$

Therefore

$$C^{(1)} = \left[\frac{6\mu\Omega}{P_a}\right] 1/2 = 2.01 \times 10^{-3} \text{ in. .}$$

At bearing 2:

$$\Lambda = 1.5$$
$$\Omega = 5236 \text{ rad/sec}$$
$$R = 1.0625 \text{ in.}$$
$$P_a = 12 \text{ psig}$$
$$\mu = 4.4 \times 10^{-9} \text{ lb. - sec/in.}^2$$

Therefore

$$C^{(2)} = 2.94 \times 10^{-3} \text{ in.}$$

If the shaft is to have no misalignment then the "y" displacement in both bearings should be the same. Then

$$Y^{(2)} = \frac{y}{C^{(2)}} = Y^{(1)} \frac{C^{(1)}}{C^{(2)}} = .827 \qquad (14)$$

Therefore

$$H_{P_4} = 1 + Y^{(2)} \cos \phi_{P_4}$$

$$H_{P_4} = .586$$

Referring to Figures 4 and 3 and recalling that all shoes have the same pivot film thickness

$$\xi = 68^\circ; \ \varepsilon = 0.61$$

$$C_{L_6} = 0.33$$

the preload on bearing 2 is given by

$$W_6 = C_{L_6} P_a R^{(2)} L^{(2)} = 8.94 \text{ pounds}$$

The operating conditions at bearing 1 for the shaft in the vertical orientation are given as follows:

a. Pivot film thickness

$$h_p^{(1)} = H_p C^{(1)} = .398 \times 2.01 \times 10^{-3}$$

$$h_p^{(1)} = .800 \times 10^{-3} \text{ inches}$$

b. Minimum film thickness

$$h_m^{(1)} = H_m C^{(1)} = .315 \times 2.01 \times 10^{-3}$$

$$h_m^{(1)} = .633 \times 10^{-3} \text{ inches}$$

c. Shoe load

$$W^{(1)} = C_L^{(1)} \times P^a R^{(1)} L^{(1)} = .592 \times 12 \times .75 \times 1.5$$

$$W^{(1)} = 8 \text{ pounds}$$

d. Pivot circle setting C'/C

C' is the difference between the radius of the pivot circle and the radius of the shaft. The clearance for the spring-loaded shoe is given by

$$H_{P_3}^{(1)} = (C'/C)^{(1)} (1 - \varepsilon' \cos \beta)$$

for $\varepsilon' = 0$

$$C'/C^{(1)} = .398$$

e. Friction loss

Figure 10 is a plot of the friction factor F versus pivot film thickness taken from figure 6 at $\phi/\alpha = 0.65$. The total friction power loss for the three shoes is given by

$$F_p^{(1)} = 3 \times F^{(1)} P_a C^{(1)} L^{(1)} R^{(1)} \Omega \qquad (15)$$

$$F_p^{(1)} = 3 \times .995 \times 12 \times 2.01 \times 10^{-3} \times .75 \times 1.5 \times 5236 \times \left(.1129 \frac{\text{watts}}{\text{in\#/sec}}\right)$$

$$F_p^{(1)} = 47.88 \text{ watts}$$

The operating conditions at bearing 2 for the shaft in the vertical orientation are given as follows:

a. Pivot film thickness

$$h_p^{(2)} = H_p^{(2)} C^{(2)} = .586 \times 2.94 \times 10^{-3}$$

$$h_p^{(2)} = 1.723 \times 10^{-3} \text{inches}$$

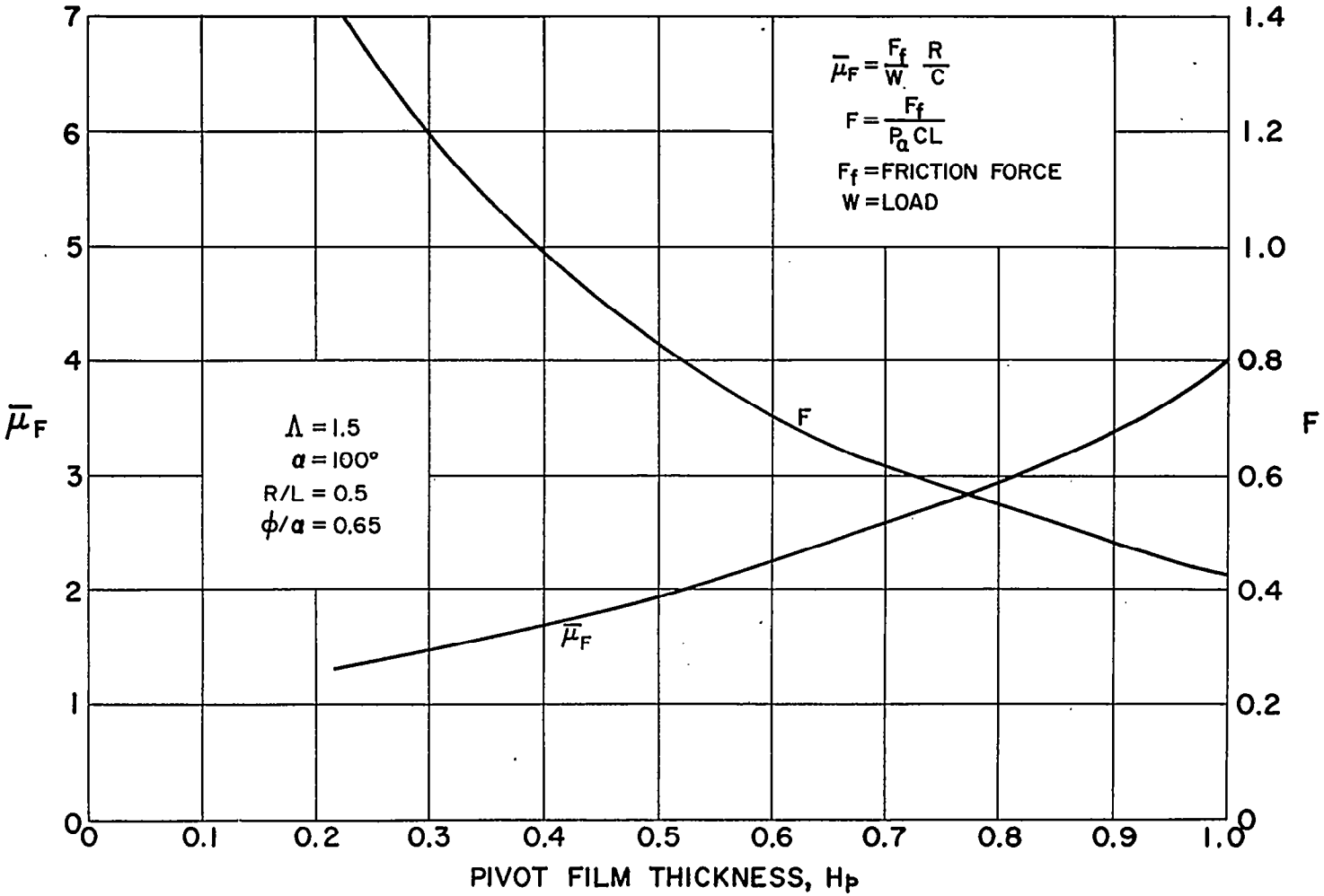

Fig. 10 - Friction Coefficient and Friction Factor vs. Pivot Film Thickness for R/L = 0.5, α = 100°, ϕ/α = 0.65, Λ = 1.5

b. Minimum film thickness

$$h_m^{(2)} = H_m^{(2)} C^{(2)} = .409 \times 2.94 \times 10^{-3}$$

$$h_m^{(2)} = 1.202 \times 10^{-3} \text{inches}$$

c. Shoe load

$$W^{(2)} = 8.94 \text{ pounds}$$

d. Pivot circle setting

$$C'/C^{(2)} = H_p^{(2)} = .586$$

e. Friction loss

$$F_p^{(2)} = 3 \times F^{(2)} \cdot P^a C^{(2)} R^{(2)} L^{(2)} \omega$$

$$= 3 \times .721 \times 12 \times 2.94 \times 10^{-3} \times 1.0625 \times 2.125 \times 5236 \times .1129$$

$$F_p^{(2)} = 101.85 \text{ watts}$$

6.3. System Rigid Body Critical Speeds

The "Lumped Parameter" program is an approximate analysis of the dynamical behavior of the rotor and journal bearing system. It gives a complete description of the rotor motion over a wide range of operating conditions. It indicates the critical speed ranger as well as the approximate threshold. Furthermore, it can produce this information with very little computer running time. This gives it an unique advantage over the "orbit program". However, being an approximate threatment, the lumped parameter program should be used primarily to provide a qualitative picture of the rotor motion and to indicate regions of operation where the "orbit program" should be employed.

The analysis considers a rigid rotor with four degrees of freedom - motions in X and Y directions, and the rotation of shaft in the X-Y and Y-Z planes. The equations of motion are therefore the same as those in the dynamical analysis outlined in Appendix IV. The principle approximation lies in the treatment of forces and moments which represent the bearing characteristics. It is assumed that the force systems acting on the rotor that is produced by the bearing film can be described by four springs, two at each end placed in the X and Y directions respectively. It also takes into consideration damping and unbalance in the formulation. The program then gives the quasi-steady-state solution of this system of four differential equations. To perform the actual calculations, the spring constants and the damping characteristics have to be established from the steady-state field maps. Accuracy of the result is then dependent entirely upon these coefficient. Thus, this program can be used only to give a qualitative description of the rotor motion.

Figure 11 is a cross-plot taken from the field map that shows the load coefficient vs the pivot film thickness. For a given film thickness, the steady-state stiffness is proportional to the slope of Figure 11. The shoe stiffness vs pivot film thickness is plotted on Figure 12. The values obtained from this plot were used in the lumped parameter program to obtain rigid body critical. Since the damping coefficient is difficult to obtain accurately, a range of coefficients that would produce amplification factor between 6 and 12 is used. The amplification factor "AF" is defined as

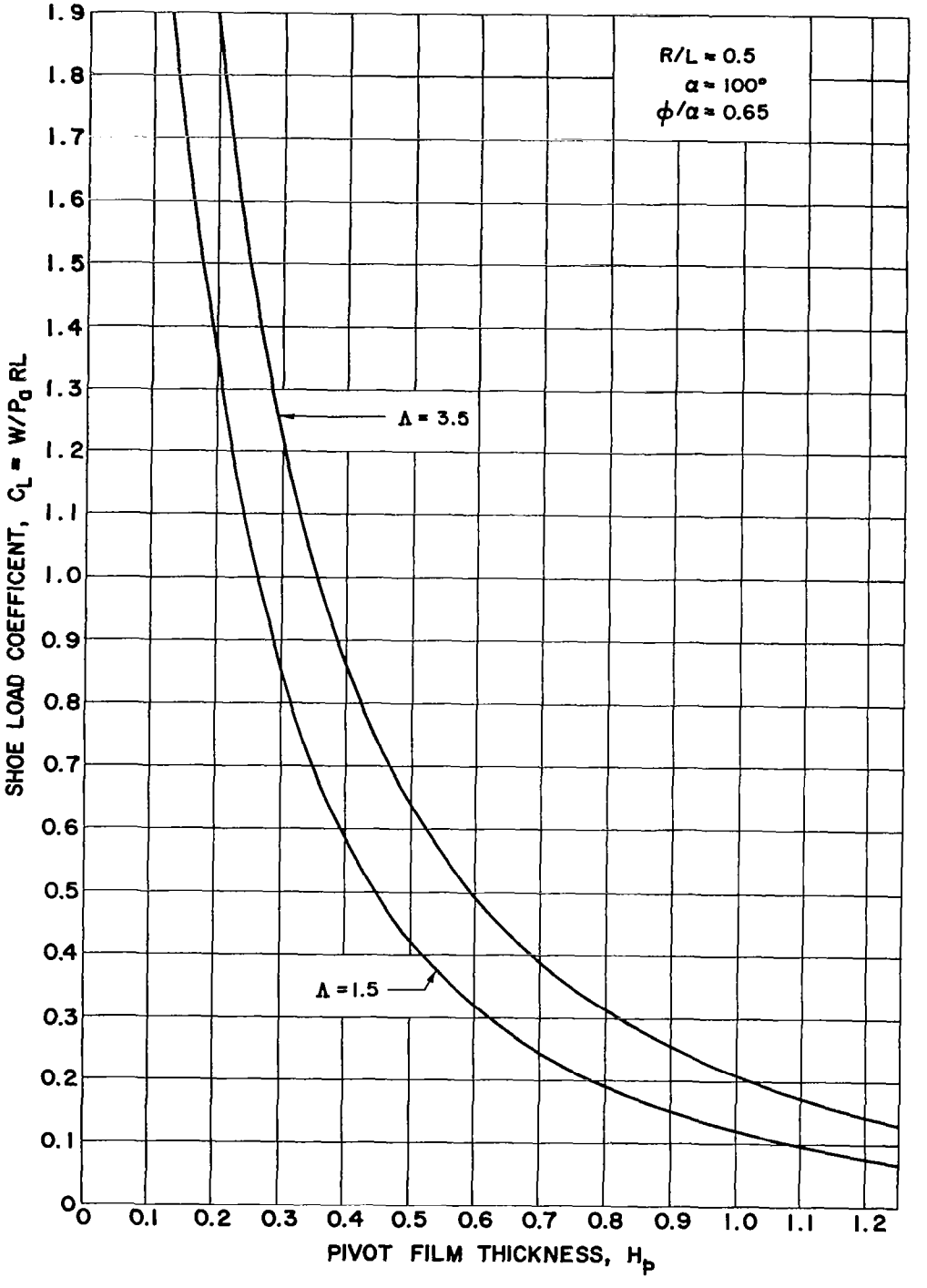

Fig. 11 - Shoe Load Coefficient vs. Pivot Film Thickness for R/L = 0.5, α = 100°, ϕ/α = 0.65, Λ = 15 and 3.5

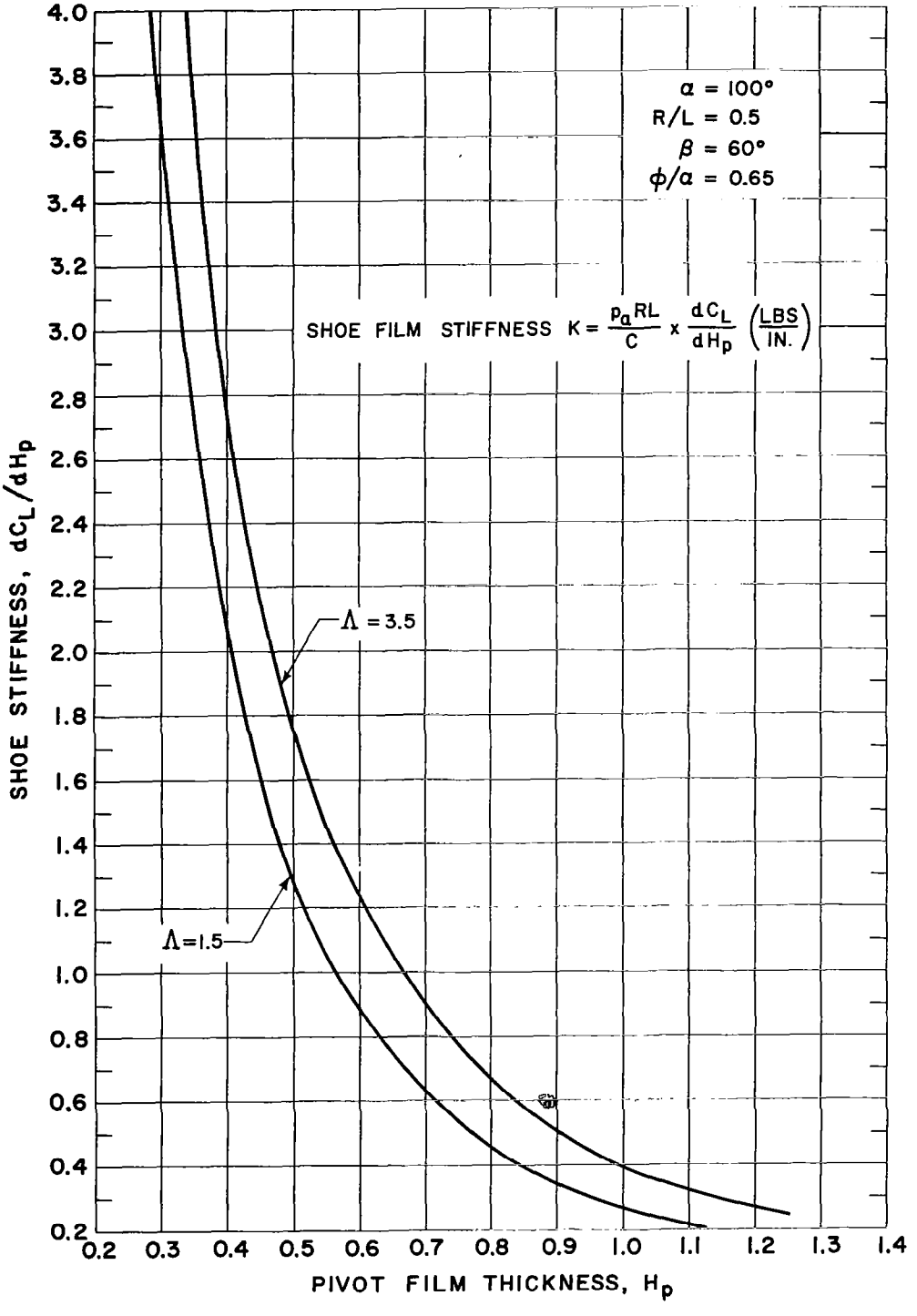

Fig. 12 - Shoe Film Stiffness Factor vs. Pivot Film Thickness (in the Pivot Direction) for R/L = 0.5, α = 100° ϕ/α = 0.65, Λ = 1.5 and 3.5

$$AF = \frac{\omega_{cr}}{C/M} = \frac{\sqrt{K/M}}{C/M} \tag{16}$$

where

ω_{cr} = critical frequency

K = film stiffness

M = mass of shaft

The amplification factors used in constructing Table 3 (which applies to vertical shaft operation) are 6, 8, 10 and 12. The film stiffnesses for the first four cases are the same. They were taken from the Figure 12 for $\Lambda = 1.5$ and they are:

$x_1 = 13{,}700$ lb/in $\qquad x_2 = 7400$ lb/in

$y_1 = 4600$ lb/in $\qquad y_2 = 2500$ lb/in

where the subscript 1 and 2 refer to bearings 1 and 2.

In the fifth case the stiffnesses are taken as a function of shaft speed obtained by plotting lines of constant load on the curve for shoe stiffness vs pivot film thickness for various values of Λ. The damping coefficients used in this case are the same as those for Case 3 in Table 3.

Figure 13 shows the response curve for Case 1. The ordinate is non-dimensionalized by e_μ where

$$e_\mu = \frac{R}{M}\sqrt{m_1^2 + m_2^2 + 2\, m_1 m_2 \cos\beta} \tag{17}$$

and

R = the radius at which the unbalance masses m_1 and m_2 are placed

M = shaft mass

β = the angle between m_1 and m_2

Table 3

SYSTEM RIGID BODY CRITICAL SPEEDS

Case		Bearing 1		Bearing 2	
		x_1	y_1	x_2	y_2
1.	Damp. (lb-sec/in)	3.25	1.87	2.38	1.38
	Freq. (CPM)	12,400	7,160	6,200	3,340
	Amp. (micro inches)	41	42	106	102
2.	Damp. (lb-sec/in)	2.44	1.41	1.79	1.03
	Freq. (CPM)	12,400	7,160	6,200	3,340
	Amp. (micro inches)	54	55	133	132
3.	Damp. (lb-sec/in)	1.95	1.12	1.43	0.83
	Freq. (CPM)	12,400	7,160	6,200	3,340
	Amp. (micro inches)	68	70	156	160
4.	Damp. (lb-sec/in)	1.62	0.94	1.19	0.69
	Freq. (CPM)	12,400	7,160	6,200	3,340
	Amp. (micro inches)	82	83	174	185
5.	Damp. (lb-sec/in)	3.25	1.87	2.38	1.38
	Freq. (CPM)	15,500	9,150	8,360	4,980
	Amp. (micro inches)	84	98	239	250

For all cases in Table 3 $e_\mu = 11.68 \times 10^{-6}$ inches.

Table 3 shows that the rigid body criticals lie between 3300 and 15,500 rpm and that the maximum anticipated critical amplitude is about 250 micro inches.

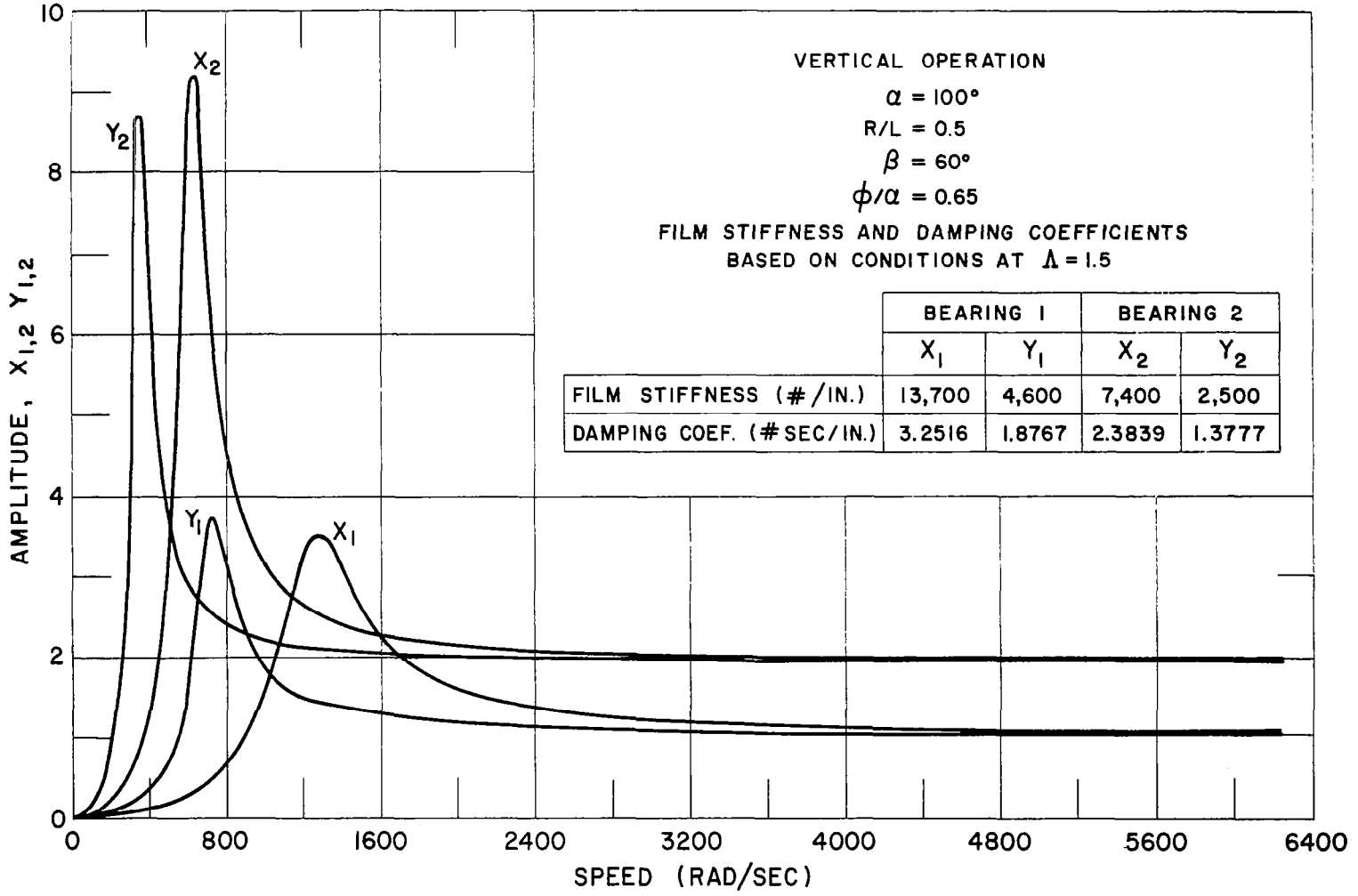

Fig. 13 - Shaft Response at Bearings 1 and 2 vs. Shaft Speed for R/L = 0.5, $\alpha = 100°$, $\phi/\alpha = 0.65$

6.4 Dynamical Analysis

6.4.1 Selection of the Analytical Method

The one dimensional Reynolds equation can be written in the form

$$\frac{\partial}{\partial x}\left(\frac{h^3}{12\mu}\frac{\partial p}{\partial x}\right) = \frac{\partial h}{\partial t} + \frac{\Omega}{2}\frac{\partial h}{\partial x} + h\left\{-\frac{h^2}{12\mu}\frac{\partial p}{\partial x}\frac{\partial (\ell n\ p)}{\partial x} + \frac{\Omega}{2}\frac{\partial (\ell n\ p)}{\partial x} + \frac{\partial (\ell n\ p)}{\partial t}\right. \quad (18)$$

where the terms in the brackets appear if the fluid is compressible.

Let $$h = f\ (x_o,\ y_o)$$

and $$\dot{h} = f\ (\dot{x}_o,\ \dot{y}_o)$$

Also, let the pressure P be given

$$P = P_1 + P_2$$

where P_1 is defined by

$$\frac{\partial}{\partial x}\ \frac{h^3}{12\mu}\frac{\partial P_1}{\partial x}\ = \frac{\Omega}{2}\frac{\partial h}{\partial x}$$

then

$$P_1 = f\ (x,\ x_o,\ y_o)$$

and the force

$$\vec{F}_1 = \vec{f}\ (x_o,\ y_o)$$

P_2 is defined by

$$\frac{\partial}{\partial x}\left(\frac{h^3}{12\mu}\frac{\partial P_2}{\partial x}\right) = \frac{\partial h}{\partial t}$$

then

$$P_2 = \phi\ (x,\ x_o,\ y_o,\ \dot{x}_o,\ \dot{y}_o)$$

and the corresponding force

$$\vec{F}_2 = \vec{\phi}\ (x_o,\ y_o,\ \dot{x}_o,\ \dot{y}_o)$$

or, since $\frac{\partial h}{\partial t}$ is linear in $\dot{x}_o$ $\dot{y}_o$

$$\vec{F}_2 = \vec{\psi}_a (x_o, y_o)\, \dot{x}_o + \vec{\psi}_b (x_o, y_o)\, \dot{y}_o$$

Therefore, for the incompressible case

$$\vec{F} = \vec{f} (x_o, y_o) + \vec{\psi}_a (x_o, y_o)\, \dot{X}_o + \vec{\psi}_b (x_o, y_o)\, \dot{Y}_o$$

The above equation says that for the incompressible case, the film force can be represented by functions that can be thought of as being related to steady-state film stiffness and damping.

But, because of the residual terms in Equation 18, this resolution cannot be made (7,9). These terms introduce a "past history" effect. The mathematics to prove this assertion are not straight forward, but it is easy to show by the following physical illustration that such must be the case:

Consider the shaft concentric in the bearing and then move very slowly to x_o, y_o and then suddenly accelerated to velocity $\dot{x}_o$, $\dot{y}_o$. As the shaft moves, the density will change and ρh will not be constant. Alternatively, move the shaft very rapidly from the concentric position to x_o, y_o and then jump to the same velocity $\dot{x}_o$, $\dot{y}_o$. In the compressible case, the fluid does not have to move out of the way - the density can change, but a sudden motion will tend to keep ρh a constant. Therefore, the two methods of approaching the same x_o, y_o, $\dot{x}_o$, $\dot{y}_o$ result in different density distributions and therefore different pressure distributions so that in the compressible, case it does not matter how the shaft got to a particular point in the bearing. In the incompressible case where the fluid, completely fills the bearing, the condition of the fluid is known once the x_o, y_o, $\dot{x}_o$ and $\dot{y}_o$ are known. This is certainly not true for the compressible case - the "past history" terms of the Reynolds equation must be taken into account.

A sound approach to the dynamical problem is to couple the Reynolds equation with the equations of motion for all the degrees of freedom and to trace these motions in time starting from an arbitrary set of initial conditions. This type of approach is generally referred to as an "orbit" analysis and is the method that has been selected to do the dynamic studies for this program.

6.4.2 Dynamical Equations

The dynamics of the shaft and the shoes are examined in detail in Appendix IV. The equations for the shaft motion are given as two translation equations for the coordinates of the shaft mass center (x_m and y_m) and two rotational coordinates (α_1 and α_2) for the rigid shaft. These equations are summarized as follows:

$$m \ddot{x} = \sum_{n=1}^{6} \iint p \sin\theta \, R \, d\theta \, dz - |\vec{F}_u| \sin(\Omega t) \tag{19}$$

$$m \ddot{y} = \sum_{n=1}^{6} \iint p \cos\theta \, R \, d\theta \, dz - |\vec{F}_u| \cos(\Omega t) + W_y \tag{20}$$

$$I_T \ddot{\alpha}_1 - I_p \Omega \dot{\alpha}_2 = \sum_{n=1}^{6} z \, p \sin\theta \, R \, d\theta \, dz - |\vec{M}_u| \cos(\Omega t + \psi_u) \tag{21}$$

$$I_T \ddot{\alpha}_2 + I_p \Omega \dot{\alpha}_1 = \sum_{n=1}^{6} z \, p \cos\theta \, R \, d\theta \, dz + |\vec{M}_u| \sin(\Omega t + \psi_u) \tag{22}$$

where

$|\vec{F}_u|$ is the magnitude of the unbalance force

and

$|\vec{M}_u|$ is the magnitude of the unbalance moment.

The first two equations express the relation between the acceleration and the forces on the shaft mass center. The forces consist of the sum of the film forces of the six shoes, plus the shaft unbalance force, plus a gravitational force. The second two equations express the relation between angular acceleration

of the shaft about the mass centers and the sum of the gyroscopic moment, the moment due to the six bearing film pressures and the shaft unbalance moment.

The shoe dynamics are summarized as follows:

$$M_{shoe}\,\rho_{G2}\,\ddot{C}' + I_p\,\ddot{\delta} = R^2 \iint p \sin(\theta - \theta_p)\left|1 + \frac{d}{R}\right| d\theta\, d\eta + M_f \qquad (23)$$

$$I_R\,\ddot{\gamma} = R \iint p \cos(\theta - \theta_p)(\eta - \eta_B)\, d\theta\, d\eta + M_f \qquad (24)$$

$$M_{shoe}\,(\ddot{C}' + \rho_{G2}\,\ddot{\delta}) = R \iint p \cos(\theta - \theta_p)\, d\theta\, d\eta - F_p - k\,C' \qquad (25)$$

Equation 23 is the expression to be solved for determining the pitch angle (δ) of the shoe. The first term on the left accounts for the pitching moment that would exist on a spring loaded shoe that is translating with acceleration $\ddot{C}'$ and has its mass center located at distance ρ_{G2} from the pivot point. If the shoe has its mass center at the pivot, or, if the shoe had a fixed pivot, this term would be zero. In the present case, $\ddot{C}'$ is of the same order as $\ddot{\delta}$ during the transient and $M_{shoe}\,\rho_{G2}$ is of the same order as I_p, therefore the pitch of the spring loaded shoe would be significantly influenced by any squeeze film oscillation that might take place. The first term on the right represents the moment of the film pressures about the pivot point which is located at radial distance "d" from the face of the shoe. M_f is the pivot friction moment which is zero when $\dot{\delta}$ is zero, minus when $\dot{\delta} < 0$ and plus when $\dot{\delta} > 0$. If M_f is equal to or greater than the sum of the other two moments in Equation 23 then δ = constant.

Equation 24 is the roll equation and is similar to Equation 23. The difference between the two equations is that the mass center of the bearing is assumed to be in the plane of the pivot circle therefore no coupling with the shoe translation exists. Any attachment made to the shoe (or cut-out from the shoe) that causes the mass center to be shifted from the pivot circle plane would be detramental to the roll motion of the shoe since the roll film stiffness to restrain this motion is small compared to the pitch stiffness.

Equation 25 is the expression which governs the translation of the spring loaded shoes. The first two terms on the left represent the cross-coupling that exists between the translation C' and the pitch δ when the shoe mass center is not at the pivot. The first term on the right is the force resulting from the film pressures. The second term is the force of the spring preload. It is this force which is principly responsible for producing the bearing stiffness. The third term is the force that arises when the preload spring, with stiffness "k" is displaced on amount C'.

The bearing film pressures are obtained by writing the Reynolds equation

$$\vec{\nabla} \cdot (H^3 P \vec{\nabla} P) = \Lambda \frac{\partial PH}{\partial \theta} + \frac{\partial PH}{\partial T} \tag{26}$$

in the time-discretized model

$$\nabla^2 \psi^{(n+1)} - \frac{\Lambda \psi^{(n+1)}}{\psi^{(n)} H^{(n)} \Delta T} = \frac{\Lambda \psi^{(n)}}{\psi^{(n)} H^{(n)} \Delta T} + F(\psi^{(n)}, H^{(n)}) \tag{27}$$

where

$$F = \frac{\Lambda \psi_\theta}{\psi H} - \frac{(\nabla\psi)^2}{\psi} + \frac{\nabla\psi \nabla H}{H} + \frac{\psi \nabla^2 H}{H}$$

$$\psi = PH$$

and (n) and (n+1) represent the n-th and the (n+1) the time intervals. Equation 27 is integrated at each time step in a column-wise implicit method which is outlined in Reference (20).

The final equation necessary for the dynamical analysis is the expression which relates the bearing film clearance to all the degrees of freedom that exist between the shoes and the shaft. This relation is given as

$$h = C + (x_m + \alpha_1 z) \sin\theta + (y_m + \alpha_2 z) \cos\theta + (d + R)\delta \sin\varphi + [(C' - C) + (z - z_B)\gamma] \cos\varphi \tag{28}$$

6.4.3 The Nonlinear Orbit Program

In order to determine the dynamic response of the bearing system, the equations of motion summarized in the previous section must be solved. For the case being considered they comprise a set of 18 equations, one for each degree of freedom. Since these equations are couples through the film pressure, this set has to be solved in conjunction with the diffusion equation 27. This is accomplished by the "Orbit Program", in which the complete nonlinear equations pertinent to the problem are integrated in small time steps by numerical methods[7]. The integration procedures are as follows:

Step 1: Set initial conditions of all degrees of freedom and ψ-distributions for all shoes.

Step 2: Do steps 3 through 6 for each shoe.

Step 3: Compute clearance distribution and all necessary spatial derivatives. Also check for failure (negative clearance).

Step 4: Integrate pressures to obtain force and torque terms on right hand side of shoe pitch, roll, and translation Equations 23,24,25, and contributions to right hand sides of shaft dynamics Equations 19 through 22.

Step 5: Integrate shoe dynamics equations through one time interval.

Step 6: Integrate diffusion Equation 27 through one time interval.

Step 7: Sum shoe contributions to total shaft forces and moments.

Step 8: Integrate shaft dynamics equations through one time interval.

Step 9: Has integration proceeded to desired limit? If not, go back to step 2.

Step 10: Print and plot output; terminate.

6.4.4 Validation of Nonlinear Orbit Program

The Nonlinear Orbit Program is a theoretical analysis of the behavior of a system consisting of a rigid rotor and two journal bearings with three pivoted pads each. One pad of each bearing is preloaded by a compressed spring; shaft axial motion is neglected and the shoe yaw mode is also neglected. The equations of motion for the resulting eighteen degrees of freedom of the system are solved together with the time dependent Reynolds equation for each shoe by a numerical process which integrates forward in time until a stationary periodic motion is achieved.

The check of the accuracy of this approach is taken in two parts - a steady-state comparison and an experimental comparison. Both comparisons are made using the data obtained from and for the experimental gas bearing SA-2 test rig built at FIRL under AEC Contract No. AT(30-1)-2512.

6.4.4.1 Steady-State Comparison

This check is made using the appropriate field maps obtained from Reference(19). These curves were obtained analytically by a numerical solution of the steady-state Reynolds equations. The comparison of the steady-state data with the dynamics program is shown in Table 4. The excellent agreement implies that the dynamics equations are written and solved in a manner that is capable of producing the steady-state operating condition-should one exist. The actual computations are shown in Appendix V of this report. A comparison between the steady-state predictions for leading and trailing edge film thicknesses and experimentally obtained measurements is shown on Figure 14.

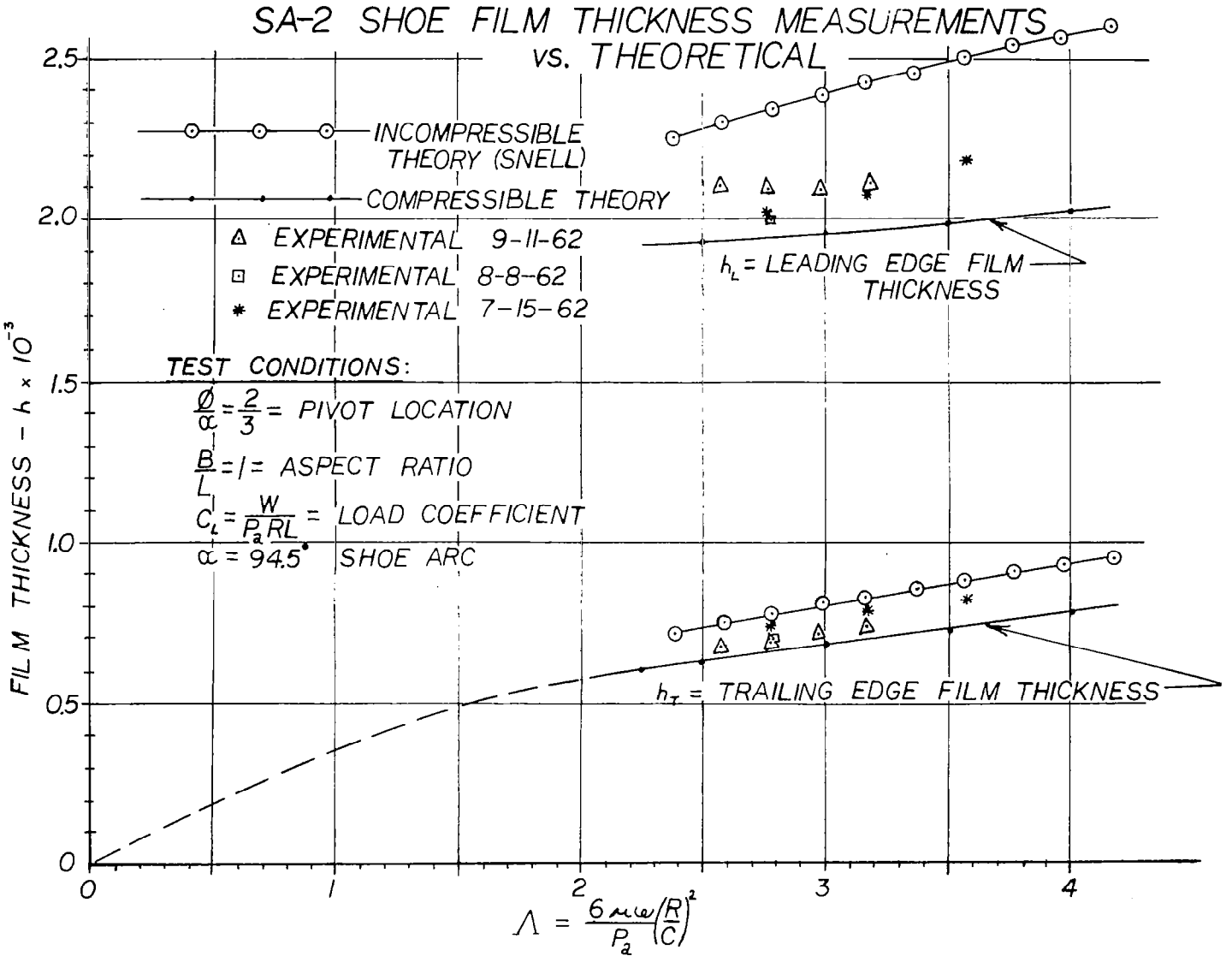

Fig. 14 - Comparison Between Measured and Computed Values of Tilting Pad Film Thickness

Table 4

VALIDATION OF THE TIME-TRANSIENT DYNAMICS PROGRAM

Steady-State Comparison

	Dynamics Program	Steady-State	% Difference
Pivot Film Thickness - shoe 1, 2	0.378	0.38	1/2
Pivot Film Thickness - shoe 3	0.537	0.52	3
Shoe Lead Angle - shoe 1, 2	89.2°	90°	1
Shoe Eccentricity ε - shoe 1, 2	0.69	0.7	1
Shoe Lead Angle - shoe 3	76.1°	77°	1
Shoe Eccentricity ε - shoe 3	0.61	0.63	3
Pivot Circle Preload C'/C	0.431	0.435	1
Pivot Circle Eccentricity ε'	0.176	0.195	10

6.4.4.2 Experimental Comaprison

The experimental run used in this phase of the comparison was made on 4-7-64 for a journal bearing system which is similar to that designed by FIRL for the turbine-compressor. In this run, two capcitance probes measured absolute X-Y shaft motion in the same plane. A third probe measured the absolute motion of a fixed shoe; a fourth probe measured the absolute motion of a spring loaded shoe. Both shoe probes looked at buttons corner mounted along the leading edge.

In formulating the physical data for the dynamic following items had to be approximated:

a) The unbalance force was estimated to be 340 miligrams with an uncertainty of $\pm$ 100 milligrams. The effect of the unbalance force is to change the orbit amplitude.

b) The estimate of the unbalance moment .002 in-lb could be in error up to 15%. The effect of the unbalance moment is to change the amount of conical motion in the shaft orbit.

c) The machined-in clearance C was taken as 1.5 mils. Due to hand lapping, thermal expansion etc., this figure could be in error by $\pm$ 0.2 mils. The effect of this error would be to change Λ and thereby alter the shaft pivot circle eccentricity. This would result in a phase change in the shaft orbit due to an apparent change in the ratio of the vertical to horizontal film stiffness.

d) The oscilloscope sweep rate used in determining the shoe motions had an error of 3%. The sweep rate for the X-Y probes had an error of 10%.

e) Other secondary quantitites adding to the errors in determining the prevailing conditions during the experimental test run were the shaft speed, the shaft radius, and the ambient pressure.

Table 5 shows the comparison between the analysis and the experimental data. A_A is the amplitude of a fixed shoe, A_B is the amplitude of a spring loaded shoe. X and Y are the amplitudes of the shaft motions in the plane of the probe station.

Plots of the computed and experimental motions of the various degrees of freedom are given in Appendix V; the computations made in forming the table of this section are also included in Appendix V.

To within the known accuracy of the actual experimental operating conditions, the capability of the dynamics program to mimic the experiment is considered good.

Table 5

DYNAMIC COMPARISON BETWEEN COMPUTED AND EXPERIMENTAL PROBE MEASUREMENTS - SA-2 RIG

	A_A		A_B		X		Y	
	Analytic	Experimental	Analytic	Experimental	Analytic	Experimental	Analytic	Experimental
Amplitude μ in.	245	200	147	280	120	110	60	180
Frequency rpm	15000	15000	15000	15000	15000	13700	15000	14000

6.4.5 Nonlinear Orbit Results

The nonlinear orbit analysis is used to analyze two cases. The first, called the base case, represents the final design as determined by steady-state considerations with zero pivot friction moment. The second, case 2, represents the final design with a high pivot friction moment.

The plots in this section were made using a General Dynamics SC4020.

6.4.5.1 Base Case - Design Point

The design specifications on which this case is based are:

1. Shaft Parameters

Design Speed	50,000 rpm
Static Load	0.0 lb. (vertical shaft)
Diameter at bearing 1	1.500 in.
Diameter at bearing 2	2.125 in.
Distance from shaft mass to	
Bearing 1	+7.04 in.
Bearing 2	-2.96 in.
Plane of Turbine	-6.08 in.
Polar Moment	0.030 in-lb/sec^2
Transverse Moment	0.60 in-lb/sec^2
Unbalance Force	2.22 lb.
Unbalance Moment (about C.G.)	12.32 in-lb.
Phase Angle between unbalance force and moment	90°

2. Shoe Parameters

	Bearing 1	Bearing 2	Units
Ambient Pressure	12	12	psia
Wrap Angle	100	100	degrees
Width (axially)	1.500	2.125	in.
R/L	0.5	0.5	--
Weight	0.118	0.236	lb.
Moment of Inertia*			
Pitch	0.66×10^{-4}	2.39×10^{-4}	$in\text{-}lb/sec^2$
Roll	0.67×10^{-4}	2.58×10^{-4}	$in\text{-}lb/sec^2$
Machined in Clearance	0.0020	0.0029	in.
Pivot Friction Moment	0.0	0.0	in-lb
Pivot Distance from face of shoe	0.094	0.094	in.
Pivot Location (ϕ/α)	0.65	0.65	--
Preload Spring Constant	80.4	80.4	lb per in.
Preload	8	9	lb.
Lub Viscosity	3.6×10^{-9}	4.1×10^{-9}	$lb\text{-}sec/in^2$

*The calculation for moments of inertia can be found in Appendix VI.

The unbalance force is computed by assuming a 0.0005 in-oz unbalance in the plane of the turbine.

3. Discussion of Results

The pitches of the shoes of bearing 1 (Fig. 15) are seen to have a once-per-rev frequency. A shoe numbering convention is adopted so that the shoes of bearing 1 are numbered 1,2,3 in the direction of rotation with shoe 1 being the first "fixed" shoe after the spring loaded shoe; shoes of bearing 2 are likewise numbered 4,5,6. The "peak to peak" pitch angles "δ_i" are gotten from the non-dimensional plots (Figs. 15, 16).

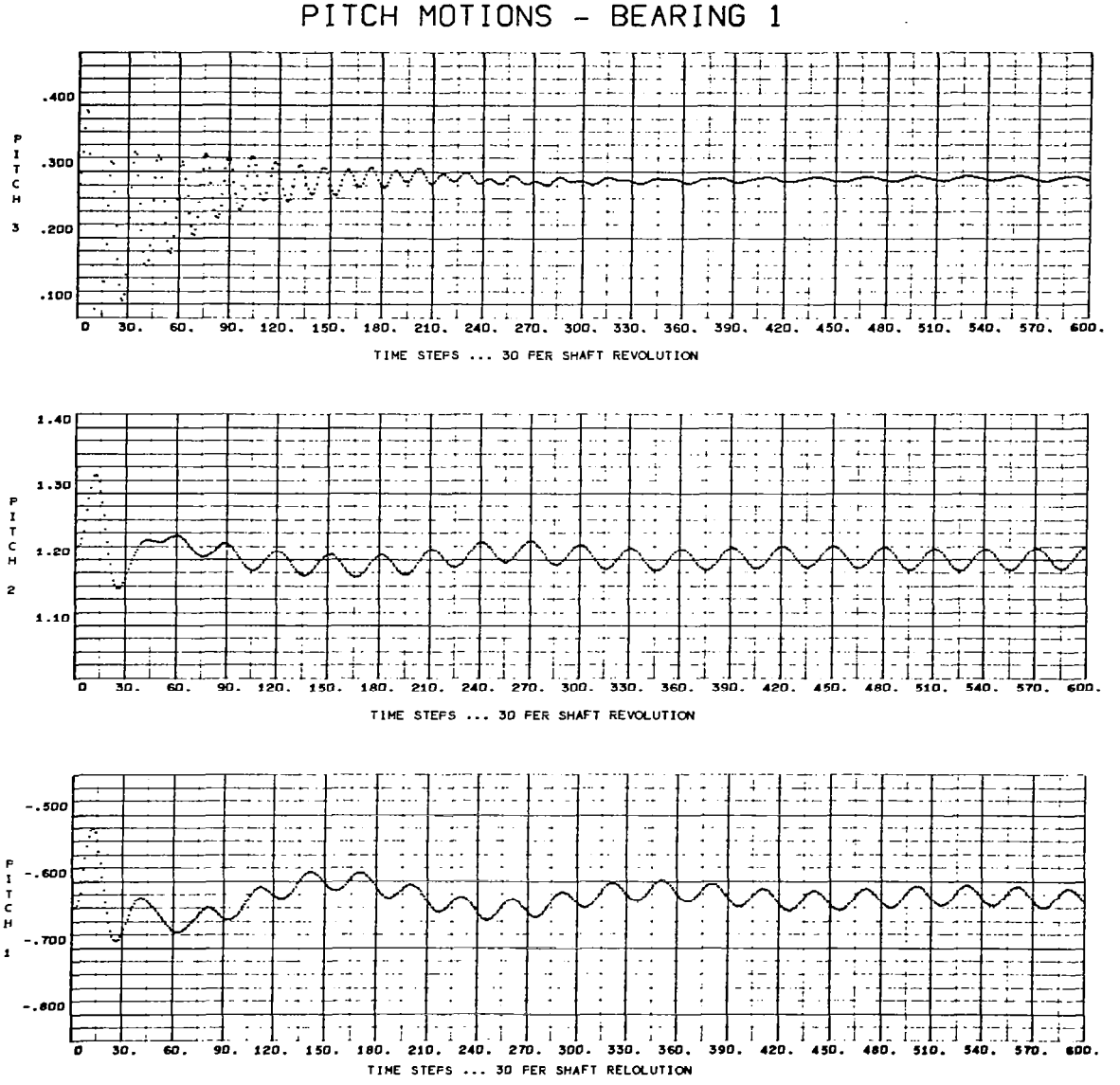

Fig. 15 - Base Case - Non-Dimensional Pitch Amplitudes $\frac{\delta R^{(1)}}{C^{(1)}}$ vs. Time for the Three Shoes of Bearing 1

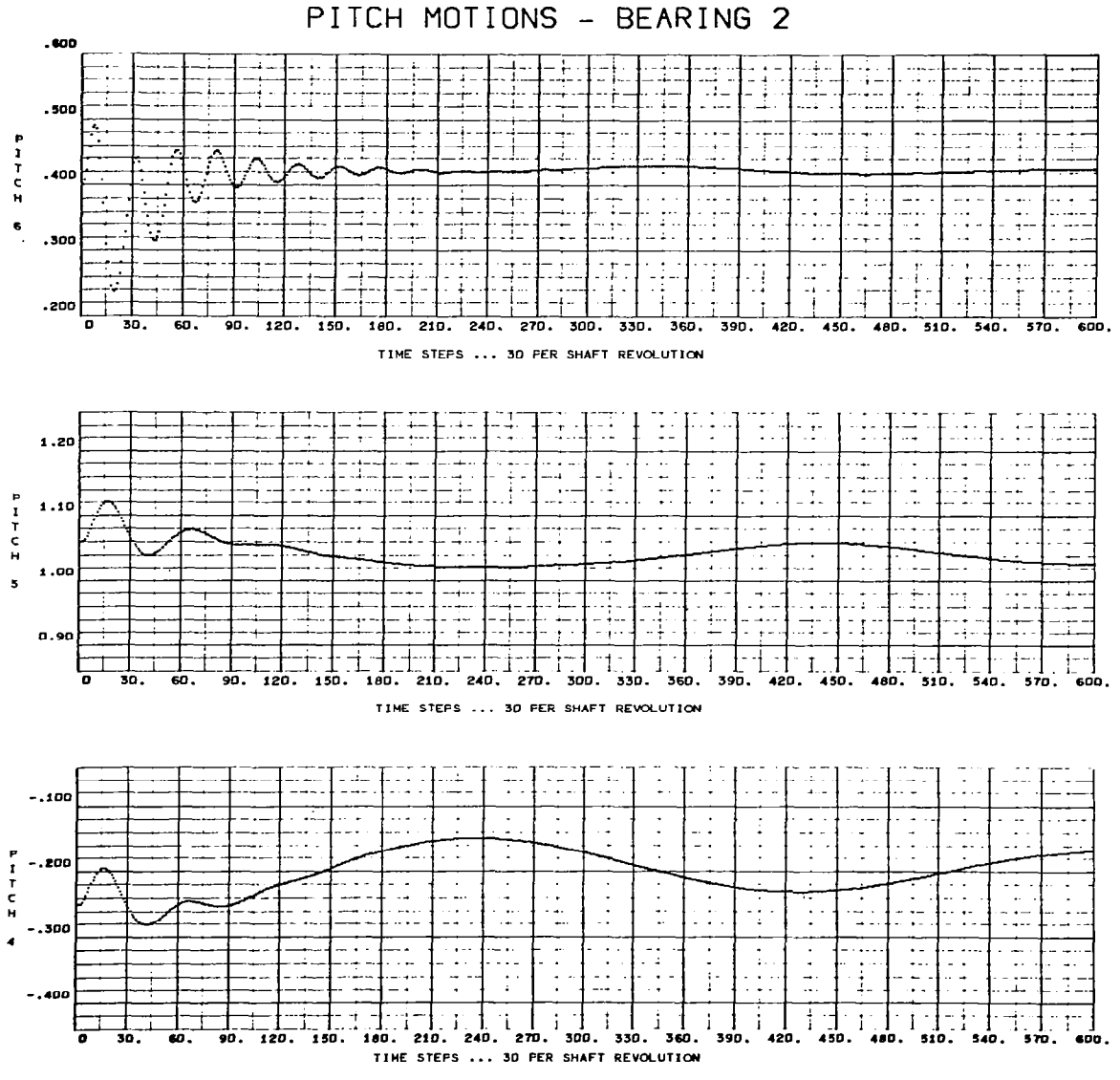

Fig. 16 - Base Case - Non-Dimensional Pitch Amplitudes $\frac{\delta R^{(1)}}{C^{(1)}}$ vs. Time for the Three Shoes of Bearing 2

The non-dimensional pitch angle of the i^{th} shoe is

$$\text{Pitch "i"} = \Delta_i = \delta_i \frac{R^{(1)}}{C^{(1)}} \quad i = 1, 3 \qquad \text{(Brg. 1)} \qquad (29)$$

$$\text{Pitch "i"} = \Delta_i = \delta_i \frac{R^{(2)}}{C^{(2)}} \quad i = 3,6 \qquad \text{(Brg. 2)}$$

The peak to peak pitch angle of shoe 1 is gotten by observing that the lower graph on Figure 15 (ordinate called Pitch 1) shows an amplitude excursion of approximately 0.032. Therefore, the pitch amplitude is

$$\delta_i = \Delta_i \frac{C^{(1)}}{R^{(1)}} = 0.032 \times \frac{0.002}{0.75} = 8.53 \times 10^{-5} \text{ radians}$$

For the shoes of bearing 1, the distance from the pivot point to the shoe leading edge is 0.806 inches, therefore the shoe leading edge will translate

$$\bar{d}_1 = l_1 \delta_1 = 0.806 \times 8.53 \times 10^{-5} \qquad (30)$$

$$\bar{d}_1 = 69 \text{ micro inches}$$

Shoe 2 has the same characteristics as shoe 1 except that the pitch motion is 120° out of phase with shoe 1.

Shoe 3, the spring loaded shoe, shows a transient twice-per-rev tendency which is seen to damp out after about 10 shaft revolutions. During the twice-per-rev period the pivot film thickness is also oscillating at about twice per-rev which gives the appearance of squeeze film vibration triggered by the fact that the initial conditions used in the program did not exactly put the spring loaded shoe in equilibrium with the shaft. After the first 10 revolutions, the pitching motion of shoe 3 damps to an anplitude of approximately 1/3 of that of shoes 1 or 2. Since the analysis

does not account for the fact that there may be a friction force restraining the free motion of the spring loaded pivot pin, it is possible that the transient twice-per-rev could be sustained with a constant amplitude.

The pitching motions of shoes 4,5,6 of bearing 2 are completely different from those of bearing 1. The frequency of shoe 4 is approximately 1/12 of the running speed or about 4170 cpm and the pitch angle is:

$$\delta_4 = \frac{\Delta_4 \, C^{(2)}}{R^{(2)}} = \frac{0.07 \times 2.94 \times 10^{-3}}{1.0625} = 19.4 \times 10^{-5} \text{ radians}$$

which is more than twice as great as the pitch of shoe 1.

The leading edge translation is

$$\bar{d}_4 = l_2 \, \delta_4 = 1.142 \times 19.4 \times 10^{-5}$$

$$\bar{d}_4 = 225 \text{ micro inches}$$

Figures 17 and 18 show the rolling motions of the shoes. The RMS roll angles of shoes 1, 3, 4 and 6 give the indication that the shaft is running skewed in the bearings. The roll angle for the i^{th} shoe is given by

$$\gamma_i = \Gamma_i \frac{C^{(1)}}{L^{(1)}} \qquad i = 1, 3 \qquad \text{(Brg. 1)} \qquad (31)$$

and

$$\gamma_i = \Gamma_i \frac{C^{(2)}}{L^{(2)}} \qquad i = 3, 6 \qquad \text{(Brg. 2)}$$

From Figure 17, for shoe 1 the peak to peak excursion in Γ is about 0.018 and

$$\gamma_1 = \frac{0.018 \times 0.002}{1.5} = 2.4 \times 10^{-5} \text{ radians}$$

The axial edge of the shoe would translate

$$\bar{e}_1 = \frac{L^{(1)}}{2} \gamma_1 = 0.75 \times 2.4 \times 10^{-5} \qquad (32)$$

$$\bar{e}_1 = 18 \text{ micro inches}$$

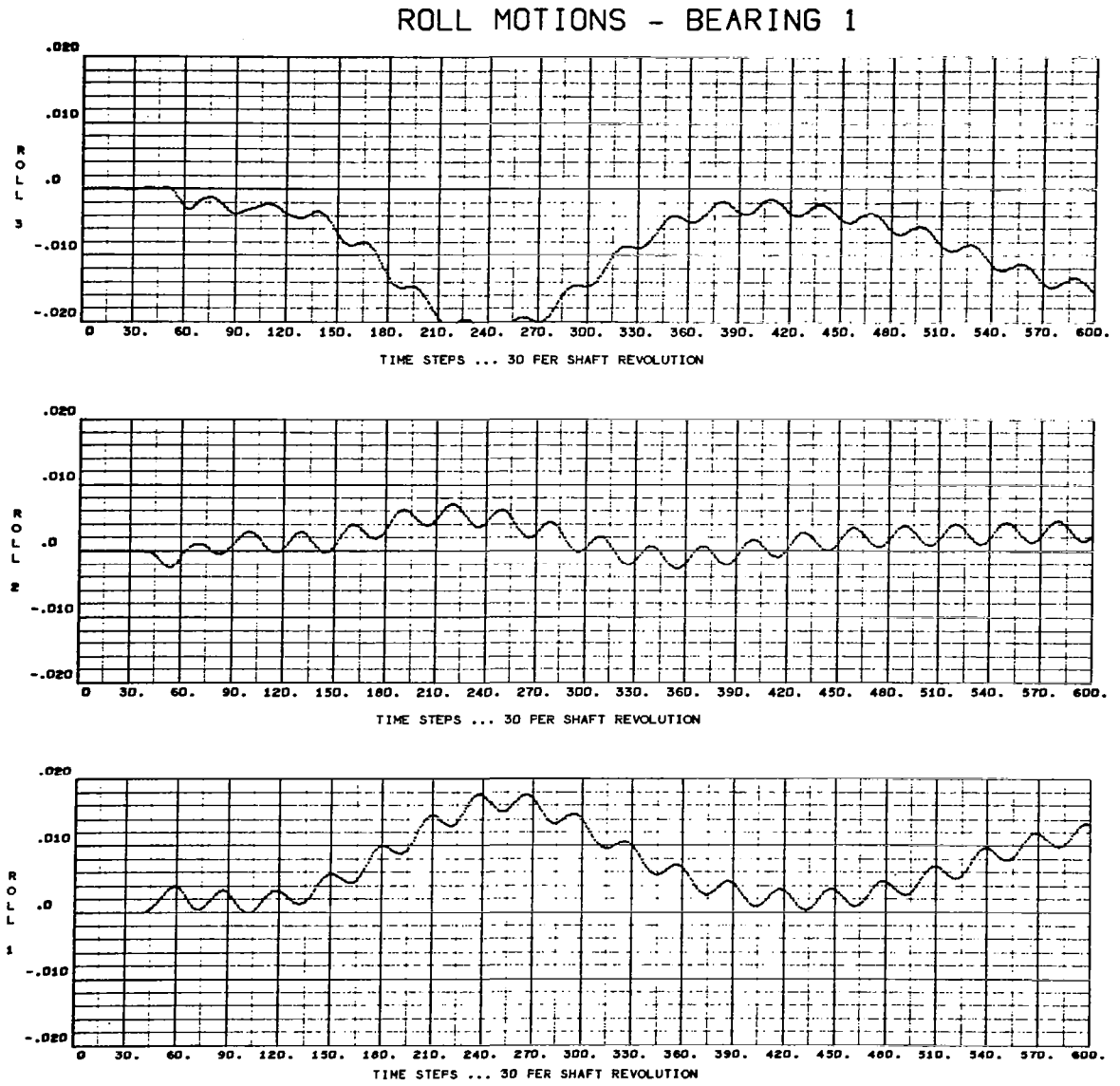

Fig. 17 - Base Case - Non-Dimensional Roll Amplitudes $\left(\frac{\gamma_L^{(1)}}{C^{(1)}}\right)$ vs. Time for the Three Shoes of Bearing 1

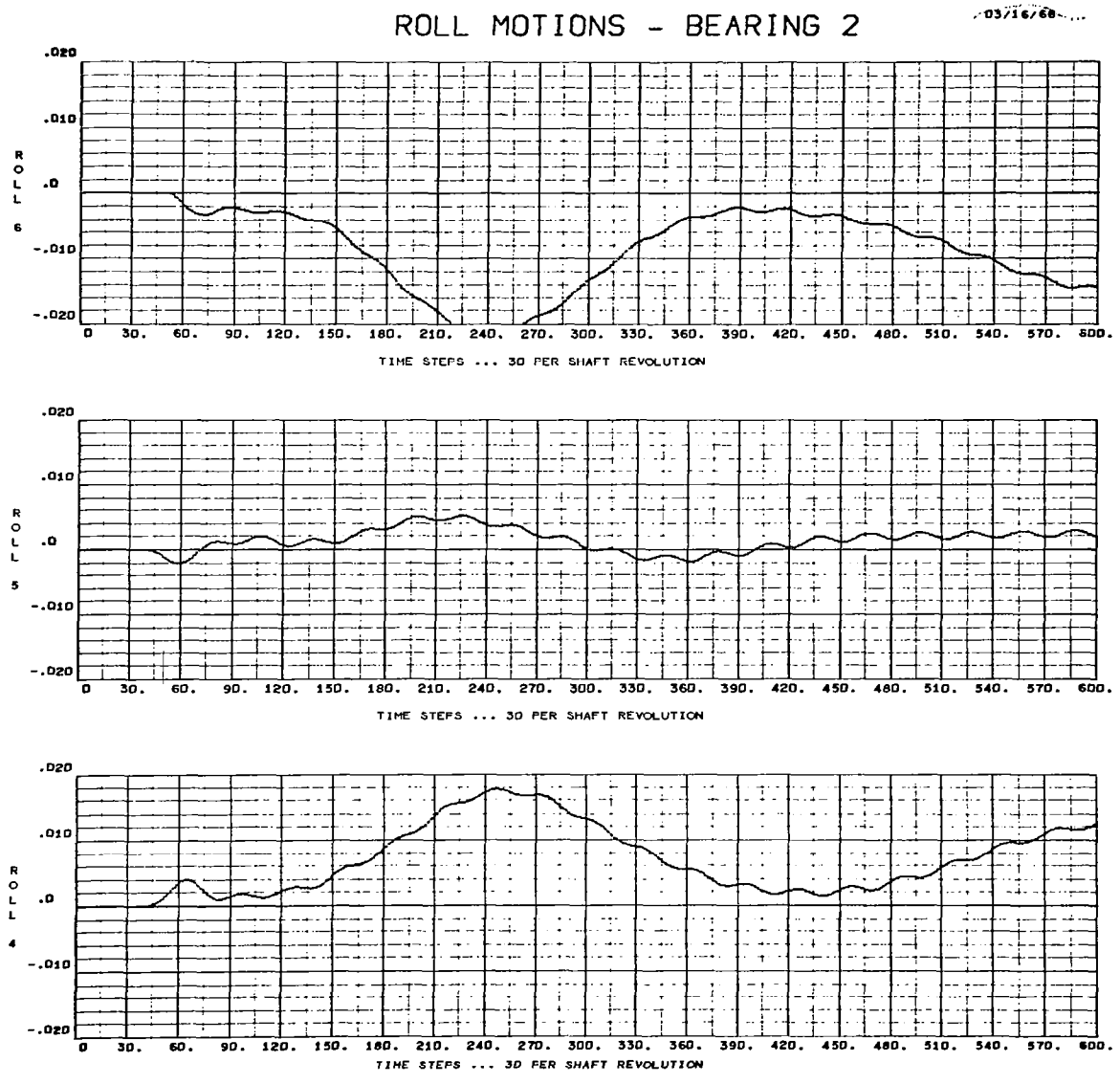

Fig. 18 - Base Case - Non-Dimensional Roll Amplitudes $\left(\frac{\gamma_L^{(1)}}{C^{(1)}}\right)$ vs. Time for the Three Shoes of Bearing 2

As is usually the case, the angular motion of the shoe in roll is small compared to the pitch motion. The yaw motion of the shoe is not computed in the analysis but expected to have an amplitude somewhat smaller than the roll amplitude.

There are two frequencies noticeable from Figures 17 and 18; one is the once-per-rev which is more pronounced in bearing 1, and the other is again about 1/12 of the shaft speed.

From Figure 19 it is seen that the spring loaded pivot of bearing 2 translates with a frequency of about 4000 cpm while the corresponding pivot of bearing 1 translates very little. This implies that bearing 1 is near the center of oscillation for the shaft motion. The amplitude of translation is given by

$$C_p = (C'/C - 1) = 0.075 \qquad (33)$$

$$C' = 150 \text{ micro inches}$$

(C_p is a displacement and the "minus" direction for C_p is a translation towards the shaft).

Figure 20 shows the peak to peak "x" translation of the shaft mass center as

$$x = X\, C^{(1)} = 0.014 \times 0.002 = 28 \text{ micro inches}$$

and the "y" translation as

$$y = Y\, C^{(1)} = 0.075 \times 0.002 = 150 \text{ micro inches}$$

The nominal 4000 cpm "y" motion of the shaft is coupled strongly to the translation of shoe 6 and the pitch motions of bearing 2. The "x" motion shows the distinct once-per-rev frequency of the pitches of bearing 1 and also an envelope of lower order harmonics that are a consequence of the film force since the only other term in the "x" equation is the once-per-rev unbalance force.

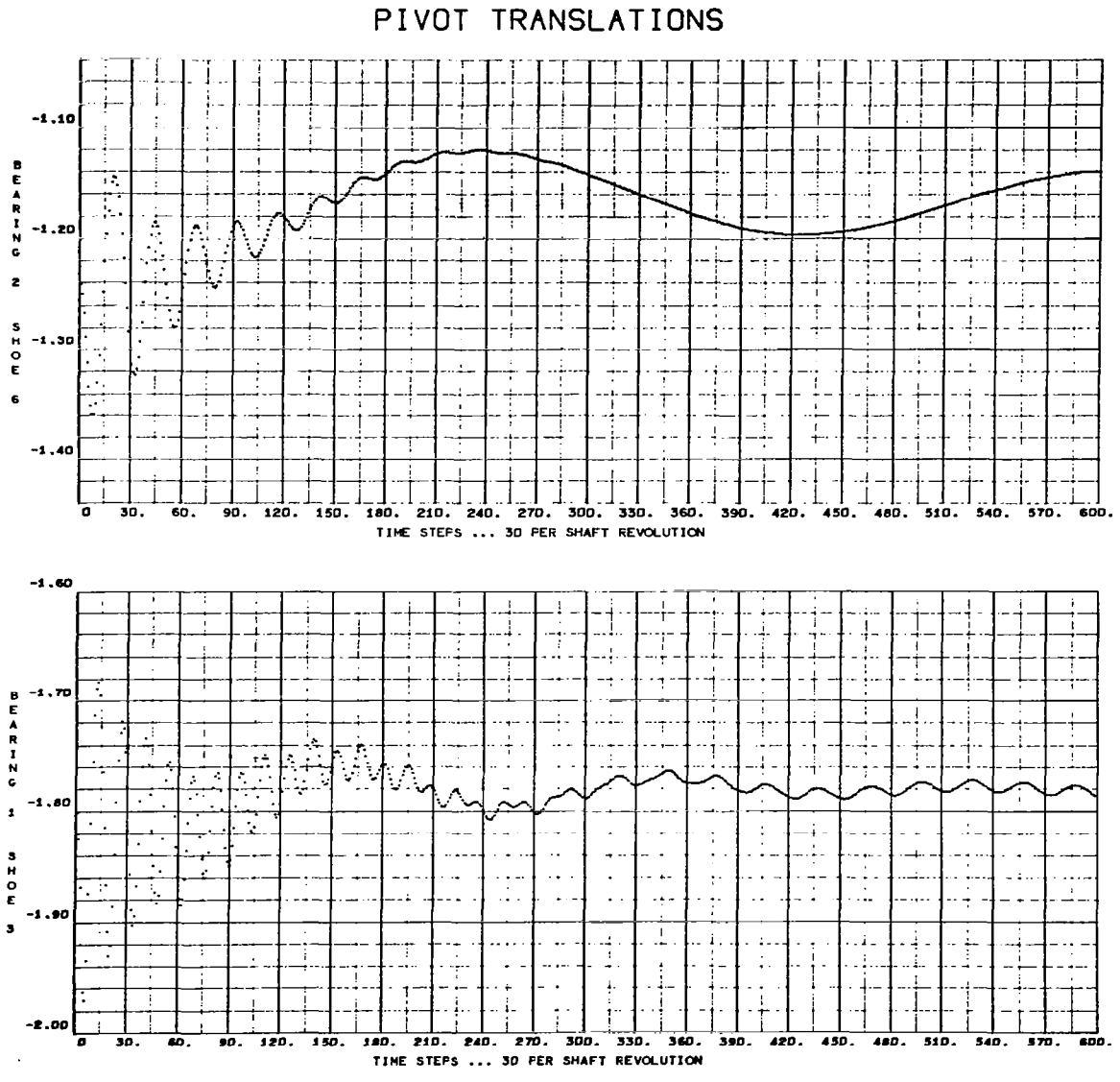

Fig. 19 - Base Case - Non-Dimensional Pivot Translation $\left(\frac{C'}{C} - 1\right)$ vs. Time for Shoes 3 and 6

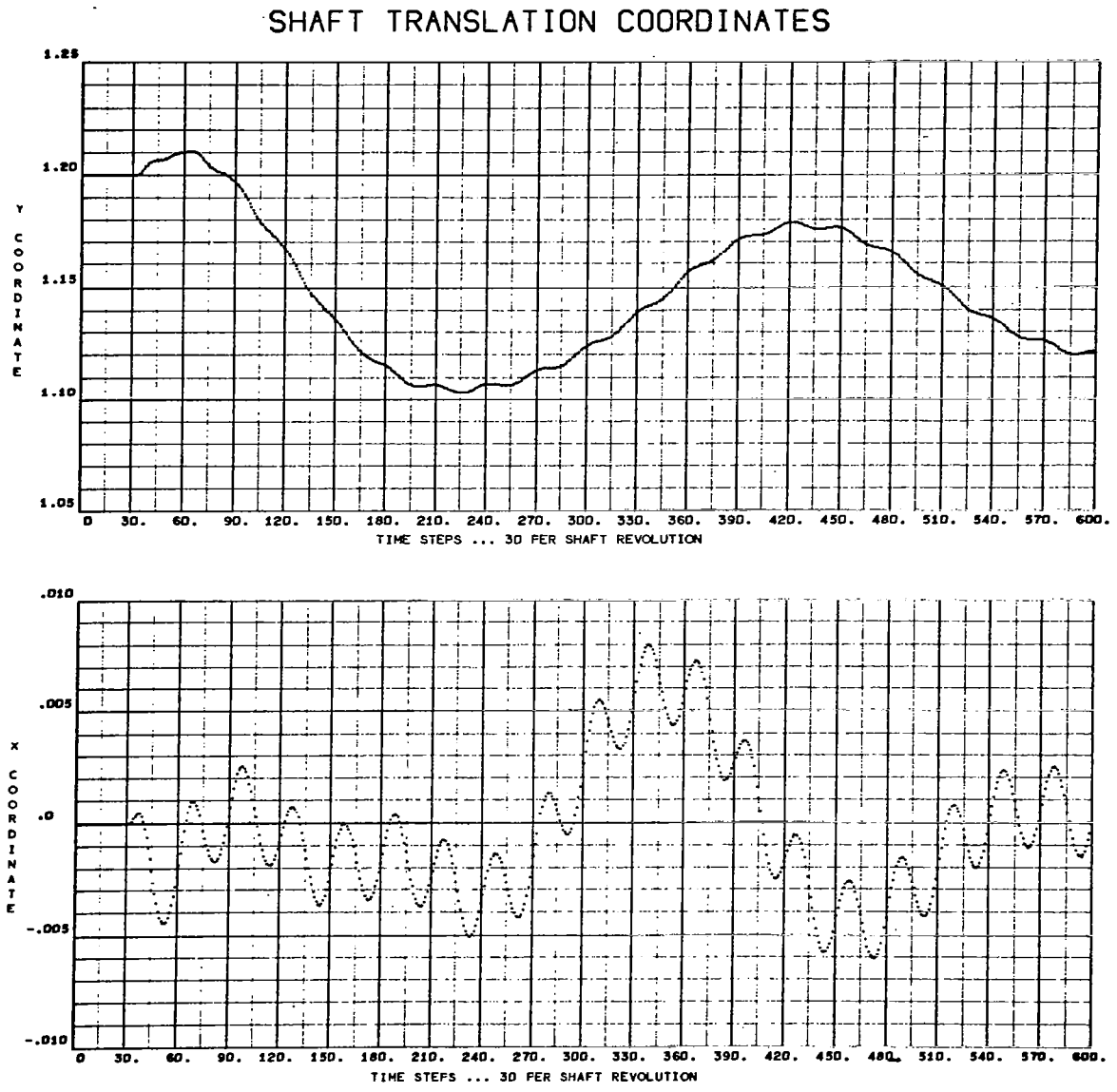

Fig. 20 - Base Case - Non-Dimensional Shaft Mass Center Coordinates $\frac{x}{c^{(1)}}$, $\frac{y}{c^{(1)}}$ vs. Time

The vector combination of "x" and "y" result in the "orbit" plot of Figure 21. After the transient has dissipated the orbit plot essentially looks like an ellipse with a major axis ("y" direction) of about 150 micro inches, a minor axis ("x" direction) of 30 micro inches and a superimposed horizontal oscillation that has a peak to peak amplitude of about 10 micro inches. The orbit plot of the validation case showed a relatively "clean" orbit whereas Figure 21 does not. It is possible that the clean orbit comes about when the unbalance force dominates the orbit motion.

Figure 22 shows that the motion is primarily conical and that the shaft is cocked, on the average, away from pivot 3 and towards pivot 6. The mean angle of inclination is

$$\bar{\alpha}_2 = \frac{\bar{A}_2 \, C^{(1)}}{L^{(1)}} = \frac{0.012 \times 0.002}{1.5} = 1.6 \times 10^{-5} \text{ radians}$$

The maximum inclination of the shaft is about twice the average. This implies that a 2.667 inch diameter thrust bearing would translate towards the thrust stator 0.04×10^{-3} inches at the outside edge. The imposed thrust bearing misalignment is considered exceptable.

Figure 23 shows the x and y forces on the shaft mass center due to the integrated film pressures in the 6 shoes.

$$f_x = F_x \quad P_a \, R^{(1)} \, L^{(1)} = 0.1 \times 12 \times 0.75 \times 1.5 = 1.32 \text{ pounds (peak to peak)} \quad (34)$$

$$f_y = F_y \, P_a \, R^{(1)} \, L^{(1)} = .27 \text{ pounds (peak to peak)}$$

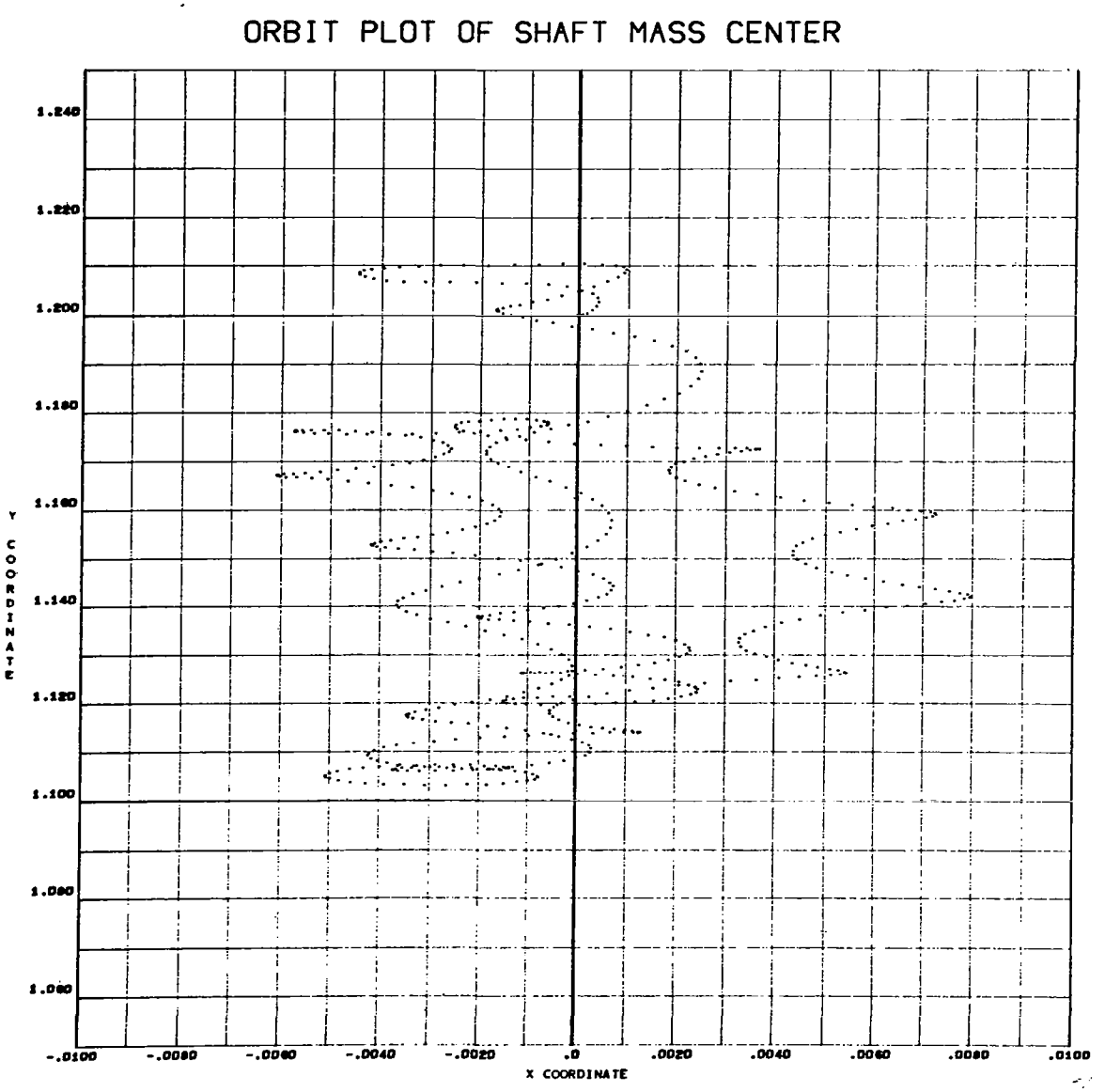

Fig. 21 - Base Case - Orbit Plot of Shaft Mass Center

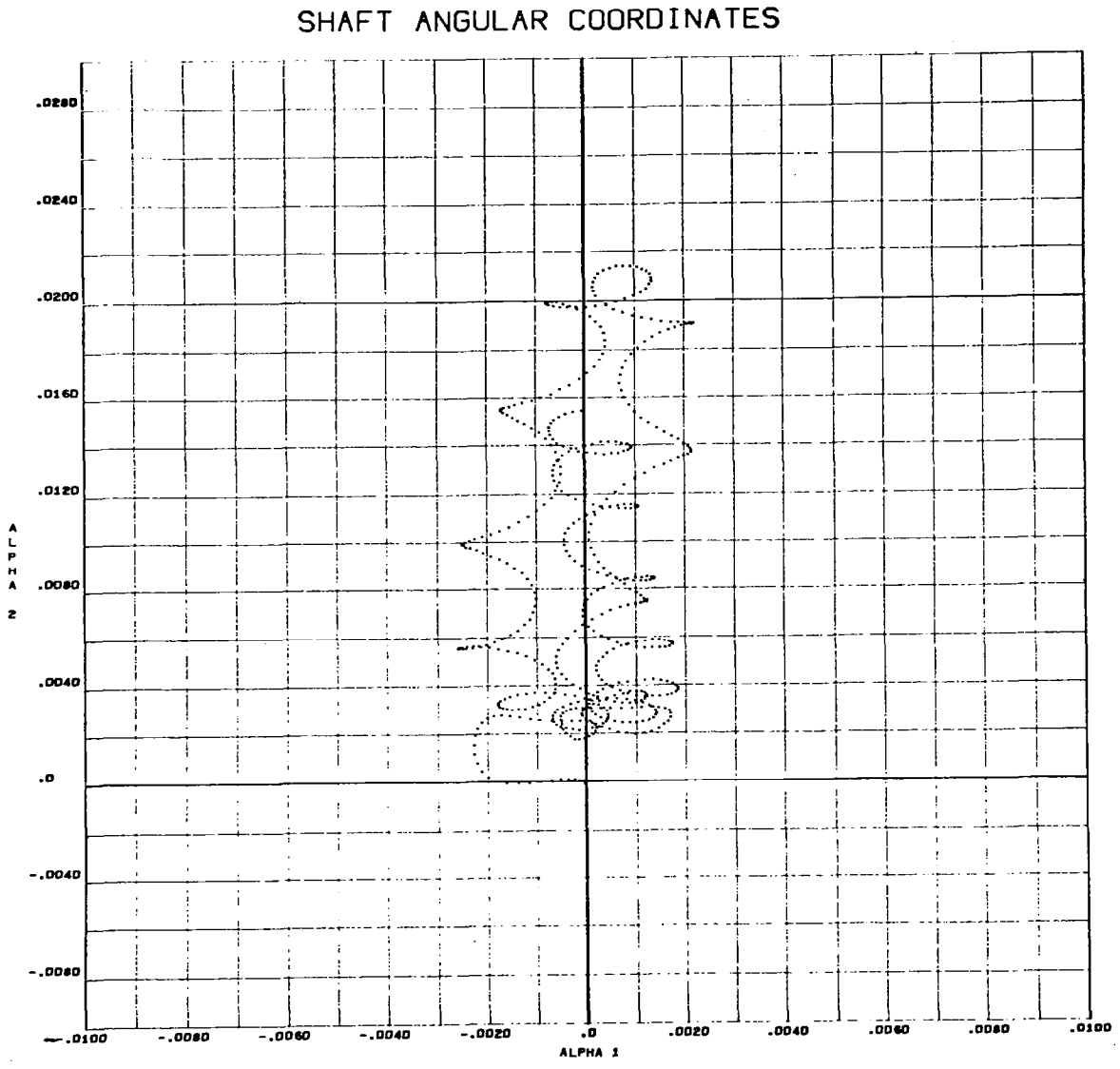

Fig. 22 - Base Case - Non-Dimensional Shaft Angular Coordinates

$$\left(\frac{\alpha_1 L^{(1)}}{C^{(1)}} \text{ vs. } \frac{\alpha_2 L^{(1)}}{C^{(1)}}\right)$$

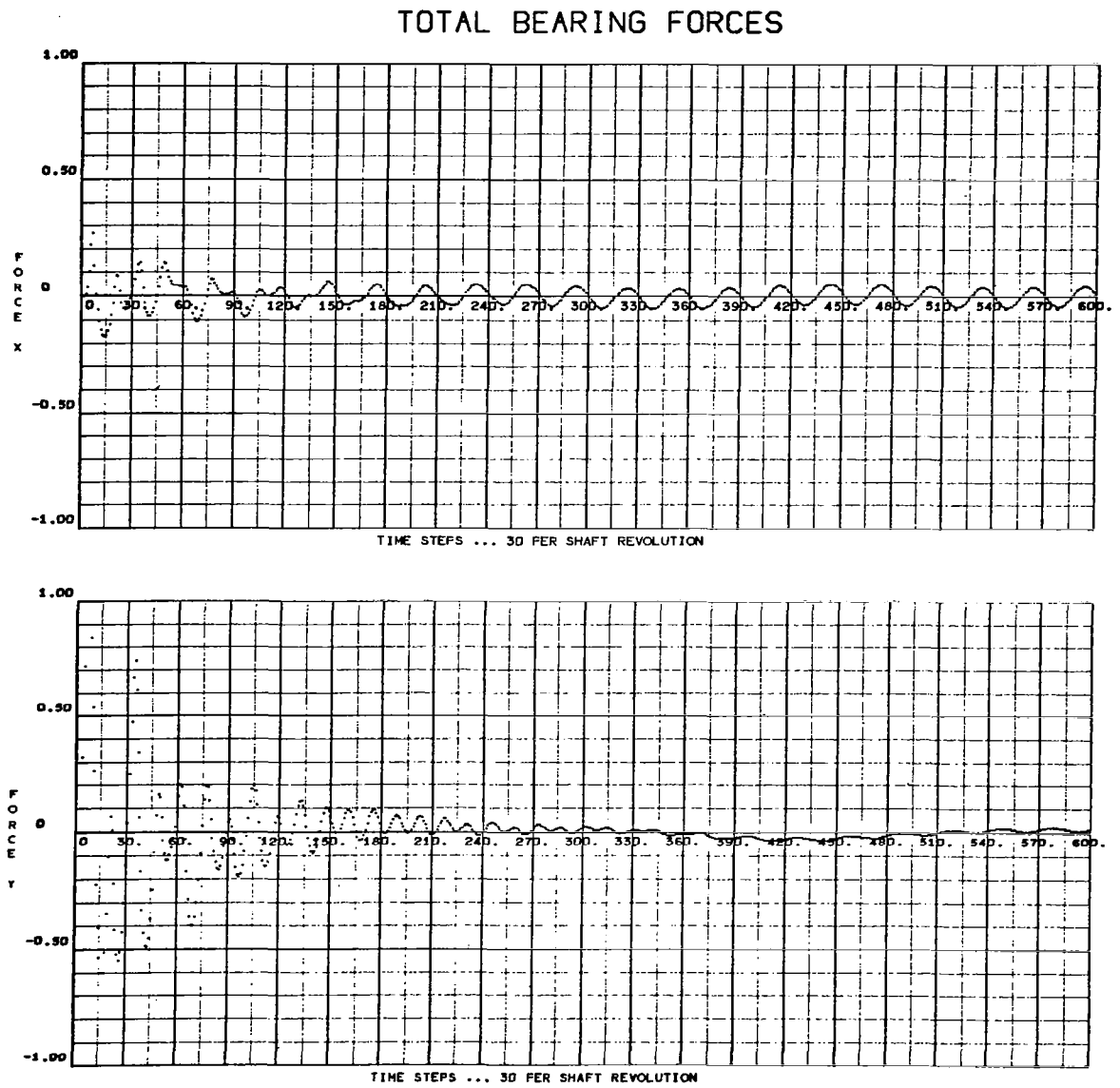

Fig. 23 - Base Case - Non-Dimensional Bearing Forces

$$\left(\frac{W_x}{P_a R^{(1)} L^{(1)}} , \frac{W_y}{P_a R^{(1)} L^{(1)}} \right) \text{ vs. Time}$$

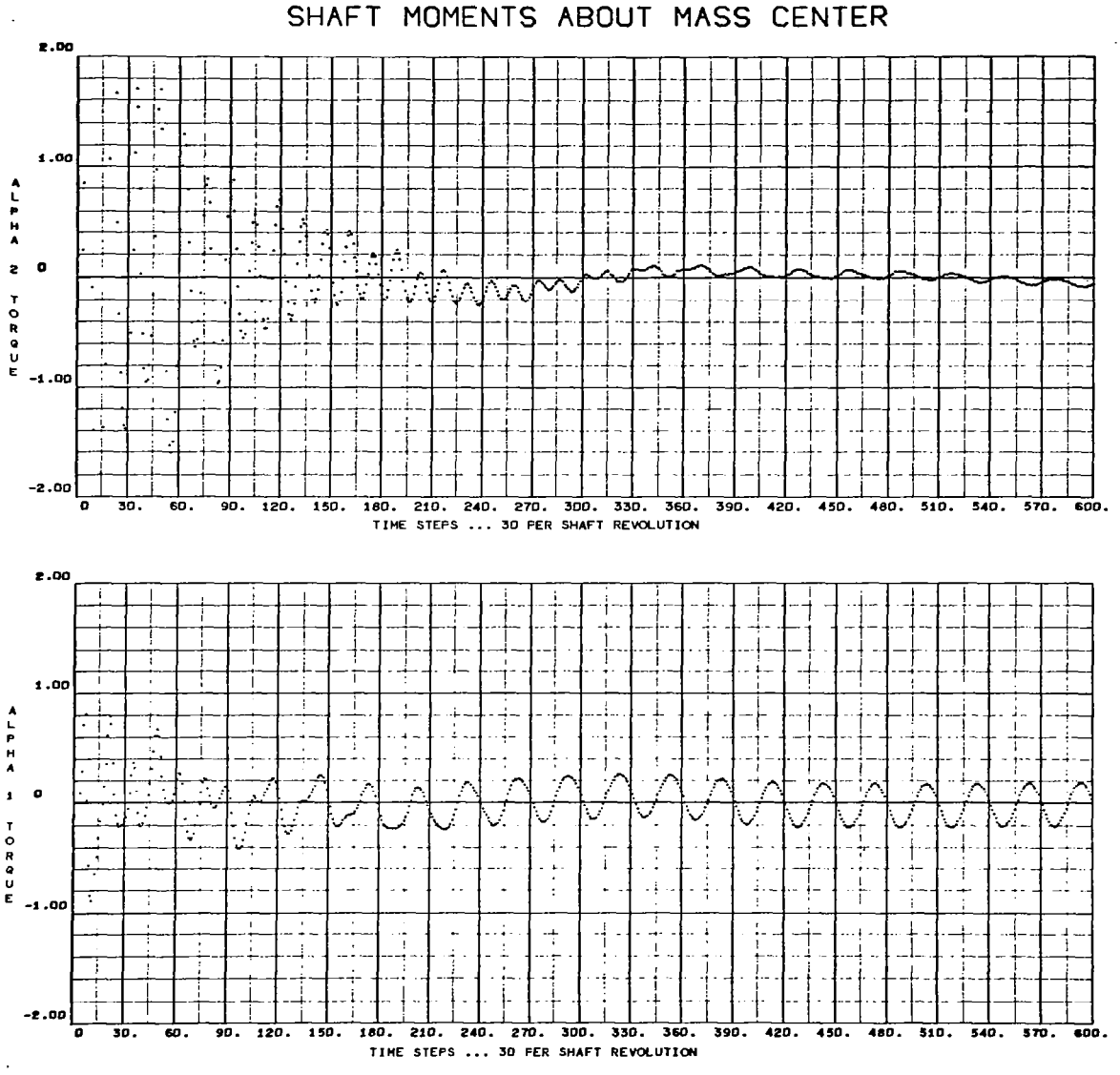

Fig. 24 - Base-Case - Non-Dimensional Torques $\left(\frac{T_{\alpha_1}}{P_a R^{(1)} (L^{(1)})^2} , \frac{T_{\alpha_2}}{P_a R^{(1)} (L^{(1)})^2} \right)$

About Shaft Mass Center vs. Time

Both forces have average values of zero. Figure 24 shows the α_2 torque (causes motion in the y-z plane) is amall compared to the α_1 torque (x-z plane). The α_2 torque is given by

$$t_{\alpha_1} = T_{\alpha_1} P_a R^{(1)} (L^{(1)})^2 \tag{35}$$

$$= 0.4 \times 12 \times 0.75 \times (1.5)^2 = 8.11 \text{ inch-pounds (peak to peak)}$$

The α_2 torque is only about 20% of the α_1 torque.

To explain the nominal 4000 cpm frequency that is associated with many of the motions of the bearing-rotor system consider the shaft motion in the y-direction only. Refering to Figure 25.

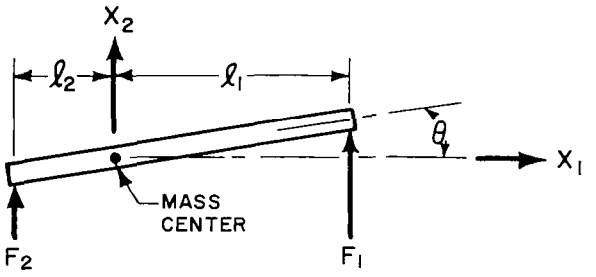

Fig. 25 - Shaft Vibration Coordinates

The moment and force equation are written as

$$F_1 \ell_1 - F_2 \ell_2 = I \ddot{\theta} \tag{36}$$

$$m \ddot{X}_2 = F_1 + F_2 \tag{37}$$

where m and I are the mass and inertia of the shaft and F_1 and F_2 are the bearing forces. In terms of the bearing stiffnesses k_1 and k_2

$$F_1 = - (X_2 + \ell_1 \theta) k_1$$

$$F_2 = - (X_2 - \ell_2 \theta) k_2$$

Substituting in 36 and 37 and rearranging

$$I\ddot{\theta} + (\ell_1^2 k_1 + \ell_2^2 k_2)\theta + (\ell_1 k_1 - \ell_2 k_2) X_2 = 0 \tag{38}$$

$$m X_2 + (k_1 + k_2) X_2 + (\ell_1 k_1 - \ell_2 k_2)\theta = 0 \tag{39}$$

Letting

$$\theta = \bar{\theta}\, e^{i\omega t}$$

$$X_2 = \bar{X}_2\, e^{i\omega t}$$

$$\omega_T^2 = \frac{k_1 + k_2}{m}$$

$$B = \ell_1 k_1 - \ell_2 k_2$$

The determinant of equations 38 and 39 is set equal to zero for determining the natural frequencies

$$\begin{vmatrix} (\omega_c^2 - \omega^2) & B/I \\ B/m & (\omega_T^2 - \omega^2) \end{vmatrix} = 0 \tag{40}$$

Note that the $\ddot{\theta}$ equation contains an X_2 term and the $\ddot{X}_2$ equation contains and θ term. This cross coupling is a consequence of the fact that the product of the distance from the mass center to the bearing times the bearing stiffness is not the same for both bearings. Therefore the system rigid body natural frequencies are not just the conical (ω_c) and the translatory (ω_T) frequencies but they are combinations of the two coupled by the term B.

Solving equation 40

$$\omega^2 = (\omega_T^2 + \omega_c^2) \pm \sqrt{(\omega_c^2 - \omega_T^2)^2 + \frac{4B^2}{Im}} \qquad (41)$$

The bearing stiffness in the "y" direction is essentially determined by the two fixed pivot shoes since the third shoe is backed by a soft spring. Using the pivot film thicknesses determined by steady-state considerations and Figure 12

$$k = 2 \frac{P_a RL}{C} \frac{dC_L}{dH_P} \cos^2 \beta$$

where B is the angle between the pivot axis and the vertical.

$$\omega_c^2 = \frac{\ell_1^2 k_1 + \ell_2^2 k_2}{I}$$

$$k_1 = 6750 \text{ lb/in}$$

$$k_2 = 4650 \text{ lb/in}$$

Substituting into Equation 41

$$\omega_1 = 8715 \text{ cpm}$$

$$\omega_L = 4655 \text{ cpm}$$

The lower of the two frequencies (ω_2) probably explains the source of the nominal 4000 cpm frequency that appears in the base case. The results of this simple analysis are seen to correspond very closely to case 5 of Table 3 from the system rigid body critical speed analysis.

6.4.5.2 Case 2 - High Pivot Friction Moment

Case 2 is the same as the base case except that the pivot friction moment is changed from 0.0 to 0.1 inch pounds on all shoes. This moment is about ten times larger than is expected to actually exist with

the FIRL pivot design. The dynamics program is written so that the pivot friction moment opposes the pitch and roll motions. If the moment of the film force pivot becomes less than the pivot friction moment then the shoe will remain in a fixed position until the film moment again exceeds the pivot friction moment. Thus the program accounts for the "stick-slip" characteristic of the pivot.

Figure 26 shows that the pitches of bearing 1 settle near the values that are predicted by the steady-state program which are:

$$\Delta_1 = -0.64;\ \Delta_2 = 1.22;\ \Delta_3 = 0.28$$

In Figure 27 the pitches for bearing 2 also settle near the steady-state values of

$$\Delta_4 = -0.25;\ \Delta_5 = 1.06\ \Delta_3 = 0.40$$

The rolls of the six shoes are not shown because the pivot friction moment is large enough to keep all shoes in their initial attitude of zero roll. It appears that if the conical mode of the shaft were small there would be no need for the roll motions of the shoe to exist. Its elimination would also improve the fretting and corrosion problem.

Figure 28 shows that spring loaded shoe of bearing 1 essentially retains the translation frequency and amplitude characteristics it had when the pivot friction moment was zero, but the frequency of shoe 6 has increased to about 5500 cpm. The dynamics equation for the shoe translation shows that the pitch motion influences the translation motion so the frequency difference is not surprising.

Comparing Figure 29 to Figure 20 shows that the "x-y" motions of the shaft become more restrained and that the once-per-rev excitation in the "x" direction has become attenuated. This suggests that the "x" motion of the shaft is greatly influenced by the pitch motions of the shoes for the zero pivot friction moment.

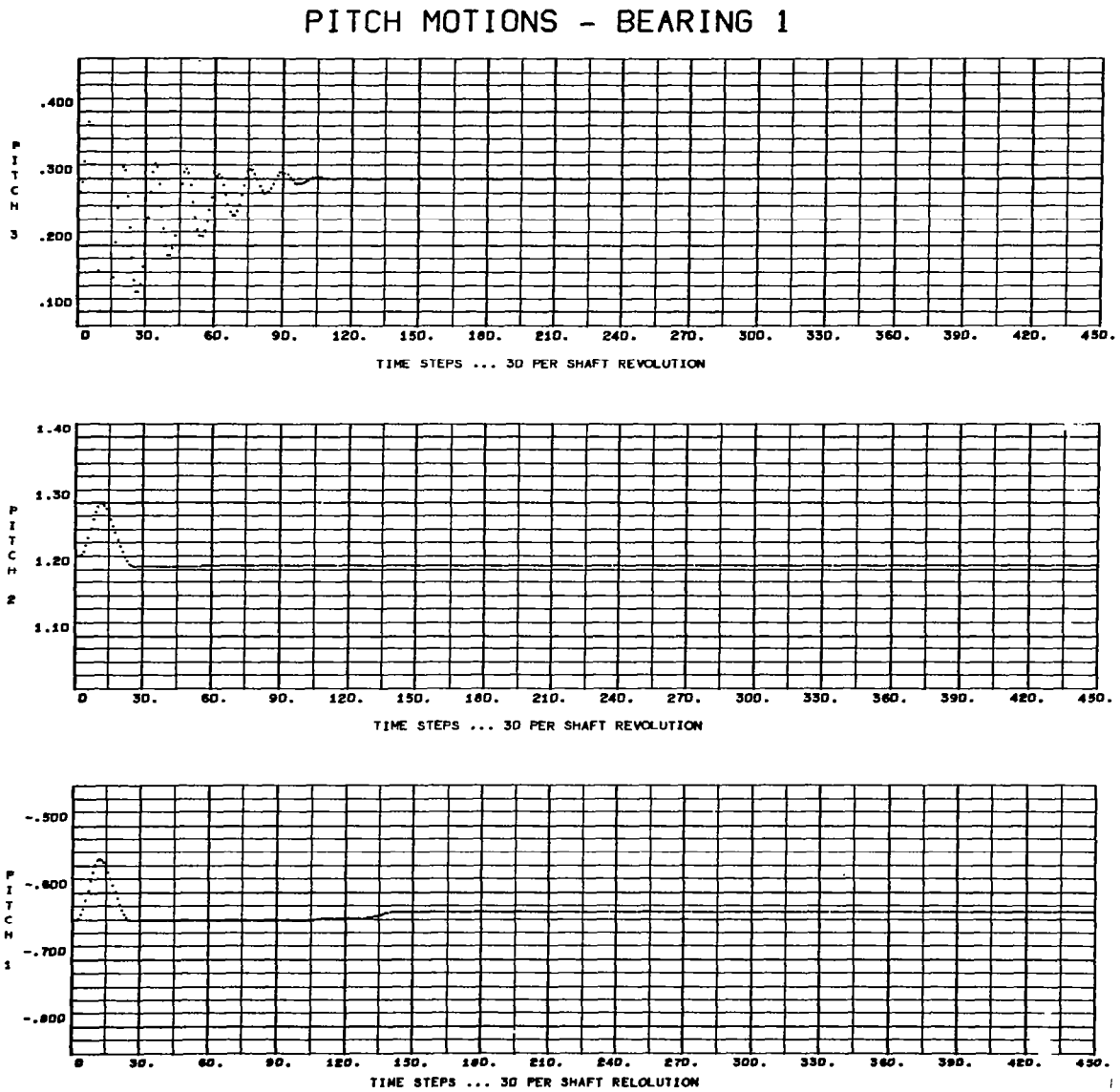

Fig. 26 - Case 2 - Non-Dimensional Pitch Amplitudes $\left(\frac{\delta R^{(1)}}{C^{(1)}}\right)$ vs. Time for the Three Shoes of Bearing 1

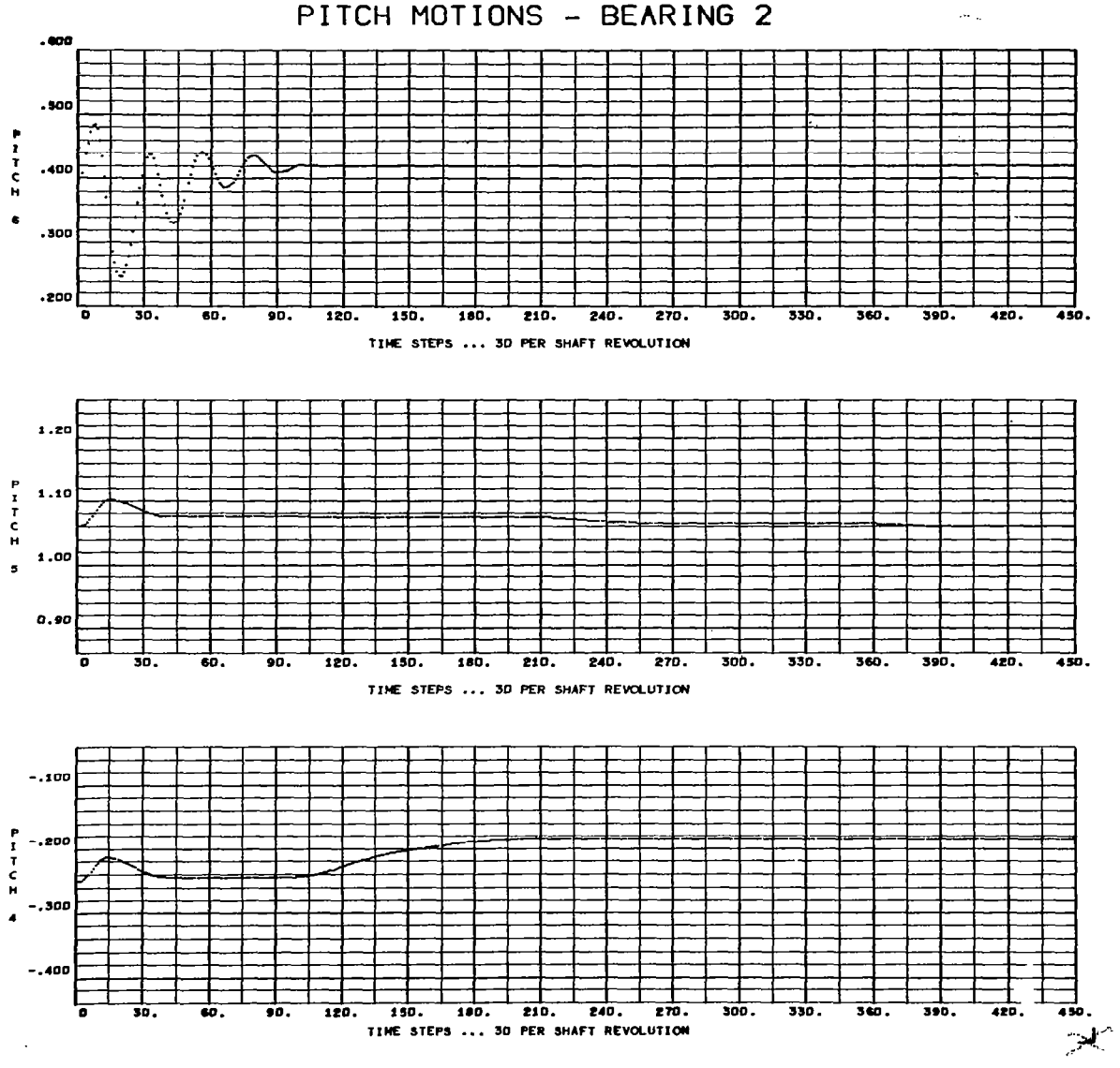

Fig. 27 - Case 2 - Non-Dimensional Pitch Amplitudes $\left(\frac{\delta R^{(1)}}{C^{(1)}}\right)$ vs. Time for the Three Shoes of Bearing 2

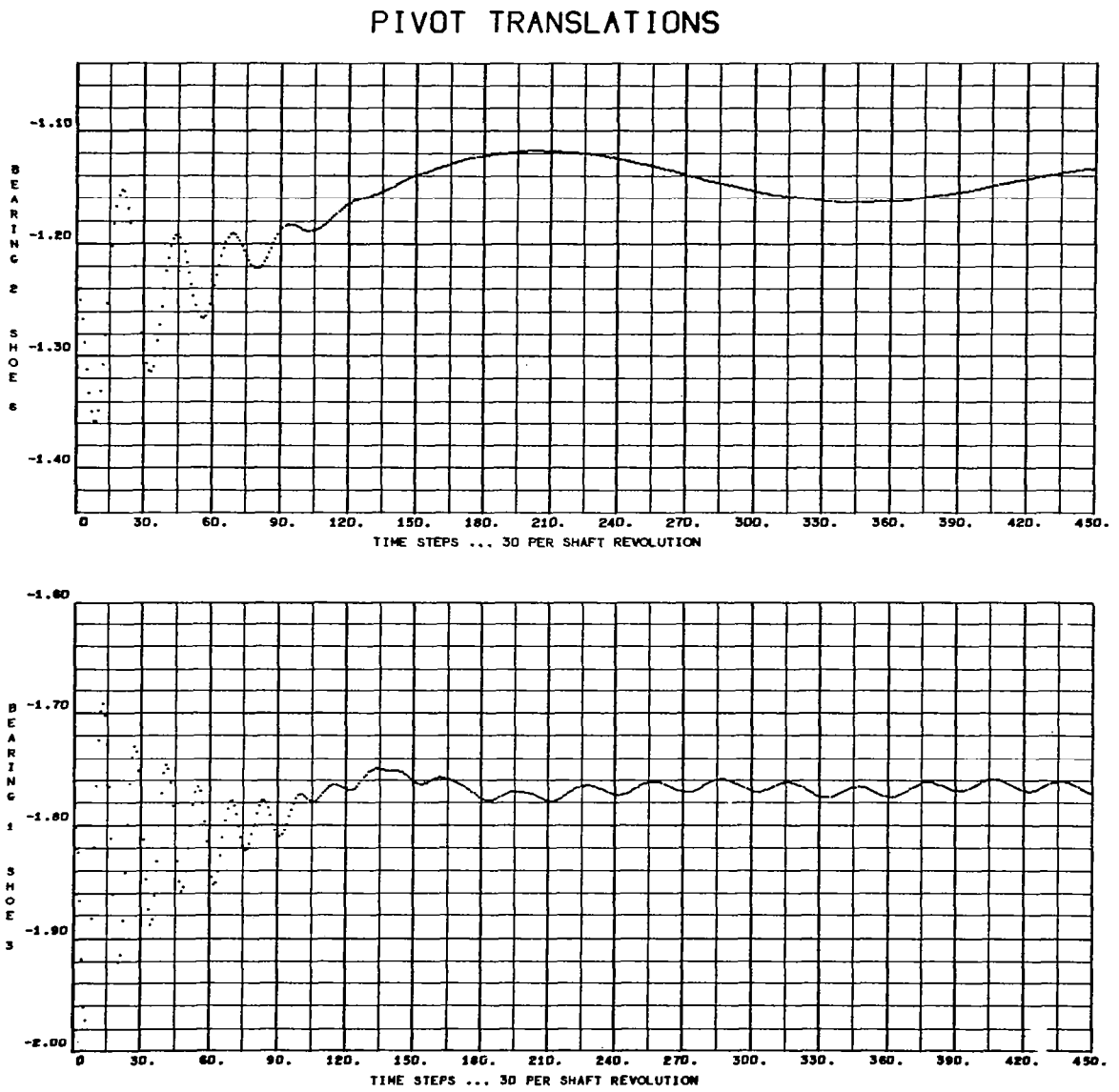

Fig. 28 - Case 2 - Non-Dimensional Pivot Translation $\left(\frac{C'}{C}\right)$ - 1 vs. Time for Shoes 3 and 6

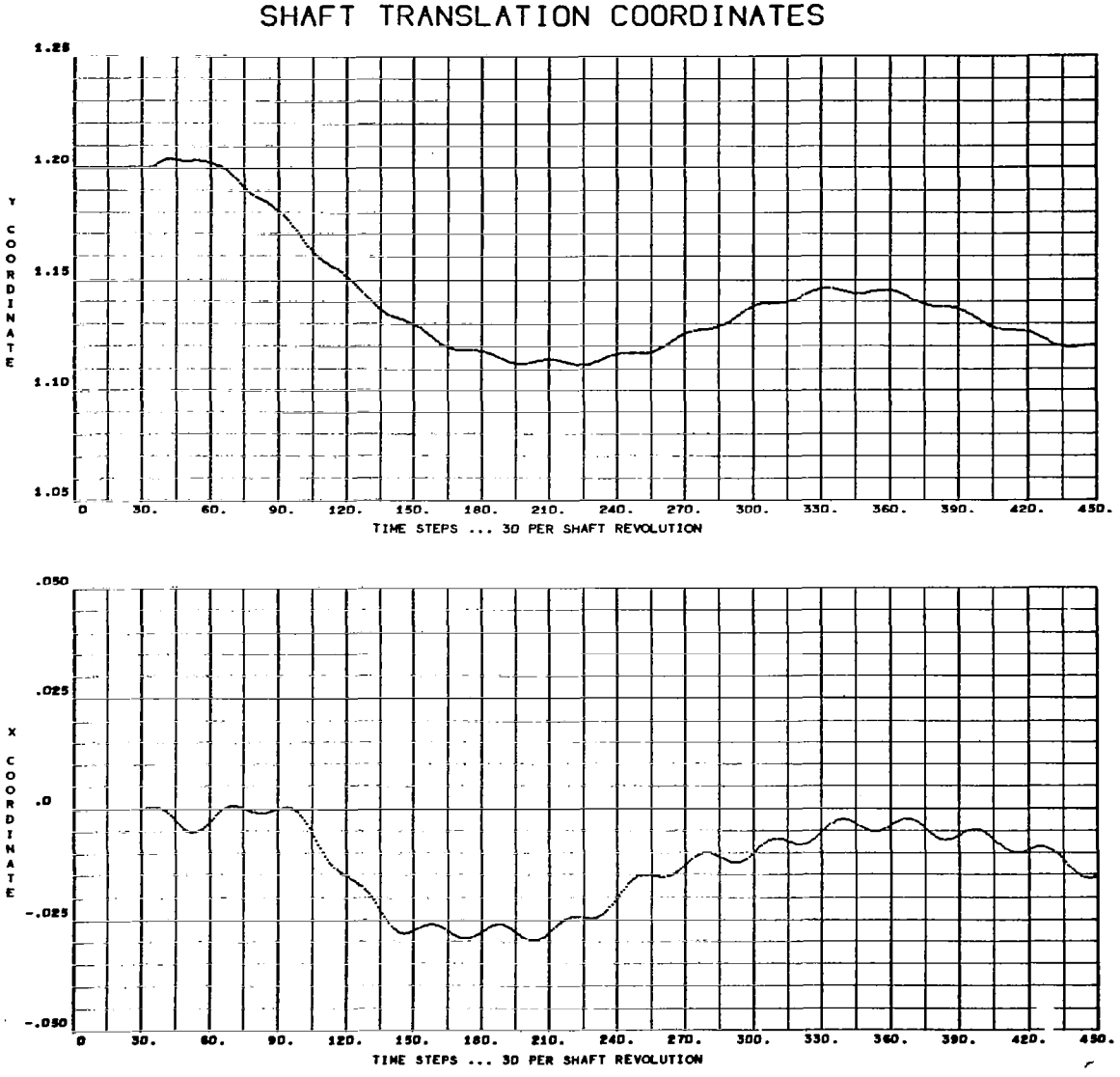

Fig. 29 - Case 2 - Non-Dimensional Shaft Mass Center Coordinates

$$\left(\frac{x}{c^{(1)}} \; ; \; \frac{y}{c^{(1)}}\right) \text{ vs. Time}$$

Figures 30 and 31 indicate that the shaft mass center is slightly more displaced towards the spring loaded shoes then it was in the base case. This is probably accounted for by the fact that shoes 3 and 6 have suffered a slight drop on load capacity because they have not rolled to make an average adjustment to the shaft inclination. The shaft is inclined towards shoe 6 and away from shoe 3. This inclination is slightly less than it was for the base case.

Figures 32 and 33 show the shaft forces and moments to be essentially the same as they were for zero pivot friction moment.

The principal conclusion from this case is that if the pivot friction moment becomes large while the shaft is rotating at design speed the shoes will acquire a fixed orientation but the rotor bearing system will remain stable. There is, of course, the possibility that if the shaft speed is continually changed - as it would be during coast-down - there is a chance that the bearing could become unstable.

Using the average values from Case 2, some of the bearing characteristics are listed in Table 6.

Table 6

BEARING CHARACTERISTICS OBTAINED FROM DYNAMICS PROGRAM

Bearing 1				Bearing 2		
Shoe	1	2	3	4	5	6
h_p (mils)	0.828	0.798	0.832	1.799	1.853	1.755
F_p (watts)	15.5	15.9	15.4	32.6	31.6	33.4
F_p (total) = 46.8 watts				F_p (total) = 97.6 watts		
Pivot Circle Eccentricity ε' = 0.003				Pivot Circle Eccentricity C' = 0.016		
Pivot Circle Setting C'/C_2 = 0.415				Pivot Circle Setting C'/C_2 = 0.607		

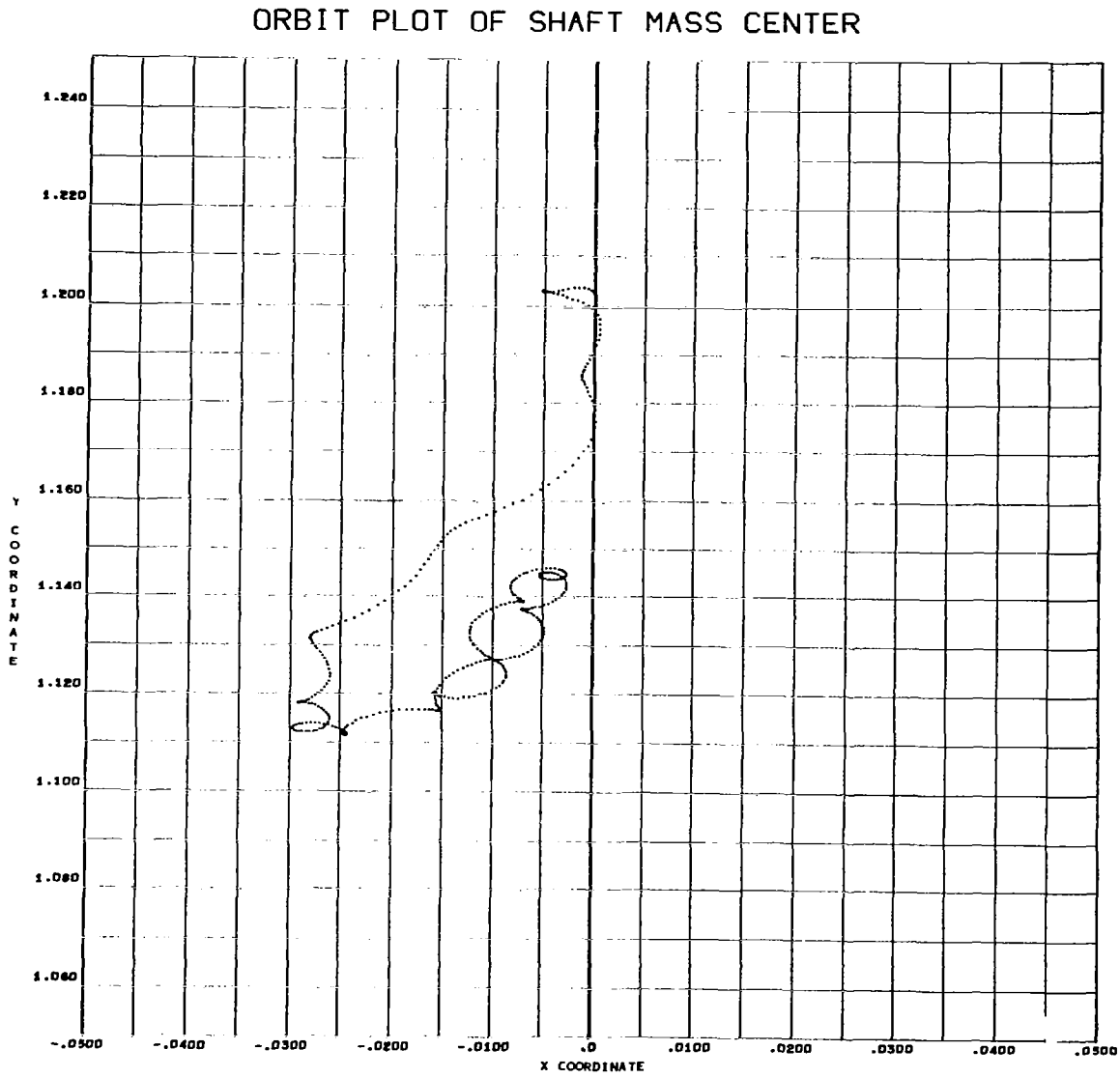

Fig. 30 - Case 2 - Orbit Plot of Shaft Mass Center

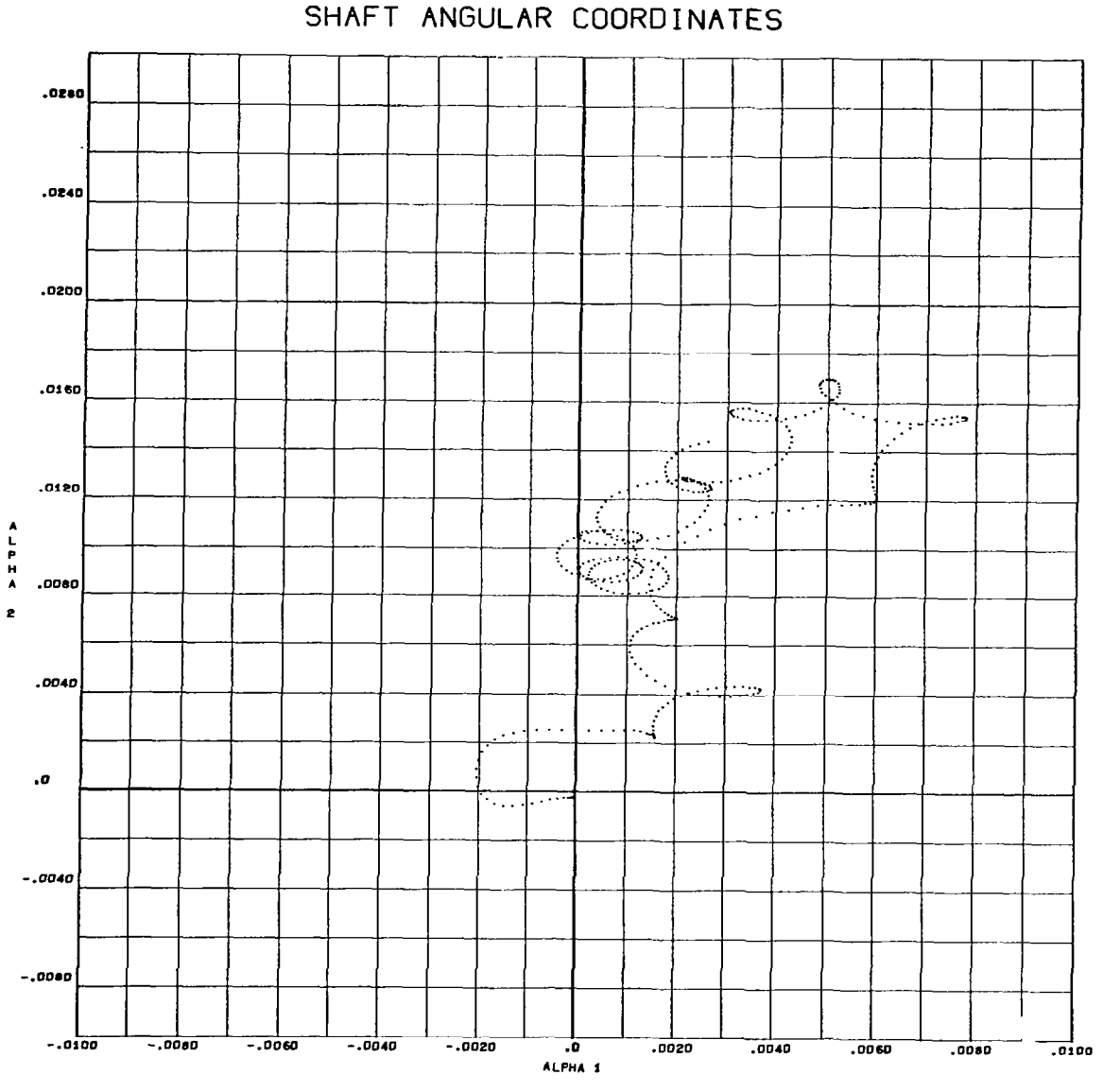

Fig. 31 - Case 2 - Non-Dimensional Shaft Angular Coordinates

$$\left(\frac{\alpha_1 L^{(1)}}{C^{(1)}} \text{ vs. } \frac{\alpha_2 L^{(1)}}{C^{(1)}} \right)$$

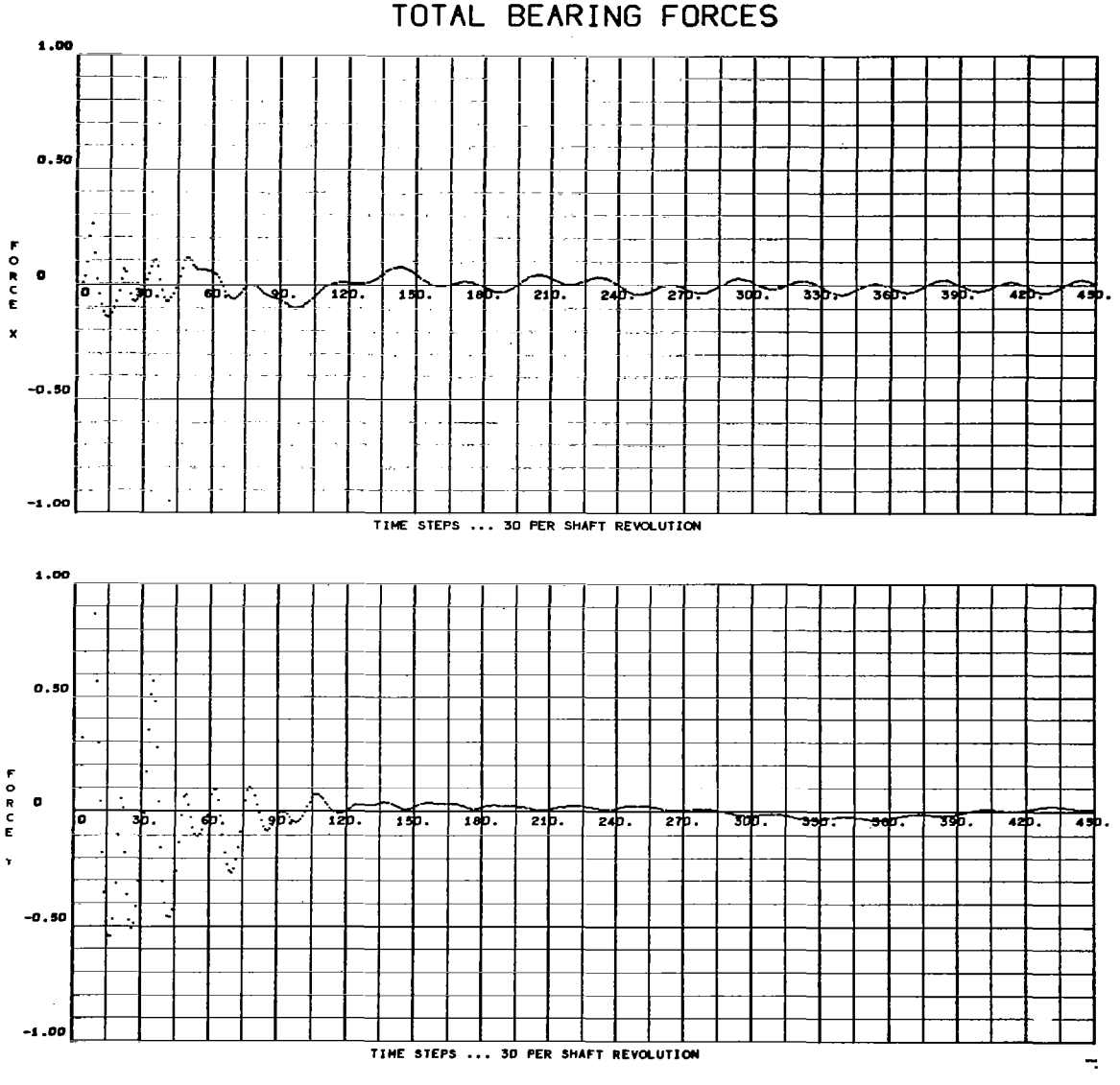

Fig. 32 - Case 2 - Non-Dimensional Bearing Forces

$$\frac{W_x}{P_a R^{(1)} L^{(1)}}, \quad \frac{W_y}{P_a R^{(1)} L^{(1)}} \qquad \text{vs. Time}$$

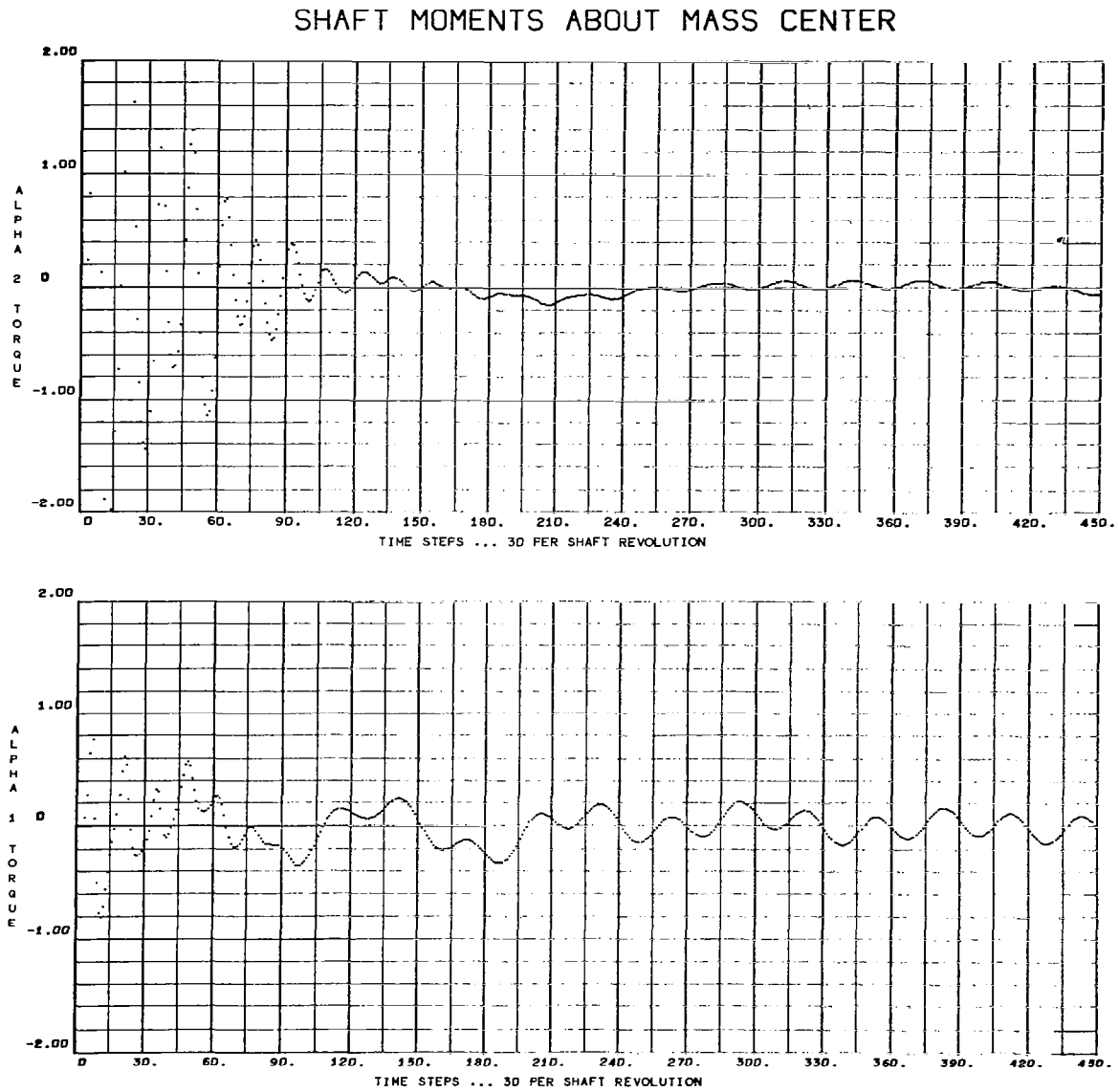

Fig. 33 - Case 2 - Non-Dimensional Torques $\left(\frac{T_{\alpha_1}}{P_a R^{(1)} (L^{(1)})^2} , \frac{T_{\alpha_2}}{P_a R^{(1)} (L^{(1)})^2} \right)$

About Shaft Mass Center vs. Time

6.4.5.3 Conclusions from the Dynamical Study

The journal bearing design has been shown to operate stably. The film thicknesses are moderate and the total journal bearing losses are less than 150 watts. The system will continue to operate stably if the pivots freeze near their steady-state operating conditions. The thrust bearing will see a slight swashing motion since the shaft cannot translate without causing conical motion.

The amplitudes and frequencies of the shoe motions, together with dynamic load along the pivot axis, constitutes vital information in the analysis of the pivot point with respect to fatigue, fretting corrosion and geometric design. The force along the pivot axis and the moments about the pivot point are computed by the Orbit analysis and are available for this type of study. A detailed analysis of the pivot was considered too time consuming and too expensive to be undertaken on this project, therefore the pivot was designed principally from past experience.

The analysis indicates the design is suitable for testing. Emphasis should be placed on studying the effects on the turbine compressor performed due to the non-symmetric bearing system with respect to the rotor c.g. Also, since the motions of the shoes of bearing 1 differ considerably from those of bearing 2, the relative life and performance of the pivots should be compared.

7. THRUST BEARING ANALYSIS

7.1 Basic Configuration

The turbine-compressor thrust bearing consists of a main thrust bearing and a reverse thrust bearing. The thrust collar is at the compressor end of the rotor and has a plain face (dead ended) which forms one surface of the main thrust bearing. The plain annular area on the turbine side of the thrust collar forms one side of the reverse thrust bearing. The other face of the main thrust bearing, shown on Figure 34, is a combination of a dead ended hydrodynamic spiral groove bearing and an inherently compensated hydrostatic bearing. The hydrostatic capability, used during start-up and shut-down, is accomplished by a circumferential row of feeding orifice at the mid-radius of the face. The stationary face of the reverse thrust bearing, shown on Figure 35, is principally an inherently compensated hydrostatic bearing, but hydrodynamic capability is also provided as an emergency measure by a series of Rayleigh steps. During operation at design speed, the thrust load is directed towards the main thrust bearing with a small amount of preload contributed by the hydrodynamic action of the reverse thrust bearing.

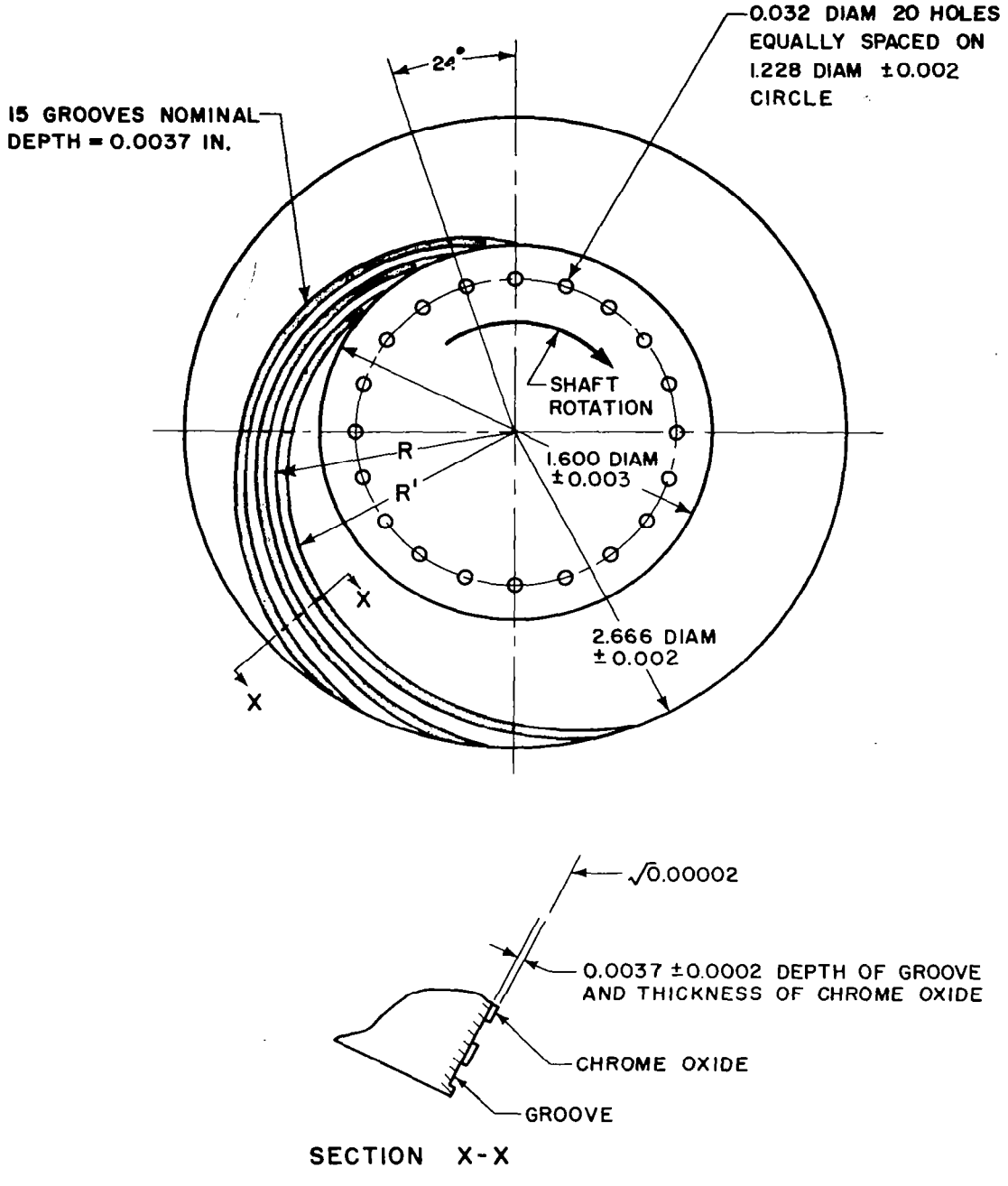

Fig. 34 - Main Thrust Bearing - Manufacturing Dimensions

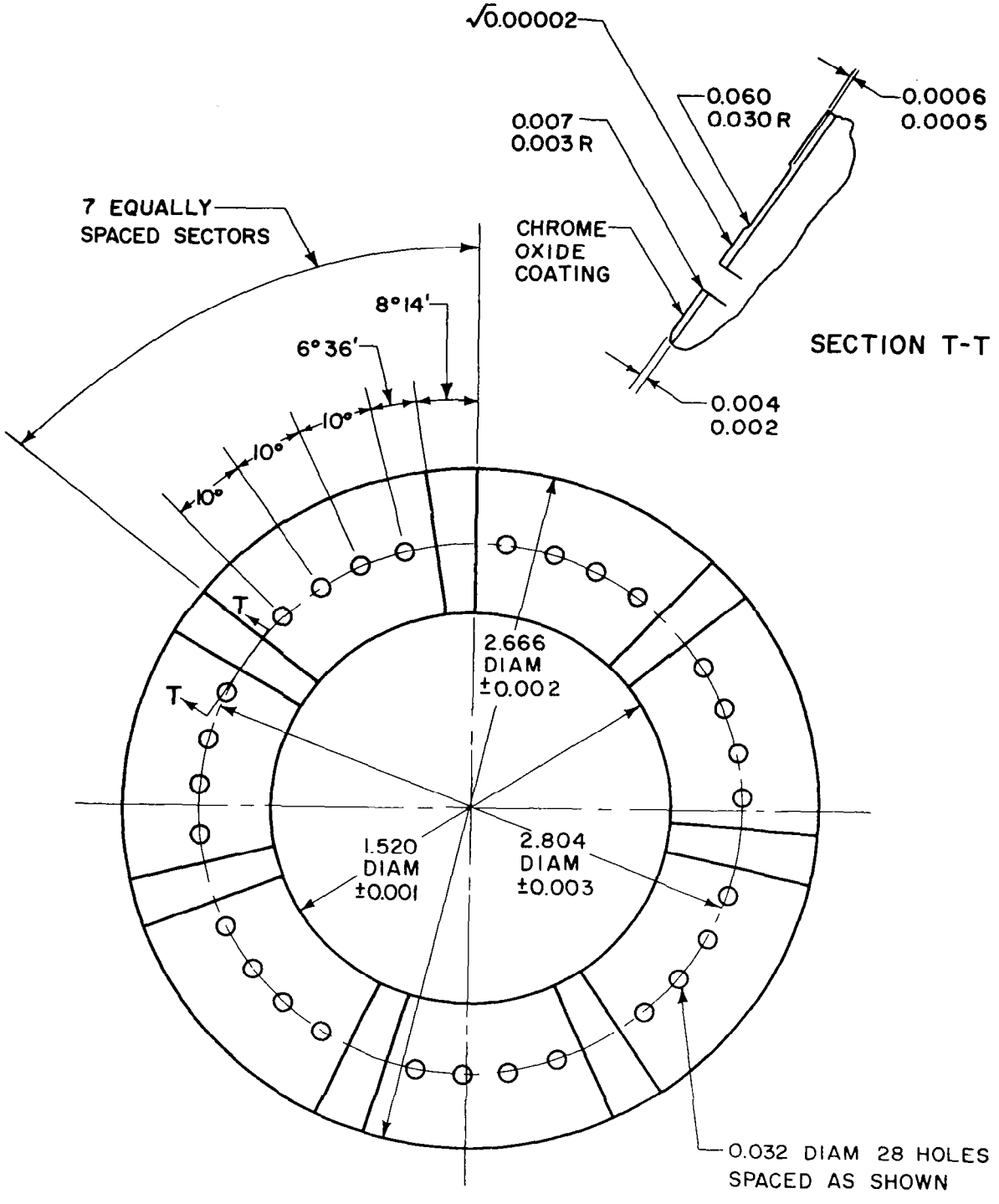

Fig. 35 - Reverse Thrust Bearing - Manufacturing Dimensions

7.2 Main Hydrodynamic Thrust Bearing

7.2.1 Load Capacity

The main hydrodynamic bearing was analyzed using Muijdermann's results, Reference (5). Muijdermann develops the geometric criteria necessary to optimize the bearing for load carrying capacity. The values applied to the compressor thrust bearing are as follows (see Fig. 36).

no. of grooves,	$k = 15$
radius ratio,	$\lambda = 0.6$
groove angle,	$\alpha_{max} = 11.7°$
compression ratio,	$\delta_{max} = 0.31$
ridge/groove ratio,	$\gamma_{max} = 1.19$
load factor,	$C_L = \frac{Wh^2}{\mu \omega R_3^4} = 0.336$

The subscript max means that the value of the parameter is the value that will yield maximum load carrying capacity. The parameters k, λ, α_{max}, γ_{max} are the geometric variables that can be fixed by manufacture of the bearing. Both the compression ratio and the load factor depend upon the bearing operating clearance.

The groove depth of the spiral groove was obtained by optimizing this parameter for load capacity at the design condition. The groove depth selected was $h_o = .00371$ inches.

The technique for obtaining the variation of load with clearance is described in Appendix VII. Fig. 37 depicts this variation at 25,000, 50,000 and 60,000 RPM.

7.2.2 Friction Loss

Two separate areas contribute to the frictional drag of the thrust bearing. The first is the circular area contained inside R_2, the second is the annular area containing the spiral groove. The expression for the power loss in watts for the ungrooved region is:

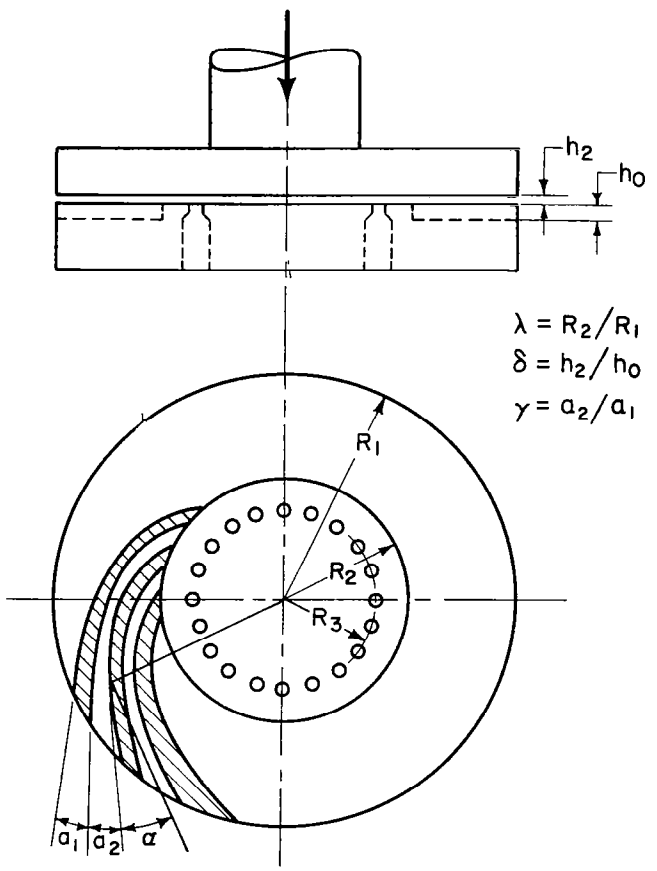

Fig. 36 - Dead-Ended Spiral Groove Bearing with Hydrostatic Lift-off Geometric Parameters

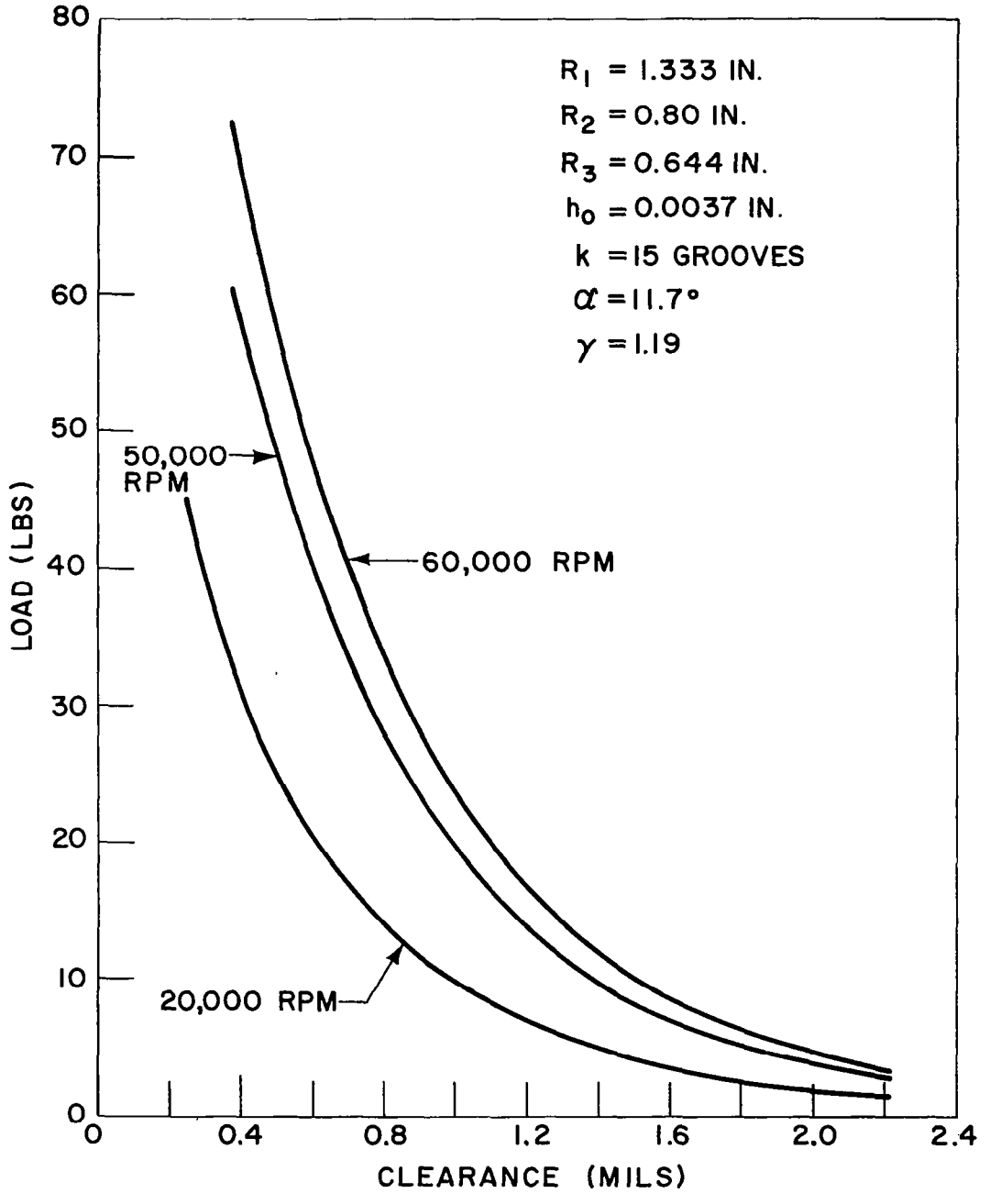

Fig. 37 - Load vs. Clearance for the Spiral Groove Bearing

$$P_f = \frac{.177 \ \mu \ \omega^2 \ R_2^4}{h} \tag{42}$$

The friction loss for the grooved portion was obtained from Reference (5). Both the derivation of Equation (42) and the methods for obtaining the friction loss in the grooved region is indicated in Appendix VII. The total power loss, P, is the summation of the losses in the two regions, and its variation with load at 25,000, 50,000 and 60,000 rpm is shown on Figure 38.

7.2.3 Axial Stiffness

The axial stiffness of the spiral groove thrust bearing is obtained from measuring the slope of the load vs clearance curves. The results are plotted on Figure 39.

7.2.4 Thermal Distortion

The general expression for thermal distortion of the thrust collar is derived in Appendix VII and is given as

$$y_{max} = \frac{P \ \alpha'}{6 \ K \ \pi} \tag{43}$$

The distortion was calculated to be 1.78×10^{-5} in. If this figure were doubled to include both the runner and the stator, the distortion is still not significant.

7.2.5 Bearing Righting Moment Capability

A rough approximation to the righting moment can be obtained by considering springs of spring constant equal to the axial bearing stiffness to act at the effective bearing mid-length. If we divide the bearing into 16 sectors the tilting stiffness can be approximated by

$$K_T = \frac{M_{xx}}{\psi} = \frac{S_A \ R_1^2}{8} [\sin^2 \theta_1 + \sin^2 \theta_2 + \sin^2 \theta_3 + \sin^2 \theta_4] \tag{44}$$

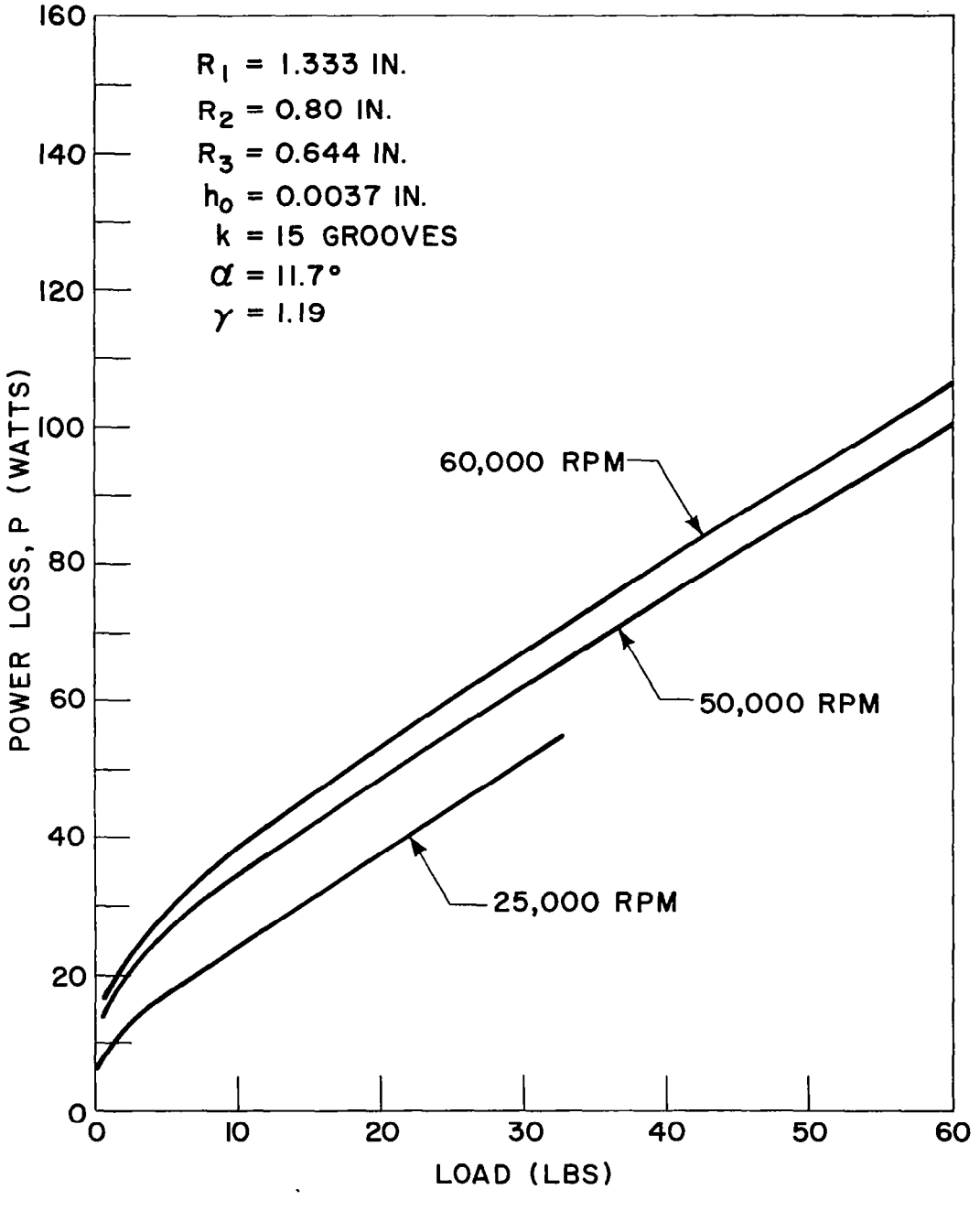

Fig. 38 - Load vs. Power Loss for the Spiral Groove Bearing

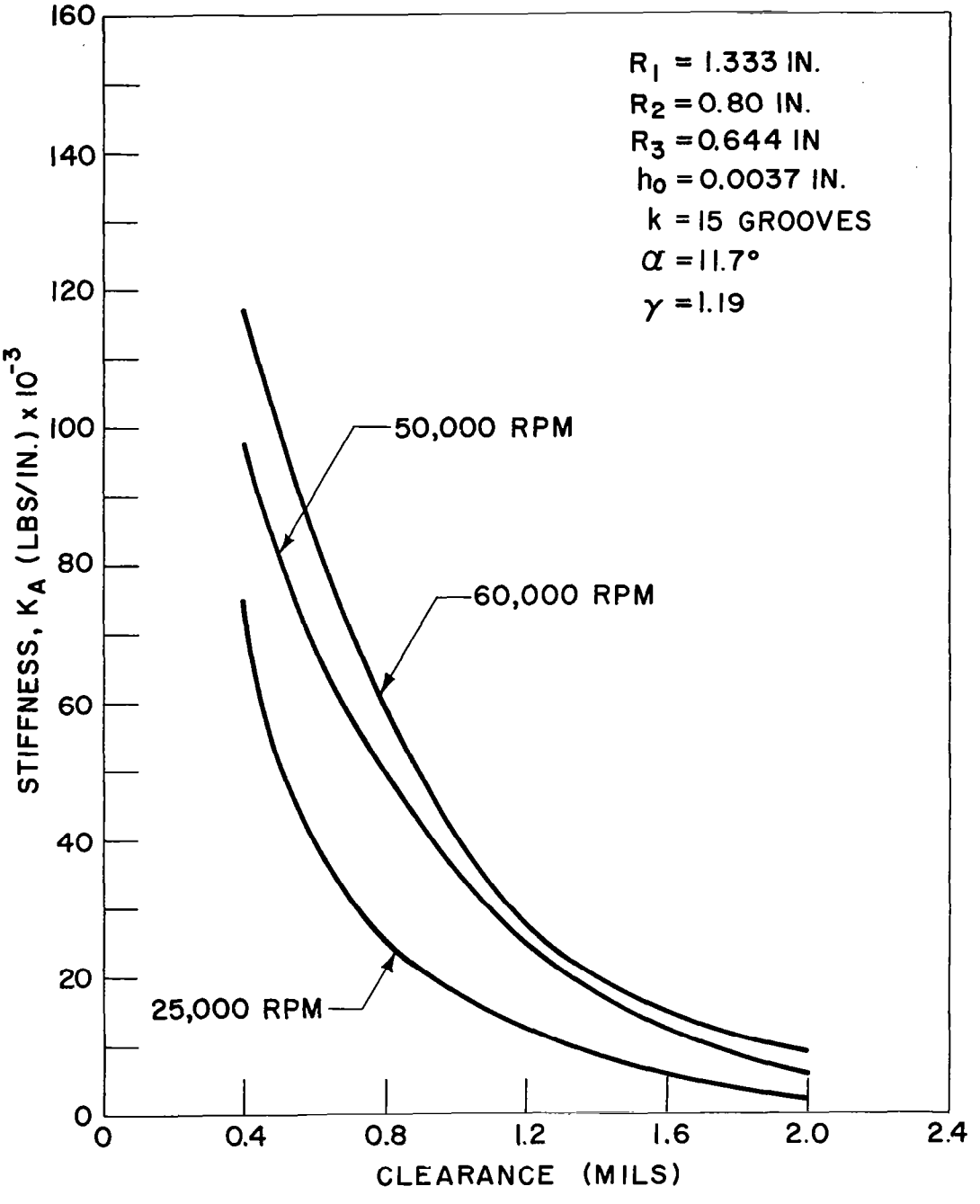

Fig. 39 - Stiffness vs. Clearance for the Dead Ended Spiral Groove Bearing

where

$$\theta_i = 22\text{-}1/2^\circ + \theta_{i-1}{}^\circ$$

At the design condition K_T = 15,549 in-lbs/rad.

7.2.6 Synchronous Vibrations of Thrust Bearing

Because the rotating collar cannot be aligned exactly perpendicular to the axis of rotation, there will be an angular swashing of the collar as it rotates. This produces a forcing function on the stationary collar and causes it to vibrate. This type of vibration has been analyzed by Whittey and Williams as described in Reference (21). The analysis is described in Appendix VII with a calculation of the swashing amplitudes at the design condition. The torsional stiffness of the stationary collar supporting structure was taken as 70,000 in-lbs/rad as per information supplied by Pratt and Whitney Aircraft.

The pertinent equations are

$$\varepsilon_{max} = \varepsilon_o \left(\frac{\omega^2}{\omega_c^2 - \omega^2} \right) \tag{46}$$

and

$$\xi_{max} = \frac{\varepsilon_o}{1 - \frac{\omega^2 I_T}{K_T}} \tag{47}$$

7.2.7 Tabulation of Performance at Design Conditions

Table 7

Rotor Speed N = 50,000 rpm

Thrust Load W = 15 lbs

Minimum clearance h_2 = 1.14 mils

Friction loss P_f = 41 watts

Axial stiffness K_A = 28,000 lbs/in.

Thermal distortion $y_{max} = 1.787 \times 10^{-5}$ in.

Torsional stiffness of fluid film $K_T = 15,549 \frac{\text{in-lbs}}{\text{rad}}$

Maximum relative swash between plates = .18 ε_o

Maximum absolute swash of stationary plate = 1.18 ε_o

where ε_o = initial angular misalignment

7.2.8 Mechanical Design

The basic mechanical design of the main thrust bearing is shown on Figure 34. A comprehensive design layout drawing for this bearing has been completed by Pratt and Whitney Aircraft Reference (10), and should be consulted for detailed information concerning the bearing construction features and installation in the compressor.

The coordinates for the groove configuration are shown on Figure 40. The grooves are formed by masking the face of the stationary thrust plate and then flame coating with chrome oxide. To improve heat transfer and thus minimize thermal distortion, and also to reduce weight a good grade of aluminum is recommended for the base material of the bearing parts. The chrome oxide coating applied to both rubbing surfaces will prevent galling if for some reason film clearance is lost.

θ°	R-in	R'-in
0	0.8000	0.7691
10	0.8294	0.7974
20	0.8600	0.8268
30	0.8916	0.8572
40	0.9245	0.8888
50	0.9585	0.9215
60	0.9938	0.9554
70	1.0303	0.9905
80	1.0683	1.0271
90	1.1075	1.0647
100	1.1482	1.1039
110	1.1906	1.1446
120	1.2344	1.1867
130	1.2798	1.2303
140	1.3269	1.2756
150	1.3758	1.3227
160	1.4264	1.3713

Note: See Figure 34 for definition of R and R'

Fig. 40 - Groove Coordinates

Concerning the alignment of the main thrust bearing it was decided to incorporate a relatively rigid mount. From the discussions of the swashing effect of a misaligned collar it was determined that the rigid mount does not substantially effect the relative displacement between the opposed members, as long as the initial installation of the collar is reasonably precise (within .0002 TIR). The major reason a flexible mount was considered was to adjust for gross distortions of the surrounding structure, which may result from thermal strains. The cooling scheme provided for the entire turbine-compressor was designed so that thermal distortions would be minimized and

this eliminated the necessity of a complex self aligning mount for the thrust bearing.

7.3 Reverse Thrust Bearing

7.3.1 Hydrodynamic Performance

The reverse thrust bearing hydrodynamic analysis was accomplished with the design charts published in Reference (2). Optimization was designed for the 25 lb load condition, or half the maximum load occurring under transient conditions.

The hydrodynamic capability of the bearing is shown on Figure 41.

7.3.2 Mechanical Design

A comprehensive design layout drawing of the reverse thrust bearing is shown in Reference (10). The configuration of the bearing face is shown on Figure 35. The bearing surface is coated with chrome oxide as is the surface of the opposed thrust collar. The step grooves are formed by appropriate masking of the face before flame spraying the chrome oxide and then grinding to final dimensions.

7.4 Pre-Loaded Hydrostatic Thrust Pair

7.4.1 Discussion of Analysis

During start-up and shut-down there are periods when the rotor speed is insufficient to generate hydrodynamic load capacity. During these operating conditions support is enhanced by externally pressurizing both the main and reverse thrust bearings. There are two problems concerned with the design of the externally pressurized bearing system. The first is to insure that the load is adequately supported; the second is to safeguard against self excited instabilities. The problem of stability is concerned with a phenomenon known as "pneumatic hammer". Characteristic of this type of instability is a violent chattering of the opposed bearing surfaces which, if not checked, can cause loss of clearance and damage to bearing surfaces.

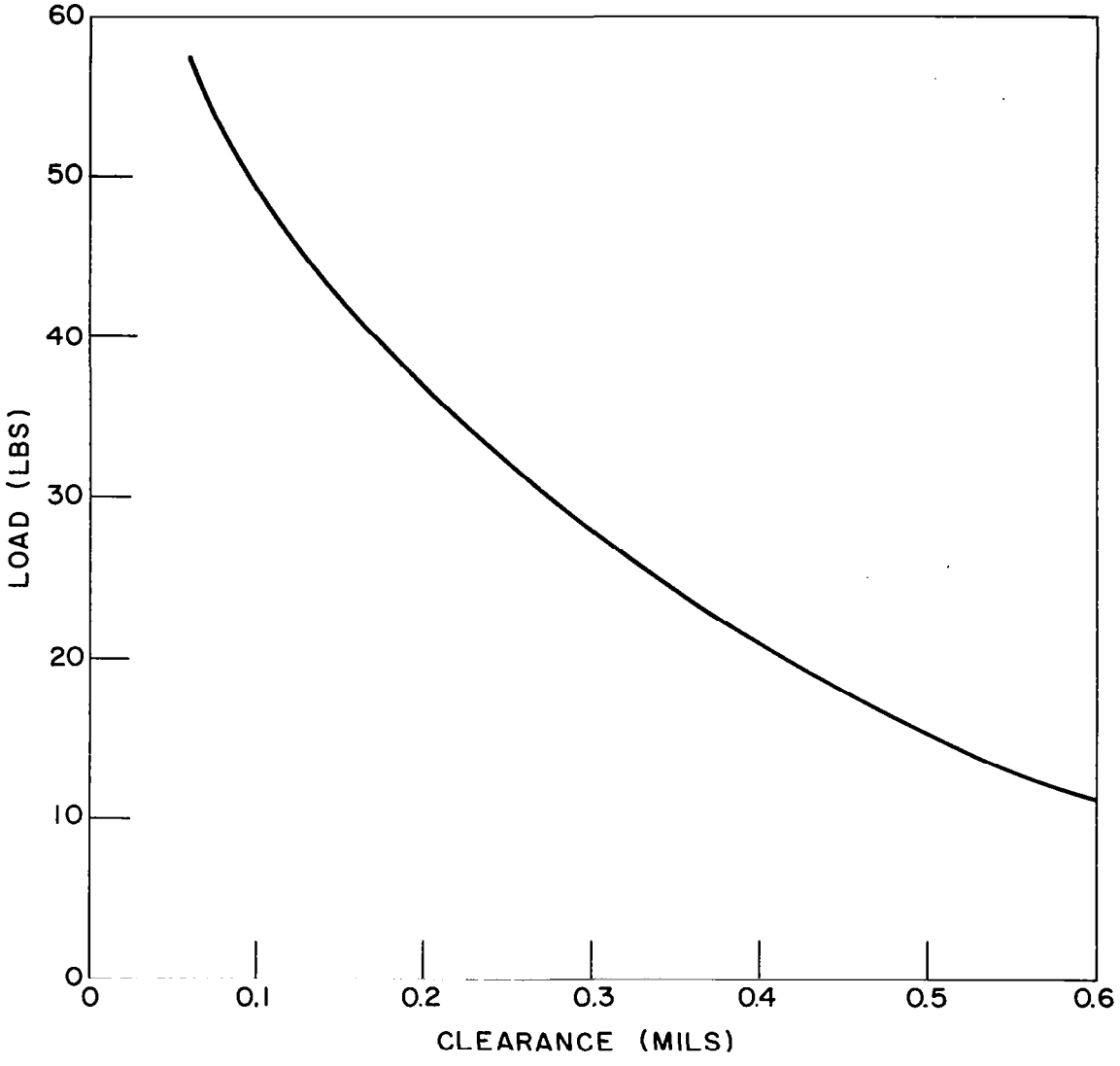

Fig. 41 - Hydrodynamic Characteristics of the Reverse Thrust Bearing

One of the questionable aspects of the external pressurization incorporated into the main thrust bearing is how much, if any, will the grooved portion contribute to load capacity at zero speed. It would be conservative to assume that the grooved portion contributes nothing to load capacity, and the bearing was sized on this basis. However, with regards to stability this assumption is not conservative since no account would be taken of the compressibility affects of the fluid contained with the grooves. The approach taken herein was to investigate load capacity and stability without considering the effects of the grooves and then to recheck stability by adjusting the bearing O.D. to include a portion of the grooved area. If both the conservative load capacity analysis and conservative stability analysis shows acceptable performance then the configuration was considered workable.

The general approach to the instability problem is that described by L. Licht in References (11) and (12). Modifications were made to incorporate inherent compensation and to make allowance for the grooved region. In the general theory deviations from the equilibrium conditions are expressed in terms of lumped parameters. The pressure distribution is assumed to vary quasi-statically so that the effect of the frequency of vibration is ignored. Also, the pressure profile is assumed to be known. In general, this simplified theory will permit reasonable approximations regarding stability, and comparisons between theory and experiments indicate that conservative results can be anticipated.

A complete development of both the steady-state and stability analysis is included in Appendix VII. From the complexity of the governing relations it is obvious that hand computation over a wide range of parameters is a lengthy task. Thus to obtain performance information over an adequate spectrum of operating conditions required development of computer programs. Two programs were used. The first program considered that the hydrostatic bearing did not include any portion of the grooved region and thus will produce conservative results in regard to load capacity. Because the grooved portion is not considered in this analysis and because inherent compensation is used

the computer results indicated stable operation for the bearing throughout its entire operating range.

To investigate the consequences of the grooved portion on stability a bearing consisting of a combination of inherent compensation with a recess area that is not directly fed must be examined. A somewhat similar bearing was analyzed for the bearings of the turbo-altermator used in the same Brayton-cycle as the turbine-compressor for which this report is pertinent. The analysis for the alternator bearing is fully described in Reference (13). The variance in geometry, however, did require that certain modifications be made to the alternator computer program which also dilutes the accuracy of the analysis. Nevertheless it is felt that a good indication of stability characteristics is provided.

7.4.2 Pre-Loaded Pair Performance

Performance was obtained, using the computer programs over a variety of operating conditions. Load and flow characteristics were determined using program 1 for supply pressures of 100, 80 and 60 psia. These results are shown on Figures 42 thru 47. Negative total loads imply that the external load is applied toward the main bearing. Using program 2, which is the modified version of the program described in Reference (13), stability characteristics were ascertained. Figure 48 indicates the effects of varying the groove depth in the spiral groove. The critical groove depth is that depth at which instability will be initiated. Figure 49 indicates the critical load as a function of supply pressure. For most of the range of each curve the greater the groove depth, the greater is the load the bearing can withstand before reaching the unstable region. This seems contrary to the usual conditions. The reason is that as the groove depth increases, the influence of the grooved region on bearing performances decreases. Since flow resistance is an inverse function of the clearance to the third power, a slight increase in groove depth decreases the grooved regions resistance substantially. A point is reached when the bearing will operate as if the grooved region was essentially at ambient conditions. At this point stability is no longer a problem since

the bearing is inherently compensated and there are no passages for compressibility effects to set in. The design performance parameters, extracted from the performance curves are on Table 7.

Table 8

Forward Load = 50 lbs

Reaction bearing clearance=8.5 mils
Main bearing clearance=1.5 mils
Supply pressure = 100 psia
Reaction bearing flow = .052 lbs/sec
Main bearing flow = .006 lbs/sec
Critical load = 132 lbs

Reverse Load = 100 lbs

Reaction bearing clearance=0.8 mils
Main bearing clearance=9.2 mils
Supply pressure=100 psia
Reaction bearing flow=.005 lbs/sec
Main bearing flow=.040 lbs/sec

Note: Reverse load stability is not critical because reverse bearings do not have any significant recessed areas.

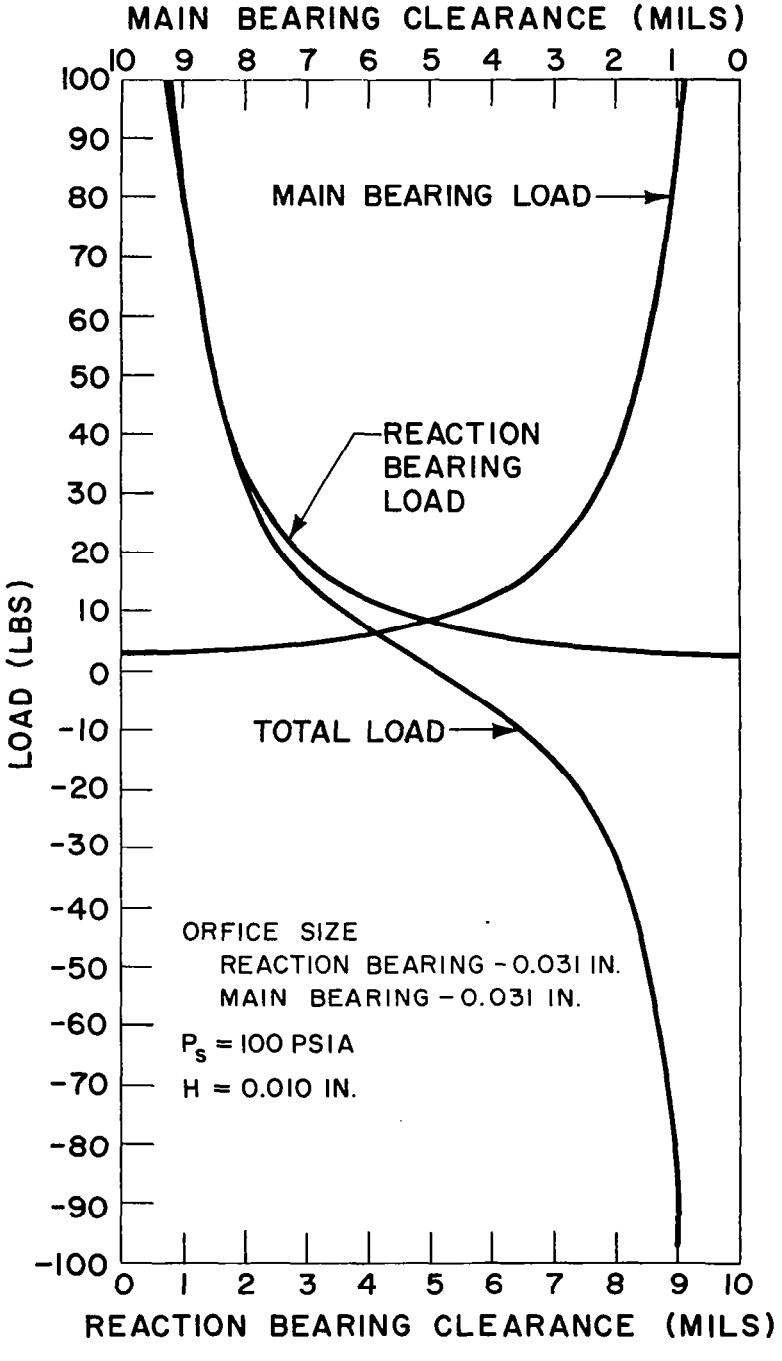

Fig. 42 - Load vs. Clearance - Preloaded Pair - P_s = 100 psia

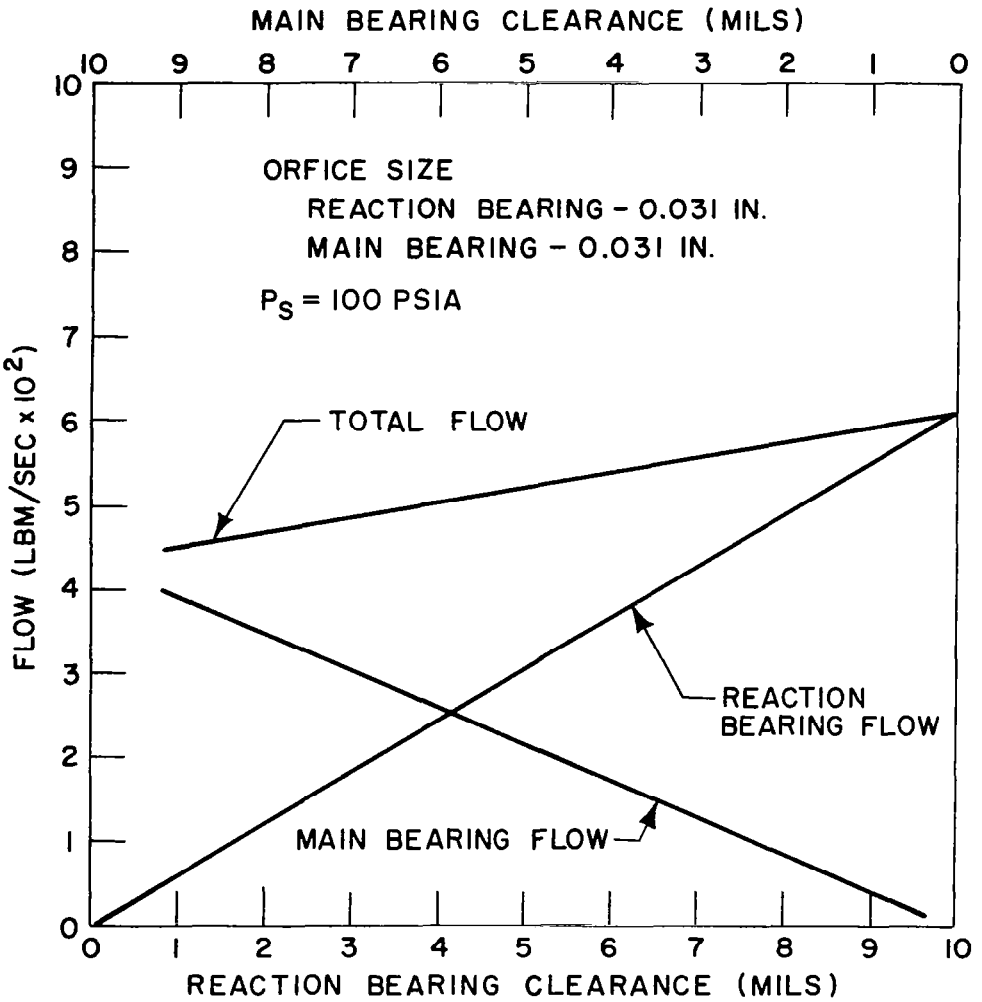

Fig. 43 - Flow vs. Clearance - Preloaded Pair - P_s = 100 psia

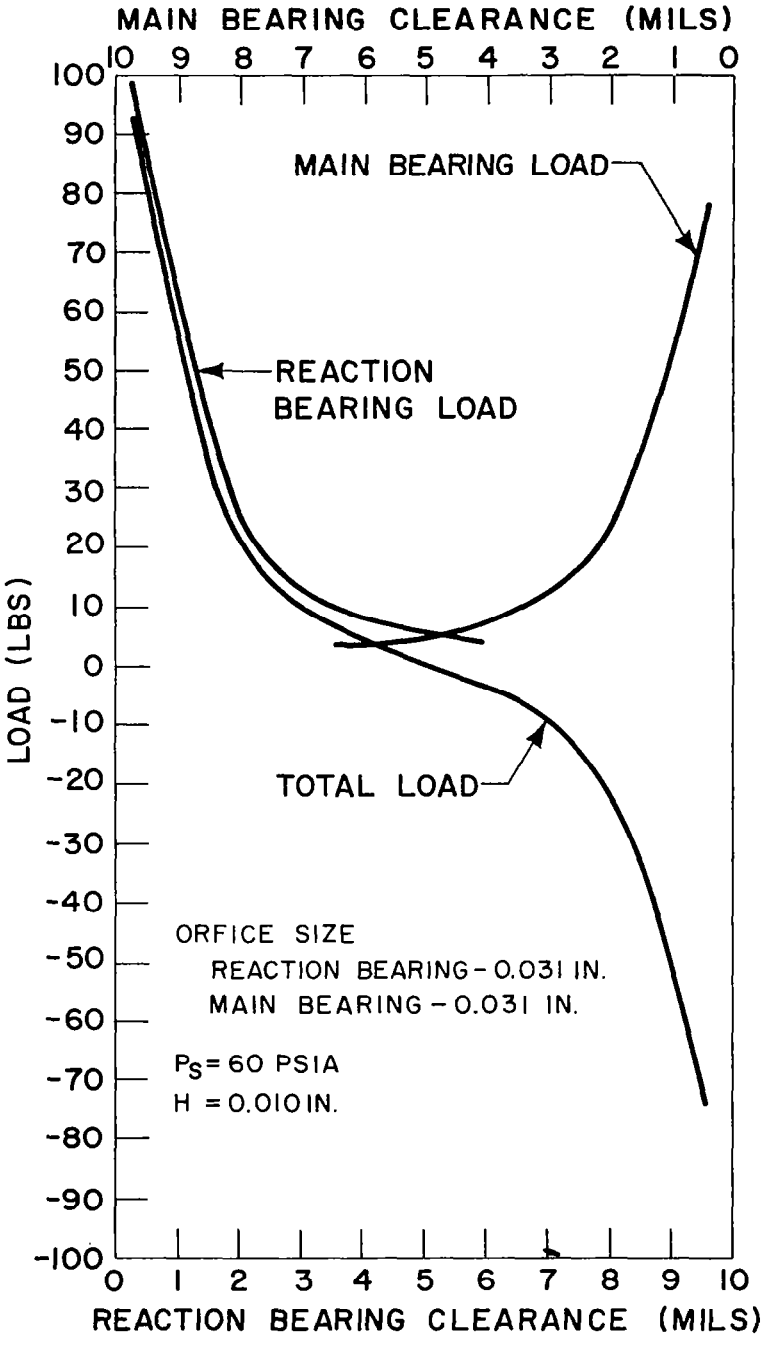

Fig. 44 - Load vs. Clearance - Preloaded Pair - P_s = 80 psia

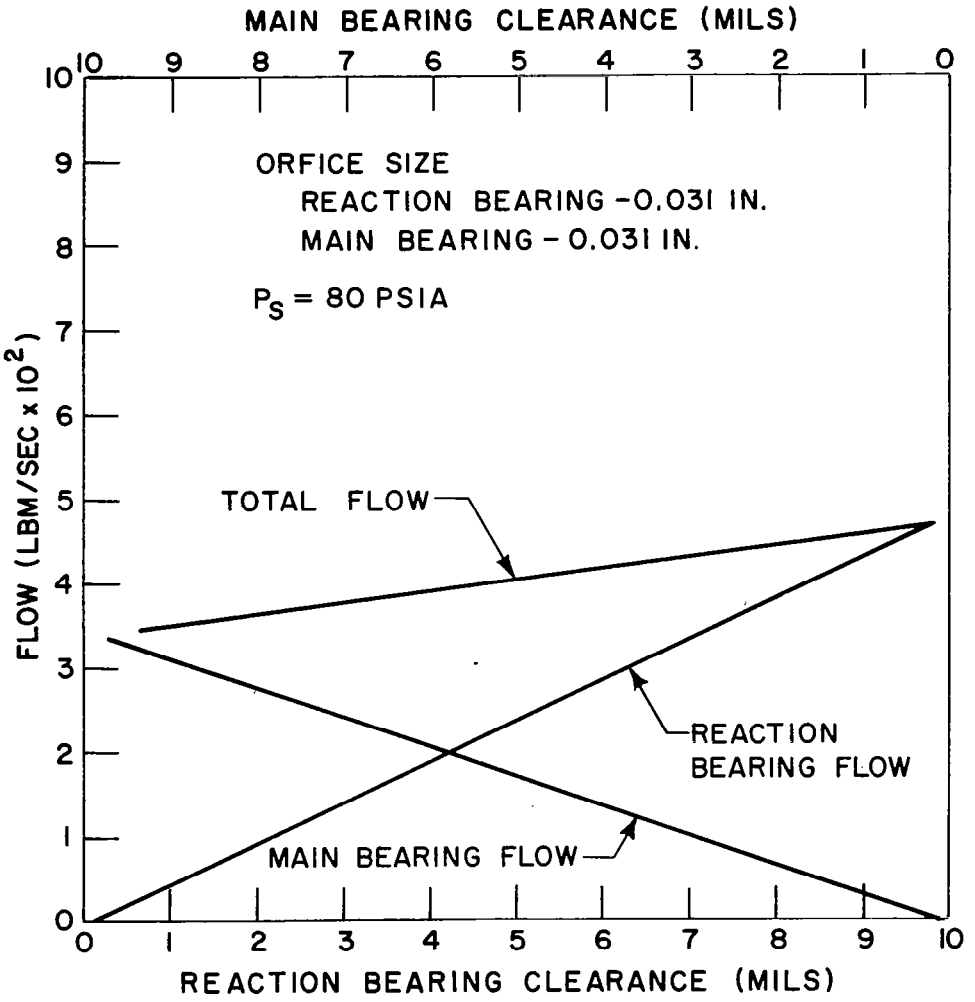

Fig. 45 - Flow vs. Clearance - Preloaded Pair - P_s = 80 psia

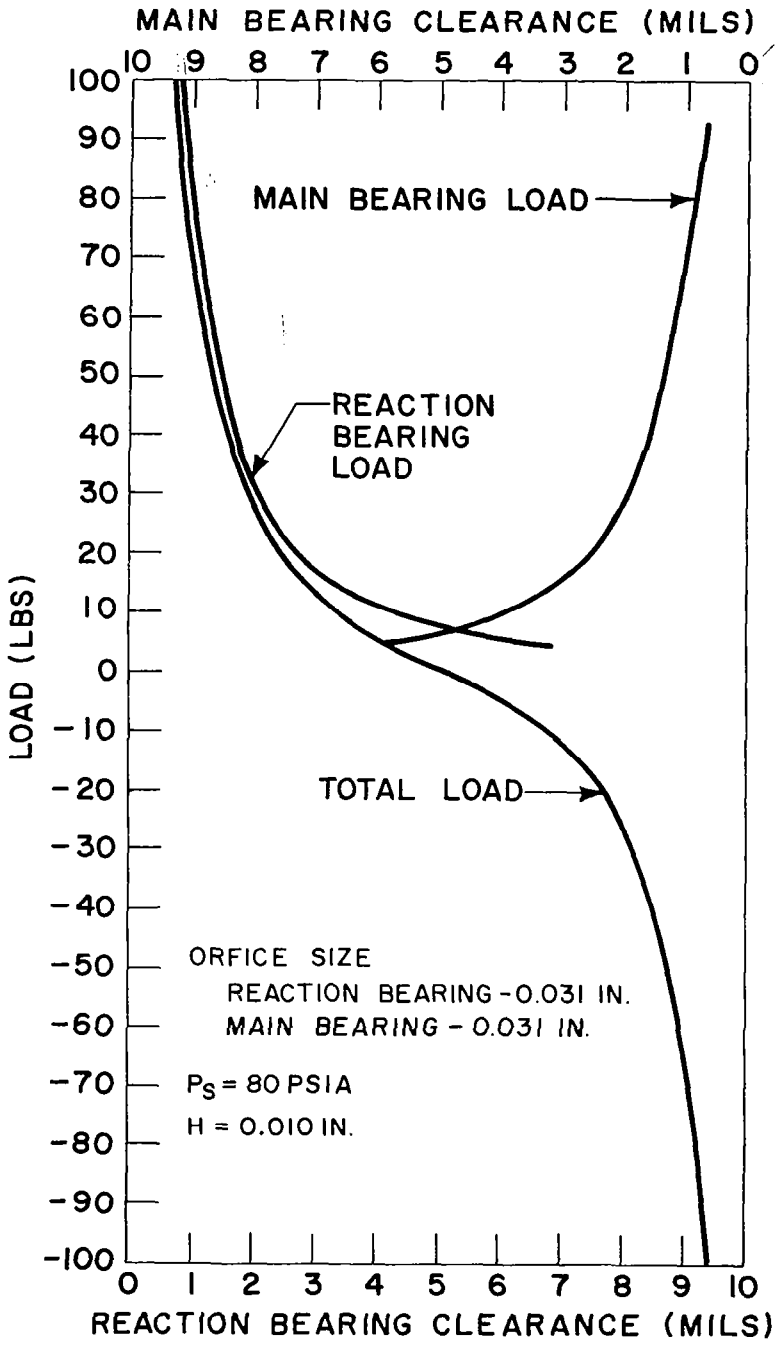

Fig. 46 - Load vs. Clearance - Preloaded Pair - P_s = 60 psia

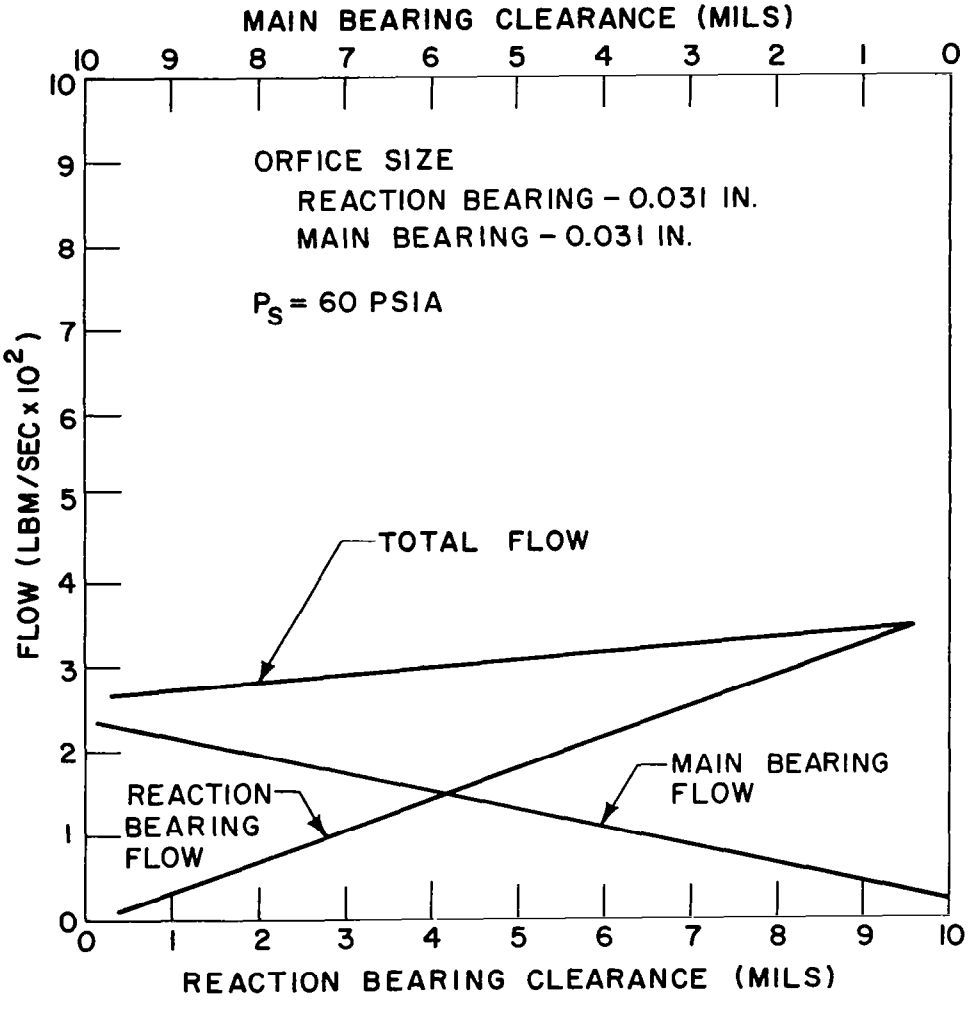

Fig. 47 - Flow vs. Clearance - Preloaded Pair - P_s = 60 psia

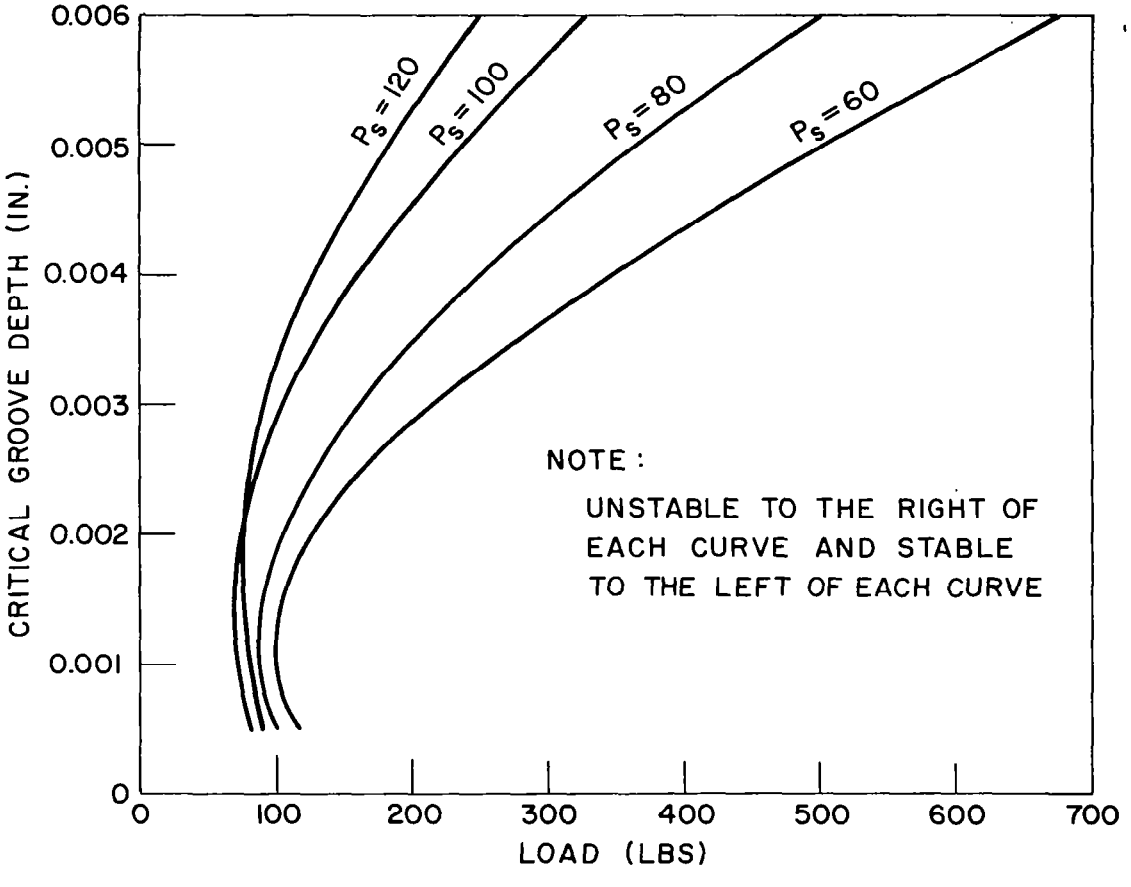

Fig. 48 - Spiral Groove Thrust Bearing Critical Groove Depth vs. Load at Various Supply Pressures

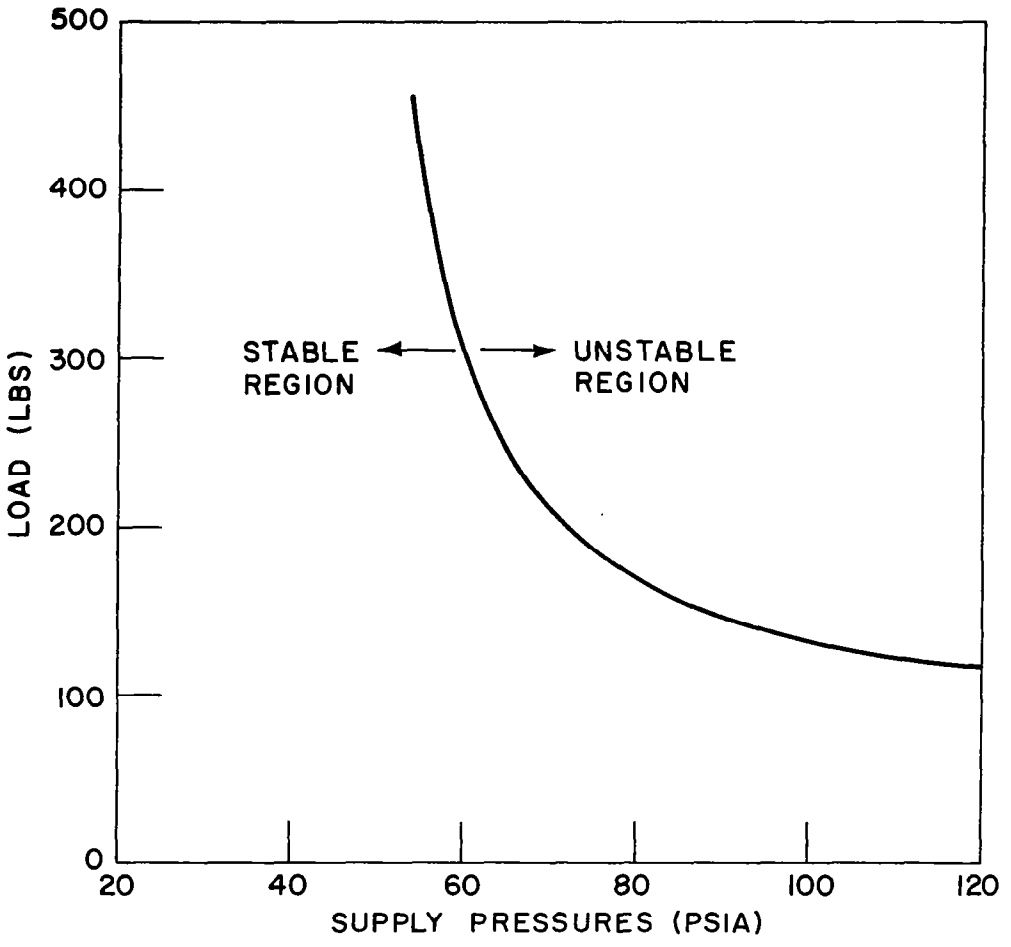

Fig. 49 - Spiral Groove Thrust Bearing Critical Load vs. Supply Pressure at .00371 in. Groove Depth

8. REFERENCES

(1) Gross, W. A., *Gas Film Lubrication*, John Wiley and Sons, Inc., Copyright 1962.

(2) Wildmann, M., Glaser, J., Moore, D. E., Road, L., Cooper, S., *The Gas-Lubricated Stepped Thrust Bearings, a Comprehensive Study*, ASME, 64-Lubs-6.

(3) Rippel, H., *Cast Bronze Thrust Bearing Design Manual*, to be published.

(4) Wilcock, D. F., *The Hydrodynamic Pocket Bearing*, Transactions of the ASME, April 1965.

(5) Muijderman, E. A. *Spiral Groove Bearings*, Ph.D Thesis, March 1964, University of Delft, Netherlands.

(6) Wildmann, M. *Grooved-Plate, Gas-Lubricated Thrust Bearings, with Special Reference to the Spiral Groove Bearings*, 64-Lub-25.

(7) Castelli, V., Elrod, H. G., *Solution of the Stability Problem for 360 Deg. Self-Acting, Gas-Lubricated Bearings*, ASME paper No. 64-Lubs-10.

(8) Elrod, H. G., McCabe, J. T., *An Analysis of the Trailing-Edge Effect in Slider and Partial Arc Gas-Lubricated Bearings*, FIRL Interim Report No. I-A2049-22, December 1964, Contract Nonr-2342 (00) Task NR 062-316.

(9) Marsh, H., *The Stability of Aerodynamic Gas Bearings*, Mechanical Engineering Science, Monograph No. 2, June 1965, Inst. of Mech. Eng., 1 Birdcage Walk, Westminster, SW1, England.

(10) Pratt & Whitney Aircraft Preliminary Layout Drawing L-67680 for Engineering Order 702930-17, *No. 1 Bearing Area Turbo Compressor (Franklin Institute Bearing)*.

(11) Licht, L., Fuller, D. D., Sternlicht, B., *Self Excited Vibrations of an Air-Lubricated Thrust Bearing*, ASME Transactions, Vol. 80, No. 2, 1958.

(12) Licht, L., *Air Hammer Instability Pressurized-Journal Gas Bearing*, Journal of Basic Engineering, June 1961.

(13) Shapiro, W., McCabe, J. T., Chu, T. Y., Castelli, V., *Hybrid Gas Bearings for a Brayton Cycle Turbine - Alternator,* Franklin Institute Report F-B2263, April 1965.

(14) Burgdorfer, A., *The Influence of the Molecular Mean Free Path on the Performance of Hydrodynamic Gas-Lubricated Bearings,* Trans. Amer. Soc. Mech. Engrs., J. of Basic Engrg., 1959, 80.

(15) Taylor, G. I., *The Stability of a Viscous Liquid Contained Between Two Rotating Cylinders,* Phil. Trans. Roy. Soc. 1923 223 (Series A), 289.

(16) Brand, R. S., *Inertia Forces in Lubricating Films,* Trans. Soc. Mech. Engrs., J. of Appl. Mech., 1955 22 (Series E), 362

(17) Schlechting, H., *Boundary Layer Theory,* McGraw-Hill, New York.

(18) Elrod, H. G., Burgdorfer, A., *Refinements of the Theory of Infinitely-Long Self-Acting, Gas-Lubricated Journal Bearings,* First Interm. Symp. Gas-Lubricated Bearings, Washington, D. C., Oct. 26 - 28, 1959, pp 93-118 (Also FIRL Interim Report I-A2049-10, Jan. 1960, OTS No. AEC - 4688; ASTIA No. AD-232705).

(19) Gunter, E. J., Hinkle, J. G., Fuller, D. D., *Design Guide for Gas-Lubricated Tilting-Pad Journal and Thrust Bearings with Special References to High-Speed Rotors,* prepared by FIRL Report I-A2922-3-1, U. S. Atomic Energy Commission Report NYO-2512-1 dated November 1964.

(20) Castelli, V., Pirvics, J., *Equilibrium Characteristics of Axial Groove Gas-Lubricated Bearings,* Columbia University, Department of Mechanical Engineering, Lubrication Research Laboratory Report, November 1, 1965.

(21) Whitley, S., Williams, L. G., *The Gas-Lubricated Spiral Groove Thrust Bearing,* United Kingdom Atomic Energy Authority, I. G. Report 28 (RD/CA), February 18, 1959.

APPENDIX I

A REVIEW OF THE DERIVATION AND THE FINITE DIFFERENCE FORM OF THE REYNOLDS EQUATION

In order to accept the use of Reynolds equation in the steady-state and dynamics analyses, it is advisable to first review the assumptions and restriction involved in its derivation.

The gas in the clearance space can be considered as a continuum, provided that the radial clearance be at least one hundred times greater than the molecular mean free path[14]. Under the anticipated bearing operating conditions, the bearing lubricant argon has a molecular mean free path of 4.7×10^{-6} inches. This implies that the Reynolds equation is applicable for clearance down to about 0.47×10^{-3} inches, which is smaller than all of the design clearances. It might be noted here that the molecular mean free path of ambient air is 2.52×10^{-6} inches.

The upper limit for laminar flow in the clearance space is usually associated with the on-set of the formation of ring vortices. The criterion given by G. I. Taylor[15] for the critical Reynolds number is

$$Re_c = \sqrt{R/C}$$

for Bearing 1

$$Re_c = 796$$

the Reynolds number is given by

$$Re = \frac{\rho \Omega R C}{\mu}$$

and for the conditions prevailing at bearing 1

$$Re = \frac{0.1373 \times 10^{-6} \times 5236 \times 0.75 \times .002}{3.6 \times 10^{-9}}$$

$$Re = 300$$

The flow conditions within the film can therefore be considered as laminar.

The inertia forces of the gas lubricant have been shown by Brand[16] to be negligible when

$$Re < R/C$$

a condition which is obviously satisfied.

The flow in the bearing clearance is governed by the Navier-Stokes[17] equation. Using the above assumptions together with the fact that since the film height is small compared to the other dimensions of the bearing, the velocity component normal to the bearing surface (y direction) is negligible compared to the x and z components and that the variation of the velocity in the x, z directions is also negligible compared with the y direction.

The Navier-Stoken equation can now be reduced to

$$\frac{\partial p}{\partial x} = \frac{\partial}{\partial y}\left(\mu \frac{\partial u}{\partial y}\right) \qquad \text{(I-1)}$$

$$\frac{\partial p}{\partial y} = 0 \qquad \text{(I-2)}$$

$$\frac{\partial p}{\partial z} = \frac{\partial}{\partial y}\left(\mu \frac{\partial w}{\partial y}\right) \qquad \text{(I-3)}$$

Equation (I-2) states that there is no pressure variation across the film. Equations (I-1) and (I-3) can be integrated using the "no-slip" boundary condition

at $y = o$ $u = o$

and at $y = h$ $u = U$

The integrated results gives the velocity profile in the circumferential direction as

$$u = \frac{y\ (y - h)}{2\mu} \frac{\partial p}{\partial x} + \frac{Uy}{h} \tag{I-4}$$

and in the axial direction as

$$w = \frac{y\ (y - h)}{2\mu} \frac{\partial p}{\partial z} \tag{I-5}$$

where the "entrance" effects at the bearing edges have been ignored.

Letting

$$x = R\theta$$

$$z = L\zeta$$

$$t = \frac{2T}{\Omega}$$

the equation of flow continuity can be written

$$\frac{1}{R} \frac{\partial}{\partial \theta} \{ \int_o^h \rho u \, dy \} + \frac{1}{L} \frac{\partial}{\partial \zeta} \{ \int_o^h \rho w \, dy \} \quad \frac{\partial}{\partial T} \int_o^h \frac{\Omega \rho}{2} \, dy \tag{I-6}$$

Substituting I-4 and I-5 into I-6

$$\frac{\partial}{\partial \theta} \left[\frac{\rho h^3}{\mu} \frac{\partial p}{\partial \theta} \right] + \left(\frac{R}{L}\right)^2 \frac{\partial}{\partial \zeta} \left[\frac{\rho h^3}{\mu} \frac{\partial p}{\partial \zeta} \right] = 6R^2 \Omega \left[\frac{\partial\ (\rho h)}{\partial \theta} + \frac{\partial \rho}{\partial T} \right] \tag{I-7}$$

where $\Omega = RU$

To further simplify equation (I-7) the following additional assumptions are made:

a) $p \propto \rho$

Although the compression and expansion of a gas at high frequency is usually adiabatic, the thinness of the film and the relatively large metal mass of the bearing surfaces make the process more nearly isothermal[18]. This assumption essentially assumes the bearing fluid as a "perfect" gas which obeys the ploytropic relation $p\ \rho^{-n}$ = constant where n is taken as 1 (isothermal).

b) $\mu = \mu_a$

For pressure variation of less that about 100 psi the viscosity of an isothermal gas is essentially constant.

c) For the steady-state analysis

$$\frac{\partial}{\partial T} = 0$$

Using the following definitions

$$p = p_a P$$

$$h = CH$$

$$\Lambda = \frac{6\mu\Omega}{p_a} \left(\frac{R}{C}\right)^2$$

equation I-7 becomes

$$\frac{\partial}{\partial\theta}\left[PH^3 \frac{\partial P}{\partial\theta}\right] + \left(\frac{R}{L}\right)^2 \frac{\partial}{\partial\zeta}\left[PH^3 \frac{\partial P}{\partial\zeta}\right] = \Lambda \frac{\partial}{\partial\theta}(PH) \qquad \text{(I-8)}$$

The expression for the local film clearance for a bearing pad of wrap angle α is obtained by choosing a set of coordinate x, y, z with the origin at the shoe center of curvature in the axial mid-plane of the bearing (Figure 1). The translation of the shaft in the bearing is given by x and y; the angular coordinates of the rigid shaft are given by α_1 and α_2.

The local film clearance "h" can be thought of as consisting of the following components:

a. the concentric clearance: "C"

b. the displacement of the shaft mass center from the origin: $x \sin \theta + y \cos \theta$

c. the rotation of the shaft about the mass center: $z\alpha_1 \sin \theta + z\alpha_2 \cos \theta$ where $-L/2 \leq z \leq L/2$

Combining the above three components

$$h = C + \left[x + (z - L/2)\ \alpha_1\right] \sin \theta + \left[y + (z - L/2)\ \alpha_2\right] \cos \theta \quad \text{(I-9)}$$

Letting

$$x = CX$$

$$y = CY$$

$$\zeta = z/L - 1/2$$

$$\alpha_1 = \frac{CA_1}{L}$$

$$\alpha_L = \frac{CA_2}{L}$$

equation I-9 becomes

$$H = 1 + \left(X + A_1\ \zeta\right) \sin \quad + \left(Y + A_2\ \zeta\right) \cos \theta \quad \text{(I-10)}$$

The shaft friction moment f_m is given by

$$f_m = \int_0^L \int_{\zeta}^{\zeta+\alpha} \tau R^2 d\theta dz \quad \text{(I-11)}$$

where

$$\tau = \mu \left.\frac{du}{dy}\right|_{y=h}$$

From equation (I-4) with $x = R\theta$

$$\left.\frac{du}{dy}\right|_{y=h} = \frac{h}{2\mu R} \frac{\partial p}{\partial \theta} + \frac{R\Omega}{h}$$

Dividing I-11 by $P_a RL$ and using the previously defined non-dimensional variables

$$F_m = \frac{f_m}{P_a RCL} = \int_{-1/2}^{1/2} \int_{\zeta}^{\zeta+\alpha} \left(H \frac{\partial P}{\partial \theta} + \frac{\Lambda}{3H} \right) d\theta d\zeta$$

Finite Difference Form of the Reynolds Equation

The use of "P" as the dependent variable in Equation (I-8) has the disadvantage that the pressure varies very rapidly near the trailing edge; $\frac{\partial P}{\partial \theta}$ has an even larger variation and, in addition, $\frac{\partial P}{\partial \theta}$ changes sign across the point of maximum pressure. In order to facilitate the numerical process, the dependent variable is chosen as $Q = P^2H^2$. The selection of Q is made because it tends to be constant on the bearing interior and vary linearly at the edges. Therefore, derivatives of Q are relatively smooth and do not tend to change sign; a condition which greatly enhances numerical stability.

In Equation (I-8), letting $Q = P^2H^2$, the first term on the left hand side becomes

$$\frac{\partial}{\partial \theta} \left[PH^3 \frac{\partial}{\partial \theta} \right] = \frac{\partial P}{\partial \theta} \left[\frac{H}{2} \frac{\partial Q}{\partial \theta} - Q \frac{\partial H}{\partial \theta} \right] = -\frac{1}{2} \frac{\partial H}{\partial \theta} \frac{\partial Q}{\partial \theta} + \frac{H}{2} \frac{\partial^2 Q}{\partial \theta^2} - Q \frac{\partial^2 H}{\partial \theta^2}$$

Therefore, the Reynolds equation in terms of Q is written

$$-\frac{1}{2} \frac{\partial H}{\partial \theta} \frac{\partial Q}{\partial \theta} + \frac{H}{2} \frac{\partial^2 Q}{\partial \theta^2} - Q \frac{\partial^2 H}{\partial \theta^2} + \left(\frac{R}{L} \right)^2 \left[-\frac{1}{2} \frac{\partial H}{\partial \zeta} \frac{\partial Q}{\partial \zeta} + \frac{H}{2} \frac{\partial^2 Q}{\partial \zeta^2} \right] - Q \frac{\partial^2 H}{\partial \zeta^2} = \frac{\Lambda}{2\sqrt{Q}} \frac{\partial Q}{\partial \theta} \quad \text{(I-12)}$$

Letting the grid interval counter "i" run in the circumferential direction and the counter "j" in the axial direction, the derivitives of Q can be approximated as follows:

$$\frac{\partial Q}{\partial \theta} = \frac{Q_{i+1,j} - Q_{i-1,j}}{2\Delta\theta} \tag{I-13}$$

$$\frac{\partial^2 Q}{\partial \theta^2} = \frac{Q_{i+1,j} - 2Q_{i,j} + Q_{i-1,j}}{(\Delta\theta)^2} \tag{I-14}$$

$$\frac{\partial \theta}{\partial \zeta} = \frac{Q_{i,j+1} - Q_{i,j-1}}{2\Delta\zeta} \tag{I-15}$$

$$\frac{\partial^2 Q}{\partial \zeta^2} = \frac{Q_{i,j+1} - 2Q_{i,j} + Q_{i,j-1}}{(\Delta\zeta)^2} \tag{I-16}$$

Substituting (I-13) through (I-16) into (I-12) and solving for $Q_{i,j}$

$$\begin{aligned} Q_{i,j} = 4\Delta\theta \left[\frac{H_{i,j}}{(\Delta\theta)^2} + \frac{\partial^2 H_{i,j}}{\partial\theta^2} + \left(\frac{R}{L}\right)^2 \left(\frac{H_{i,j}}{(\Delta\zeta)^2} + \frac{\partial^2 H_{i,j}}{\partial\zeta^2} \right) \right] \times \\ \left\{ \left[-\frac{\partial H_{i,j}}{\partial\theta} + \frac{2H_{i,j}}{\Delta\theta} - \frac{\Lambda}{\sqrt{Q_{i,j}}} \right] Q_{i+1,j} \right. \\ + \left[\frac{\partial H_{i,j}}{\partial\theta} + \frac{2H}{\Delta\theta} + \frac{\Lambda}{\sqrt{Q_{i,j}}} \right] Q_{i-1,j} \\ + \left[\left(\frac{R}{L}\right)^2 \Delta\theta \left(-\frac{\partial H_{i,j}}{\partial\zeta} + \frac{2H_{i,j}}{(\Delta\zeta)^2} \right) \right] Q_{i,j+1} \\ \left. + \left[\left(\frac{R}{L}\right)^2 \Delta\theta \left(\frac{\partial H_{i,j}}{\partial\zeta} + \frac{2H_{i,j}}{(\Delta\zeta)^2} \right) \right] Q_{i,j-1} \right\} \end{aligned} \tag{I-17}$$

Equation (I-17) is not linear because the term $\sqrt{Q_{i,j}}$ appears on the right hand side. This situation is circumvented by using a relaxation procedure in which the previous value of $Q_{i,j}$ is used for the right hand

side of Equation (I-17). As the process converges, this approximation becomes better and better. Letting $\bar{Q}_{i,j}$ be the value of Q computed by Equation (I-17) and $\bar{\bar{Q}}_{i,j}$ be the previous value of Q, then the new value of Q is given by

$$Q_{i,j} = \Gamma \bar{Q}_{i,j} + (1-\Gamma)\, \bar{\bar{Q}}_{i,j} \qquad \text{(I-18)}$$

when Γ is a relaxation factor.

The convergence procudure is accelerated by increasing Γ; numerically stability is enhanced by reducing Γ. It is usually desirable to change Γ as the relaxation process proceeds. An average suitable value of Γ is 0.9. Equation (I-18) is applied to all the interior points of the grid array.

The dervitives of H at the point (i,j) are gotten from Eauation (I-10). They are

$$\frac{\partial H}{\partial \theta} = (X + A_1\zeta) \cos\theta - (Y + A_2\zeta) \sin\theta$$

$$\frac{\partial^2 H}{\partial \theta^2} = -(X + A_1\zeta) \sin\theta - (Y + A_2\zeta) \cos\theta = 1-H$$

$$\frac{\partial H}{\partial \zeta} = A_1 \sin\theta + A_2 \cos\theta$$

$$\frac{\partial^2 H}{\partial \zeta^2} = 0$$

Briefly, the numerical method of solution consists of specifying the clearance distribution H, the bearing number Λ, the warp angle α, the ratio R/L, the pressure boundary conditions and the initial pressure distribution in the bearing. Successive values of the pressure distribution are computed (that obey the given boundary conditions) until the finite difference representation of the Reynolds equation is satisfied within some predetermined truncation constant.

APPENDIX II

FIELD MAPS FOR $\Lambda = 0.5, 3.5, 5.0, 10.0$

$(R/L = 0.5, \alpha = 100^0)$

COMPUTER RESULTS FOR $\alpha = 80^0$

This appendix contains the field maps for Λ's other than the design Λ ($\Lambda = 1.5$). This information was used to determine the optimum design Λ and to determine the influence of pivot location on load, friction, etc.
The field maps are given for:

$\Lambda = 0.5, 3.5, 5$ and 10

$R/L = 0.5$

$\alpha = 100°$

Figure II-9 shows the friction factors vs. pivot film thickness for $\Lambda = 3.5$.

Following the field maps is a tabular listing of the 80° wrap angle computer results which could be used for plotting field maps. At the beginning of the project it was hoped that performance curves for a four pad (80° wrap angle) bearing could be plotted. This phase of the project was dropped in favor of more pressing requirements. The data is presented here as Table II-1 for future reference.

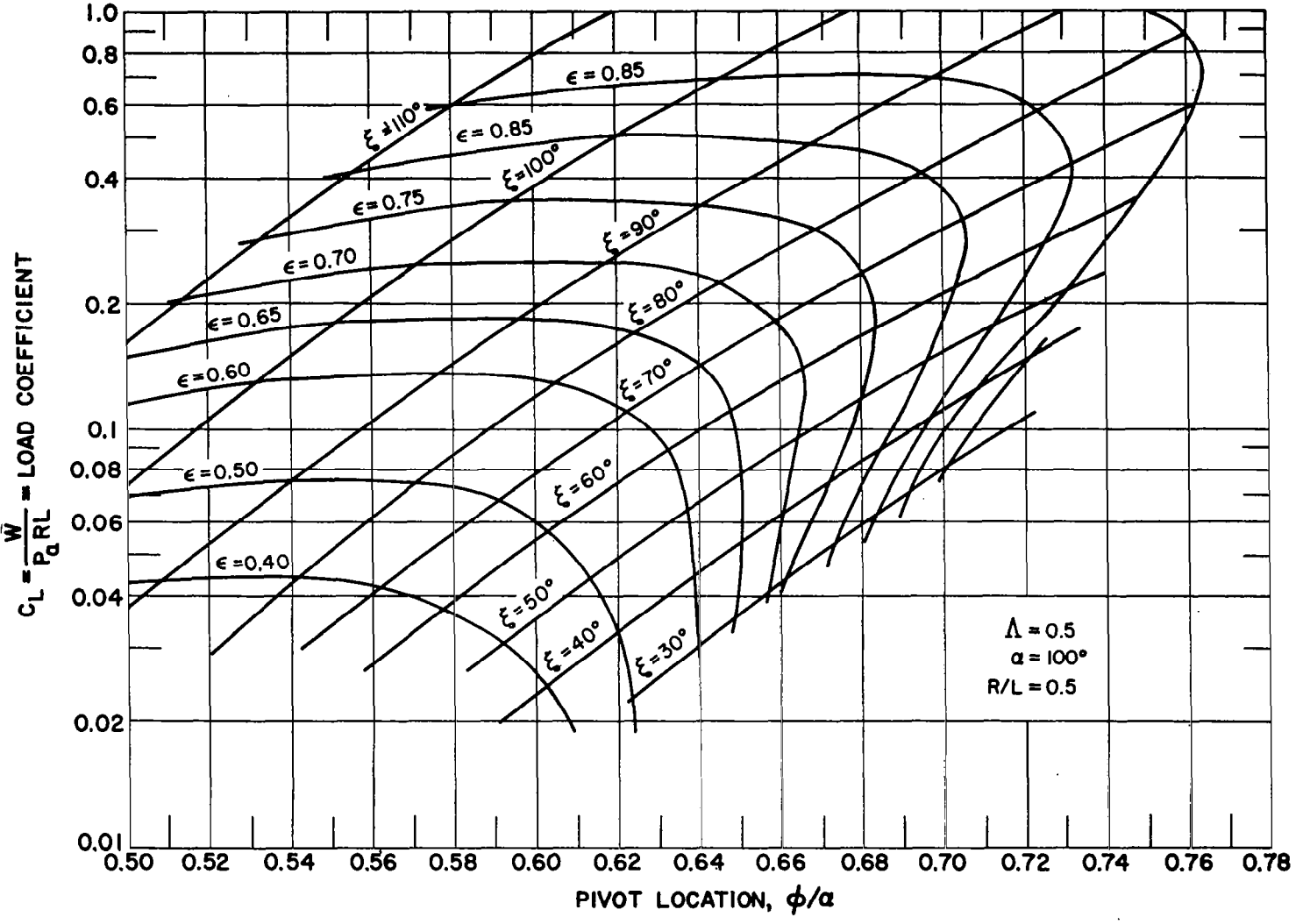

Figure II-1

Load Coefficient vs. Pivot Location for R/L = 0.5, α = 100°, Λ = 0.5

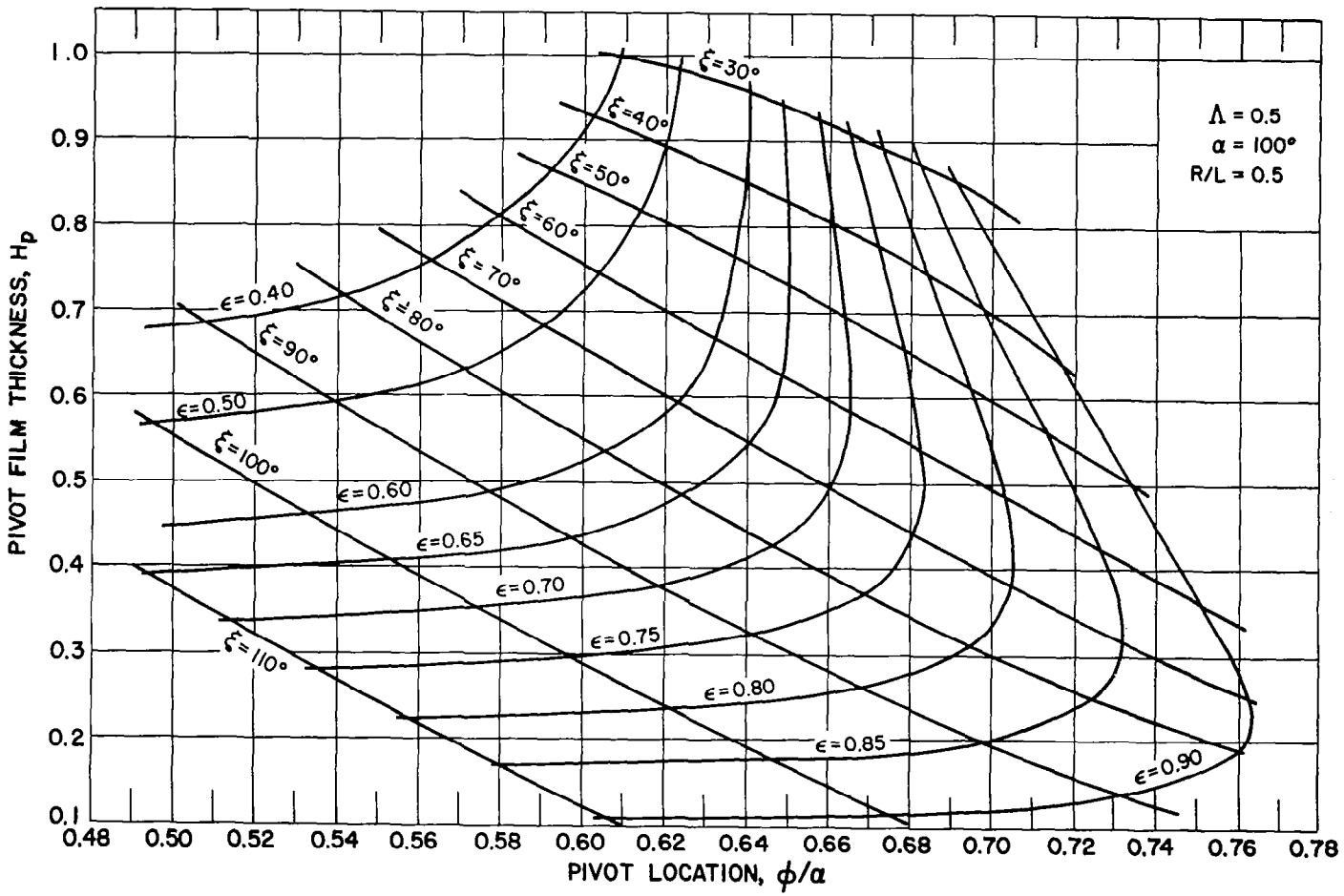

Figure II-2

Pivot Film Thickness vs. Pivot Location for R/L = 0.5, α = 100°, Λ = 0.5

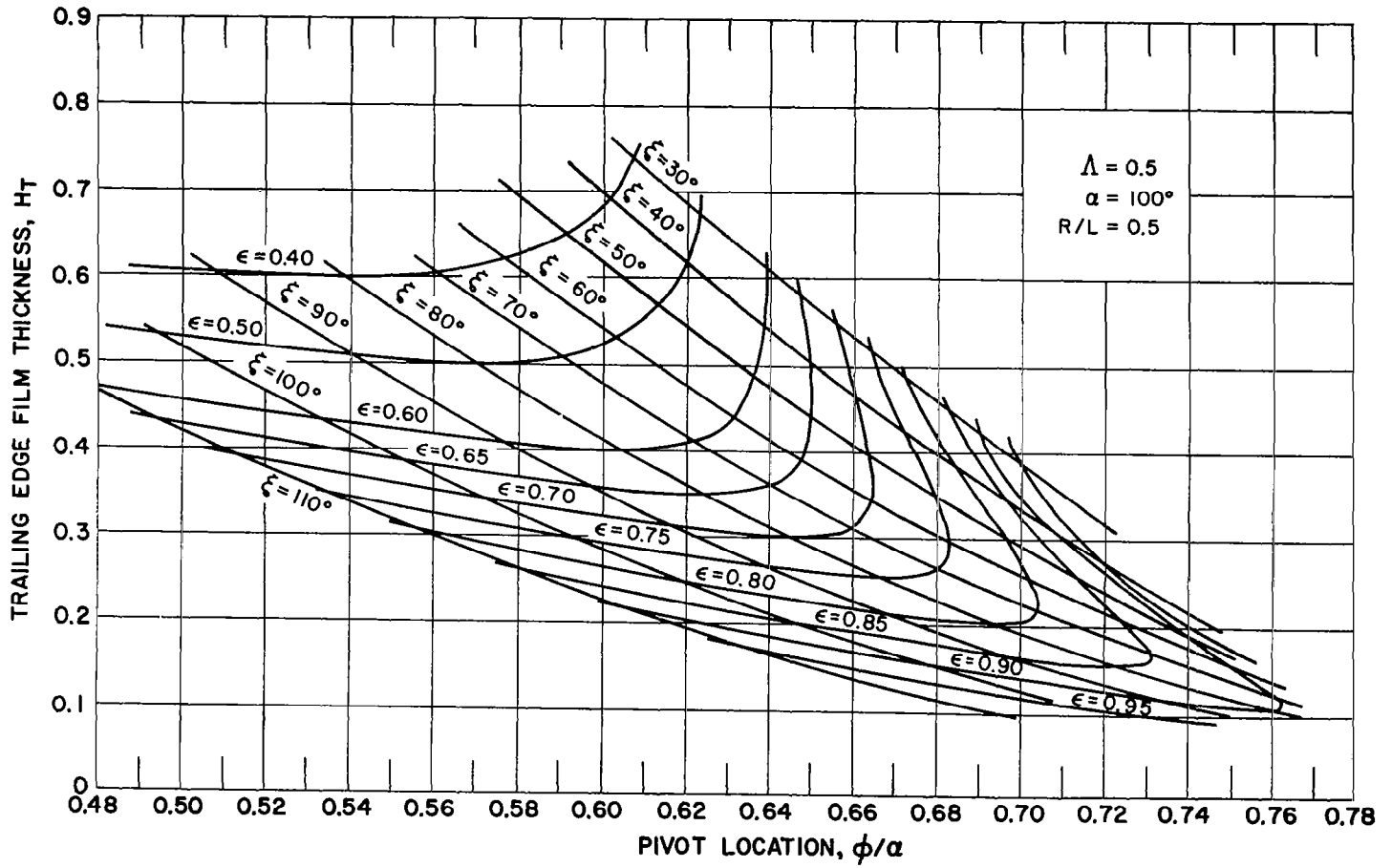

Figure II-3

Trailing Edge Film Thickness vs. Pivot Location for R/L = 0.5, α = 100°, Λ = 0.5

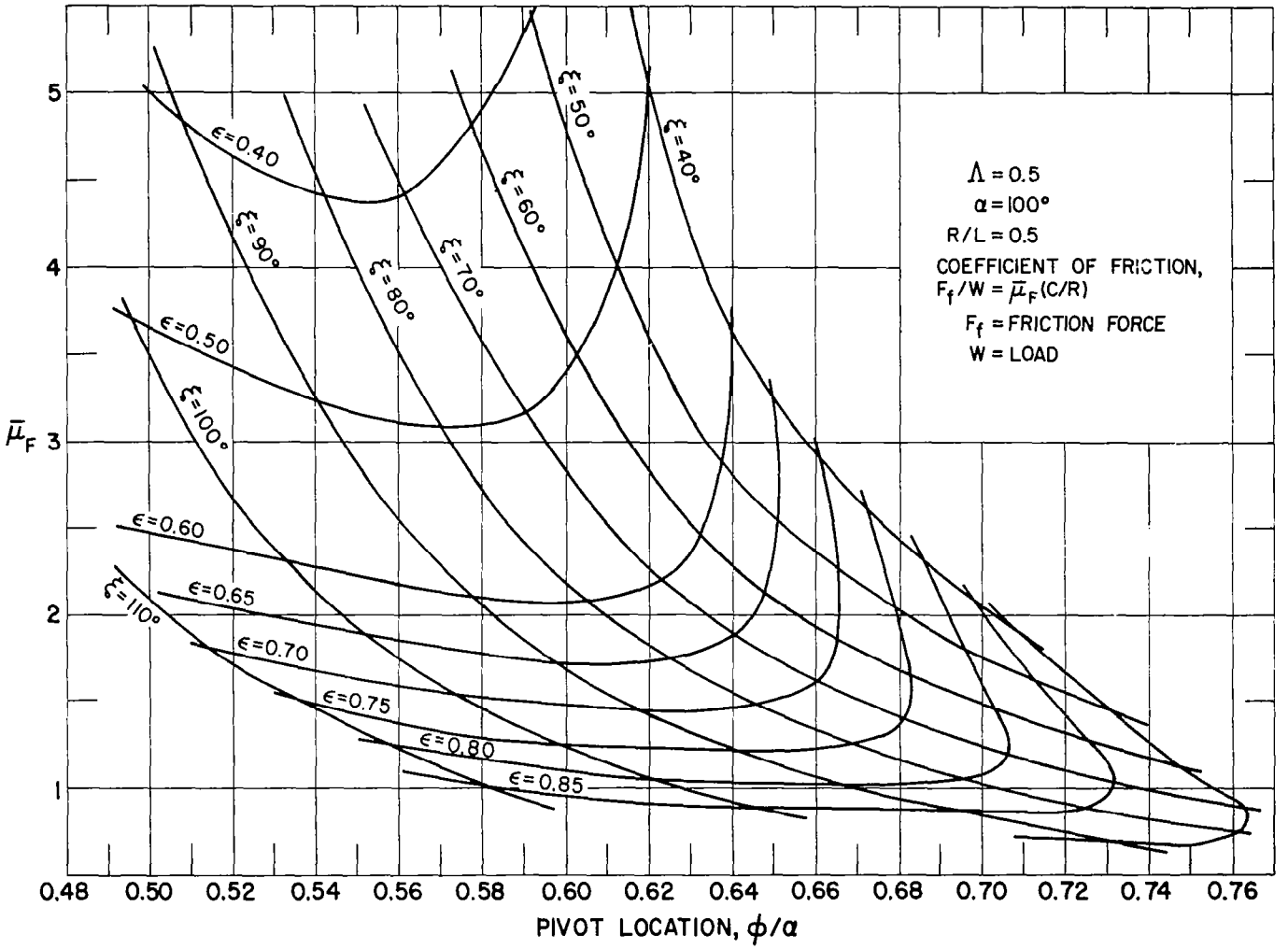

Figure II-4

Friction Factor vs. Pivot Location for R/L = 0.5, α = 100°, Λ = 0.5

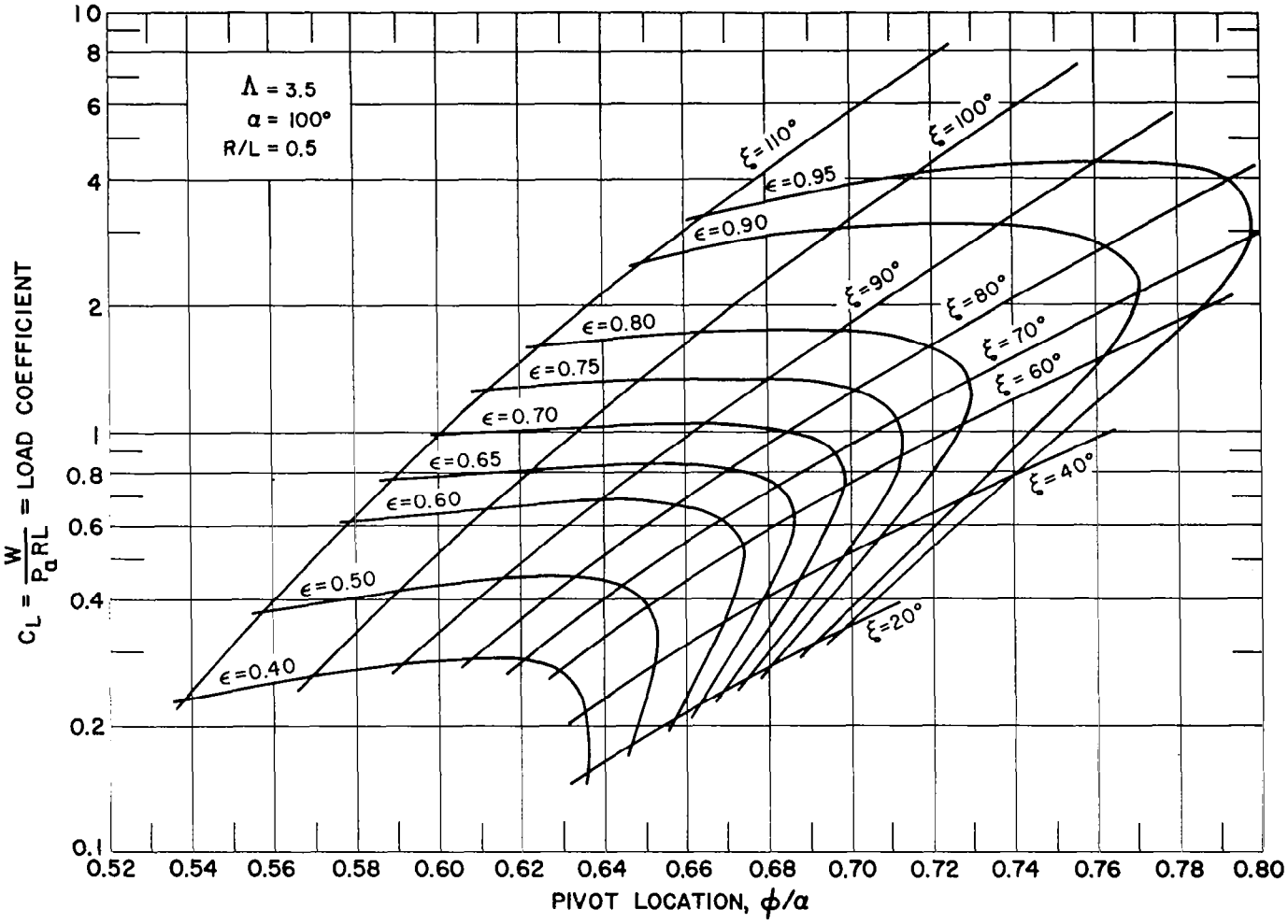

Figure II-5

Load Coefficient vs. Pivot Location for R/L = 0.5, α = 100°, Λ = 3.5

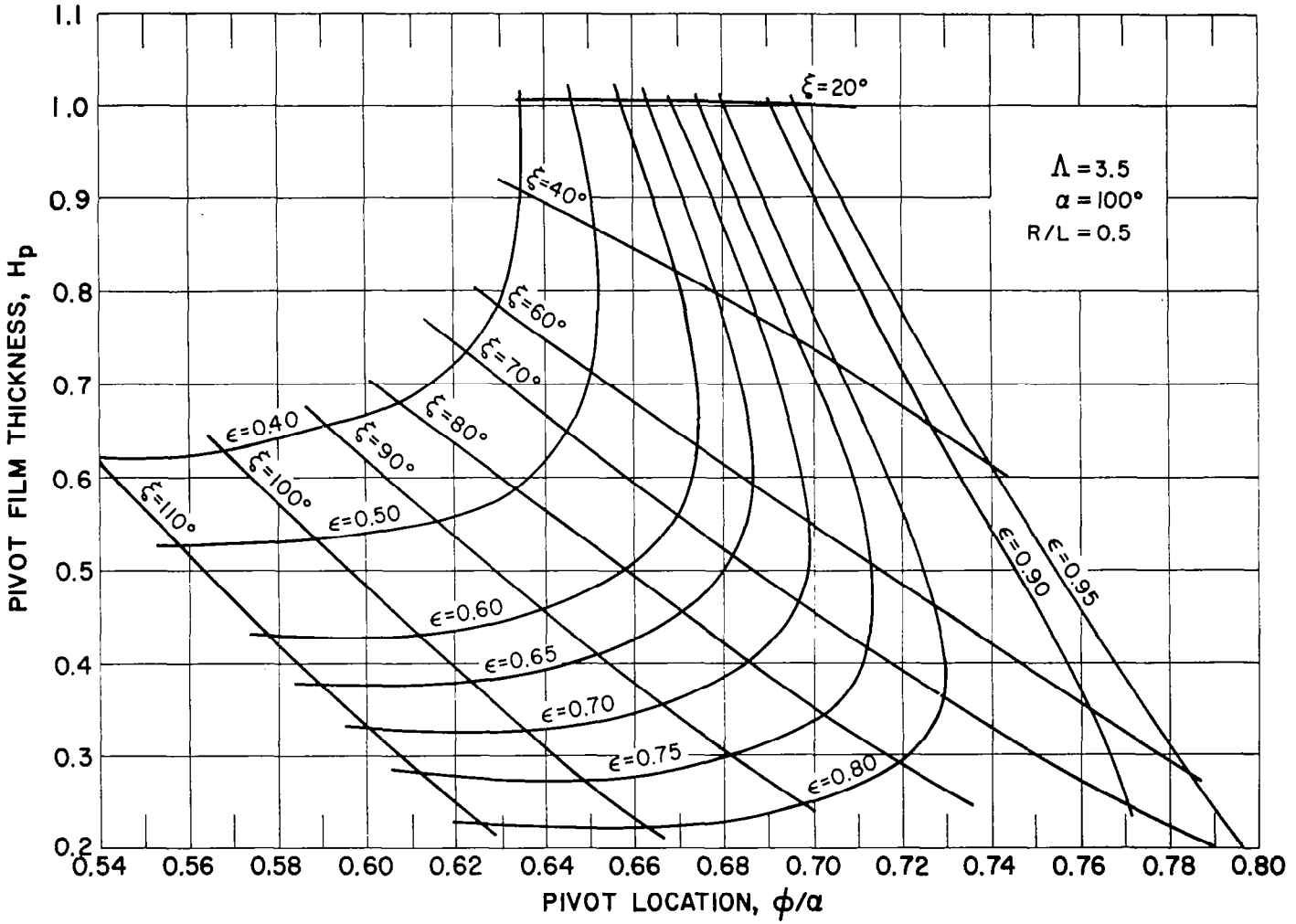

Figure II-6

Pivot Film Thickness vs. Pivot Location for R/L = 0.5, α = 100°, Λ = 3.5

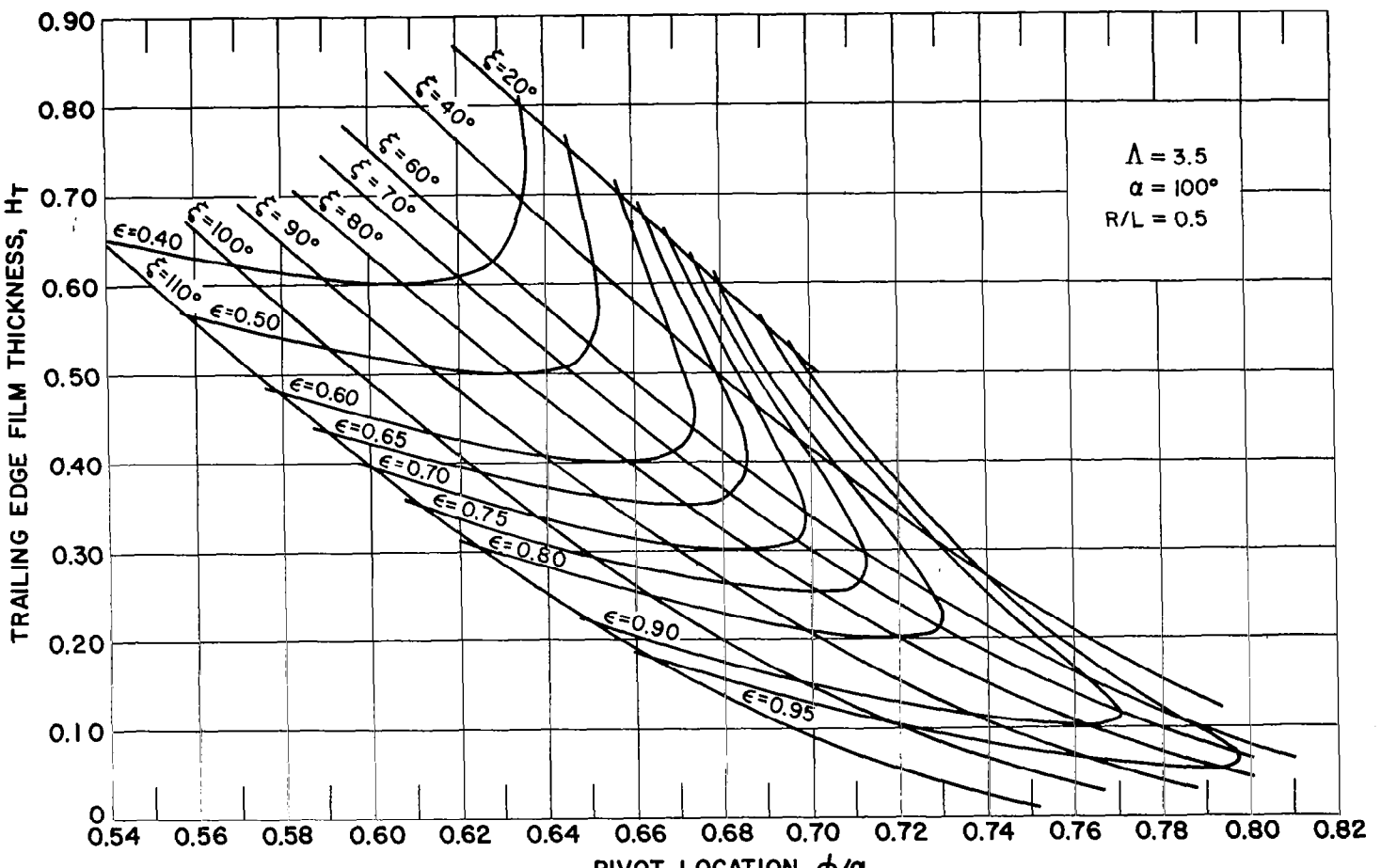

Figure II-7

Trailing Edge Film Thickness vs. Pivot Location for R/L = 0.5, α = 100°, Λ = 3.5

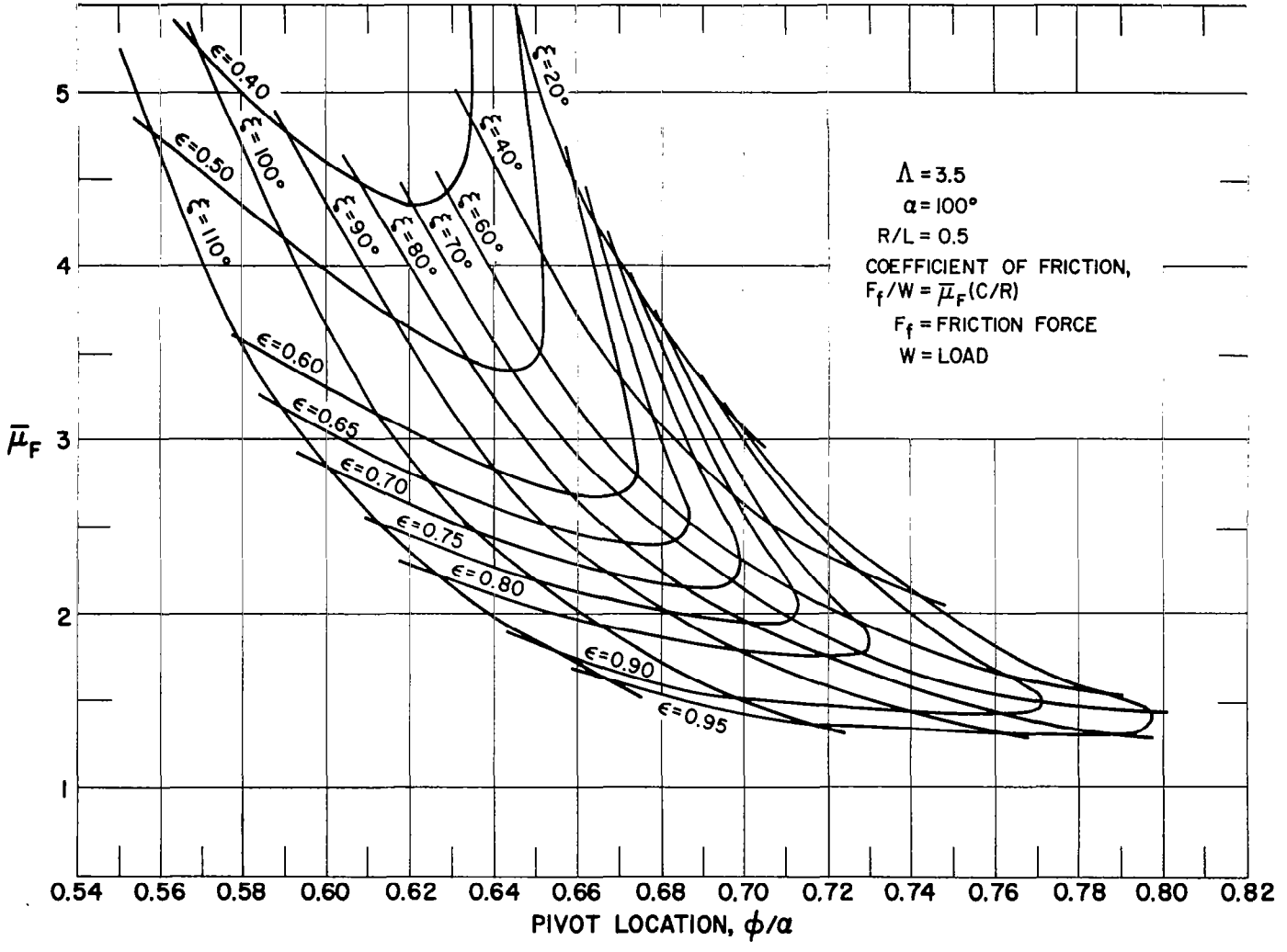

Figure II-8

Friction Factor vs. Pivot Location for R/L = 0.5, α = 100°, Λ = 3.5

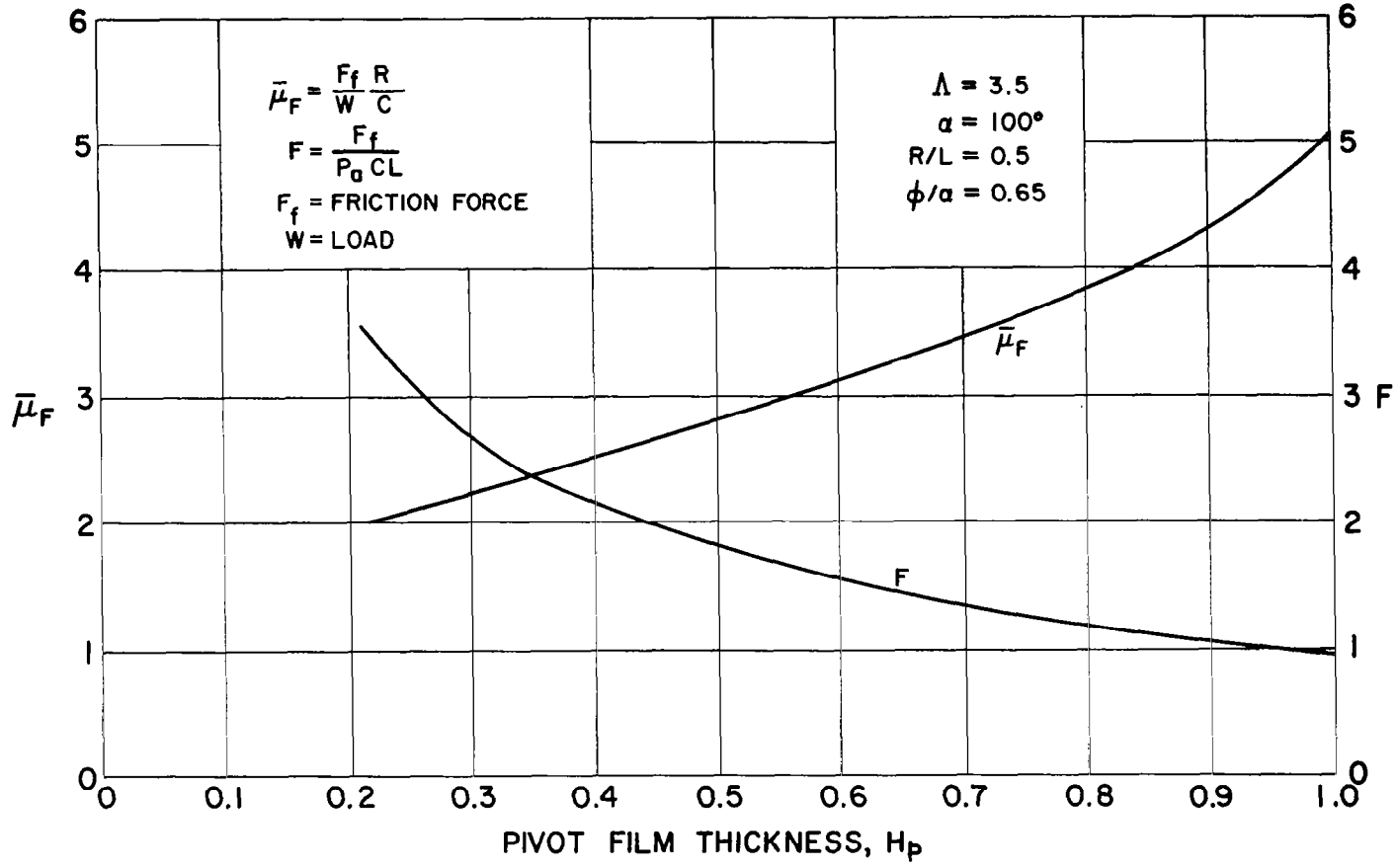

Figure II-9

Friction Coefficient and Friction Factor vs. Pivot Film Thickness for R/L = 0.5, $\alpha = 100°$, $\phi/\alpha = 0.65$, $\Lambda = 3.5$

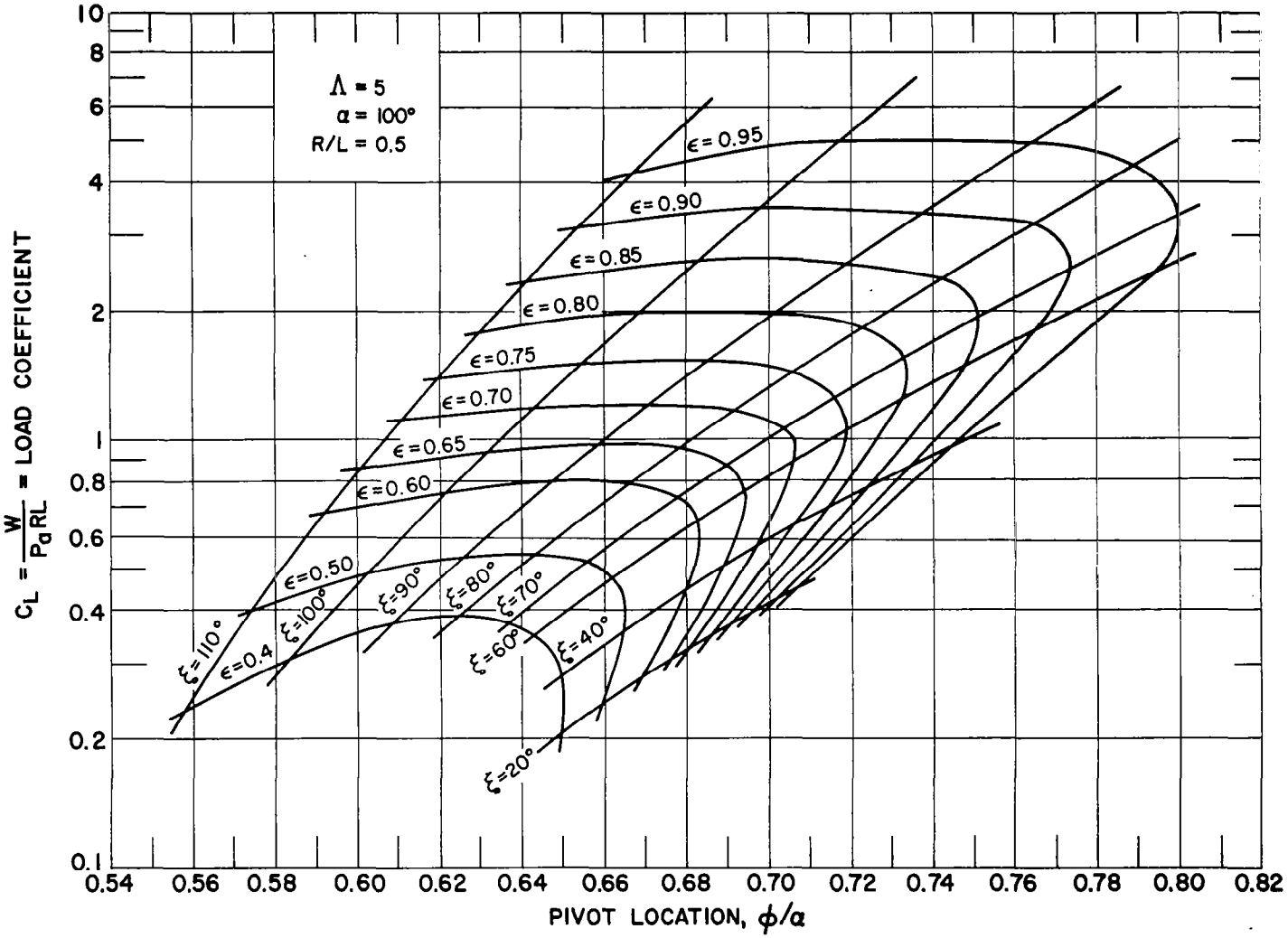

Figure II-10

Load Coefficient vs. Pivot Location for R/L = 0.5, α = 100°, Λ = 5

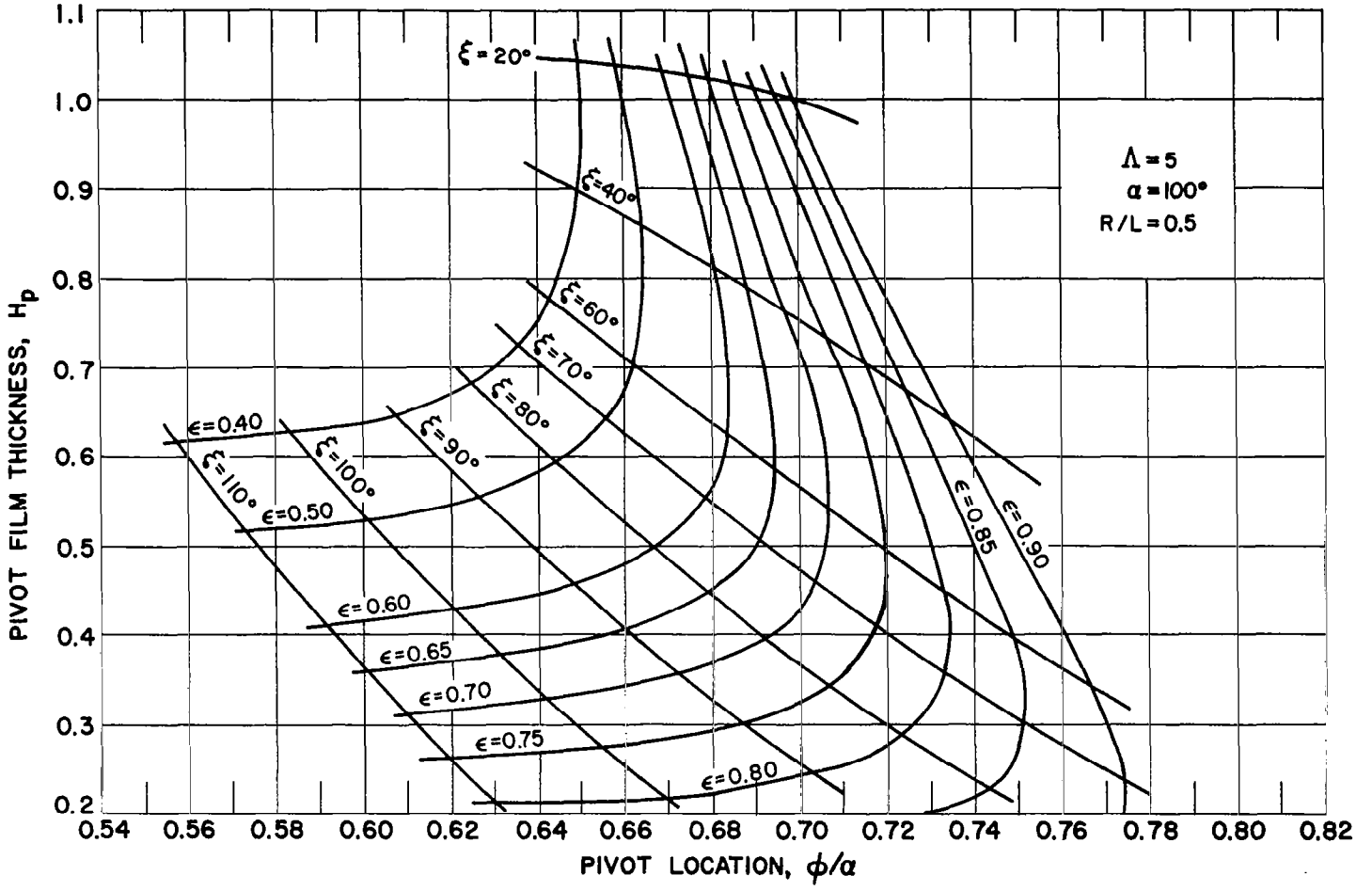

Figure II-11

Pivot Film Thickness vs. Pivot Location for R/L = 0.5, α = 100°, Λ = 5

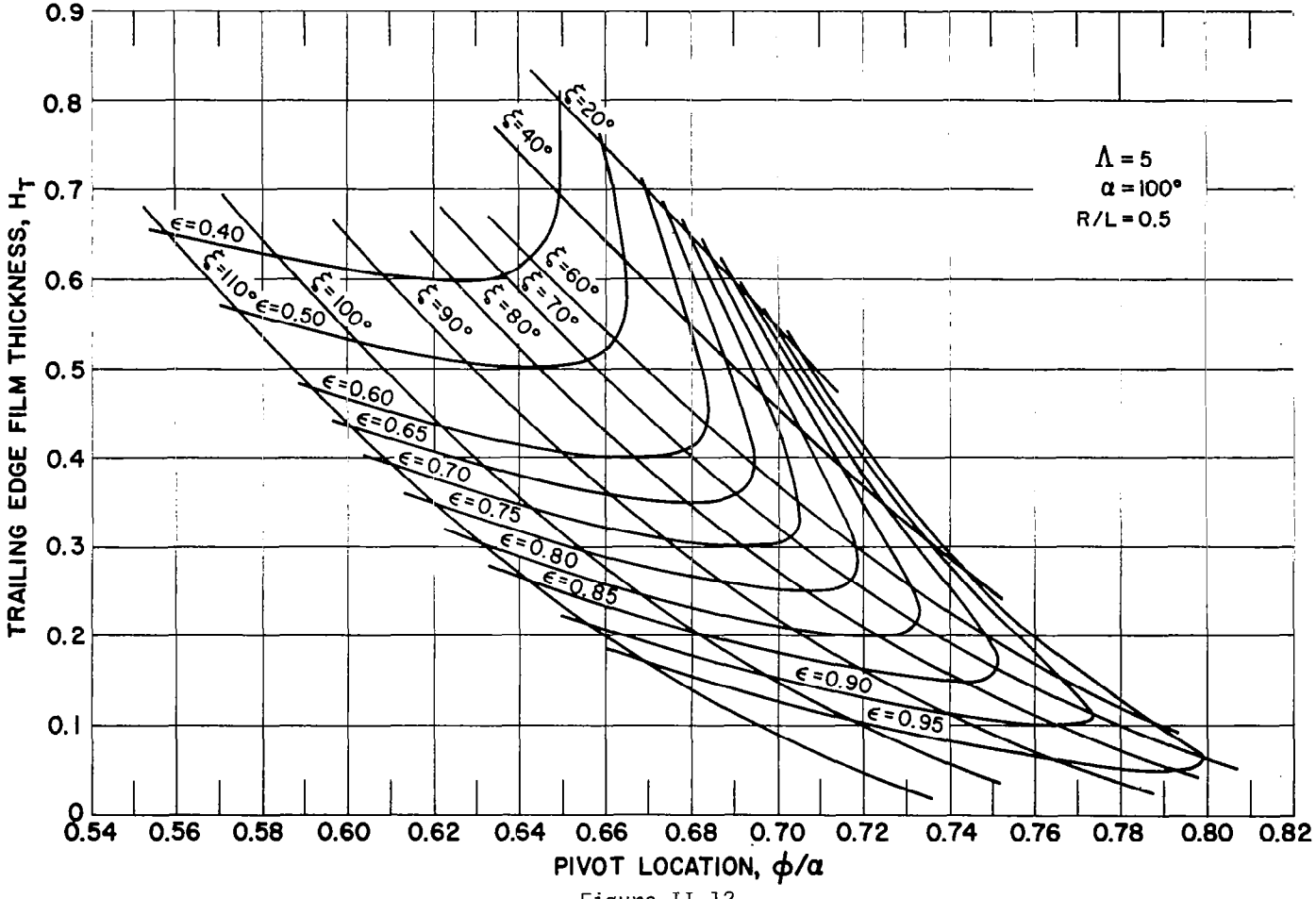

Figure II-12

Trailing Edge Film Thickness vs. Pivot Location for R/L = 0.5, α = 100°, Λ = 5

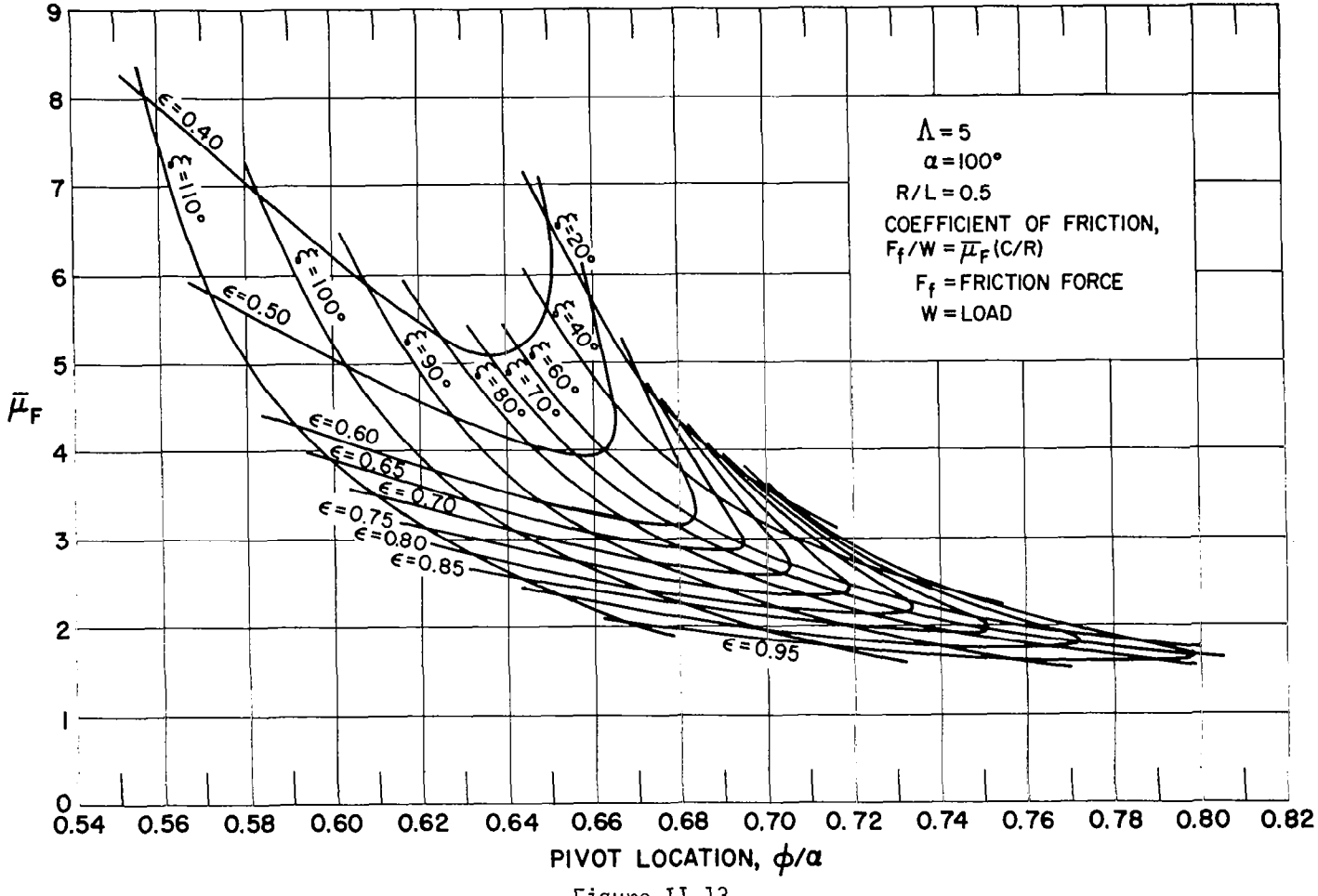

Figure II-13

Friction Factor vs. Pivot Location for R/L = 0.5, α = 100°, Λ = 5

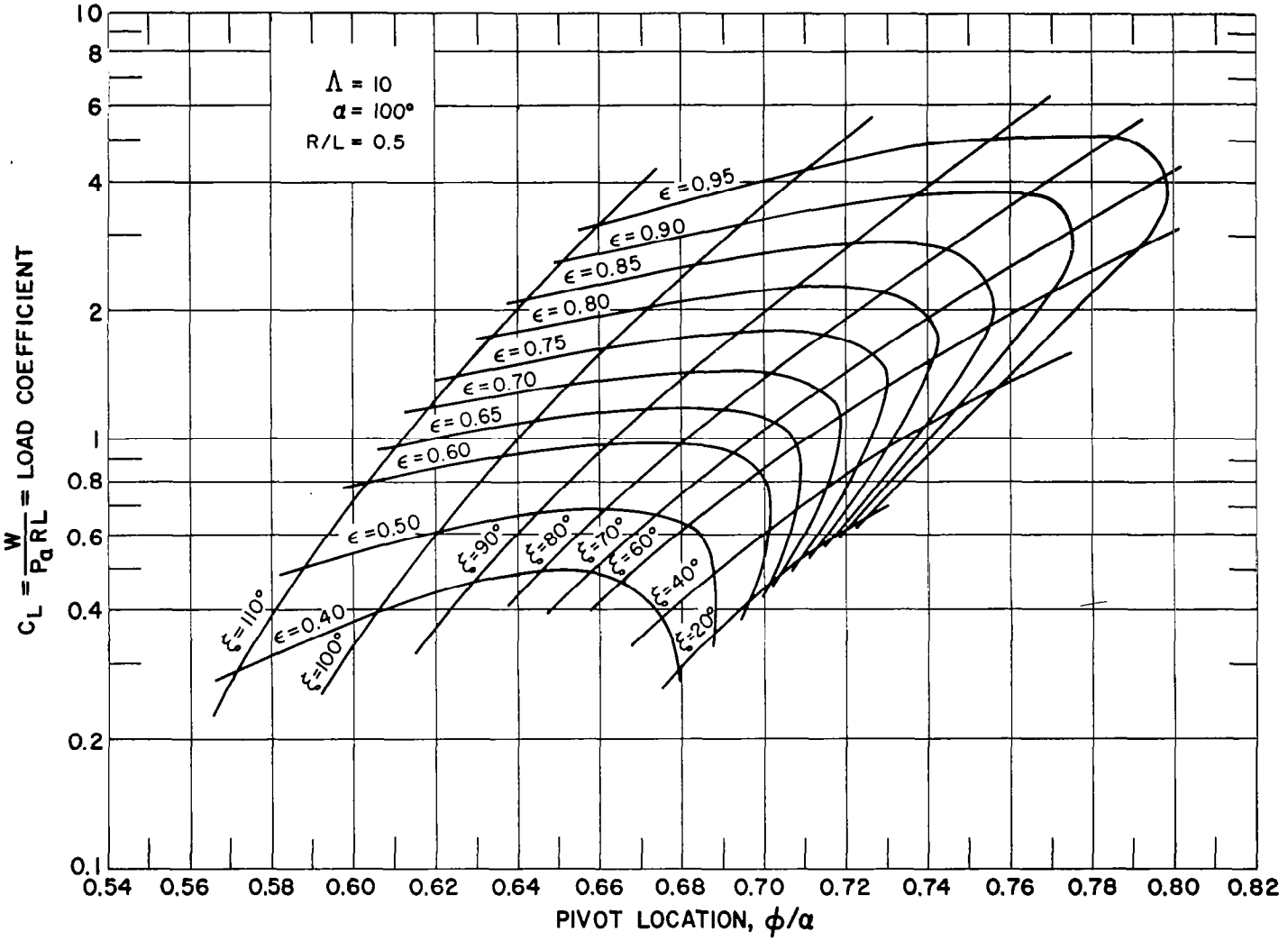

Figure II-14

Load Coefficient vs. Pivot Location for R/L = 0.5, α = 100°, Λ = 10

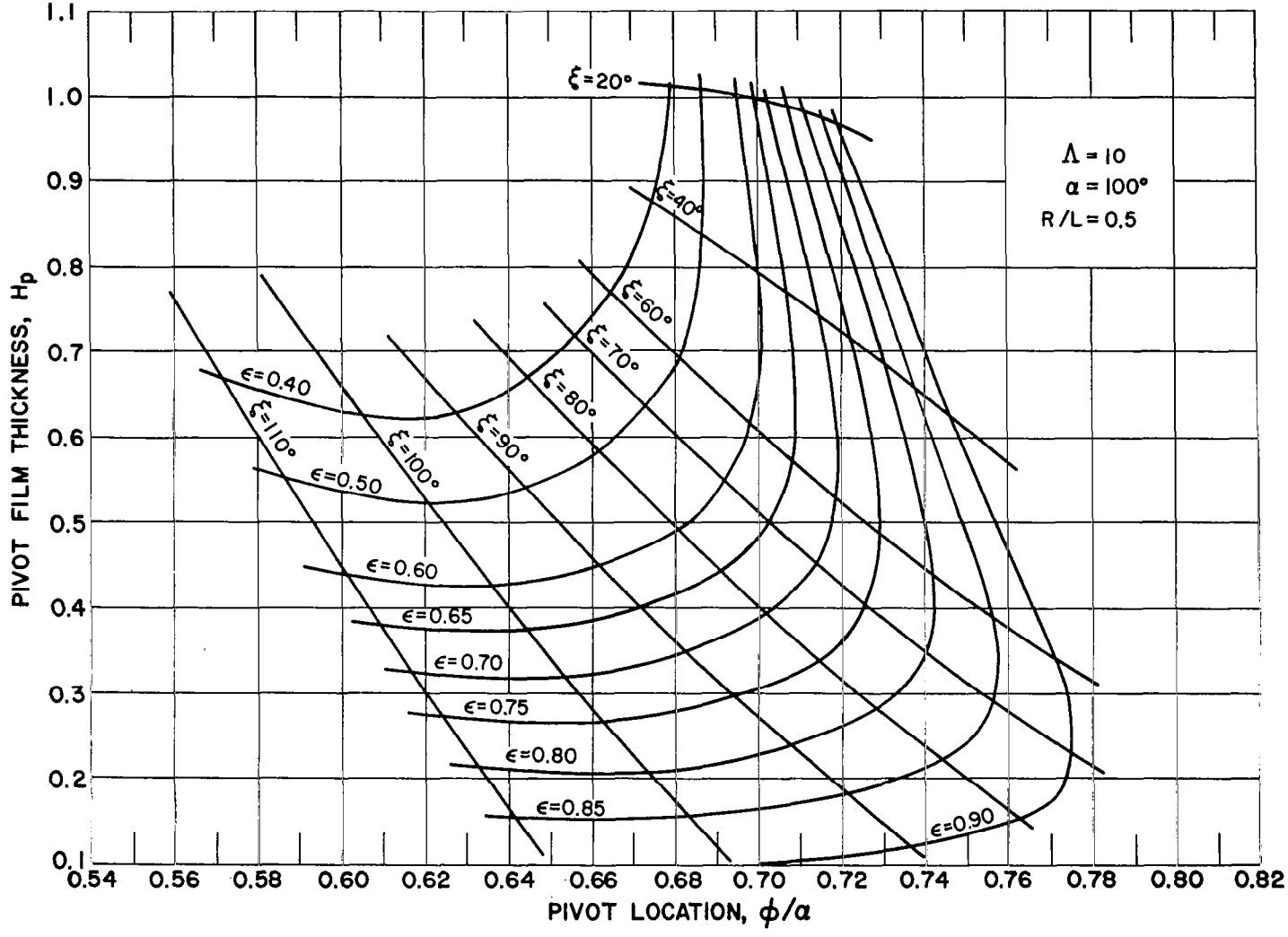

Figure II-15

Pivot Film Thickness vs. Pivot Location for R/L = 0.5, α = 100°, Λ = 10

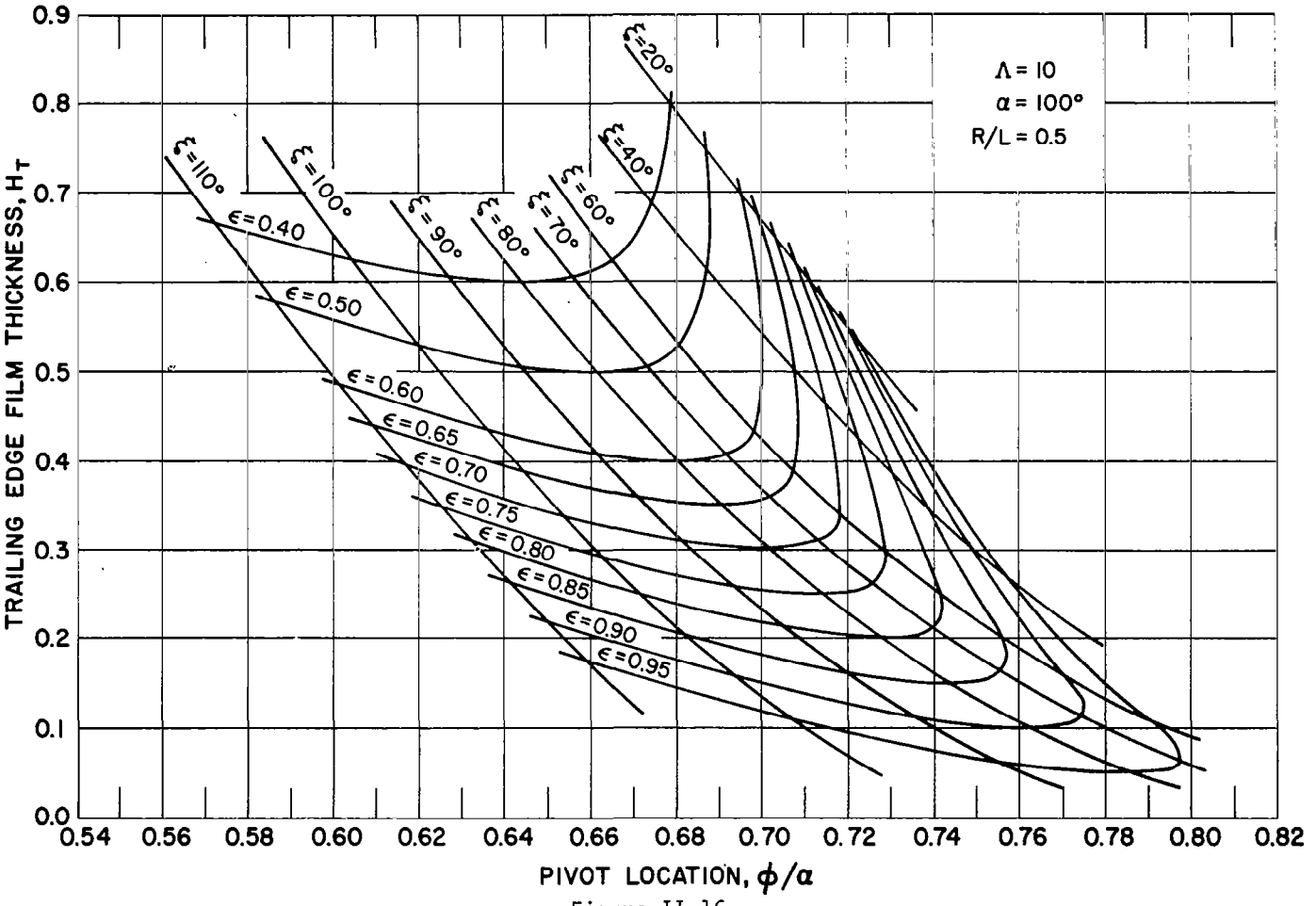

Figure II-16

Trailing Edge Film Thickness vs. Pivot Location for R/L = 0.5, α = 100°, Λ = 10

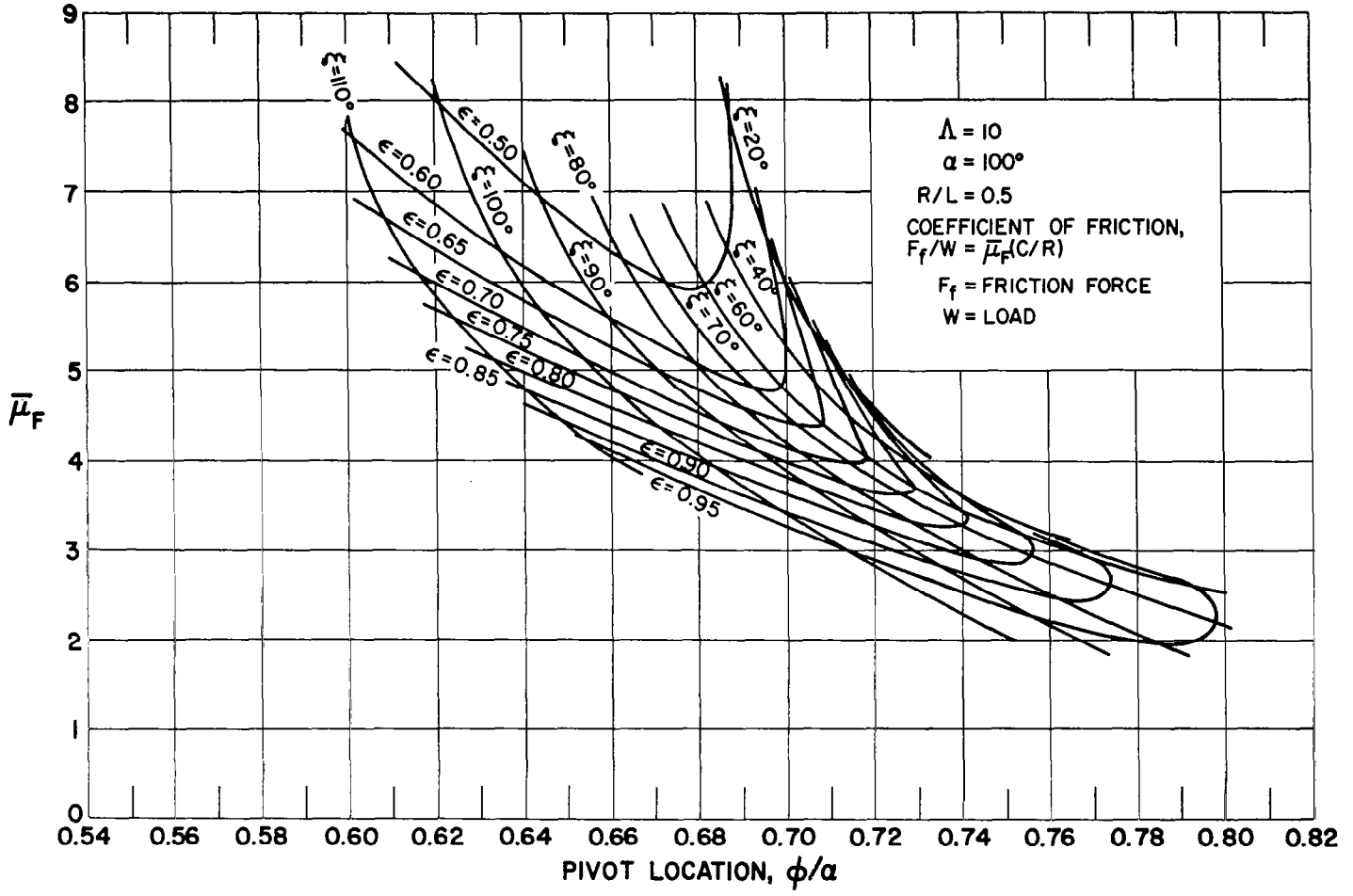

Figure II-17

Friction Factor vs. Pivot Location for R/L = 0.5, α = 100°, Λ = 10

Nomenclature for Table II-1

The following nomenclature pertains to the computer output listing constituting Table II-1.

1. First page

$$\Lambda = \frac{6\mu\Omega}{P_a}\left(\frac{R}{C}\right)^2$$

where

μ = lubricant viscosity

Ω = shaft speed

P_a = ambient pressure

R = radius of shaft

C = radius of shoe minus radius of shaft

R/L = shaft radius over shoe length

α = wrap angle of shoe

ϕ/α = pivot angle from shoe leading edge over wrap angle

$\text{Log}_{10}C_L$ = log to base 10 of load coefficient

C_L = load coefficient = $\frac{W}{P_a RL}$

ε = e/c

where

e = eccentricity

ξ = angle from line of centers to shoe leading edge

The ninth column contains a 3 digit code for Λ, R/L, and α.

The tenth column is a "1" for the first of the two card output for each case.

The eleventh column is a two digit code for ε and ξ.

The codes were used for sorting and automatic plotting.

2. Second page

The first three columns are the Λ, R/L, α and ϕ/α repeated from the first page as are the plotting codes contained in columns 10, 11 and 12. Column 11 is a "2" signifying that this is the second of the two cards.

H_T = trailing edge film thickness
$= 1 + \varepsilon \cos(\xi+\alpha)$

H_p = pivot film thickness
$= 1 + c \cos(\xi+\phi)$

F_r = total friction = $\sqrt{F_{rn}^2 + F_{rp}^2}$

where

F_{rn} = Friction normal to line of centers =

$$1/2 \iint \left[\frac{\partial PH}{\partial \theta} - P\frac{\partial H}{\partial \theta} + \frac{\Lambda}{3H}\right] \sin\theta \, d\theta dz$$

F_{rp} = Friction force paralled to line of centers =

$$1/2 \iint \left[\frac{\partial PH}{\partial \theta} - P\frac{\partial H}{\partial \theta} + \frac{\Lambda}{3H}\right] \cos\theta \, d\theta dz$$

$\bar{\mu}_F$ = Friction factor =

$$\{1/2 \iint \frac{\partial PH}{\partial \theta} - P\frac{\partial H}{\partial \theta} + \frac{\Lambda}{3H} \, d\theta dz\} / C_L$$

$$= \frac{F}{W}\left(\frac{R}{C}\right)$$

where F is the friction force, and W is the total load

δ = the attitude angle -- the angle between the displacement direction and the load direction.

Note that the third and fourth pages, etc. are the same as pages one and two except that they refer to additional cases.

TABLE II-1 - TABULAR LISTING OF 80° WRAP ANGLE COMPUTER RESULTS FOR FIELD MAP PLOTTING

Λ	R/L	α	ϕ/α	$\log_{10} C_L$	C_L	ϵ	ξ	PLOTTING CODE
0.50	0.500	80.0	0.6567	-0.8166	0.1526	0.8000	70.0	258 1 28
0.50	0.500	80.0	0.6690	-0.6626	0.2175	0.8000	80.0	258 1 29
0.50	0.500	80.0	0.6729	-0.5236	0.2995	0.8000	90.0	258 1 23
0.50	0.500	80.0	0.6625	-0.4223	0.3782	0.8000	100.0	258 1 25
0.50	0.500	80.0	0.6322	-0.3774	0.4193	0.8000	110.0	258 1 21
0.50	0.500	80.0	0.5750	-0.4200	0.3802	0.8000	120.0	258 1 24
0.50	0.500	80.0	0.6744	-0.7459	0.1795	0.8500	70.0	258 1 48
0.50	0.500	80.0	0.6918	-0.5616	0.2744	0.8500	80.0	258 1 49
0.50	0.500	80.0	0.7005	-0.3917	0.4058	0.8500	90.0	258 1 43
0.50	0.500	80.0	0.6924	-0.2651	0.5432	0.8500	100.0	258 1 45
0.50	0.500	80.0	0.6609	-0.2030	0.6266	0.8500	110.0	258 1 41
0.50	0.500	80.0	0.6019	-0.2226	0.5990	0.8500	120.0	258 1 42
0.50	0.500	80.0	0.6936	-0.6674	0.2151	0.9000	70.0	258 1 78
0.50	0.500	80.0	0.7179	-0.4464	0.3577	0.9000	80.0	258 1 79
0.50	0.500	80.0	0.7333	-0.2364	0.5802	0.9000	90.0	258 1 73
0.50	0.500	80.0	0.7288	-0.0762	0.8392	0.9000	100.0	258 1 75
0.50	0.500	80.0	0.6952	0.0069	1.0160	0.9000	110.0	258 1 71
0.50	0.500	80.0	0.6319	0.0070	1.0162	0.9000	120.0	258 1 72
0.50	0.500	80.0	0.7153	-0.5792	0.2635	0.9500	70.0	258 1 38
0.50	0.500	80.0	0.7488	-0.3108	0.4889	0.9500	80.0	258 1 39
0.50	0.500	80.0	0.7751	-0.0382	0.9157	0.9500	90.0	258 1 33
0.50	0.500	80.0	0.7337	-0.5938	0.2548	0.9700	70.0	258 1 88
0.50	0.500	80.0	0.7668	-0.2692	0.5380	0.9700	80.0	258 1 89
1.00	0.500	80.0	0.6321	-0.8167	0.1525	0.7000	60.0	358 1 57
1.00	0.500	80.0	0.6416	-0.6975	0.2007	0.7000	70.0	358 1 58
1.00	0.500	80.0	0.6471	-0.5864	0.2592	0.7000	80.0	358 1 59
1.00	0.500	80.0	0.6456	-0.4964	0.3189	0.7000	90.0	358 1 53
1.00	0.500	80.0	0.6548	-0.7199	0.1906	0.8000	60.0	358 1 27
1.00	0.500	80.0	0.6707	-0.5637	0.2731	0.8000	70.0	358 1 28
1.00	0.500	80.0	0.6827	-0.4130	0.3864	0.8000	80.0	358 1 29
1.00	0.500	80.0	0.6863	-0.2844	0.5195	0.8000	90.0	358 1 23
1.00	0.500	80.0	0.6763	-0.1957	0.6373	0.8000	100.0	358 1 25
1.00	0.500	80.0	0.6487	-0.1598	0.6921	0.8000	110.0	358 1 21
1.00	0.500	80.0	0.6758	-0.7575	0.1748	0.8500	60.0	358 1 47
1.00	0.500	80.0	0.6924	-0.5439	0.2858	0.8500	70.0	358 1 48
1.00	0.500	80.0	0.7063	-0.3462	0.4506	0.8500	80.0	358 1 49
1.00	0.500	80.0	0.7120	-0.1800	0.6607	0.8500	90.0	358 1 43
1.00	0.500	80.0	0.7026	-0.0634	0.8642	0.8500	100.0	358 1 45
1.00	0.500	80.0	0.6728	-0.0090	0.9796	0.8500	110.0	358 1 41
1.00	0.500	80.0	0.6888	-0.6921	0.2032	0.9000	60.0	358 1 77
1.00	0.500	80.0	0.7100	-0.4556	0.3503	0.9000	70.0	358 1 78
1.00	0.500	80.0	0.7295	-0.2302	0.5886	0.9000	80.0	358 1 79
1.00	0.500	80.0	0.7407	-0.0321	0.9288	0.9000	90.0	358 1 73
1.00	0.500	80.0	0.7344	0.1134	1.2983	0.9000	100.0	358 1 75
1.00	0.500	80.0	0.7026	0.1867	1.5370	0.9000	110.0	358 1 71
1.00	0.500	80.0	0.7025	-0.6252	0.2371	0.9500	60.0	358 1 37
1.00	0.500	80.0	0.7294	-0.3619	0.4346	0.9500	70.0	358 1 38

Λ	R/L	α	ϕ/a	H_T	H_P	FR	μ_F	δ	PLOTTING CODE
0.50	0.500	80.0	0.6567	0.3072	0.5697	0.2209	1.5391	57.46	258 2 28
0.50	0.500	80.0	0.6690	0.2482	0.4491	0.2697	1.3177	46.48	258 2 29
0.50	0.500	80.0	0.6729	0.2122	0.3541	0.3235	1.1480	36.16	258 2 23
0.50	0.500	80.0	0.6625	0.2000	0.2872	0.3738	1.0507	27.00	258 2 25
0.50	0.500	80.0	0.6322	0.2122	0.2455	0.4117	1.0452	19.42	258 2 21
0.50	0.500	80.0	0.5750	0.2482	0.2238	0.4326	1.2169	14.00	258 2 24
0.50	0.500	80.0	0.6744	0.2639	0.5253	0.2422	1.4334	56.05	258 2 48
0.50	0.500	80.0	0.6918	0.2013	0.3954	0.3070	1.1887	44.66	258 2 49
0.50	0.500	80.0	0.7005	0.1629	0.2950	0.3828	1.0023	33.96	258 2 43
0.50	0.500	80.0	0.6924	0.1500	0.2272	0.4562	0.8922	24.60	258 2 45
0.50	0.500	80.0	0.6609	0.1629	0.1877	0.5120	0.8679	17.13	258 2 41
0.50	0.500	80.0	0.6019	0.2013	0.1681	0.5435	0.9660	11.85	258 2 42
0.50	0.500	80.0	0.6936	0.2206	0.4775	0.2690	1.3294	54.51	258 2 78
0.50	0.500	80.0	0.7179	0.1543	0.3372	0.3585	1.0654	42.57	258 2 79
0.50	0.500	80.0	0.7333	0.1137	0.2313	0.4731	0.8670	31.34	258 2 73
0.50	0.500	80.0	0.7288	0.1000	0.1637	0.5920	0.7495	21.69	258 2 75
0.50	0.500	80.0	0.6952	0.1137	0.1282	0.6836	0.7136	14.38	258 2 71
0.50	0.500	80.0	0.6319	0.1543	0.1122	0.7347	0.7661	9.45	258 2 72
0.50	0.500	80.0	0.7153	0.1773	0.4253	0.3042	1.2276	52.78	258 2 38
0.50	0.500	80.0	0.7488	0.1073	0.2733	0.4356	0.9483	40.10	258 2 39
0.50	0.500	80.0	0.7751	0.0644	0.1611	0.6364	0.7398	27.99	258 2 33
0.50	0.500	80.0	0.7337	0.1600	0.3936	0.3089	1.2900	51.31	258 2 88
0.50	0.500	80.0	0.7668	0.0885	0.2425	0.4707	0.9316	38.65	258 2 89
1.00	0.500	80.0	0.6321	0.4638	0.7541	0.3169	2.2132	69.43	358 2 57
1.00	0.500	80.0	0.6416	0.3938	0.6360	0.3688	1.9566	58.67	358 2 58
1.00	0.500	80.0	0.6471	0.3422	0.5337	0.4269	1.7538	48.23	358 2 59
1.00	0.500	80.0	0.6456	0.3106	0.4510	0.4862	1.6241	38.35	358 2 53
1.00	0.500	80.0	0.6548	0.3872	0.6954	0.3521	1.9649	67.62	358 2 27
1.00	0.500	80.0	0.6707	0.3072	0.5566	0.4290	1.6707	56.34	358 2 28
1.00	0.500	80.0	0.6827	0.2482	0.4381	0.5220	1.4367	45.39	358 2 29
1.00	0.500	80.0	0.6863	0.2122	0.3455	0.6237	1.2771	35.10	358 2 23
1.00	0.500	80.0	0.6763	0.2000	0.2803	0.7200	1.2023	25.89	358 2 25
1.00	0.500	80.0	0.6487	0.2122	0.2396	0.7968	1.2257	18.10	358 2 21
1.00	0.500	80.0	0.6758	0.3489	0.6534	0.3582	2.1864	65.94	358 2 47
1.00	0.500	80.0	0.6924	0.2639	0.5077	0.4561	1.6995	54.61	358 2 48
1.00	0.500	80.0	0.7063	0.2013	0.3834	0.5810	1.3727	43.50	358 2 49
1.00	0.500	80.0	0.7120	0.1629	0.2875	0.7251	1.1685	33.04	358 2 43
1.00	0.500	80.0	0.7026	0.1500	0.2222	0.8674	1.0683	23.79	358 2 45
1.00	0.500	80.0	0.6728	0.1629	0.1837	0.9818	1.0662	16.18	358 2 41
1.00	0.500	80.0	0.6888	0.3106	0.6182	0.3834	2.0109	64.90	358 2 77
1.00	0.500	80.0	0.7100	0.2206	0.4609	0.5062	1.5387	53.20	358 2 78
1.00	0.500	80.0	0.7295	0.1543	0.3274	0.6751	1.2216	41.64	358 2 79
1.00	0.500	80.0	0.7407	0.1137	0.2265	0.8892	1.0201	30.74	358 2 73
1.00	0.500	80.0	0.7344	0.1000	0.1612	1.1181	0.9169	21.25	358 2 75
1.00	0.500	80.0	0.7026	0.1137	0.1260	1.3057	0.9023	13.80	358 2 71
1.00	0.500	80.0	0.7025	0.2723	0.5805	0.4133	1.8574	63.80	358 2 37
1.00	0.500	80.0	0.7294	0.1773	0.4105	0.5709	1.3992	51.65	358 2 38

B23

Λ	R/L	α	ϕ/α	$\text{LOG}_{10}\,C_L$	C_L	ϵ	ξ	PLOTTING CODE
1.00	0.500	80.0	0.7566	-0.0977	0.7985	0.9500	80.0	358 1 39
1.00	0.500	80.0	0.7781	0.1547	1.4278	0.9500	90.0	358 1 33
1.50	0.500	80.0	0.6130	-0.8234	0.1502	0.5500	60.0	458 1 37
1.50	0.500	80.0	0.6164	-0.7455	0.1797	0.5500	70.0	458 1 38
1.50	0.500	80.0	0.6164	-0.6805	0.2087	0.5500	80.0	458 1 39
1.50	0.500	80.0	0.6114	-0.6360	0.2312	0.5500	90.0	458 1 33
1.50	0.500	80.0	0.5996	-0.6191	0.2404	0.5500	100.0	458 1 35
1.50	0.500	80.0	0.6222	-0.7740	0.1683	0.6000	60.0	458 1 87
1.50	0.500	80.0	0.6275	-0.6834	0.2073	0.6000	70.0	458 1 88
1.50	0.500	80.0	0.6290	-0.6052	0.2482	0.6000	80.0	458 1 89
1.50	0.500	80.0	0.6250	-0.5487	0.2827	0.6000	90.0	458 1 83
1.50	0.500	80.0	0.6133	-0.5218	0.3007	0.6000	100.0	458 1 85
1.50	0.500	80.0	0.5915	-0.5314	0.2942	0.6000	110.0	458 1 81
1.50	0.500	80.0	0.6319	-0.7242	0.1887	0.6500	60.0	458 1 17
1.50	0.500	80.0	0.6392	-0.6204	0.2397	0.6500	70.0	458 1 18
1.50	0.500	80.0	0.6427	-0.5288	0.2959	0.6500	80.0	458 1 19
1.50	0.500	80.0	0.6399	-0.4594	0.3472	0.6500	90.0	458 1 13
1.50	0.500	80.0	0.6283	-0.4218	0.3786	0.6500	100.0	458 1 15
1.50	0.500	80.0	0.6055	-0.4242	0.3765	0.6500	110.0	458 1 11
1.50	0.500	80.0	0.6420	-0.6754	0.2112	0.7000	60.0	458 1 57
1.50	0.500	80.0	0.6518	-0.5570	0.2774	0.7000	70.0	458 1 58
1.50	0.500	80.0	0.6574	-0.4501	0.3547	0.7000	80.0	458 1 59
1.50	0.500	80.0	0.6561	-0.3666	0.4299	0.7000	90.0	458 1 53
1.50	0.500	80.0	0.6544	-0.6323	0.2332	0.7500	60.0	458 1 97
1.50	0.500	80.0	0.6657	-0.4929	0.3214	0.7500	70.0	458 1 98
1.50	0.500	80.0	0.6735	-0.3685	0.4281	0.7500	80.0	458 1 99
1.50	0.500	80.0	0.6380	-0.1898	0.6460	0.7500	110.0	458 1 91
1.50	0.500	80.0	0.6652	-0.5805	0.2627	0.8000	60.0	458 1 27
1.50	0.500	80.0	0.6799	-0.4250	0.3759	0.8000	70.0	458 1 28
1.50	0.500	80.0	0.6909	-0.2822	0.5222	0.8000	80.0	458 1 29
1.50	0.500	80.0	0.6938	-0.1644	0.6848	0.8000	90.0	458 1 23
1.50	0.500	80.0	0.6836	-0.0860	0.8204	0.8000	100.0	458 1 25
1.50	0.500	80.0	0.6570	-0.0579	0.8752	0.8000	110.0	458 1 21
2.00	0.500	80.0	0.6213	-0.7292	0.1866	0.5500	60.0	158 1 37
2.00	0.500	80.0	0.6252	-0.6521	0.2228	0.5500	70.0	158 1 38
2.00	0.500	80.0	0.6256	-0.5898	0.2571	0.5500	80.0	158 1 39
2.00	0.500	80.0	0.6209	-0.5487	0.2827	0.5500	90.0	158 1 33
2.00	0.500	80.0	0.6095	-0.5358	0.2912	0.5500	100.0	158 1 35
2.00	0.500	80.0	0.6303	-0.6780	0.2099	0.6000	60.0	158 1 87
2.00	0.500	80.0	0.6360	-0.5894	0.2574	0.6000	70.0	158 1 88
2.00	0.500	80.0	0.6378	-0.5152	0.3053	0.6000	80.0	158 1 89
2.00	0.500	80.0	0.6340	-0.4631	0.3443	0.6000	90.0	158 1 83
2.00	0.500	80.0	0.6226	-0.4410	0.3623	0.6000	100.0	158 1 85
2.00	0.500	80.0	0.5975	-0.4809	0.3304	0.6000	110.0	158 1 81
2.00	0.500	80.0	0.6398	-0.6275	0.2358	0.6500	60.0	158 1 17
2.00	0.500	80.0	0.6474	-0.5264	0.2976	0.6500	70.0	158 1 18
2.00	0.500	80.0	0.6509	-0.4396	0.3634	0.6500	80.0	158 1 19
2.00	0.500	80.0	0.6482	-0.3758	0.4209	0.6500	90.0	158 1 13

Λ	R/L	α	ϕ/a	H_T	H_P	FR	μ_F	δ	PLOTTING CODE
1.00	0.500	80.0	0.7566	0.1073	0.2667	0.8148	1.0860	39.47	358 2 39
1.00	0.500	80.0	0.7781	0.0644	0.1593	1.1860	0.8857	27.75	358 2 33
1.50	0.500	80.0	0.6130	0.5787	0.8206	0.4135	2.9428	70.96	458 2 37
1.50	0.500	80.0	0.6164	0.5237	0.7307	0.4582	2.7256	60.69	458 2 38
1.50	0.500	80.0	0.6164	0.4832	0.6515	0.5046	2.5853	50.68	458 2 39
1.50	0.500	80.0	0.6114	0.4584	0.5855	0.5496	2.5437	41.09	458 2 33
1.50	0.500	80.0	0.5996	0.4500	0.5338	0.5899	2.6299	32.04	458 2 35
1.50	0.500	80.0	0.6222	0.5404	0.7970	0.4297	2.7262	70.22	458 2 87
1.50	0.500	80.0	0.6275	0.4804	0.6982	0.4829	2.4863	59.80	458 2 88
1.50	0.500	80.0	0.6290	0.4362	0.6117	0.5393	2.3200	49.68	458 2 89
1.50	0.500	80.0	0.6250	0.4091	0.5404	0.5948	2.2483	40.00	458 2 83
1.50	0.500	80.0	0.6133	0.4000	0.4854	0.6448	2.2938	30.94	458 2 85
1.50	0.500	80.0	0.5915	0.4091	0.4464	0.6853	2.4979	22.68	458 2 81
1.50	0.500	80.0	0.6319	0.5021	0.7718	0.4481	2.5321	69.45	458 2 17
1.50	0.500	80.0	0.6392	0.4371	0.6639	0.5115	2.2755	58.86	458 2 18
1.50	0.500	80.0	0.6427	0.3892	0.5700	0.5803	2.0911	48.59	458 2 19
1.50	0.500	80.0	0.6399	0.3599	0.4935	0.6492	1.9952	38.81	458 2 13
1.50	0.500	80.0	0.6283	0.3500	0.4356	0.7119	2.0084	29.73	458 2 15
1.50	0.500	80.0	0.6055	0.3599	0.3955	0.7628	2.1684	21.56	458 2 11
1.50	0.500	80.0	0.6420	0.4638	0.7450	0.4688	2.3651	68.64	458 2 57
1.50	0.500	80.0	0.6518	0.3938	0.6276	0.5448	2.0921	57.86	458 2 58
1.50	0.500	80.0	0.6574	0.3422	0.5262	0.6295	1.8901	47.41	458 2 59
1.50	0.500	80.0	0.6561	0.3106	0.4447	0.7162	1.7753	37.51	458 2 53
1.50	0.500	80.0	0.6544	0.4255	0.7148	0.4912	2.2430	67.65	458 2 97
1.50	0.500	80.0	0.6657	0.3505	0.5888	0.5837	1.9327	56.75	458 2 98
1.50	0.500	80.0	0.6735	0.2952	0.4801	0.6893	1.7141	46.12	458 2 99
1.50	0.500	80.0	0.6380	0.2614	0.2907	0.9907	1.6362	18.96	458 2 91
1.50	0.500	80.0	0.6652	0.3872	0.6846	0.5185	2.0998	66.78	458 2 27
1.50	0.500	80.0	0.6799	0.3072	0.5481	0.6304	1.7846	55.61	458 2 28
1.50	0.500	80.0	0.6909	0.2482	0.4316	0.7640	1.5575	44.72	458 2 29
1.50	0.500	80.0	0.6938	0.2122	0.3407	0.9105	1.4161	34.50	458 2 23
1.50	0.500	80.0	0.6836	0.2000	0.2768	1.0525	1.3669	25.31	458 2 25
1.50	0.500	80.0	0.6570	0.2122	0.2368	1.1702	1.4248	17.44	458 2 21
2.00	0.500	80.0	0.6213	0.5787	0.8146	0.5473	3.1361	70.30	158 2 37
2.00	0.500	80.0	0.6252	0.5237	0.7249	0.6062	2.9086	59.99	158 2 38
2.00	0.500	80.0	0.6256	0.4832	0.6461	0.6674	2.7750	49.96	158 2 39
2.00	0.500	80.0	0.6209	0.4584	0.5807	0.7271	2.7525	40.33	158 2 33
2.00	0.500	80.0	0.6095	0.4500	0.5298	0.7810	2.8742	31.24	158 2 35
2.00	0.500	80.0	0.6303	0.5404	0.7906	0.5683	2.8910	69.57	158 2 87
2.00	0.500	80.0	0.6360	0.4804	0.6921	0.6381	2.6464	59.12	158 2 88
2.00	0.500	80.0	0.6378	0.4362	0.6062	0.7120	2.4902	48.98	158 2 89
2.00	0.500	80.0	0.6340	0.4091	0.5355	0.7852	2.4375	39.28	158 2 83
2.00	0.500	80.0	0.6226	0.4000	0.4814	0.8520	2.5166	30.19	158 2 85
2.00	0.500	80.0	0.5975	0.4091	0.4445	0.9050	2.9399	22.20	158 2 81
2.00	0.500	80.0	0.6398	0.5021	0.7651	0.5919	2.6777	68.82	158 2 17
2.00	0.500	80.0	0.6474	0.4371	0.6576	0.6748	2.4184	58.21	158 2 18
2.00	0.500	80.0	0.6509	0.3892	0.5644	0.7646	2.2442	47.93	158 2 19
2.00	0.500	80.0	0.6482	0.3599	0.4888	0.8551	2.1687	38.14	158 2 13

Λ	R/L	α	ϕ/α	$LOG_{10} C_L$	C_L	ϵ	ξ	PLOTTING CODE
2.00	0.500	80.0	0.6368	-0.3437	0.4533	0.6500	100.0	158 1 15
2.00	0.500	80.0	0.6121	-0.3681	0.4285	0.6500	110.0	158 1 11
2.00	0.500	80.0	0.6497	-0.5781	0.2642	0.7000	60.0	158 1 57
2.00	0.500	80.0	0.6595	-0.4633	0.3441	0.7000	70.0	158 1 58
2.00	0.500	80.0	0.6650	-0.3626	0.4339	0.7000	80.0	158 1 59
2.00	0.500	80.0	0.6636	-0.2859	0.5177	0.7000	90.0	158 1 53
2.00	0.500	80.0	0.6638	-0.5897	0.2572	0.7500	60.0	158 1 97
2.00	0.500	80.0	0.6745	-0.4391	0.3639	0.7500	70.0	158 1 98
2.00	0.500	80.0	0.6811	-0.3088	0.4912	0.7500	80.0	158 1 99
2.00	0.500	80.0	0.6438	-0.1327	0.7368	0.7500	110.0	158 1 91
2.00	0.500	80.0	0.6749	-0.5321	0.2937	0.8000	60.0	158 1 27
2.00	0.500	80.0	0.6883	-0.3660	0.4305	0.8000	70.0	158 1 28
2.00	0.500	80.0	0.6977	-0.2195	0.6033	0.8000	80.0	158 1 29
2.00	0.500	80.0	0.6991	-0.1028	0.7892	0.8000	90.0	158 1 23
2.00	0.500	80.0	0.6882	-0.0275	0.9387	0.8000	100.0	158 1 25
2.00	0.500	80.0	0.6618	-0.0027	0.9937	0.8000	110.0	158 1 21
3.50	0.500	80.0	0.6221	-0.7384	0.1827	0.4500	50.0	558 1 46
3.50	0.500	80.0	0.6251	-0.6752	0.2113	0.4500	60.0	558 1 47
3.50	0.500	80.0	0.6262	-0.6238	0.2378	0.4500	70.0	558 1 48
3.50	0.500	80.0	0.6244	-0.5887	0.2578	0.4500	80.0	558 1 49
3.50	0.500	80.0	0.6283	-0.6899	0.2042	0.5000	50.0	558 1 76
3.50	0.500	80.0	0.6328	-0.6180	0.2410	0.5000	60.0	558 1 77
3.50	0.500	80.0	0.6351	-0.5575	0.2770	0.5000	70.0	558 1 78
3.50	0.500	80.0	0.6342	-0.5134	0.3066	0.5000	80.0	558 1 79
3.50	0.500	80.0	0.6288	-0.4898	0.3237	0.5000	90.0	558 1 73
3.50	0.500	80.0	0.6175	-0.4927	0.3216	0.5000	100.0	558 1 75
3.50	0.500	80.0	0.6347	-0.6450	0.2265	0.5500	50.0	558 1 36
3.50	0.500	80.0	0.6407	-0.5637	0.2731	0.5500	60.0	558 1 37
3.50	0.500	80.0	0.6445	-0.4937	0.3208	0.5500	70.0	558 1 38
3.50	0.500	80.0	0.6446	-0.4398	0.3632	0.5500	80.0	558 1 39
3.50	0.500	80.0	0.6397	-0.4080	0.3909	0.5500	90.0	558 1 33
3.50	0.500	80.0	0.6282	-0.4035	0.3949	0.5500	100.0	558 1 35
3.50	0.500	80.0	0.6414	-0.6027	0.2496	0.6000	50.0	558 1 86
3.50	0.500	80.0	0.6490	-0.5111	0.3083	0.6000	60.0	558 1 87
3.50	0.500	80.0	0.6543	-0.4309	0.3707	0.6000	70.0	558 1 88
3.50	0.500	80.0	0.6556	-0.3674	0.4291	0.6000	80.0	558 1 89
3.50	0.500	80.0	0.6512	-0.3266	0.4714	0.6000	90.0	558 1 83
3.50	0.500	80.0	0.6396	-0.3141	0.4852	0.6000	100.0	558 1 85
3.50	0.500	80.0	0.6482	-0.5618	0.2743	0.6500	50.0	558 1 16
3.50	0.500	80.0	0.6577	-0.4603	0.3465	0.6500	60.0	558 1 17
3.50	0.500	80.0	0.6646	-0.3691	0.4274	0.6500	70.0	558 1 18
3.50	0.500	80.0	0.6673	-0.2950	0.5070	0.6500	80.0	558 1 19
3.50	0.500	80.0	0.6636	-0.2441	0.5701	0.6500	90.0	558 1 13
3.50	0.500	80.0	0.6518	-0.2229	0.5986	0.6500	100.0	558 1 15
3.50	0.500	80.0	0.6558	-0.5249	0.2986	0.7000	50.0	558 1 56
3.50	0.500	80.0	0.6668	-0.4108	0.3884	0.7000	60.0	558 1 57
3.50	0.500	80.0	0.6755	-0.3074	0.4927	0.7000	70.0	558 1 58
3.50	0.500	80.0	0.6797	-0.2214	0.6006	0.7000	80.0	558 1 59
3.50	0.500	80.0	0.6770	-0.1592	0.6931	0.7000	90.0	558 1 53

Λ	R/L	α	ϕ/α	H_T	H_P	FR	μ_F	δ	PLOTTING CODE
2.00	0.500	80.0	0.6368	0.3500	0.4318	0.9386	2.2131	29.05	158 2 15
2.00	0.500	80.0	0.6121	0.3599	0.3933	1.0061	2.5158	21.03	158 2 11
2.00	0.500	80.0	0.6497	0.4638	0.7361	0.6186	2.4952	68.02	158 2 57
2.00	0.500	80.0	0.6595	0.3938	0.6212	0.7174	2.2216	57.24	158 2 58
2.00	0.500	80.0	0.6650	0.3422	0.5208	0.8274	2.0323	46.80	158 2 59
2.00	0.500	80.0	0.6636	0.3106	0.4403	0.9407	1.9377	36.92	158 2 53
2.00	0.500	80.0	0.6638	0.4255	0.7057	0.6349	2.6354	66.89	158 2 97
2.00	0.500	80.0	0.6745	0.3505	0.5811	0.7561	2.2166	56.04	158 2 98
2.00	0.500	80.0	0.6811	0.2952	0.4744	0.8953	1.9442	45.51	158 2 99
2.00	0.500	80.0	0.6438	0.2614	0.2887	1.3026	1.8884	18.50	158 2 91
2.00	0.500	80.0	0.6749	0.3872	0.6748	0.6690	2.4301	66.01	158 2 27
2.00	0.500	80.0	0.6883	0.3072	0.5404	0.8154	2.0193	54.93	158 2 28
2.00	0.500	80.0	0.6977	0.2482	0.4263	0.9905	1.7505	44.18	158 2 29
2.00	0.500	80.0	0.6991	0.2122	0.3373	1.1838	1.6002	34.07	158 2 23
2.00	0.500	80.0	0.6882	0.2000	0.2746	1.3744	1.5621	24.94	158 2 25
2.00	0.500	80.0	0.6618	0.2122	0.2352	1.5364	1.6494	17.05	158 2 21
3.50	0.500	80.0	0.6221	0.7107	0.9237	0.8186	4.8059	80.23	558 2 46
3.50	0.500	80.0	0.6251	0.6553	0.8460	0.8858	4.4957	69.99	558 2 47
3.50	0.500	80.0	0.6262	0.6103	0.7743	0.9573	4.3166	59.90	558 2 48
3.50	0.500	80.0	0.6244	0.5771	0.7110	1.0299	4.2855	50.05	558 2 49
3.50	0.500	80.0	0.6283	0.6786	0.9109	0.8341	4.3740	79.74	558 2 76
3.50	0.500	80.0	0.6328	0.6170	0.8239	0.9124	4.0536	69.38	558 2 77
3.50	0.500	80.0	0.6351	0.5670	0.7439	0.9968	3.8538	59.19	558 2 78
3.50	0.500	80.0	0.6342	0.5302	0.6737	1.0840	3.7879	49.26	558 2 79
3.50	0.500	80.0	0.6288	0.5076	0.6153	1.1695	3.8741	39.70	558 2 73
3.50	0.500	80.0	0.6175	0.5000	0.5696	1.2480	4.1669	30.60	558 2 75
3.50	0.500	80.0	0.6347	0.6465	0.8971	0.8514	4.0222	79.22	558 2 36
3.50	0.500	80.0	0.6407	0.5787	0.8006	0.9421	3.6902	68.74	558 2 37
3.50	0.500	80.0	0.6445	0.5237	0.7122	1.0416	3.4730	58.44	558 2 38
3.50	0.500	80.0	0.6446	0.4832	0.6351	1.1460	3.3769	48.43	558 2 39
3.50	0.500	80.0	0.6397	0.4584	0.5715	1.2497	3.4251	38.83	558 2 33
3.50	0.500	80.0	0.6282	0.4500	0.5225	1.3461	3.6563	29.74	558 2 35
3.50	0.500	80.0	0.6414	0.6143	0.8823	0.8706	3.7277	78.69	558 2 86
3.50	0.500	80.0	0.6490	0.5404	0.7760	0.9755	3.3815	68.08	558 2 87
3.50	0.500	80.0	0.6543	0.4804	0.6790	1.0927	3.1497	57.66	558 2 88
3.50	0.500	80.0	0.6556	0.4362	0.5950	1.2178	3.0346	47.55	558 2 89
3.50	0.500	80.0	0.6512	0.4091	0.5265	1.3442	3.0515	37.90	558 2 83
3.50	0.500	80.0	0.6396	0.4000	0.4744	1.4632	3.2313	28.83	558 2 85
3.50	0.500	80.0	0.6482	0.5822	0.8664	0.8922	3.4732	78.14	558 2 16
3.50	0.500	80.0	0.6577	0.5021	0.7501	1.0130	3.1211	67.39	558 2 17
3.50	0.500	80.0	0.6646	0.4371	0.6444	1.1512	2.8760	56.83	558 2 18
3.50	0.500	80.0	0.6673	0.3892	0.5535	1.3019	2.7437	46.62	558 2 19
3.50	0.500	80.0	0.6636	0.3599	0.4803	1.4572	2.7336	36.91	558 2 13
3.50	0.500	80.0	0.6518	0.3500	0.4253	1.6057	2.8716	27.85	558 2 15
3.50	0.500	80.0	0.6558	0.5500	0.8489	0.9156	3.2718	77.53	558 2 56
3.50	0.500	80.0	0.6668	0.4638	0.7226	1.0553	2.8988	66.66	558 2 57
3.50	0.500	80.0	0.6755	0.3938	0.6082	1.2188	2.6403	55.96	558 2 58
3.50	0.500	80.0	0.6797	0.3422	0.5104	1.4019	2.4930	45.62	558 2 59
3.50	0.500	80.0	0.6770	0.3106	0.4325	1.5953	2.4604	35.84	558 2 53

Λ	R/L	α	ϕ/a	$\text{LOG}_{10} C_L$	C_L	ϵ	ξ	PLOTTING CODE
5.00	0.500	80.0	0.6370	-0.6498	0.2240	0.4500	50.0	658 1 46
5.00	0.500	80.0	0.6396	-0.5896	0.2573	0.4500	60.0	658 1 47
5.00	0.500	80.0	0.6401	-0.5431	0.2864	0.4500	70.0	658 1 48
5.00	0.500	80.0	0.6377	-0.5123	0.3074	0.4500	80.0	658 1 49
5.00	0.500	80.0	0.6427	-0.5996	0.2514	0.5000	50.0	658 1 76
5.00	0.500	80.0	0.6466	-0.5319	0.2938	0.5000	60.0	658 1 77
5.00	0.500	80.0	0.6483	-0.4770	0.3334	0.5000	70.0	658 1 78
5.00	0.500	80.0	0.6467	-0.4387	0.3641	0.5000	80.0	658 1 79
5.00	0.500	80.0	0.6406	-0.4209	0.3794	0.5000	90.0	658 1 73
5.00	0.500	80.0	0.6288	-0.4284	0.3729	0.5000	100.0	658 1 75
5.00	0.500	80.0	0.6486	-0.5534	0.2797	0.5500	50.0	658 1 36
5.00	0.500	80.0	0.6540	-0.4769	0.3335	0.5500	60.0	658 1 37
5.00	0.500	80.0	0.6570	-0.4136	0.3859	0.5500	70.0	658 1 38
5.00	0.500	80.0	0.6562	-0.3671	0.4294	0.5500	80.0	658 1 39
5.00	0.500	80.0	0.6504	-0.3414	0.4556	0.5500	90.0	658 1 33
5.00	0.500	80.0	0.6384	-0.3421	0.4549	0.5500	100.0	658 1 35
5.00	0.500	80.0	0.6548	-0.5095	0.3094	0.6000	50.0	658 1 86
5.00	0.500	80.0	0.6617	-0.4243	0.3765	0.6000	60.0	658 1 87
5.00	0.500	80.0	0.6660	-0.3519	0.4448	0.6000	70.0	658 1 88
5.00	0.500	80.0	0.6662	-0.2963	0.5054	0.6000	80.0	658 1 89
5.00	0.500	80.0	0.6609	-0.2622	0.5467	0.6000	90.0	658 1 83
5.00	0.500	80.0	0.6487	-0.2555	0.5552	0.6000	100.0	658 1 85
5.00	0.500	80.0	0.6611	-0.4678	0.3406	0.6500	50.0	658 1 16
5.00	0.500	80.0	0.6696	-0.3735	0.4231	0.6500	60.0	658 1 17
5.00	0.500	80.0	0.6755	-0.2912	0.5115	0.6500	70.0	658 1 18
5.00	0.500	80.0	0.6769	-0.2258	0.5946	0.6500	80.0	658 1 19
5.00	0.500	80.0	0.6721	-0.1823	0.6572	0.6500	90.0	658 1 13
5.00	0.500	80.0	0.6597	-0.1673	0.6803	0.6500	100.0	658 1 15
5.00	0.500	80.0	0.6683	-0.4660	0.3420	0.7000	50.0	658 1 56
5.00	0.500	80.0	0.6780	-0.3488	0.4479	0.7000	60.0	658 1 57
5.00	0.500	80.0	0.6852	-0.2469	0.5664	0.7000	70.0	658 1 58
5.00	0.500	80.0	0.6878	-0.1641	0.6853	0.7000	80.0	658 1 59
5.00	0.500	80.0	0.6838	-0.1060	0.7834	0.7000	90.0	658 1 53
10.00	0.500	80.0	0.6519	-0.7315	0.1856	0.3500	40.0	758 1 95
10.00	0.500	80.0	0.6514	-0.6727	0.2125	0.3500	50.0	758 1 96
10.00	0.500	80.0	0.6501	-0.6278	0.2356	0.3500	60.0	758 1 97
10.00	0.500	80.0	0.6472	-0.5970	0.2529	0.3500	70.0	758 1 98
10.00	0.500	80.0	0.6420	-0.5828	0.2614	0.3500	80.0	758 1 99
10.00	0.500	80.0	0.6562	-0.6719	0.2129	0.4000	40.0	758 1 25
10.00	0.500	80.0	0.6568	-0.6073	0.2470	0.4000	50.0	758 1 26
10.00	0.500	80.0	0.6564	-0.5560	0.2780	0.4000	60.0	758 1 27
10.00	0.500	80.0	0.6542	-0.5196	0.3023	0.4000	70.0	758 1 28
10.00	0.500	80.0	0.6494	-0.4994	0.3167	0.4000	80.0	758 1 29
10.00	0.500	80.0	0.6605	-0.6190	0.2404	0.4500	40.0	758 1 45
10.00	0.500	80.0	0.6623	-0.5481	0.2831	0.4500	50.0	758 1 46
10.00	0.500	80.0	0.6628	-0.4908	0.3230	0.4500	60.0	758 1 47
10.00	0.500	80.0	0.6613	-0.4480	0.3565	0.4500	70.0	768 1 48
10.00	0.500	80.0	0.6571	-0.4217	0.3787	0.4500	80.0	758 1 49

Λ	R/L	α	ϕ/α	H_T	H_P	FR	μ_F	δ	PLOTTING CODE
5.00	0.500	80.0	0.6370	0.7107	0.9144	1.1600	5.5566	79.04	658 2 46
5.00	0.500	80.0	0.6396	0.6553	0.8375	1.2544	5.2303	68.83	658 2 47
5.00	0.500	80.0	0.6401	0.6103	0.7668	1.3550	5.0776	58.79	658 2 48
5.00	0.500	80.0	0.6377	0.5771	0.7047	1.4584	5.0943	48.98	658 2 49
5.00	0.500	80.0	0.6427	0.6786	0.9010	1.1802	5.0310	78.58	658 2 76
5.00	0.500	80.0	0.6466	0.6170	0.8149	1.2896	4.7033	68.27	658 2 77
5.00	0.500	80.0	0.6483	0.5670	0.7360	1.4081	4.5269	58.13	658 2 78
5.00	0.500	80.0	0.6467	0.5302	0.6671	1.5316	4.5114	48.26	658 2 79
5.00	0.500	80.0	0.6406	0.5076	0.6101	1.6542	4.6809	38.75	658 2 73
5.00	0.500	80.0	0.6288	0.5000	0.5657	1.7688	5.0971	29.69	658 2 75
5.00	0.500	80.0	0.6486	0.6465	0.8867	1.2027	4.6049	78.11	658 2 36
5.00	0.500	80.0	0.6540	0.5787	0.7911	1.3290	4.2662	67.68	658 2 37
5.00	0.500	80.0	0.6570	0.5237	0.7040	1.4681	4.0747	57.44	658 2 38
5.00	0.500	80.0	0.6562	0.4832	0.6285	1.6153	4.0312	47.51	658 2 39
5.00	0.500	80.0	0.6504	0.4584	0.5664	1.7639	4.1529	37.96	658 2 33
5.00	0.500	80.0	0.6384	0.4500	0.5186	1.9045	4.4953	28.93	658 2 35
5.00	0.500	80.0	0.6548	0.6143	0.8713	1.2280	4.2463	77.62	658 2 86
5.00	0.500	80.0	0.6617	0.5404	0.7662	1.3732	3.9018	67.07	658 2 87
5.00	0.500	80.0	0.6660	0.4804	0.6708	1.5362	3.6962	56.72	658 2 88
5.00	0.500	80.0	0.6662	0.4362	0.5885	1.7122	3.6278	46.70	658 2 89
5.00	0.500	80.0	0.6609	0.4091	0.5216	1.8929	3.7108	37.13	658 2 83
5.00	0.500	80.0	0.6487	0.4000	0.4708	2.0663	3.9923	28.11	658 2 85
5.00	0.500	80.0	0.6611	0.5822	0.8550	1.2562	3.9427	77.11	658 2 16
5.00	0.500	80.0	0.6696	0.5021	0.7401	1.4228	3.5946	66.43	658 2 17
5.00	0.500	80.0	0.6755	0.4371	0.6362	1.6141	3.3751	55.96	658 2 18
5.00	0.500	80.0	0.6769	0.3892	0.5473	1.8254	3.2859	45.85	658 2 19
5.00	0.500	80.0	0.6721	0.3599	0.4757	2.0471	3.3365	36.23	658 2 13
5.00	0.500	80.0	0.6597	0.3500	0.4220	2.2633	3.5663	27.22	658 2 15
5.00	0.500	80.0	0.6683	0.5500	0.8370	1.2762	3.9920	76.54	658 2 56
5.00	0.500	80.0	0.6780	0.4638	0.7126	1.4699	3.5099	65.76	658 2 57
5.00	0.500	80.0	0.6852	0.3938	0.6004	1.6978	3.2067	55.19	658 2 58
5.00	0.500	80.0	0.6878	0.3422	0.5049	1.9561	3.0554	44.98	658 2 59
5.00	0.500	80.0	0.6838	0.3106	0.4287	2.2335	3.0536	35.30	658 2 53
10.00	0.500	80.0	0.6519	0.8250	0.9869	2.0998	12.2051	87.85	758 2 95
10.00	0.500	80.0	0.6514	0.7750	0.9265	2.2241	11.2865	77.88	758 2 96
10.00	0.500	80.0	0.6501	0.7319	0.8689	2.3587	10.7924	67.99	758 2 97
10.00	0.500	80.0	0.6472	0.6969	0.8157	2.5003	10.6595	58.23	758 2 98
10.00	0.500	80.0	0.6420	0.6711	0.7687	2.6438	10.9111	48.64	758 2 99
10.00	0.500	80.0	0.6562	0.8000	0.9826	2.1041	10.6506	87.50	758 2 25
10.00	0.500	80.0	0.6568	0.7429	0.9131	2.2483	9.8048	77.45	758 2 26
10.00	0.500	80.0	0.6564	0.6936	0.8468	2.4067	9.3255	67.48	758 2 27
10.00	0.500	80.0	0.6542	0.6536	0.7861	2.5756	9.1796	57.67	758 2 28
10.00	0.500	80.0	0.6494	0.6241	0.7326	2.7493	9.3561	48.05	758 2 29
10.00	0.500	80.0	0.6605	0.7750	0.9777	2.1109	9.4513	87.16	758 2 45
10.00	0.500	80.0	0.6623	0.7107	0.8989	2.2761	8.6546	77.02	758 2 46
10.00	0.500	80.0	0.6628	0.6553	0.8240	2.4603	8.1975	66.97	758 2 47
10.00	0.500	80.0	0.6613	0.6103	0.7555	2.6596	8.0311	57.09	768 2 48
10.00	0.500	80.0	0.6571	0.5771	0.6956	2.8677	8.1539	47.43	758 2 49

Λ	R/L	α	ϕ/a	$LOG_{10} C_L$	C_L	ϵ	ξ	PLOTTING CODE
10.00	0.500	80.0	0.6648	-0.5714	0.2683	0.5000	40.0	758 1 75
10.00	0.500	80.0	0.6677	-0.4943	0.3204	0.5000	50.0	758 1 76
10.00	0.500	80.0	0.6693	-0.4304	0.3712	0.5000	60.0	758 1 77
10.00	0.500	80.0	0.6687	-0.3808	0.4161	0.5000	70.0	758 1 78
10.00	0.500	80.0	0.6649	-0.3482	0.4486	0.5000	80.0	758 1 79
10.00	0.500	80.0	0.6573	-0.3352	0.4622	0.5000	90.0	758 1 73
10.00	0.500	80.0	0.6446	-0.3466	0.4502	0.5000	100.0	758 1 75
10.00	0.500	80.0	0.6690	-0.5282	0.2963	0.5500	40.0	758 1 35
10.00	0.500	80.0	0.6732	-0.4445	0.3593	0.5500	50.0	758 1 36
10.00	0.500	80.0	0.6760	-0.3736	0.4230	0.5500	60.0	758 1 37
10.00	0.500	80.0	0.6762	-0.3170	0.4819	0.5500	70.0	758 1 38
10.00	0.500	80.0	0.6731	-0.2772	0.5283	0.5500	80.0	758 1 39
10.00	0.500	80.0	0.6657	-0.2576	0.5525	0.5500	90.0	758 1 33
10.00	0.500	80.0	0.6527	-0.2633	0.5454	0.5500	100.0	758 1 35
10.00	0.500	80.0	0.6733	-0.4882	0.3250	0.6000	40.0	758 1 85
10.00	0.500	80.0	0.6788	-0.3979	0.4001	0.6000	50.0	758 1 86
10.00	0.500	80.0	0.6827	-0.3197	0.4790	0.6000	60.0	758 1 87
10.00	0.500	80.0	0.6841	-0.2553	0.5555	0.6000	70.0	758 1 88
10.00	0.500	80.0	0.6818	-0.2078	0.6197	0.6000	80.0	758 1 89
10.00	0.500	80.0	0.6746	-0.1809	0.6593	0.6000	90.0	758 1 83
10.00	0.500	80.0	0.6614	-0.1801	0.6606	0.6000	100.0	758 1 85
10.00	0.500	80.0	0.6776	-0.4512	0.3538	0.6500	40.0	758 1 15
10.00	0.500	80.0	0.6845	-0.3535	0.4431	0.6500	50.0	758 1 16
10.00	0.500	80.0	0.6897	-0.2676	0.5400	0.6500	60.0	758 1 17
10.00	0.500	80.0	0.6923	-0.1951	0.6381	0.6500	70.0	758 1 18
10.00	0.500	80.0	0.6909	-0.1388	0.7264	0.6500	80.0	758 1 19
10.00	0.500	80.0	0.6843	-0.1036	0.7879	0.6500	90.0	758 1 13
10.00	0.500	80.0	0.6709	-0.0955	0.8026	0.6500	100.0	758 1 15

Λ	R/L	α	ϕ/α	H_T	H_P	FR	μ_F	δ	PLOTTING CODE
10.00	0.500	80.0	0.6648	0.7500	0.9722	2.1202	8.4998	86.82	758 2 75
10.00	0.500	80.0	0.6677	0.6786	0.8840	2.3077	7.7463	76.58	758 2 76
10.00	0.500	80.0	0.6693	0.6170	0.8003	2.5200	7.3007	66.45	758 2 77
10.00	0.500	80.0	0.6687	0.5670	0.7241	2.7536	7.1181	56.50	758 2 78
10.00	0.500	80.0	0.6649	0.5302	0.6578	3.0015	7.1998	46.81	758 2 79
10.00	0.500	80.0	0.6573	0.5076	0.6029	3.2528	7.5757	37.42	758 2 73
10.00	0.500	80.0	0.6446	0.5000	0.5603	3.4923	8.3547	28.43	758 2 75
10.00	0.500	80.0	0.6690	0.7250	0.9662	2.1320	7.7328	86.48	758 2 35
10.00	0.500	80.0	0.6732	0.6465	0.8683	2.3435	7.0082	76.14	758 2 36
10.00	0.500	80.0	0.6760	0.5787	0.7756	2.5868	6.5714	65.92	758 2 37
10.00	0.500	80.0	0.6762	0.5237	0.6917	2.8595	6.3775	55.90	758 2 38
10.00	0.500	80.0	0.6731	0.4832	0.6190	3.1543	6.4207	46.15	758 2 39
10.00	0.500	80.0	0.6657	0.4584	0.5593	3.4581	6.7328	36.75	758 2 33
10.00	0.500	80.0	0.6527	0.4500	0.5134	3.7519	7.4037	27.78	758 2 35
10.00	0.500	80.0	0.6733	0.7000	0.9596	2.1465	7.0943	86.14	758 2 85
10.00	0.500	80.0	0.6788	0.6143	0.8518	2.3836	6.3976	75.70	758 2 86
10.00	0.500	80.0	0.6827	0.5404	0.7500	2.6616	5.9674	65.38	758 2 87
10.00	0.500	80.0	0.6841	0.4804	0.6582	2.9794	5.7616	55.27	758 2 88
10.00	0.500	80.0	0.6818	0.4362	0.5792	3.3304	5.7754	45.46	758 2 89
10.00	0.500	80.0	0.6746	0.4091	0.5148	3.6993	6.0320	36.03	758 2 83
10.00	0.500	80.0	0.6614	0.4000	0.4658	4.0614	6.6118	27.08	758 2 85
10.00	0.500	80.0	0.6776	0.6750	0.9523	2.1636	6.5626	85.79	758 2 15
10.00	0.500	80.0	0.6845	0.5822	0.8344	2.4287	5.8822	75.24	758 2 16
10.00	0.500	80.0	0.6897	0.5021	0.7234	2.7456	5.4577	64.82	758 2 17
10.00	0.500	80.0	0.6923	0.4371	0.6236	3.1164	5.2441	54.62	758 2 18
10.00	0.500	80.0	0.6909	0.3892	0.5382	3.5362	5.2295	44.73	758 2 19
10.00	0.500	80.0	0.6843	0.3599	0.4692	3.9874	5.4384	35.26	758 2 13
10.00	0.500	80.0	0.6709	0.3500	0.4174	4.4382	5.9427	26.33	758 2 15

APPENDIX III

OPERATING CONDITIONS WITH THE SHAFT HORIZONTAL

The purpose of this section is to show how the field maps can be used to compute characteristic curves for the bearing. The characteristic curve consists of plots of the total external load C_{LT} and pivot film thickness H_p vs. pivot circle eccentricity ratio ε' for various values of the preload setting C'/C. These curves are for constant Λ, constant R/L, constant wrap angle α, constant pivot location ϕ/α and for a fixed angular spacing β between pivots. These curves assume zero attitude angle (the angle between the load and the displacement directions) whereas the design data used for the case of the vertical shaft assumed zero pivot circle eccentricity. The characteristic curves are given for Λ of 1.5 (the design) and for Λ of 3.5. Two cases are shown for each Λ: 1) the spring loaded shoe is 180° from the gravity load direction; 2) the gravity load is directly into the spring loaded shoe.

Referring to Figure III-1 the pivot film thickness in terms of the shoe shaft coordinates is given by

$$H_P = 1 + \varepsilon \cos (\xi+\phi)$$

In terms of the pivot circle eccentricity ratio this equation can be written as[19]

$$H_{P_{1,2}} = C'/C \, [1 + \varepsilon' \cos (\pi-\beta)]$$

For $\beta = 60°$

$$H_{P_{1,2}} = C'/C \, (1 - 0.5 \, \varepsilon')$$

The pivot film thickness for the third shoe is given by

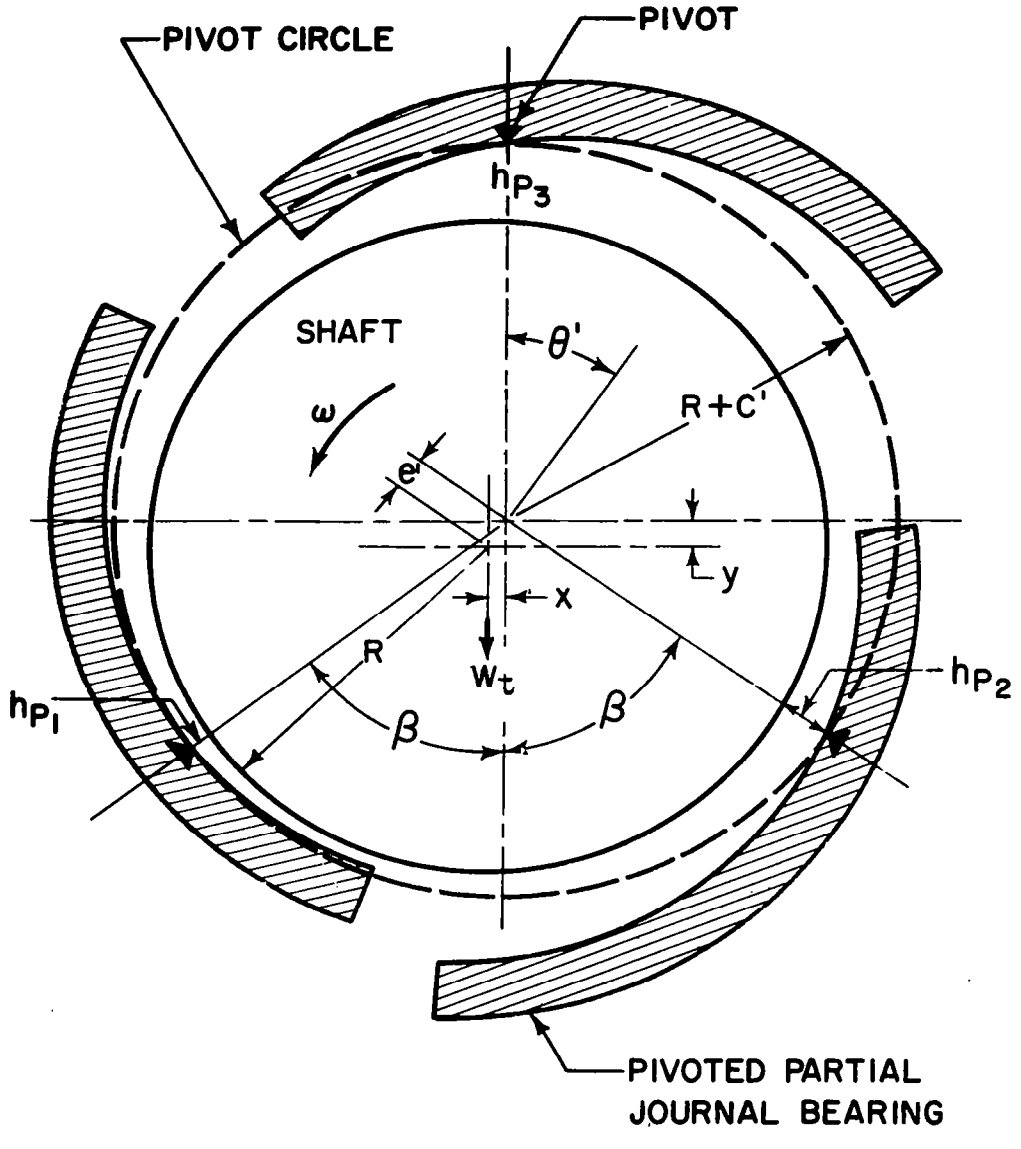

Fig. III-1 - Pivoted Pad Journal Bearing with Three Shoes

$$H_{P_3} = C'/C\ (1 + \varepsilon') \qquad \text{(III-1)}$$

Therefore, for a given pivot circle setting C'/C, the pivot film thickness can be computed for any ε'. For ease in plotting, a cross plot is constructed to give the relation between the shoe load coefficient C_L and the pivot film thickness H_P (Fig. 11).

The bearing total load coefficient C_{LT} for the load direction between shoes 1 and 2 is given by

$$C_{LT} = (C_{L_1} + C_{L_2}) \cos \beta - C_{L_3}$$

since

$$B = 60°$$
$$C_{L_1} = C_{L_2}$$
$$C_{LT} = C_{L_1} - C_{L_3}$$

For the gravity load against the spring, the total load coefficient is given by

$$C_{LT} = C_{L_3} - C_{L_1}$$

two characteristic curves are shown (Figures II-2, III-3) for $\Lambda = 1.5$ and two orientations of the gravity vector. As an example of the use of these curves consider the following problems:

Given: $\Lambda = 1.5$; R/L = 0.5; = 100°, $\phi/\alpha = 0.65$, $\beta = 60°$

P_a = 12 psia; R = 0.75 inches; L = 1.5 inches; C = 2×10^{-3} inches

W_T (external load) = 4.5 lbs.

Find: C'/C, ε', total friction loss, the minimum film thickness and the preload for both gravity orientations relative to the spring such that:

(1) $h_m \geq 0.5 \times 10^{-3}$ inches

(2) $H_{P_3} \quad 1$

For:

$H_{P_3} < 1$, from equation (III-1)

$C'/C\ (1 + \varepsilon') < 1$

or

$$C'/C < \frac{1}{1 + \varepsilon'}$$

Assume a value for C'/C.

Let C'/C = .7

$$C_{LT} = \frac{W_T}{P_a RL} = \frac{45}{12 \times .75 \times 1.5} = 0.333$$

From Figure III-2 (spring down)

$$\varepsilon' = 0.372$$

$$\frac{1}{1 + \varepsilon'} = 0.716$$

Therefore C'/C = .7 is a suitable choice.

Also from Figure III-2

$$H_{P_{1,2}} = 0.830$$

$$H_{P_3} = 0.430$$

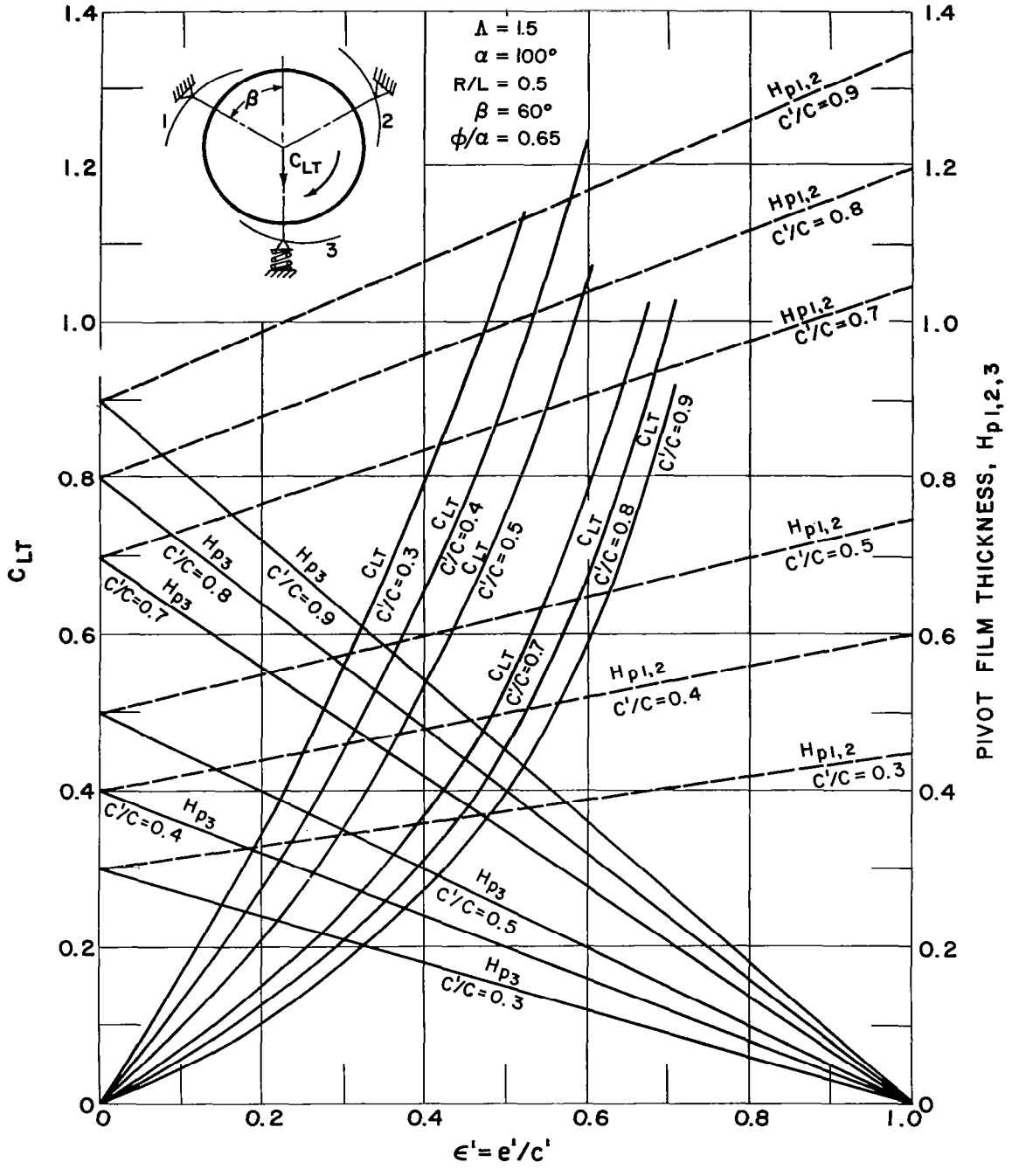

Fig. III-2 - Three Shoe Bearing Characteristics - Spring Down - R/L = 0.5, α = 100°, ϕ/α = 0.65, Λ = 1.5

The friction loss can now be obtained using the computed pivot film thickness and Figure 9

$$F_{1,2} = 0.53$$

$$F_3 = 0.94$$

$$F_P = F_T P_a C L R \omega$$

$$= (2 \times .53 + .94) \times 12 \times 2 \times 10^{-3} \times 1.5 \times .75 \times 5236 \times .1129$$

$$F_P = 31.9 \text{ watts}$$

The minimum film thickness is gotten by first reading ε and ξ from Figure 4 at $\phi/\alpha = 0.65$

For shoes 1 and 2 $\varepsilon = .61$ and $\xi = 41°$

For shoe 3 $\varepsilon = .67$ and $\xi = 83°$

Then, since ξ is less that 80°, for shoes 1 and 2 the minimum film thickness can be computed as

$$H_{m_{1,2}} = 1 + \varepsilon \cos (\xi+\alpha)$$

$$= 1 + .61 \cos (141°)$$

$$H_{m_{1,2}} = 0.526$$

and

$$h_{m_{1,2}} = H_{m_{1,2}} \times C = 1.052 \times 10^{-3} \text{ inches}$$

For shoes 3 the minimum film thickness occurs inside the trailing edge at 180° from the line of centers. Therefore

$$H_{m_3} = 1 - \varepsilon = 1 - 0.67$$

$$H_{m_3} = 0.33$$

and

$$h_{m_3} = 0.66 \times 10^{-3} \text{ inches}$$

The non-dimensional minimum film thickness could, of course, be obtained by examining Figure 5. The preload is computed by getting the load coefficient for shoe 3. The total film force is equal to the preload force. From Figure 3 (using ε and ξ for shoe 3 and $\phi/\alpha = 0.65$)

$$C_{L_3} = 0.522$$

There the preload W_3 is given by

$$W_3 = C_{L_3} \times P_a RL$$

$$= 0.522 \times 12 \times 0.75 \times 1.5$$

$$W_3 = 7.04 \text{ pounds}$$

Similarly, the load on each of the two bottom shoes is given by (or gotten from Figure 3)

$$W_{1,2} = W_3 - W_T$$

$$= 7.04 - 4.5$$

$$W_{1,2} = 2.54 \text{ pounds}$$

Next, the operating conditions will be investigated for the gravity load between the two fixed pivots.

As before

$$C_{LT} = 0.333$$

and since the spring load is constant for both configurations

$$C_{L_3} = 0.522$$

$$H_{P_3} = 0.430$$

$$F_3 = 0.94$$

$$h_{m_3} = 0.66 \times 10^{-3} \text{ inches}$$

From the load arrangement (through the pivots)

$$C_{L_{1,2}} = C_{L_3} + C_{LT}$$

$$= 0.522 + 0.333$$

$$C_{L_{1,2}} = 0.855$$

From Figure 3

$$\varepsilon = 0.75 \text{ and } \xi = 94°$$

Therefore

$$H_{P_{1,2}} = 1 + 0.75 \cos (94° + 65°)$$

$$H_{P_{1,2}} = 0.301$$

and

$$F_{1,2} = 1.19$$

Therefore

$$F_p = (2 \times 1.19 + .94) \times 12 \times 2 \times 10^{-3} \times 1.5 \times 7.5 \times 5236 \times .1129$$

$$F_p = 52.99 \text{ watts}$$

Also

$$H_{m_{1,2}} = 1 - 0.75 = .25$$

$$h_{m_{1,2}} = 0.25 \times 2 \times 10^{-3}$$

$$h_{m_{1,2}} = 0.5 \times 10^{-3} \text{ inches}$$

In terms of the pivot circle geometry, the pivot film thickness can also be expressed as

$$H_{P_3} = C'/C \ (1 + \varepsilon')$$

$$H_{P_{1,2}} = C'/C \ (1 - 0.5 \ \varepsilon')$$

Eliminating ε' from the above two equations

$$C'/C = \frac{H_{P_{1,2}} + 0.5\ H_{P_3}}{1.5}$$

$$= \frac{0.301 \times 0.5 \times 0.430}{1.5}$$

$$C'/C = 0.344$$

Also

$$\varepsilon' = \frac{H_{P_3}}{C'/C} - 1$$

$$= \frac{0.430}{.344} - 1$$

$$\varepsilon' = 0.25$$

Figure III-3 can be used to check the above calculations. Table III-1 summarizes the steady-state design conditions for the two extremes for the case of the horizontal rotor.

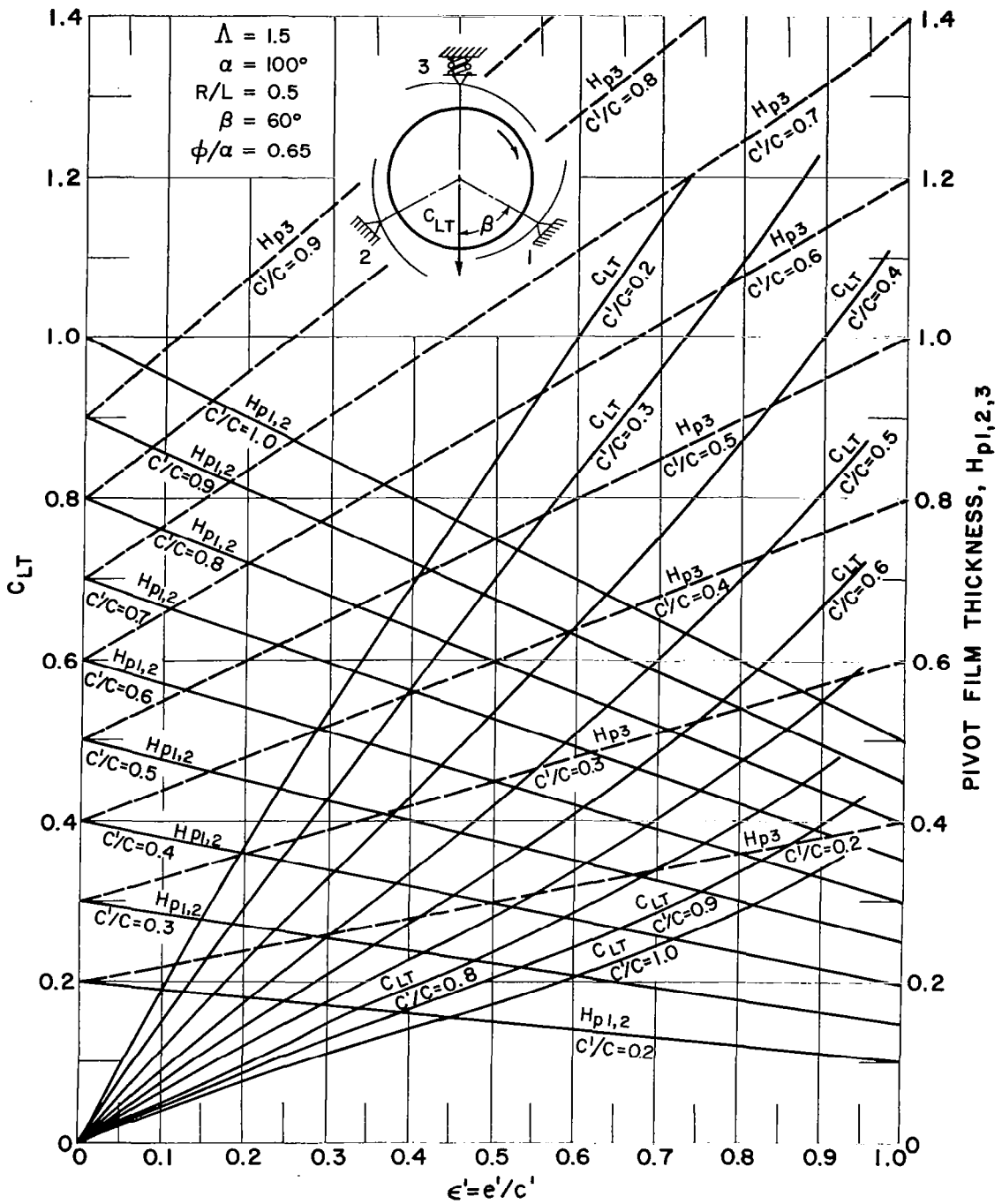

Fig. III-3 - Three Shoe Bearing Characteristics - Spring Up - R/L = 0.5, $\alpha = 100°$, $\phi/\alpha = 0.65$, $\Lambda = 1.5$

Table III-1

STEADY STATE DESIGN CONDITIONS - BEARING 1
HORIZONTAL ROTOR - MULTIPLE ORIENTATION

External load = 4.5 pounds; $\Lambda = 1.5$; $C = 2 \times 10^{-3}$ inches; $R = 0.75$ inches

	CASE 1*	CASE 2**
C'/C	0.700	0.344
ε'	0.372	0.250
Preload (lbs.)	7.04	7.04
$h_{p_{1,2}}$ (mils)	1.66	0.60
h_{p_3} (mils)	0.86	0.86
$h_{m_{1,2}}$ (mils)	1.05	0.50
h_{m_3} (mils)	0.66	0.66
F_p (Watts)	31.9	53.0

*Gravity load towards spring loaded shoe (spring down)

**gravity load between fixed pivots (spring up)

Problem 2

GIVEN: Same condition as problem 1 except:

$R = 1.0625$ inches; $L = 2.125$ inches; $C = 2.94 \times 10^{-3}$ inches;

W_T (external load) = 8.5 pounds. (conditions at Bearing 2)

FIND: C'/C, ε', total friction loss, the minimum film thickness for both gravity orientations relative to the spring such that:

(1) A shaft which passes through the bearing in problem 1 will have no steady-state misalignment.

(2) $h_m \geq 0.5 \times 10^{-3}$ inches

(3) $H_{P_3} < 1$

The total load ciefficient C_{LT} is determined by the external load as:

$$C_{LT} = \frac{W_T}{P_a RL} = 0.314$$

In problem 1 the preload setting C'/C was selected arbitrarily, but in this problem there exists a constraint on its selection, namely, the eccentricity (not the eccentricity ratio) must be the same for both bearings, i.e.,

$$e'^{(1)} = \varepsilon'^{(1)} c'^{(1)} = e'^{(2)} = \varepsilon'^{(2)} c'^{(2)}$$

or

$$\varepsilon'^{(2)} = \frac{c'^{(1)}}{c'^{(2)}} \varepsilon'^{(1)}$$

Where the superscripts refer to bearing 1 or bearing 2.

The above relation is plotted on Figure III-4 for various values of (C'/C). Also shown on Figure III-4 is a curve of ε' vs. C'/C for $C_{LT} = 0.314$. This curve is determined from Figure III-2 (the case for the spring "down"). The intersection of these two curves (point 1, Fig. III-4) gives the pivot circle coordinates ε' and C'/C that satisfy the load requirement and result in no shaft misalignment. They are

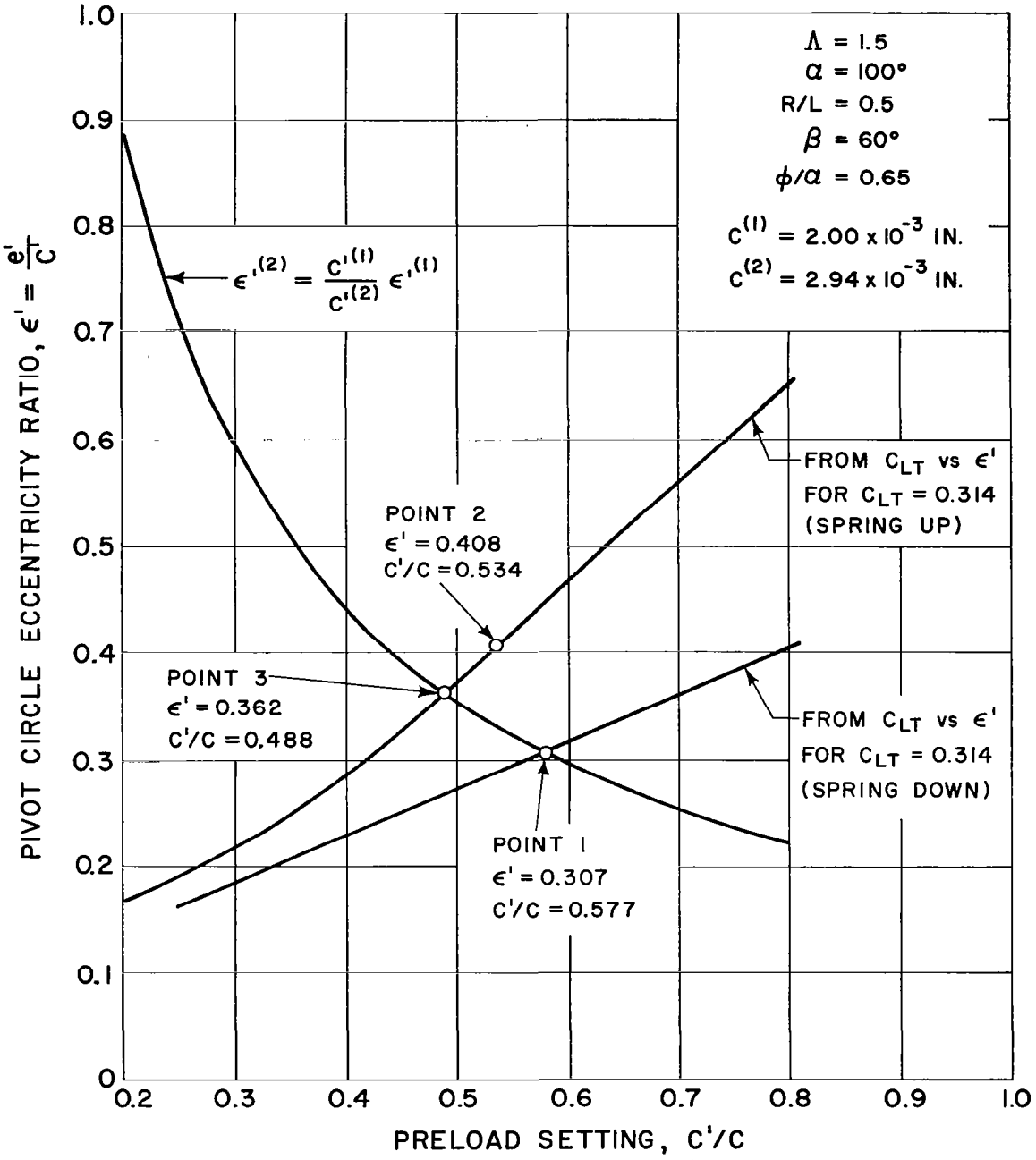

Fig. III-4 - Pivot Circle Eccentricity Ratio vs. Preload Setting - R/L = 0.5, α = 100°, ϕ/α = 0.65, Λ = 1.5

$$\varepsilon' = 0.307$$

$$C'/C = 0.577$$

then

$$H_{p_3} = C'/C\ (1 + \varepsilon') = 0.752$$

$$H_{p_{1,2}} = C'/C\ (1 - .5\ \varepsilon') = 0.487$$

From Figure 11

$$C_{L_3} = 0.218$$

Therefore the preload is

$$W_3 = C_{L_3}\ P_a RL = 5.9 \text{ pounds}$$

From Figure 5

$$H_{m_{1,2}} = 0.362$$

$$H_{m_3} = 0.487$$

Therefore

$$h_{m_{1,2}} = 1.065 \text{ inches}$$

$$h_{m_3} = 1.432 \text{ inches}$$

Also

$$F_{1,2} = 0.581$$

$$F_3 = 0.850$$

$$F_p = 94.7 \text{ watts}$$

With the spring "up" the total load coefficient, as well as the conditions at shoe three (due to maintaining the same preload) remain the same as they were with the spring "down".

Then

$$C_{L_{1,2}} = C_{L_3} + C_{LT} = 0.532$$

and

$$H_{p_{1,2}} = 0.424$$

$$H_{m_{1,2}} = 0.331$$

$$F_{p_{1,2}} = 0.950$$

$$F_p = 129.5$$

$$C'/C = \frac{H_{p_{1,2}} + 0.5\, H_{p_3}}{1.5} = 0.534$$

$$\varepsilon' = \frac{H_{p_3}}{C'/C} - 1 = 0.408$$

These coordinates are plotted on Figure III-4 as point 2. The third curve shown on Figure III-4 is the relation between ε' and C'/C for $C_{LT} = 0.314$ with the spring "up". The intersection of this curve with the ε' curve are the required coordinates (point 3) for no shaft misalignment. It can be seen from Figure III-4 that, by virtue of the fixed preload, external load, and the assymetry of the bearing radii, the shaft becomes misaligned when the gravity vector is rotated 180 degrees. The misalignment displacement in bearing 2 is gotten by taking the difference between ε' at points 2 and 3.

displacement $= (\varepsilon'_2 - \varepsilon'_3)\ (C'/C)^{(2)}_{avg}\ C^{(2)}$

$= (0.408 - 0.362) \times 0.511 \times 2.94 \times 10^3$

$= 69$ micro inches

This displacement would, of course, have an effect on the alignment of the shaft thrust collar.

Table III-2 summarizes the operating conditions for problem 2. Table III-3 shows, for various values of preload, similar results for the case where the design need only consider the gravity vector acting in one "preferred" direction. Also shown on this table are the operating conditions for the rotor in the vertical orientation.

Table III-2

STEADY-STATE DESIGN CONDITIONS - BEARING 2
HORIZONTAL ROTOR - MULTIPLE ORIENTATION

External load = 8.5 pounds, $\Lambda = 1.5$; $C = 2.94 \times 10^{-3}$ inches; $R = 1.0625$ inches

	CASE 1*	CASE 2**
C'/C	0.577	0.534
ε'	0.307	0.408
Preload (lbs.)	5.9	5.9
$h_{p_{1,2}}$ (mils)	1.430	1.248
h_{p_3} (mils)	2.205	2.205
$h_{m_{1,2}}$ (mils)	1.065	.972
h_{m_3} (mils)	1.432	1.432
F_p (watts)	94.7	129.5

*Gravity load towards spring loaded shoe (spring down).

**Gravity load between fixed pivots (spring up).

Table III-3

STEADY-STATE DESIGN CONDITIONS BEARING 1 AND 2
HORIZONTAL ROTOR - PREFERRED ORIENTATION - $\Lambda = 1.5$

$\Lambda = 1.5$

	$R/L = 0.5$			$\alpha = 100°$			$\phi/\alpha = 0.65$					
	Bearing No. 1						Bearing No. 2					
	W = 4.3 lbs Diam. = 1.5 in. $\mu = 4.1 \times 10^{-9}$ lb-sec/in^2						W = 8.5 lbs Diam. = 2.125 in. $\mu = 4.4 \times 10^{-9}$ lb-sec/in^2					
	p_a = 6 psia c = 2.836			p_a = 12 psia c = 2.006			p_a = 6 psia c = 4.163			p_a = 12 psia c = 2.943		
Preload	2	4	6	2	4	6	2	4	6	2	4	6
	SHAFT HORIZONTAL											
ε'	.596	.474	.385	.476	.354	.277	.752	.591	.491	.581	.477	.401
e'	.666	.360	.227	.585	.330	.210	1.615	.974	.662	1.273	.859	.627
c'/c	.394	.268	.208	.613	.465	.379	.516	.396	.324	.745	.612	.531
c'	1.117	.760	.590	1.230	.933	.760	2.148	1.648	1.349	2.192	1.801	1.563
$h_p(1,2)$	.785	.581	.479	.937	.766	.656	1.340	1.161	1.016	1.554	1.371	1.247
$h_p(3)$	1.784	1.120	.817	1.815	1.264	.971	3.763	2.623	2.011	3.467	2.660	2.190
$h_m(1,2)$	.669	.516	.431	.710	.616	.544	1.120	.995	.882	1.127	1.042	.974
$h_m(3)$	1.219	.890	.695	1.129	.862	.728	2.340	1.790	1.503	2.110	1.654	1.416
$F_f(1,2)$	14.115	16.410	17.700	14.048	16.400	18.112	38.150	41.615	44.647	37.263	41.503	44.753
$F_f(3)$	7.634	11.310	13.820	7.648	10.800	13.664	15.993	22.457	28.554	17.148	22.612	27.700
$F_f(T)$	35.864	44.120	49.220	35.744	43.600	49.888	92.293	105.687	117.848	91.674	105.618	117.206
	SHAFT VERTICAL											
e'	0	0	0	0	0	0	0	0	0	0	0	0
c'/c	.629	.395	.288	.905	.630	.484	.904	.630	.483	1.178	.904	.744
$c'=h_p$	1.784	1.120	.817	1.815	1.264	.971	3.763	2.623	2.011	3.467	2.660	2.190
h_m	1.219	.890	.695	1.129	.862	.728	2.340	1.790	1.503	2.110	1.654	1.416
F_f	7.634	11.310	13.820	7.648	10.800	13.664	15.993	22.457	28.554	17.148	22.612	27.700
$F_f(T)$	22.902	33.930	41.460	22.940	32.400	40.992	47.979	67.371	85.662	51.444	67.836	83.100

Note: c, c', e', h_p, h_m given in mils; F_f given in watts; preload given in lbs; $\varepsilon' = e'/c'$; subscripts refer to shoe no. or total.

Operating Conditions for $\Lambda = 3.5$

This section contains characteristic curves for a three pad bearing with $\Lambda = 3.5$, $\alpha = 100°$, $R/L = 0.5$, $\phi/\alpha = 0.65$ and a pivot separation of 120°. Figure III-6 shows the case for the gravity load between the fixed pivots; Figure III-5 shows the case where the gravity load is directed at the spring loaded show. Table III-4 is a summary for $\Lambda = 3.5$ of the operating conditions at bearings 1 and 2 for ambient pressures of 6 psig and 12 psig and for preloads of 2, 4 and 6 pounds. In this table the gravity load is directed between the fixed pivots.

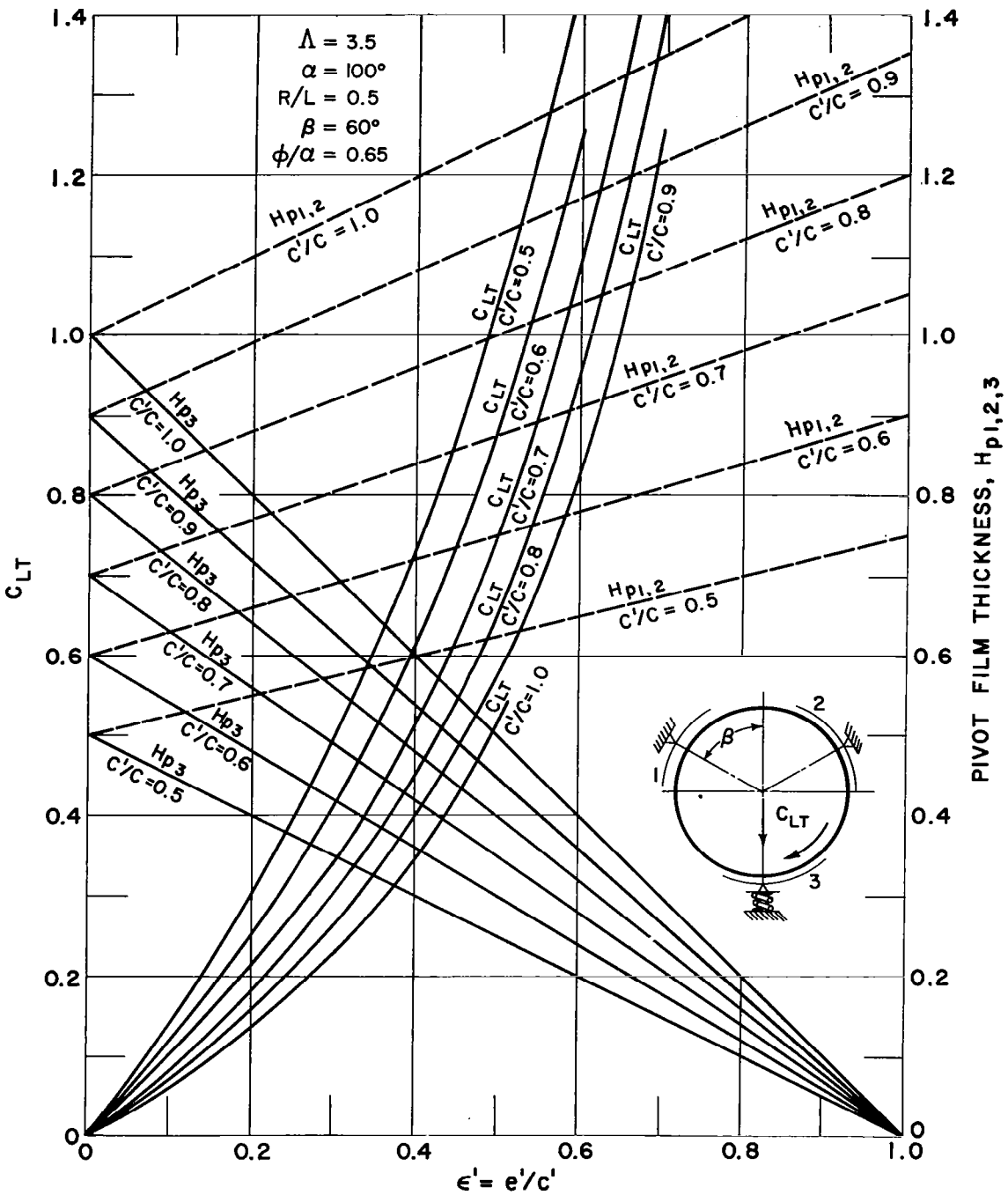

Fig. III-5 - Three Shoe Bearing Characteristics - Spring Down - R/L = 0.5, α = 100°, ϕ/α = 0.65, Λ = 3.5

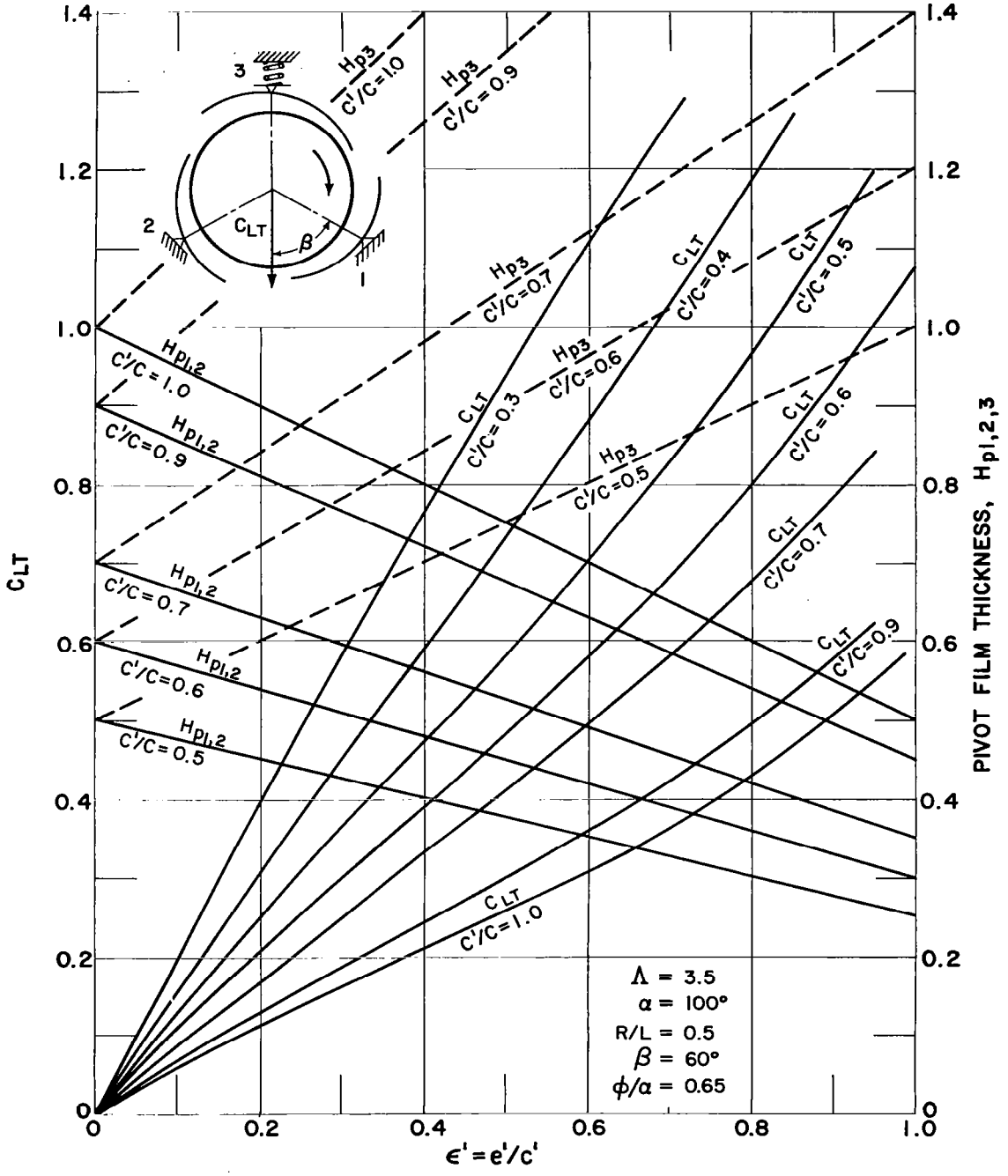

Fig. III-6 - Three Shoe Bearing Characteristics - Spring Up - R/L = 0.5, α = 100°, ϕ/α = 0.65, Λ = 3.5

Table III-4

STEADY-STATE DESIGN CONDITIONS - BEARINGS 1 AND 2
HORIZONTAL ROTOR - PREFERRED ORIENTATION - $\Lambda = 3.5$

$\Lambda = 3.5$

	R/L = 0.5			$\alpha = 100°$			$\phi/\alpha = 0.65$					
	Bearing No. 1						Bearing No. 2					
	W = 4.3 lbs Diam. = 1.5 $\mu = 4.1 \times 10^{-9} \frac{\text{lb-sec}}{\text{in}^2}$						W = 8.5 lbs Diam. = 2.125 in. $\mu = 4.4 \times 10^{-9} \frac{\text{lb-sec}}{\text{in}^2}$					
	P_a = 6 psia c = 1.857			P_a = 12 psia c = 1.313			P_a = 6 psia c = 2.725			P_a = 12 psia c = 1.927		
Preload	2	4	6	2	4	6	2	4	6	2	4	6
					SHAFT HORIZONTAL							
ε'	.582	.417	.349	.382	.336	.271	.659	.575	.451	.378	.382	.367
e'	.570	.289	.187	.390	.275	.181	1.164	.830	.547	.634	.573	.494
c'/c	.527	.374	.289	.778	.624	.509	.648	.530	.446	.871	.778	.698
c'	.979	.694	.537	1.022	.819	.668	1.766	1.444	1.215	1.678	1.499	1.345
$h_p(1,2)$	.693	.550	.444	.827	.681	.578	1.183	1.030	.940	1.362	1.214	1.098
$h_p(3)$	1.549	.984	.724	1.411	1.095	.850	2.929	2.275	1.763	2.312	2.071	1.838
$h_m(1,2)$	.615	.505	.408	.637	.551	.491	1.008	.907	.845	1.023	.938	.873
$h_m(3)$	1.120	.798	.635	1.061	.792	.652	2.202	1.643	1.354	1.869	1.557	1.324
$F_f(1,2)$	21.975	26.448	31.601	15.604	18.745	21.154	44.492	48.854	52.343	41.333	46.269	50.895
$F_f(3)$	11.182	17.113	21.294	9.948	12.043	15.184	19.411	25.081	31.842	23.442	27.453	31.154
$F_f(T)$	55.132	70.006	84.496	41.156	49.533	57.492	108.395	122.789	136.528	106.108	119.991	132.944
					SHAFT VERTICAL							
e'	0	0	0	0	0	0	0	0	0	0	0	0
c'/c	.834	.530	.390	1.075	.834	.647	1.073	.835	.647	1.200	1.075	.954
$c' = h_p$	1.549	.984	.724	1.411	1.095	.850	2.929	2.275	1.763	2.312	2.071	1.838
h_m	1.120	.798	.635	1.061	.792	.652	2.202	1.643	1.354	1.869	1.557	1.324
F_f	11.182	17.113	21.294	9.948	12.043	15.184	19.411	25.081	31.842	23.442	27.453	31.154
$F_f(T)$	33.546	51.339	63.882	29.844	36.129	45.552	58.233	75.243	95.526	70.326	82.359	93.462

Note: c, c', e', h_p, h_m, given in mils; F_f given in watts; preload given in lbs.; $\varepsilon' = e'/c'$; subscripts refer to shoe no. or total.

APPENDIX IV

THE DEVELOPMENT OF THE SHAFT AND SHOE DYNAMICAL EQUATIONS

1. Shaft Rotation Equations

The angular motion of the shaft can be obtained from the angular momentum principle. Let $\bar{N}_i$, i = 1,2,3 be a right hand set of unit vectors fixed in the shaft S; let P* be a point fixed in S and let the Newtionian x,y,z reference frame shown in Figure IV-I be designated by Q_1. Then, the angular momentum in Q_1 of the rigid body S relative to the point P* fixed in S is given by

$$Q_1 \bar{A}^{S/p*} = \left(\bar{N}_o \cdot Q_1 \bar{\omega}^{S} \right) \bar{\Phi}^{S/p*} \qquad \text{(IV-1)}$$

where

$\bar{N}_o$ is a unit vector parallel to the angular velocity of S in Q_1 i.e. $\left({}^{R}\bar{\omega}^{S} \right)$

and

$\bar{\Phi}^{S/p*}$ is value of the inertia tensor of S with respect to P* for the direction $\bar{N}_o$

Equation IV-1 can also be written

$$Q_1 \bar{A}^{S/p*} = \phi_{ij}^{S/p*} \, Q_1 \bar{\omega}_i^{S} \, \bar{N}_j$$

The angular momentum principle states that the time derivation of the angular momentum of S with respect to P* in reference frame Q_1 is equal to the sum of the moments about P* of all gravitational and contact forces acting on S, i.e.,

$$\frac{{}^{Q_1}d\left({}^{Q_1}\bar{A}^{S/p^*}\right)}{dt} = \bar{M}\ p^*$$

Let P* be the shaft mass center and let $\bar{N}_j$, $j = 1,2,3$ be mutually perpendicular principal directions of S and fixed in S for P*

Then,

$${}^{Q_1}\bar{A}^{S/p^*} = \phi_{11}^{S/p^*}\ \omega_1\ \bar{N}_1 + \phi_{22}^{S/p^*}\ \omega_2\ \bar{N}_2 + \phi_{33}^{S/p^*}\ \omega_3\ \bar{N}_3$$

where

ω_i is the $\bar{N}_i$ magnitude of the shaft angular velocity

and

$$\frac{{}^{Q_1}d\left({}^{Q_1}\bar{A}^{S/p^*}\right)}{dt} = \frac{{}^{S}d\left({}^{Q_1}\bar{A}^{S/p^*}\right)}{dt} + {}^{Q_1}\bar{\omega}^{\bar{S}} \times {}^{Q_1}\bar{A}^{S/p^*} \qquad \text{(IV-2)}$$

where

$$\frac{{}^{S}d\left({}^{Q_1}\bar{A}^{S/p^*}\right)}{dt} = \phi_{11}^{S/p^*}\ \dot{\omega}_1\ \bar{N}_1 + \phi_{22}^{S/p^*}\ \dot{\omega}_2\ \bar{N}_2 + \phi_{33}^{S/p^*}\ \dot{\omega}_3\ \bar{N}_3 \qquad \text{(IV-3)}$$

and

${}^{Q_1}\bar{\omega}^{\bar{S}}$ is the angular velocity of the $\bar{N}_i$ reference frame in the $\bar{N}_x$, $\bar{N}_y$, $\bar{N}_z$ frame

$\bar{S}$ is a reference frame with $\bar{N}_3$ along the shaft axis but not rotating with the shaft.

Let Q_2 with the unit vectors $\bar{N}_1'$, $\bar{N}_2'$, $\bar{N}_3'$ be a reference frame with $\bar{N}_2'$ parallel to $\bar{N}_y$. The relations among S, Q_2, and Q_1 are shown below in Figure IV-1

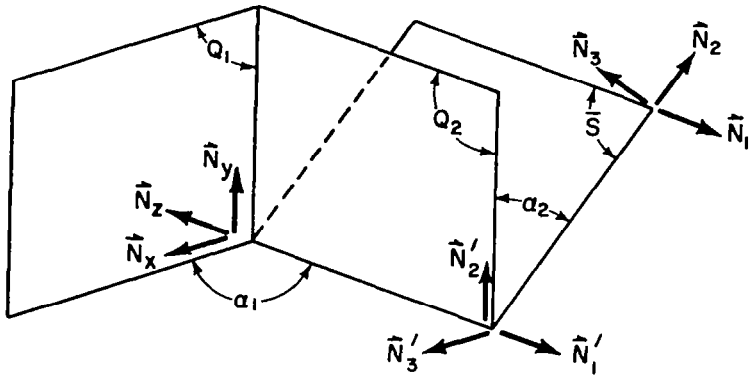

Fig. IV-1 - Shaft Reference Frames

then, the angular velocity of $\bar{S}$ in Q_1 is

$$Q_1 \underset{\omega}{} \bar{S} = Q_1 \underset{\omega}{} Q_2 + Q_2 \underset{\omega}{} \bar{S}$$

where

$$Q_1 \underset{\omega}{} Q_2 = \dot{\alpha}_1 \bar{N}_1$$

$$Q_1 \underset{\omega}{} \bar{S} = - \dot{\alpha}_2 \bar{N}_1 = \dot{\alpha}_2 \bar{N}_1'$$

Now

$$\bar{N}_1' = \cos \alpha_1 \bar{N}_x - \sin \alpha_1 \bar{N}_z$$

For small α_1

$$\bar{N}_1' = \bar{N}_x - \alpha_1 \bar{N}_z$$

Therefore

$$Q_1 \bar{\omega}^{\bar{S}} = \dot{\alpha}_1 \bar{N}_y - \dot{\alpha}_2 (\bar{N}_x - \alpha_1 \bar{N}_z)$$

Since

$$\dot{\alpha}_2 \alpha_1 << \dot{\alpha}_1$$

$$Q_1 \bar{\omega}^{\bar{S}} = \dot{\alpha}_1 \bar{N}_y - \dot{\alpha}_2 \bar{N}_x$$

Transformations between reference frames $\bar{S}$ and Q_1 result in

$$\bar{N}_2 = \bar{N}_y - \alpha_1 \quad \alpha_2 \bar{N}_x - \alpha_2 \bar{N}_z \cong \bar{N}_y - \alpha_2 \bar{N}_z$$

$$\bar{N}_3 = \alpha_1 \bar{N}_x + \alpha_2 \bar{N}_y + \bar{N}_z$$

Substituting in Equation (IV-3)

$$\frac{S_d \left(R \bar{A}^{S/p^*} \right)}{dt} = \phi_{11}^{S/p^*} \dot{\omega}_1 (\bar{N}_x - \alpha_1 \bar{N}_z) + \phi_{22}^{S/p^*} \omega_2 (\bar{N}_y - \alpha_2 \bar{N}_z) + \phi_{33}^{S/p^*} \omega_3 \quad (\alpha_1 \bar{N}_x + \alpha_2 \bar{N}_y + \bar{N}_z)$$

Consistant with the above assumption of small α_1, α_2

$$\omega_1 = -\dot{\alpha}_2$$

$$\omega_2 = \dot{\alpha}_1$$

$$\omega_3 = -\Omega$$

$$\dot{\omega}_i \alpha_j << \dot{\omega}_i$$

where Ω is the axial angular speed of the shaft, a constant.

Let

$$\phi_{11}^{S/p^*} = \phi_{22}^{S/p^*} = I_T$$

$$\phi_{33}^{S/p^*} = I_p$$

then

$$Q_{\bar{\omega}}^{S} \times Q_1 \bar{A}^{S/p^*} = - I_p \dot{\alpha}_1 \Omega \bar{N}_x - I_p \dot{\alpha}_2 \Omega \bar{N}_y$$

And equation (IV-2) becomes

$$\frac{Q_{1_d}\left(Q_1 \bar{A}^{S/p^*}\right)}{dt} = (-I_T \alpha_2 - I_p \dot{\alpha}_1 \Omega) N_x + (I_T \alpha_1 - I_p \dot{\alpha}_2 \Omega) N_y \qquad \text{(IV-4)}$$

Let the vector sum of moments due to all the graviational and contact forces about P* be given by

$$\bar{M}^{P^*} = M_x \bar{N}_x + M_y \bar{N}_y + M_z \bar{N}_z$$

Assuming that the axial driving torque is balanced by friction, windage and output torque,

$$M_z = 0$$

The shaft unbalance is considered as an external force system and, as such it can be replaced by an equivalent system consisting of a force F_u passing through P* and a moment M_u about P*. There is an infinite number of ways that the system may be represented -- one such way is shown in Figure IV-2. In this case

$$|\bar{F}_u| = Rm_2 \Omega^2$$

$$|\bar{M}_u| = 2m_1 R \rho_u \Omega^2$$

Referring to the figure below,

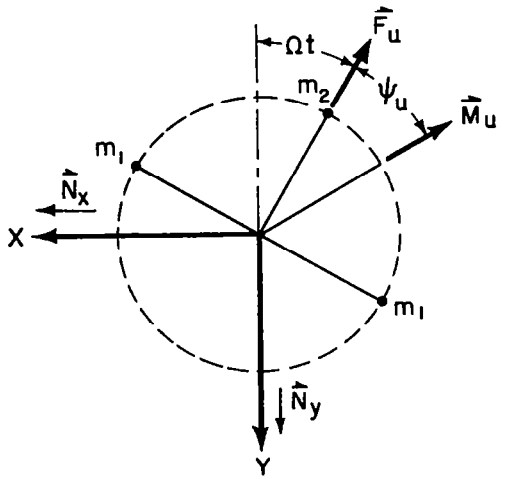

Fig. IV-2 - Shaft Unbalance Representation

the unbalance force $\bar{F}_u$ is located in the $\bar{N}_x$, $\bar{N}_y$, $\bar{N}_z$ coordinate system by the angle Ωt and the unbalance moment $\bar{M}_u$ is located by the angle $(\Omega t + \psi_u)$. The unbalance system thereby revolves synchronously with the shaft.

Let

$$M_x = T_{ux} + T_{px}$$
$$M_y = T_{uy} + T_{py} \qquad \text{(IV-5)}$$

Where T_{ux} is the $\bar{N}_x$ component of M_u, etc.

and T_{px} is the $\bar{N}_x$ component of the moment about P* produced by the shoe pressures.

Now

$$T_{ux} = \bar{M}_u \cdot \bar{N}_x = - |\bar{M}_u| \sin (\Omega t + \psi_u) \qquad \text{(IV-6)}$$

Similarly

$$T_{uy} = \bar{M}_u \cdot \bar{N}_y = - \bar{M}_u \cos (\Omega t + \psi_u)$$

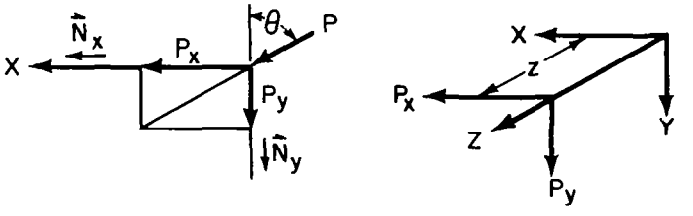

Fig. IV-3 - Bearing Forces

From Figure IV-3

$$T_{px} = -R \int_{L_1}^{L_2} \int_0^{2\pi} zP \cos \theta d\theta dz \qquad \text{(IV-7)}$$

and

$$T_{py} = R \int_{L_1}^{L_2} \int_0^{2\pi} zP \sin \theta d\theta dz \qquad \text{(IV-8)}$$

Using eqs. IV-4 through IV-8 the following equations are obtained:

$$\bar{N}_x: -I_T \ddot{\alpha}_2 - I_p \dot{\alpha}_1 \Omega = -|\bar{M}_u| \sin(\Omega t + \psi u) - R \iint zP \cos d\theta dz \qquad \text{(IV-9)}$$

$$\bar{N}_y: I_T \ddot{\alpha}_1 - I_p \dot{\alpha}_2 \Omega = -|\bar{M}_u| \cos(\Omega t + \psi u) + R \iint zP \sin d\theta dz \qquad \text{(IV-10)}$$

The coupled equations (IV-9) and (IV-10) can be integrated numerically to obtain the shaft angular coordinates α_1 and α_2.

2. Shaft Translation Equations

Let the shaft with mass "m" be considered rigid with its mass center at P*. The instantaneous position of P* can be obtained using D'Alembert's principle which states that the force system consisting of all gravitational, contact and inertia forces acting on a body S is a zero system in a Newtonian reference frame. The reference frame designated by the unit vectors $\bar{N}_x$, $\bar{N}_y$, $\bar{N}_z$ in Figure IV-1 form a Newtonian reference frame Q_1, therefore:

$$^{Q_1}\bar{F}^{P^*} = m\, {}^{Q_1}\bar{a}^{P^*} \qquad \text{(IV-11)}$$

where $^{Q_1}\bar{F}^{P^*}$ is the vector force resultant through the point P* in Q_1 of all gravitational and contact force and $^{Q_1}\bar{a}^{P^*}$ is the absolute acceleration of P* in Q_1. Assuming that the thrust bearing completely constrains the shaft in the axial direction, the gravitational and contact force system is represented by Figure IV-4.

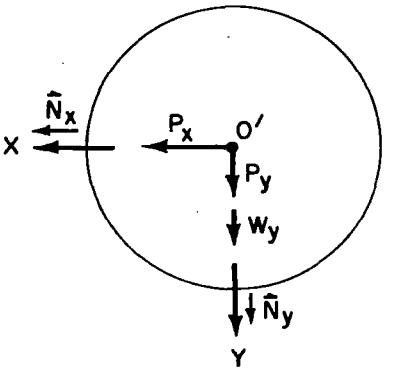

Fig. IV-4 - Shaft Forces

Let O' be the origin of the x, y, z coordinate system, then the position vector of P* relation of O' is given by

$$^{O'}\bar{P}^* = x\,\bar{N}_x + y\,\bar{N}_y \qquad \text{(IV-12)}$$

and

$$Q_1 \; \bar{a}^{\,P^*} = \frac{d^2\left(^{O'}\bar{P}^*\right)}{dt} = \ddot{x}\,\bar{N}_x + \ddot{y}\,\bar{N}_y \qquad \text{(IV-13)}$$

Let

$$Q_1 \; \bar{F}^{\,P^*} = F_x\bar{N}_x + F_y\bar{N}_y$$

From Figures IV-3 and IV-4

$$F_x = \iint P \sin\theta \, R\,d\theta\,dz - \left|\bar{F}_u\right| \sin \Omega t$$

$$F_y = \iint P \cos\theta \, R\,d\theta\,dz - \left|\bar{F}_u\right| \cos \Omega t + W_y \qquad \text{(IV-14)}$$

Using equations IV-11 through IV-14 the following equations are obtained:

$$\bar{N}_x: m\ddot{x} = \iint P \sin\theta R d\theta dz - |\bar{F}_u| \sin \Omega t \qquad \text{(IV-15)}$$

$$\bar{N}_y: m\ddot{y} = \iint P \cos\theta R d\theta sz - |\bar{F}_u| \sin \Omega t + W_y \qquad \text{(IV-16)}$$

Equations IV-15 and IV-16 can be integrated numerically to obtain the shaft mass center coordinates x and y.

3. Shoe Dynamics

For convenience a new reference frame Q_3 with three mutually perpendicular axis (X_1, X_2, X_3) is chosen. Here, the X_1 axis coincides with the Z axis while the X_3 axis passes through the pivot point. The unit vector system ($\bar{n}_1$, $\bar{n}_2$, $\bar{n}_3$) for this reference frame is shown on Figure IV-5. Since Q_3 differs from Q_1 only in the orientation of axis and the position of its center there is no relative motion between the two reference frames, thus Q_3 is also a Newtonian reference frame. In addition, X_1 is the principal axis of shoe at mass center, and the product of inertia with respect to the $\bar{N}_1$ direction vanishes. The angular velocity of a shoe in Q_3 is

$$\vec{\omega} = \dot{\delta}\vec{n}_1 + \dot{\gamma}\vec{n}_2 + \omega_3\bar{n}_3$$

where δ is the pitch angle and γ the roll angle.

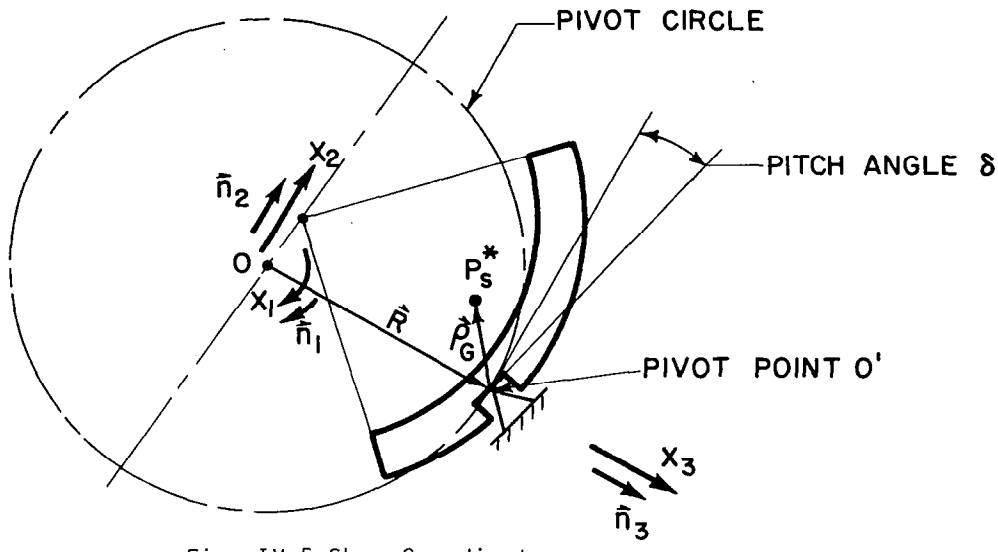

Fig. IV-5 Shoe Coordinates

In the present problem, since the angular speed in the yaw direction is small in comparison with that of the other two directions (pitch and roll), ω_3 can be neglected. Furthermore, it is assumed that $\dot{\delta}$ and $\dot{\gamma}$ are small so that the square of these quantities may also be neglected. Hence,

$$\bar{\omega} = \dot{\delta}\,\bar{n}_1 + \dot{\gamma}\,\bar{n}_2$$

Let O be the center of Q_3, O' the pivot point, and P_s^* the mass center of the shoe. $\bar{\rho}_G$ is the position vector from O' to P_s^* and $\bar{R}$ is the position vector from O to O'. Since the pivot point is allowed to move along X_3, the acceleration of P_s^* is

$$\bar{a}^{P_s^*} = \ddot{\bar{R}} + \dot{\omega} \times (\bar{\rho}_G)$$

where the dot indicates the time derivation. The second term in the above expression is due to pitch and roll motion of the shoe. It should be noted that a term $\bar{\omega} \times (\bar{\omega} \times \bar{\rho}_G)$ has been dropped because it is negligable compared to the other terms. The inertia force is then

$$\bar{I} = - M_{shoe}\bar{a}^{P*}$$

The inertia moment is

$$\bar{T} = - \sum_{i=1}^{3} \sum_{j=1}^{3} \phi_{ij}^{S/p^*} \dot{\omega}_i \bar{n}_j$$

where $\phi_{i,j}$ is the moment and product of inertia about P_s^*

$$\omega_1 = \dot{\delta} \text{ and } \omega_2 = \dot{\gamma}$$

Applying D'Alembert's Principle we have

$$\bar{I} + \bar{F} = 0$$
$$\bar{T} + \bar{M} = (\bar{\rho}_G) \times \bar{I} = 0$$

Here, $\bar{F}$ is the vector sum of all contact force and gravitational force, $\bar{M}$ is the vector sum of moments due to these forces.

The first equation states that all the forces acting at the pivot point are in equilibrium, while the second equation indicates the moment equilibrium about the same point. Since the shoe is allowed to move only in the X_3 direction, the first vector equation yields one scalar equation. From moment equilibrium we obtain two scalar equations: one for the pitch motion, the other for the roll motion. Let I_P be the pitching inertia about 0' I_R the roll inertia and ρ_{G2}, ρ_{G3} the component of ρ_G along X_2 and X_3 axis we have

$$\phi_{11}^{S/p^*} + M_{shoe}(\rho_{G2}^2 + {}^2_{G3}) = I_P$$
$$\phi_{22}^{S/p^*} + M_{shoe}\rho_{G3}^2 = I_R$$

The three equations of motion may now be written explicitly.

$$M_{shoe}\,\rho_{G2}\,\ddot{R}_p + I_P\,\ddot{\delta} = M_1 \qquad \text{(IV-17)}$$

$$I_R\,\ddot{\gamma} = M_2 \qquad \text{(IV-18)}$$

$$M_{shoe}\,(\ddot{\kappa}_p + \rho_{G2}\,\ddot{\delta}) = F_3 \qquad \text{(IV-19)}$$

Since at any time during the motion

$$R_p = R + c'$$

Where R is the shaft radius, we have

$$\ddot{R}_p = \ddot{c}'$$

Thus, the last equation becomes

$$M_{shoe}\,(\ddot{c}' + \rho_{G2}\,\ddot{\delta}) = F_3 \qquad \text{(IV-20)}$$

The moments and forces appear on the left hand side of these equations consists of contributions from film pressures, pivot friction, and preloads. They may be written explicitly as follows:

$$F_3 = R\iint P\cos(\theta - \theta_p)\,d\theta d\eta - F_p - kc'$$

$$M_1 = R^2\iint P\sin(\theta - \theta_p)\,(1 + d/R)\,d\theta d\eta$$

$$M_2 = R\iint P\cos(\theta - \theta_p)\,(y - y_B)\,d\theta d\eta + M_f$$

where θ_p is the location of pivot, d the distance from pivot to shoe surface along X_3, F_p the preload, kc' the spring force, and M_f the friction moment where

$$M_f = 0 \quad \text{for} \quad \omega = 0$$

$$= + m_f \quad \text{for} \quad \omega < 0$$

$$= - m_f \quad \text{for} \quad \omega > 0$$

In order to solve this set of equations we substitute equation (IV-20) into equation (IV-19)

$$\ddot{\delta} = \frac{M_1 - F_3 \rho_{G2}}{I_P - \rho_{G2}^2 M_{shoe}}$$

Once δ is known, (IV-18) and (IV-20) may be used to solve γ and c'

$$\ddot{\gamma} = M_2/I_R$$

$$\ddot{c}' = \frac{F_3}{M_{shoe}} - \rho_{G2} \ddot{\delta}$$

It should be noted that for the fixed shoe this substitution is unnecessary, since in this case c' = 0 and (IV-17) reduces to

$$I_P \ddot{\delta} = M_1$$

Thus, there are three equations of motion for a spring-loaded shoe and two for a fixed shoe. For the present problem, since there are a total of six shoes, two of them are spring loaded, we have a set of 16 equations of motion.

4. Bearing Film Clearance

To evaluate the film clearance the shaft axis is initially coincidnet with the z- axis and all shoe bearing surfaces lie on a cylinder of radius (R + c) having z as its axis. The film clearance is now c everywhere. Motions of the shoes and shaft alter the film thickness by the following amounts:

a. Translation of shaft; $x_m \sin\theta + y_m \cos\theta$
b. Tilting of shaft; $\alpha_1 \sin\theta + \alpha_2 \cos\theta$
c. Radial translation of shoe; $(c'-c)\cos\varphi$
d. Pitch of shoe; $(d + R)\,\delta \sin\varphi$
e. Roll of shoe; $\gamma(z - z_B)\cos\varphi$

Therefore the dimensionless film thickness is

$$H = 1 + (X_m + A_1 Z)\sin\theta + (Y_m + A_2 Z)\cos\theta$$

$$+ (D + 1)\,\Delta \sin\varphi + [(Z - Z_B)\,\Gamma + C_p]\cos\varphi.$$

To facilitate numerical calculations, all the pertinent equations are presented in non-dimensional form. For the equations of motion of the shoes and for the Reynold's equation it is natural to non-dimensionalize them with respect to the parameters of the individual bearing, since these equations only deal with one particular bearing and the influence of the others do not appear in them explicitly. Equations of motion for the rotor, on the other hand, involve contributions from both bearings. Thus, it is necessary to non-dimensionalize them with respect to one set of parameters. In the present problem, parameters of bearing 1 are chosen and dimensionless quantities of bearing 2 will be converted.

The dimensionless quantities are listed, as follows:

$$H = h_i/c_i$$

$$C' = C_i'/C_i - 1$$

$$\Lambda = \frac{6\,\mu_i\,\Omega}{P_{ai}} \left(\frac{R_i}{C_i}\right)^2$$

$$P = P_i/P_{ai}$$

$$\Delta = \delta_i\, R_i/C_i$$

$$\Gamma = \gamma_i\, L_i/C_i$$

$$D = \frac{d_i}{R_i}$$

$$TP = \frac{M_1}{P_{ai}\, R_i^2\, L_i}$$

$$TR = \frac{M_2}{P_{ai}\, R_i\, L_i^2}$$

$$FF = \frac{F_3}{P_{ai}\, R_i\, L_i}$$

$$F_s = \frac{kc'}{P_{ai}\, R_i\, L_i}$$

$$PVTFR = \frac{M_f}{P_{ai}\, R_i^2\, L_i}$$

$$Z = \eta/L_i$$

$$I\Delta = \frac{P_{ai}\, R_i^2\, L_i}{I_P - M_{shoe}\, \rho'\, G_2} \frac{R_i}{C_i} \left(\frac{2}{\Omega}\right)^2$$ - pitch inertia parameter

$$I\Gamma = \frac{P_{ai}\, R_i\, L_i^2}{I_R} \frac{L_i}{C_i} \left(\frac{2}{\Omega}\right)^2$$ - roll inertia parameter

$$\bar{M}_s = P_a R L_i / M_{shoe} C\left(\frac{\Omega}{2}\right)^2$$

$$RR_i = P_{G2}/R$$

where "i" denotes bearing 1 or 2

For the rotor we have:

$$X_M = X_m/C_1$$

$$Y_M = Y_m/C_1$$

$$A_1 = \alpha_1 L_1/C_1$$

$$A_2 = \alpha_2 L_1/C_1$$

$$T = t\,\Omega/2$$

$$G = 2\frac{I_P}{I_T}$$

$$F_X = \frac{F_x}{P_{a1} R_1 L_1}$$

$$F_Y = \frac{F_y}{P_{a1} R_1 L_1}$$

$$T_A = \frac{M_x}{P_{a1} R_1 L_1^2}$$

$$T_{AA} = \frac{M_y}{P_{a1} R_1 L_1^2}$$

$$U_F = \frac{F_u}{P_{a1} R_1 L_1}$$

$$U_M = \frac{M_u}{P_{al}\ R_1\ L_1^2}$$

$$B = P_{al}\ R_1\ L_1/M_{shaft}\ C_1\ \left(\frac{\Omega}{2}\right)^2$$

$$I = P_{al}\ R_1\ L_1^3/I_T\ C\left(\frac{\Omega}{2}\right)^2$$

$$WY = load/P_{al}\ R_1\ L_1$$

Substituting these quantities into governing equations we have

1. Reynold's Equation

$$\frac{\partial}{\partial\theta}\left(PH^3\ \frac{\partial P}{\partial\theta}\right) + \left(\frac{R}{L}\right)^2 \frac{\partial}{\partial Z}\left(PH^3\ \frac{\partial P}{\partial Z}\right) = \Lambda\ \left(\frac{\partial PH}{\partial\theta} + \frac{\partial PH}{\partial T}\right)$$

where H is given by the equation

$$H = 1 + (X_M + A_1 Z)\ \sin\theta + (Y_M + A_2 Z)\ \cos\theta + C_i'\ \cos\varphi$$
$$+ (1 + D_i)\ \sin\varphi\ \Delta_i + (Z - Z_B)\ \Gamma_i\ \cos\varphi$$

where subscript "i" denotes the i^{th} shoe

2. Shaft Motion

$$\ddot{XM} = B\ \{FX - U_F\ \sin\ (2T)\}$$

$$\ddot{YM} = B\ \{FY - U_F\ \cos\ (2T) + WY\}$$

$$\ddot{A}_2 = -G\ \dot{A}_1 + \{T_{AA} + U_M\ \sin\ (2T + \psi_u)\}\ I$$

$$\ddot{A}_1 = G\ \dot{A}_2 + \{TA - U_M\ \cos\ (2T + \psi_u)\}\ I$$

3. Shoe Motion

$$\ddot{\Delta}_i = [TP_i - (FF_i)\ (RR_i)]\ \ (I\Delta)$$

$$\ddot{\Gamma}_i = (TR_i)\ (I\Gamma)$$

$$\ddot{C}_i' = (FF_i)\ (M_s) - (\ddot{\Delta}_i)\ (RR_i)$$

APPENDIX V

COMPUTATIONS FOR STEADY-STATE AND EXPERIMENTAL COMPARISON FOR THE VALIDATION OF THE NON-LINEAR ORBIT PROGRAM

1. Pivot Film Thickness

In general, the clearance anywhere within the shoe is given by

$$H = \frac{h}{C} = 1 + (X_M + A_1 Z) \sin\theta + (Y_M + A_1 Z) \cos\theta + (C'/C - 1) \cos\psi + (D + 1)\,\Delta \sin\psi + (Z - Z_B)\,\Gamma \cos\psi \qquad (V\text{-}1)$$

using the computer data from the non-linear orbit program

C = radius of shaft - radius of shoe

$X_M = \frac{X_m}{C} \approx 0$ = horizontal coordinate of shaft mass center

$Y_M = \frac{Y_m}{C} = 0.9608$ = vertical coordinate of shaft mass center

$L = 3.3''$ = shoe axial length

$R = 2''$ = shaft radius

$A_1 = \frac{\alpha_1 L}{C} \approx 0$ = horizontal angular coordinate of shaft

$A_2 = \frac{2^L}{C} = 0.00215$ = vertical angular coordinate of shaft

$Z = z/L = Z_B = 3.45$ = axial location of bearing 1 from shaft CG

$C'/C-1 = 0$ = pivot displacement

$D = \frac{d}{R} = 0.15$ = pivot distance from face of shoe

$\Delta = \delta R/C = -0.3793$ = shoe pitch angular coordinate

$\Gamma = \gamma L/C = 0.001927$ = shoe roll angular coordinate

The journal coordinate system is shown in Figure 1.

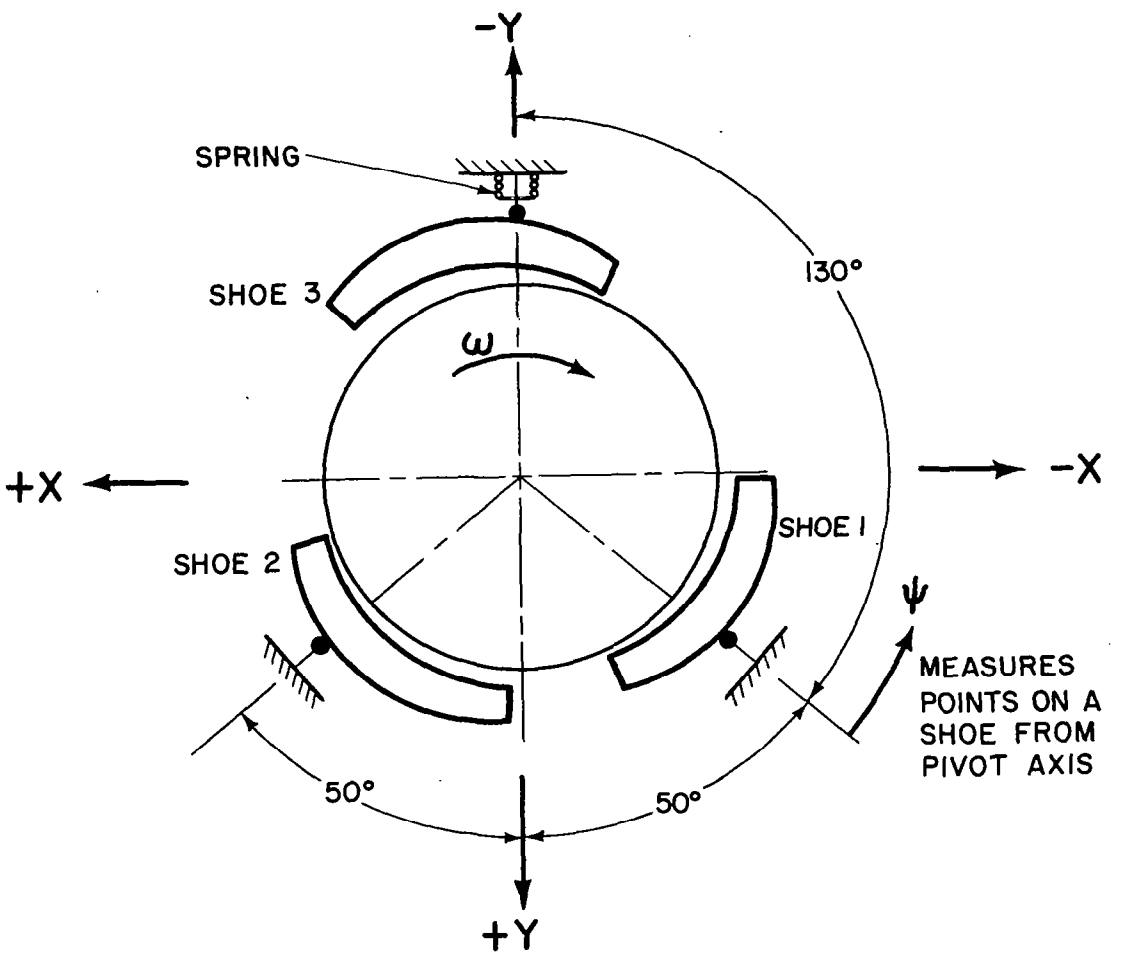

Fig. V-1 - Geometry of Three Shoe Bearing-Validation Case

Using the above data and equation (V-1) the pivot film thickness for shoe 1 is

$$H_{p_1} = 1 + (0.9608 + 0.00215 \times 3.45)\ (-0.6428)$$

$$H_{p_1} = 0.3776$$

Also

$$H_{p_2} = H_{p_1}$$

For shoe 3 the data is the same as for shoe 1 except

$$\theta = \theta_p = 0$$

$$C'/C = -1 = -1.431$$

$$\Delta = 0.3597$$

$$\Gamma = -0.0021$$

Therefore

$$H_{p_3} = 0.537$$

2. Leading Edge Film Thickness

For shoe number 1

$$\theta = \theta_L = 67°$$

$$\psi = \psi_L = 63°$$

$$H_{L_1} = 1 + (0.09608 + 0.00215 \times 3.45) \times 0.3907$$

$$H_{L_1} = 0.9896$$

For shoe number 3

$$\theta = \theta_L = 65°$$

$$H_{L_3} = 1 + (0.9608 + 0.00215 \times 3.45) \cos 65° - 1.431 \cos 65° + 1.15 \times 0.3597 \sin 65°$$

$$H_{L_3} = 1.1467$$

The shoe shaft coordinates used in the field map presentations are $\varepsilon = e/c$ and ξ which are shown in Figure (V-2)

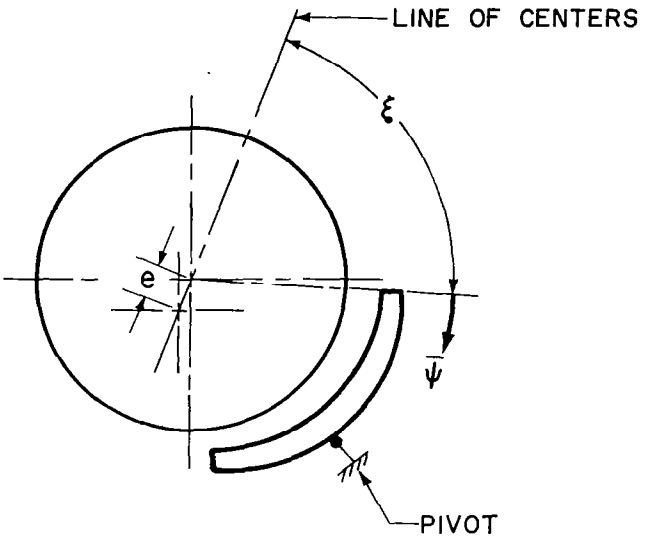

Fig. V-2 - Shoe-Shaft Coordinates-Validation Case

The film thickness is given by $H = 1 + \varepsilon \cos(\xi+\bar{\psi})$

At the shoe leading edge $H_L = 1 + \varepsilon \cos(\xi)$ (V-2)

At the pivot point $H_P = 1 + \varepsilon \cos(\xi+\bar{\psi})$ (V-3)

Using Eqs. (V-2) and (V-3) $$\frac{H_p-1}{H_L-1} = \frac{\varepsilon \cos(\xi+\bar{\psi}_p)}{\varepsilon \cos}$$

or,

$$\tan^{-1}\xi = \frac{1}{\sin\bar{\psi}_p}\left(\cos\bar{\psi}_p - \frac{H_p-1}{H_L-1}\right)$$

$$\varepsilon = (H_p-1)/\cos(\xi+\bar{\psi}_p)$$

For shoe number 1

$$\xi_1 = 89.2°$$

$$\varepsilon_1 = 0.69$$

For shoe number 3

$$\xi_3 = 76.1°$$

$$\varepsilon_3 = 0.614$$

To determine the shoe-shaft coordinates from the field map, it is necessary to know the load coefficient C_L and the pivot location ϕ/α. The load W_1 on shoe 1 was 76.7. ϕ/α for all shoes was 2/3.

Therefore,

$$C_{L_1} = \frac{W_1}{P_a RL} = \frac{76.7}{14.7 \times 2 \times 3.3} = 0.789$$

From Figures (V-3) and (V-4)

$$\varepsilon_1 = 0.7$$

$$\xi_1 = 90°$$

$$H_{P_1} = 0.38$$

Similarly, for shoe number 3

$$C_{L_3} = \frac{50}{14.7 \times 2 \times 3.3} = 0.515$$

$$\varepsilon_3 = 0.63$$

$$\xi_3 = 77°$$

$$H_{P_3} = 0.52$$

The preload setting C'/C and the pivot circle eccentricity ε' can be computed from the field map pivot film thicknesses as follows,

$$C'/C = \frac{H_{p1} + H_{p3} \cos 50°}{1 + \cos 50°} = \frac{0.38 + 0.52 \times 0.6428}{1.6428}$$

$$C'/C = 0.435$$

$$\varepsilon' = \frac{H_{p3}}{C'/C} - 1 = \frac{0.52}{0.435} - 1$$

$$\varepsilon' = 0.195$$

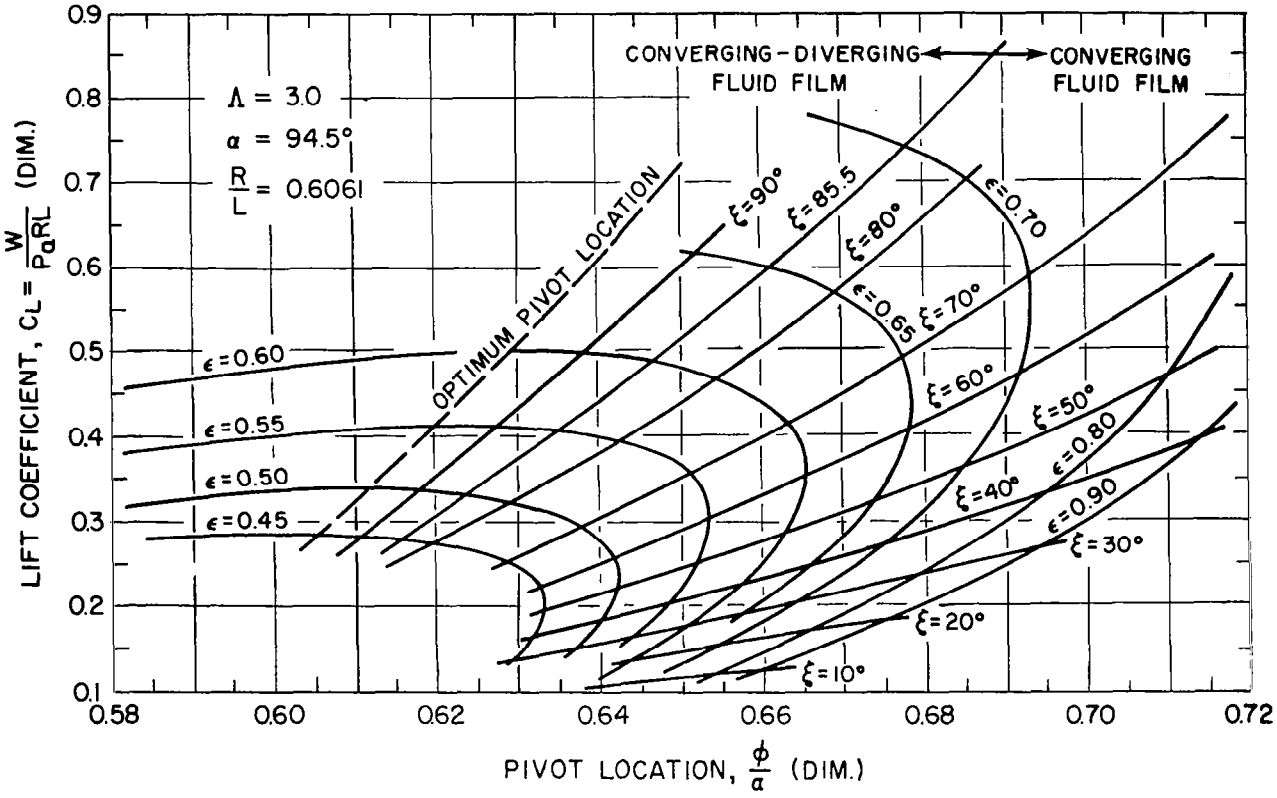

Fig. V-3 - Lift Coefficient vs. Pivot Location R/L = 0.6061, α = 94.5, Λ = 3.0

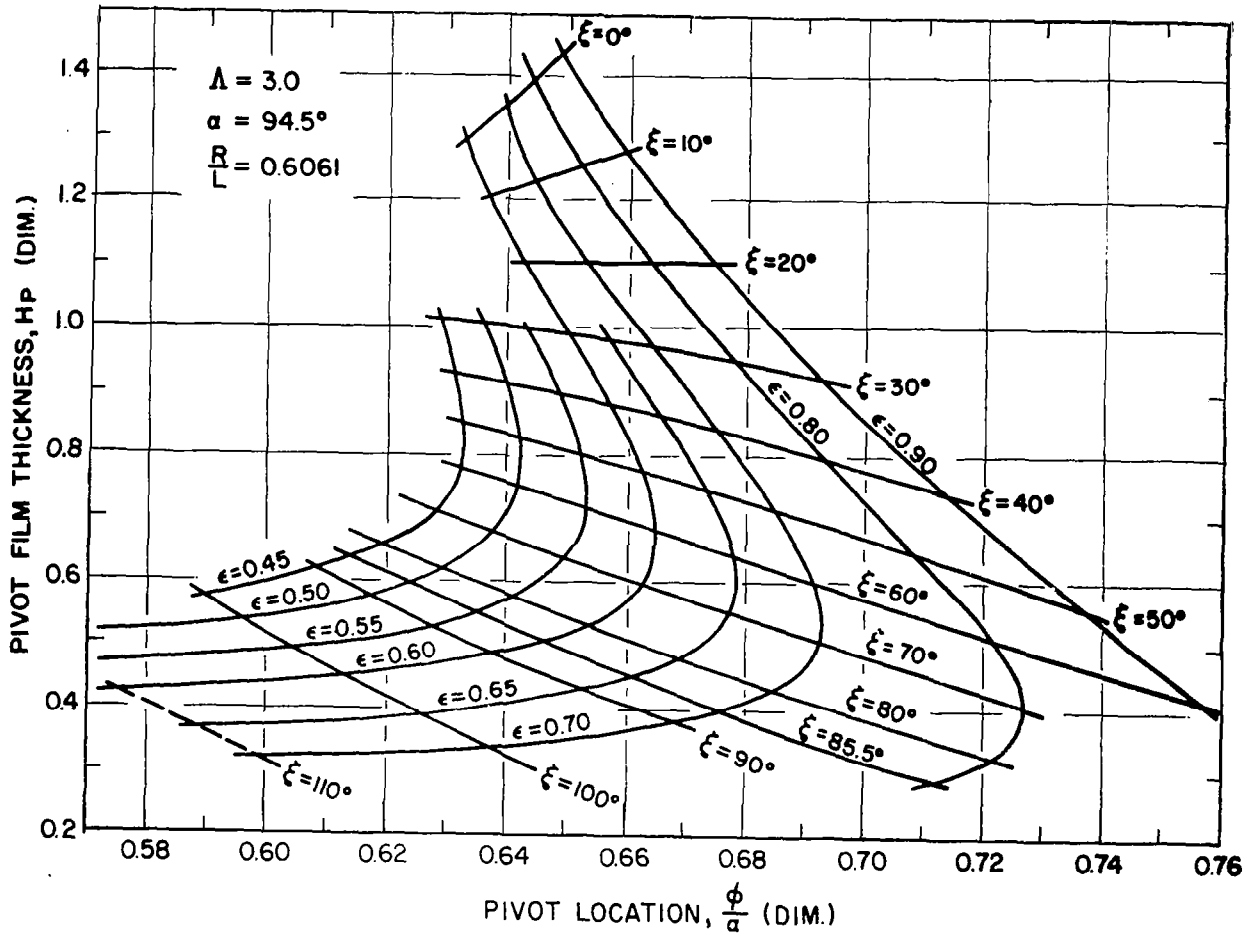

Fig. V-4 - Pivot Film Thickness vs. Pivot Location - R/L = 0.6061, α = 94.5, Λ = 3.0

From the program results,

$$C'/C - 1 = -1.431$$
$$|C'/C| = 0.431$$

The calculation for the pivot circle eccentricity C'/C from the dynamics program output is performed as follows:

The program zero for the Y displacement is taken at the center of a reference circle with radius R + C. The instantaneous center of the pivot circle depends on the displacement C'. The difference between the center of the pivot circle and the center of the reference circle is given by δy_m where,

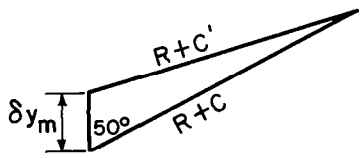

Using the law of cosines,

$$(\delta y_m)^2 + (R + C)^2 - 2(\delta y_m)\ (R + C) \cos 50° = (R + C')^2$$

Dividing through by C'

$$(R/C')^2 + 2(R/C') + 1 = (\delta y_m/C')^2 + (R/C')^2 + 2(C/C')\ (R/C') + (C/C')^2 +$$
$$-2(\delta y_m/\varepsilon')\ (R/C'\ C/C') \cos 50°$$

The orders of magnitudes of the above terms are,

$$R/C' = 0\ (10^3) \qquad C/C' = 0\ (1) \qquad \delta y_m/C' = 0\ (1)$$
$$(\delta y_m/C') = (1/\cos 50°)\ (1/C'/C - 1)$$
$$\delta y_m/C' = 2.053$$
$$\varepsilon' = e'/C' = y_M/C' - \delta y_M/C' = Y_M/(C'/C) - \delta y_M/C'$$
$$\varepsilon' = 0.176$$

Bearing 2 differs only slightly from bearing 1, therefore it was felt that no additional computations were necessary.

The dynamics program will be validated by comparing the analytically predicted shoe and rotor motions with those obtained from picture records of test runs made on a horizontal experimental test rig. The tests referred to were made on the SA-2 rig at FIRL under the sponsorship of U.S. Atomic Energy Commission (Contract No. AT (30-1)-2512). The bearing system consists of a tilting pad self-acting thrust bearing, an externally pressurized thrust bearing (providing an axial load) and two self-acting journal bearings with three pivoted pad bearings each. The top shoe of each journal bearing is spring loaded. The rig specifications are as follows:

Design Speed	18,000 rpm
Rigid Shaft Critical	7,050 rpm
Rotor Weight	97 lb
Shaft Diameter	4 in.
Shaft Length	24.68 in.
Shaft Polar Moment	.492 in. lb sec^2
Shaft Transverse Moment	12.88 in. lb sec^2
Shoe Arc Length	3.3 in.
Shoe Width	3.3 in.
Shoe Wrap Angle	94.5°
Shoe Weight	5.5 lb
Shoe Radius of Gyration for Pitch Direction	1.5 in.
Shoe Radius of Gyration for Roll Direction	1.2 in.
Pivot Distance from Face of the Shoe	.3 in.
Shoe Radial Clearance	.0015 in.
Pivot Location ϕ/α	.67
Shaft Unbalance Force	.34 grams
Shaft Unbalance Moment	.0019 in. lb

Test run number 4074 performed on 4-7-64 has been selected as the check case. The prevailing conditions during the run were:

Ambient Pressure	14.7 psia
Shaft Speed	15,000 rpm
Spring Preload	25 lb.bearings
Spring Constant	80 lb/in.
Scope Sweep	.005 sec/cm
Scope Sensitivity	20 mv/cm
Scope Screen Calibration	100 in./cm
Λ	2.98
Bearing Lubricant Viscosity (air)	2.61×10^{-9} Reyn
Pivot Friction Moment	.13 in. lb

The shaft and shoe motions were monitored by four Wayne-Kerr capacitance probes (two Wayne-Kerr Distance Meters (DM1-0), two Wayne-Kerr Vibration Meters B731A) and two Tektronix type 502 dual-beam oscilloscopes. The four probes were positioned as shown in Figure V-5.

All four probes are attached to "ground" and therefore measure absolute motions. It can be seen from the sketch of the shoe probe (Fig.V-5) that the motion measured by probe A will be a combination of pitch and roll. Referring to the trace from probe A in Figure V-12-a, 10 cycles occurred in 8 cm; therefore the frequency of this motion is:

$$\text{Frequency}_A = \frac{10 \text{ cycles} \times 60 \text{ sec/min}}{8 \text{ cm} \times 0.005 \text{ sec.cm}}$$

$$= 15{,}000 \text{ RPM}$$

which is synchronous with the shaft speed. The peak to peak amplitude measures about 200 μ-in.

The trace from probe B (looking at the spring loaded shoe) (Fig. V-12-a) accounts for a combination of pitch, roll and pivot motion. The frequency is again synchronous (15,000 rpm) and the amplitude is about 280 μ-in.

The closed curve also shown in Figure V-12-a vectorally adds the purpose of probes A and B and adds no useful information for the present purposes.

Figure V-12-b shows the absolute horizontal (probe X) and vertical (probe Y) motion of the shaft in a plane 9.181" west of the plane of the shaft cg. The trace of the X probe shows a frequency of 13,700 rpm and an amplitude of about 110 μ-in.; the Y probe indicates a frequency of 14,000 rpm with an amplitude of about 180 μ-in. The closed curve also shown on Figure V-12-b is the trace of the shaft orbit obtained by adding the outputs of probes X and Y. The picture shows a curve which is approximately an ellipse with a major axis of 190 μ-in. and a minor axis of 90 μ-in.

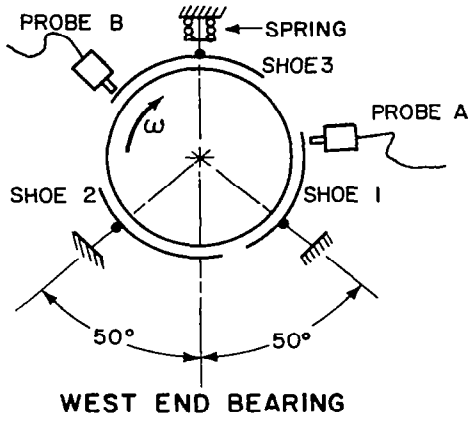

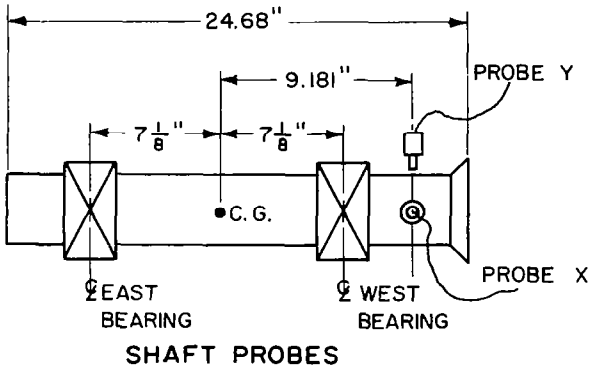

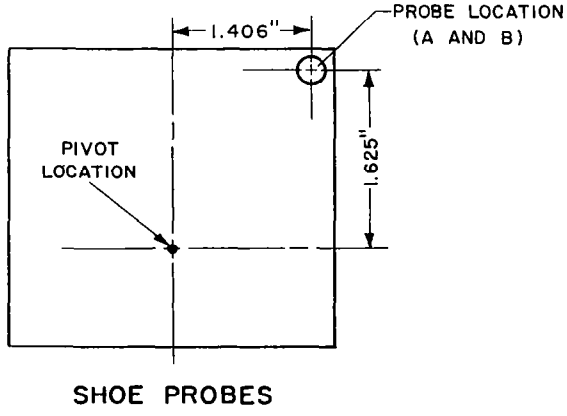

Fig. V-5 - Probe Location on SA-2 Rig-Validation of Non-Linear Orbit Program

The amplitude of the motion at each probe will be determined from the computer output in the following manner:

Probe A:

This probe looks at the inside corner of the leading edge of bearing 1 shoe 1. The magnitude of the position vector from the pivot point to the shoe probe button is 2.172 inches. At any instant, the amplitude A_A of probe A is given by

$$A_A = 2.172 \ (\sin \delta + \sin \gamma)$$

where δ and γ are the shoe pitch and roll angles which are zero when the shoe surface lies on a reference circle with radius R + C.

In the program output DEG (11) represents the absolute pitch angle of shoe 1 and DEG (5) represents its absolute roll angle.
Since the motions are small

$$\sin \delta \approx \delta \text{ and } \sin \gamma \approx \gamma$$

therefore,

$$A_A = 2.17 \times C\left[\frac{\text{DEG (11)}}{R} + \frac{\text{DEG (5)}}{L}\right]$$

or

$$A_A = 0.003258 \left[\frac{\text{DEG (11)}}{2} + \frac{\text{DEG (5)}}{3.3}\right]$$

Probe B:

Probe B looks at the inside corner of the leading edge of bearing 1 shoe 3 and is located the same distance from the pivot point as probe A. The pitch angle is given by DEG (13) and the roll by DEG (7). The motion of the pivot is measured by DEG (17).

where C = radius of shoe - radius of shaft

C' = radius of pivot circle - radius of shaft

Let the mean C' (after the system has reached a quasi-steady-state) $= \bar{C}'$. $\bar{C}'$ will be obtained from a plot of DEG (17) vs. time. Then the amplitude A_B measured by probe B is

$$A_B = 2.172\ (\sin\delta + \sin\gamma) + (C' - \bar{C}')$$

In terms of the program variables

$$A_B = 0.0015\ \{2.172\left[\frac{\text{DEG (13)}}{2} + \frac{\text{DEG (7)}}{3.3}\right] + \left[\text{DEG (17)} - \overline{\text{DEG (17)}}\right]\}$$

Probe x and y

Let the axial distance from the shaft cg to the planes of X-Y probes be $\bar{z}$ and the X, Y coordinates of the point on the Z axis in this plane be given by $\bar{x}$, $\bar{y}$. Then the motion observed by probe X is given by

$$\bar{x} = x_m + \bar{z}\sin\alpha_1 \approx x_m + \bar{z}\,\alpha_1$$

In terms of the program variables

$$\bar{x} = 0.0015\left[\text{DEG (1)} + \frac{9.181}{3.3}\,\text{DEG (3)}\right]$$

Similarly

$$\bar{y} = 0.0015\left[\text{DEG (2)} + \frac{9.181}{3.3}\,\text{DEG (4)}\right]$$

The shaft orbit is obtained by plotting $\bar{X}$ vs. $\bar{Y}$ and the frequencies are obtained by plotting A_A, A_B, $\bar{X}$ and $\bar{Y}$ all vs. time.

The computer predicted motions for various degrees of freedom are given on Figures V-6 through V-11.

Definitions:

Deg (1)	Non-Dimensional Shaft X Motions	(x/c)
Deg (2)	Non-Dimensional Shaft Y Motion	(y/c)
Deg (3)	Non-Dimensional Shaft A_1 Rotation	$\frac{(\alpha_1 L)}{c}$
Deg (4)	Non-Dimensional Shaft A_2 Rotation	$\frac{(\alpha_2 L)}{c}$
Deg (7)	Non-Dimensional Roll — Shoe 3	$\frac{(\gamma_3 L)}{c}$
Deg (13)	Non-Dimensional Pitch — Shoe 3	$\frac{(\delta_3 R)}{c}$
Deg (17)	Non-Dimensional Translation of Shoe 3	(c'/c)

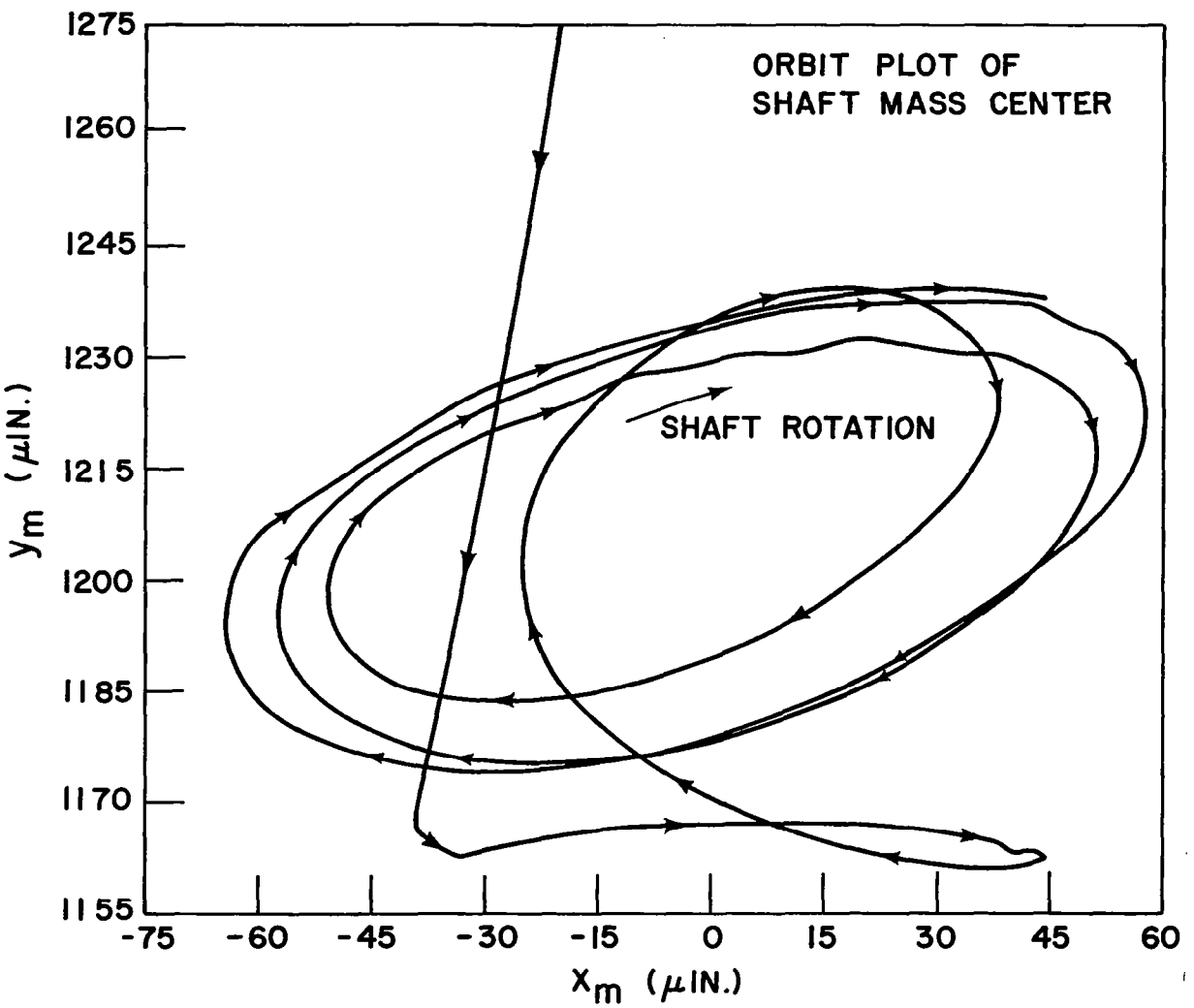

Fig. V-6 - Orbit Plot of Shaft Mass Center, SA-2 Rig, Validation of Non-Linear Orbit Program

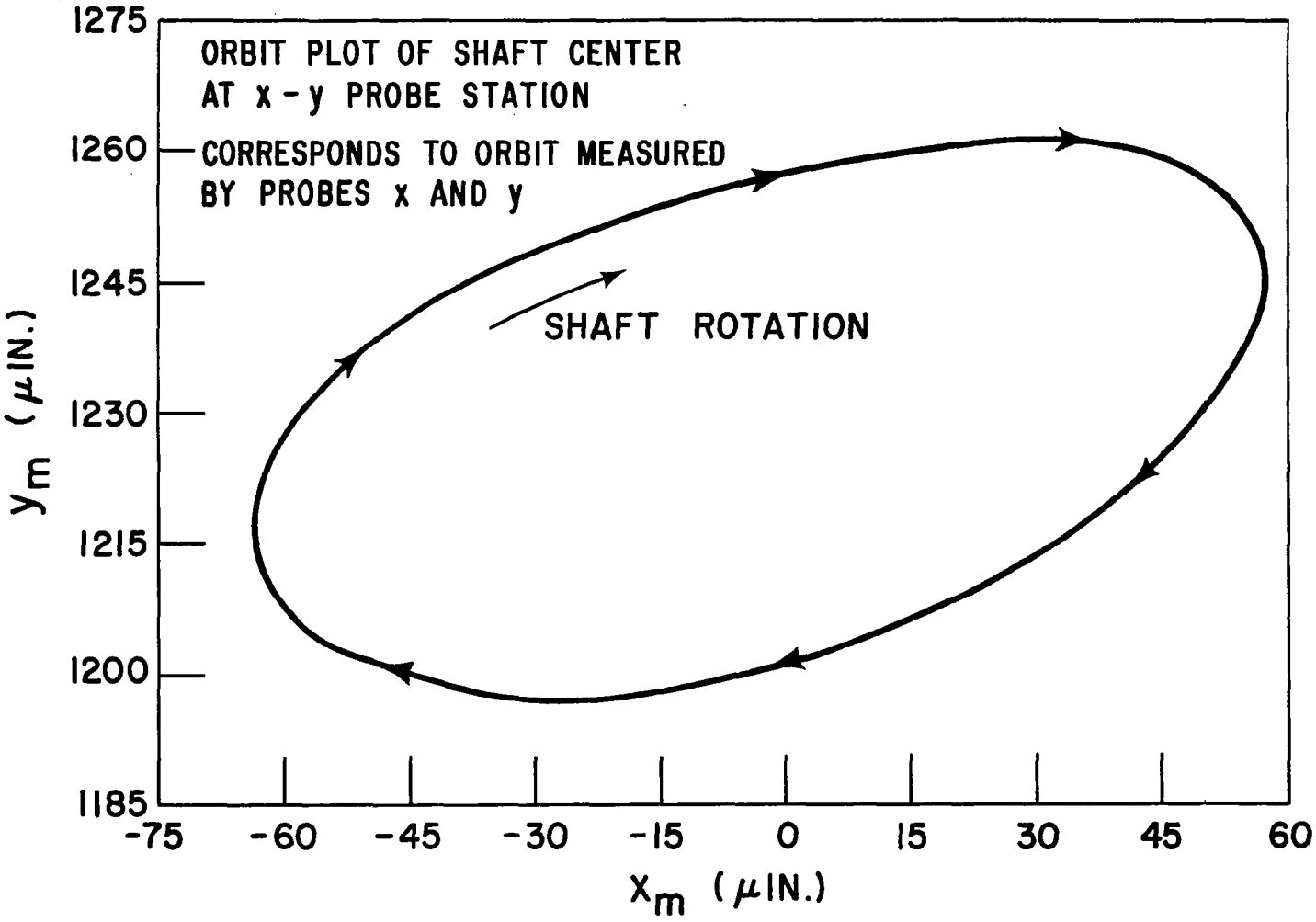

Fig. V-7 - Orbit Plot of Shaft Center at Probe Station, SA-2 Rig,
Validation of Non-Linear Orbit Program

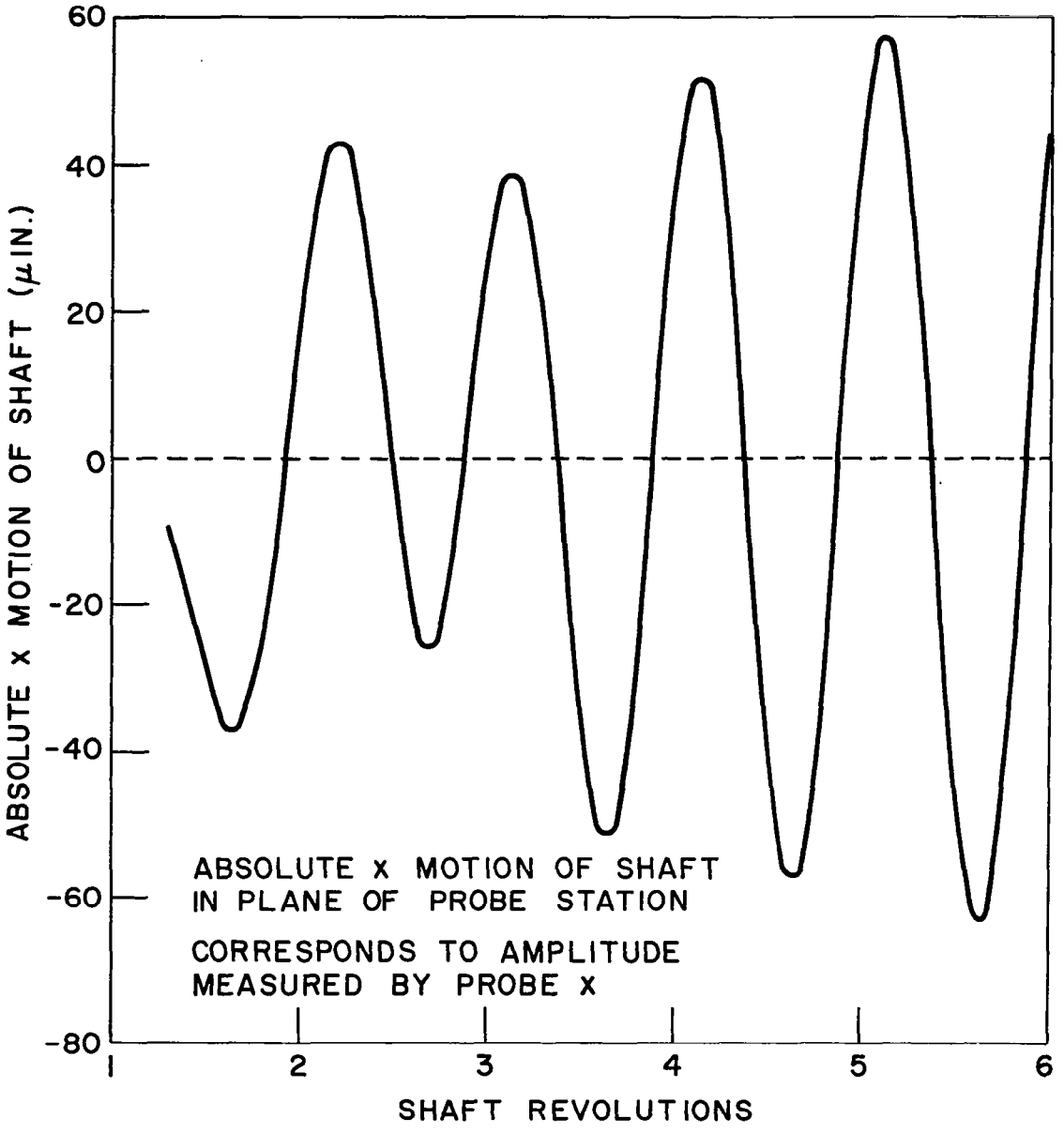

Fig. V-8 - Absolute Motion of Shaft in X Direction, SA-2 Rig, Validation of Non-Linear Orbit Program

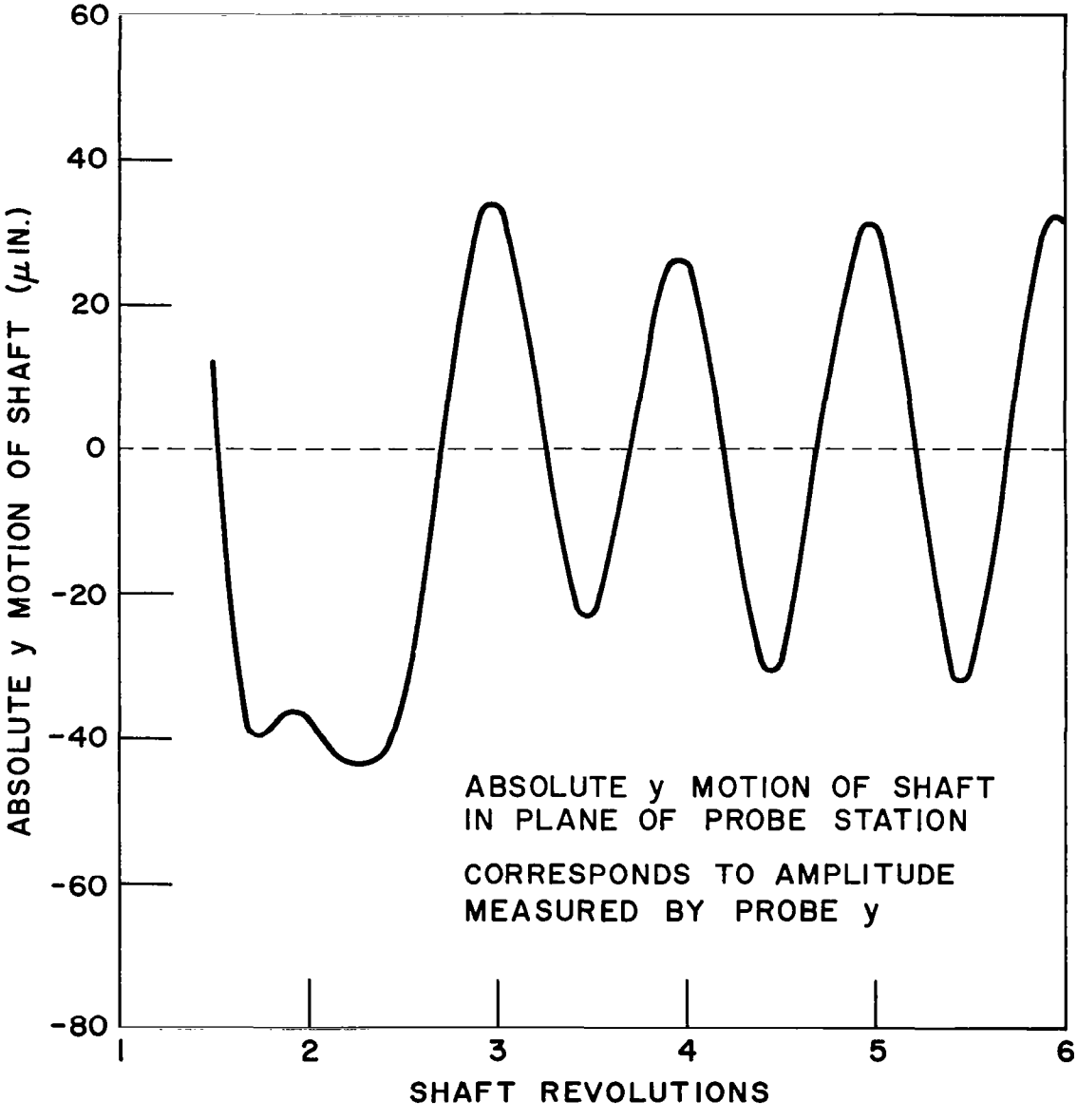

Fig. V-9 - Absolute Motion of Shaft in Y Direction, SA-2 Rig, Validation of Non-Linear Orbit Program

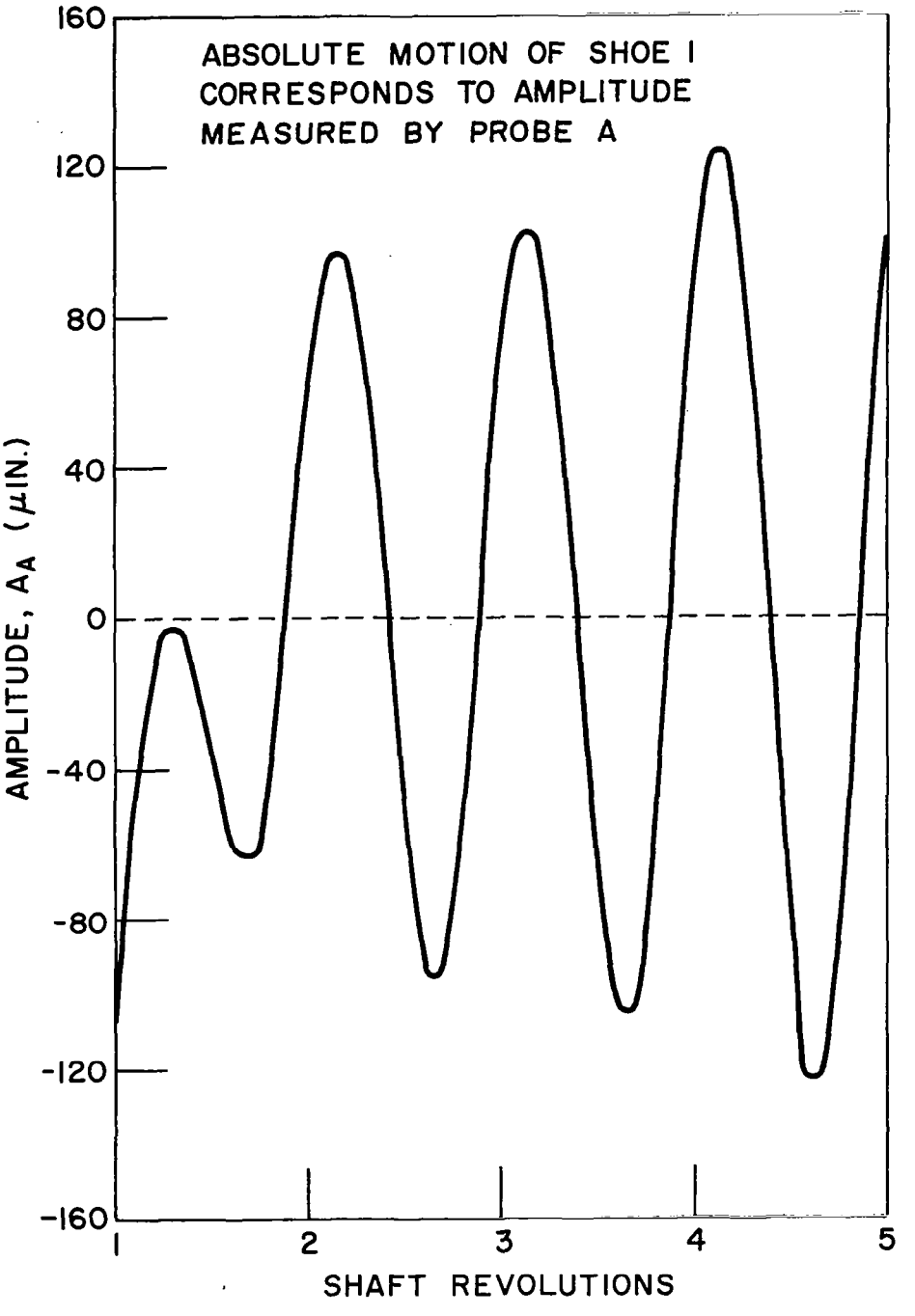

Fig. V-10 - Absolute Motion of Leading Edge of Shoe 1, SA-2 Rig, Validation of Non-Linear Orbit Program

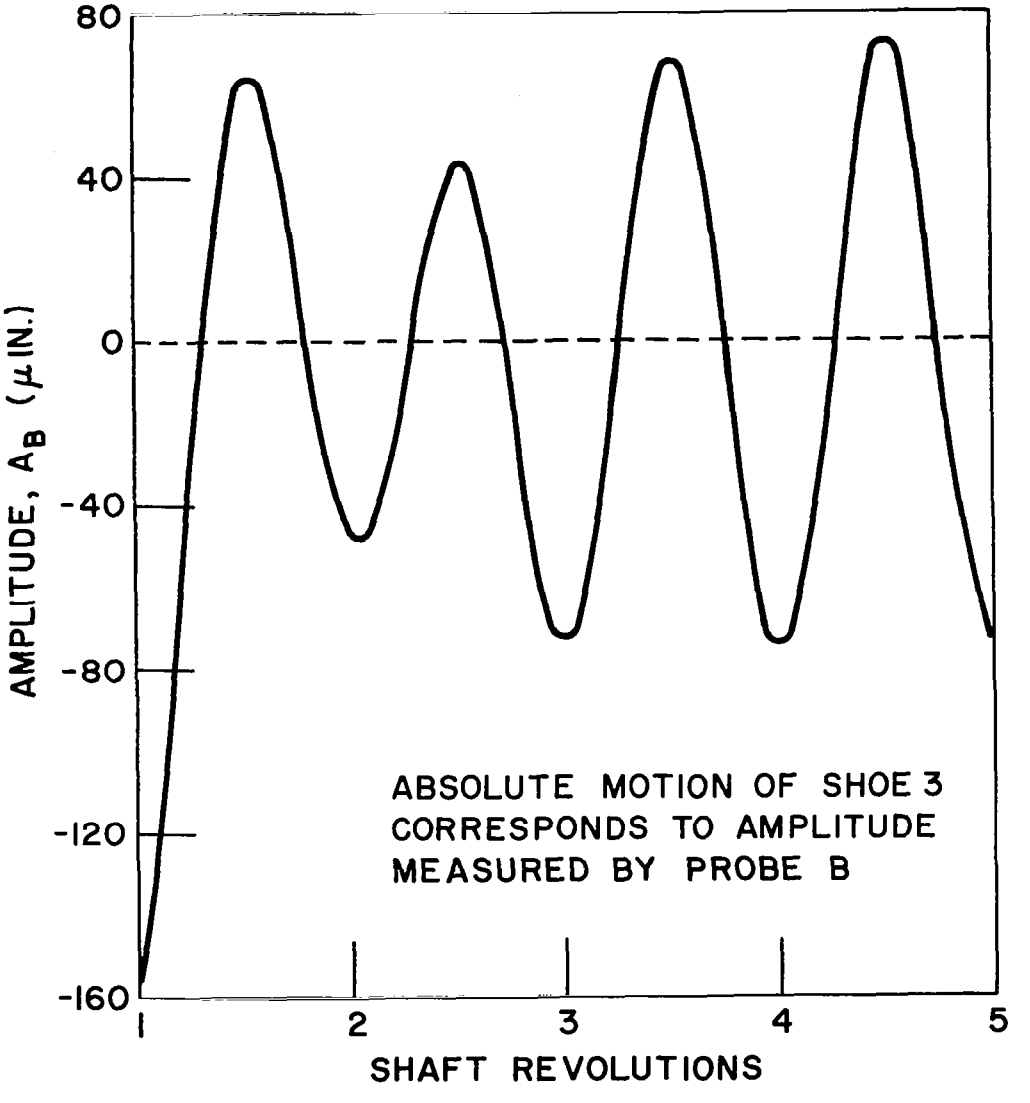

Fig. V-11 - Absolute Motion of Leading Edge of Shoel, SA-2 Rig, Validation of Non-Linear Orbit Program

RUN 4074
SHAFT SPEED = 15,000 RPM
SCOPE CALIBRATION = 100μ in./cm
SWEEP RATE = 0.005 sec/cm

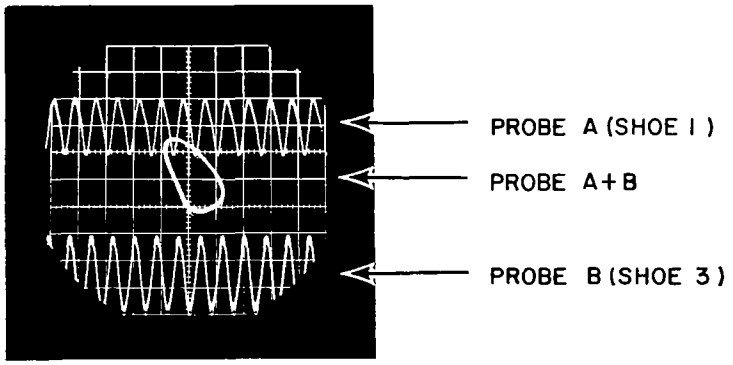

(a) Absolute Shoe Motion

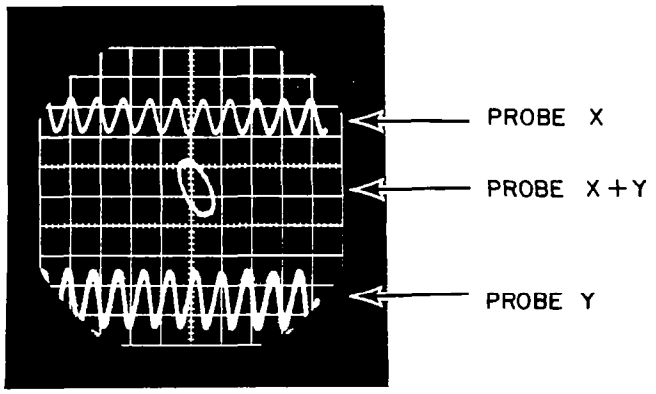

(b) Absolute Shaft Motion

Fig. V-12 - Oscilloscope Pictures of Experimental Data Used in the Validation of the Non-Linear Orbit Program

APPENDIX VI

CALCULATION OF SHOE INERTIA

The roll moment of inertia is

$$I_R = \int_v \rho(\bar{N}_2 \times \bar{P})^2 \, dv$$

$$= \rho \int_v \left[(X_1 - R)^2 + X_3^2\right] dv$$

$$= \rho V \left(\frac{L^2}{12}\right) + PL \int_{r_1}^{r_2} \int_{\theta_1}^{\theta_2} \left[R^2 - 2Rr \cos\theta + r^2 \cos^2\theta\right] r \, dr \, d\theta$$

$$= \rho V \frac{L^2}{12} + \rho L \left\{\frac{R^2 (r_2^2 - r_1^2)}{2} - \frac{2R}{3}(r_2^3 - r_1^3)(\sin\theta_2 + \sin\theta_1)\right.$$
$$\left. + \frac{r_2^4 - r_1^4}{16}(\sin 2\theta_2 + \sin 2\theta_1) + \frac{r_2^4 - r_1^4}{8}\alpha\right\}$$

$$= \rho V \left\{\frac{L^2}{12} + R^2 + \frac{r_2^2 + r_1^2}{4}\left[1 + \frac{1}{2}(\sin 2\theta_2 + \sin 2\theta_1)\right]\right.$$
$$\left. - \frac{4R}{3} \frac{r_2^3 + r_1^3}{r_2^2 - r_1^2}(\sin\theta_2 + \sin\theta_1)\right\}$$

	Bearing 1	Bearing 2	Units
ρV	3.04×10^{-4}	6.12×10^{-4}	$\frac{\text{lb sec}^2}{\text{in.}}$
L	1.5	2.125	in.
R	0.656	0.968	in.
$r_2 - r_1$	3/16	3/16	in.
θ_1	35	35	degrees
θ_2	65	65	degrees
I_p	0.66×10^{-4}	2.39×10^{-4}	in lb sec^2
I_R	0.67×10^{4}	2.58×10^{-4}	in lb sec^2

APPENDIX VII

ANALYTICAL DEVELOPMENT OF THRUST BEARING PERFORMANCE

1. Spiral Groove Thrust Bearing

a. Load Capacity

Figure 36 diagrammatically depicts the geometric parameters for the dead-ended Spiral Groove Thrust Bearing. When analyzing this bearing the portion inside the radius R_2 is considered to be a solid area at the same level as the land area in the grooved portion.

A comprehensive analytical treatment of this bearing that is applicable to both compressible and incompressible lubricants is described in Reference 5, and the information from this reference was used for calculating the hydrodynamic performance of this bearing. Section 7.2.1 indicates the groove depth to clearance ratio optimized on the basis of load carrying capacity. Figure VII-1, extracted from Reference 5, shows the relationship between load factor, C_L, and compression ratio δ. The equation relating clearance, load and speed is:

$$h_2^2 = \frac{C_L \mu R_1^4 \Omega}{W} \qquad \text{(VII-1)}$$

For the design condition of 50,000 RPM and 15 lbs. load an operating clearance h_2 is established from equation (VII-1).

The groove depth is then

$$h_o = \frac{h_2}{\delta_{max}} \qquad \text{(VII-2)}$$

Fixing of the groove depth permits off-design performance to be calculated. Load vs. clearance can be determined by the following process.

(1) Assume a clearance h_2

(2) Solve for δ using

$$\delta = h_2/h_o \qquad \text{(VII-3)}$$

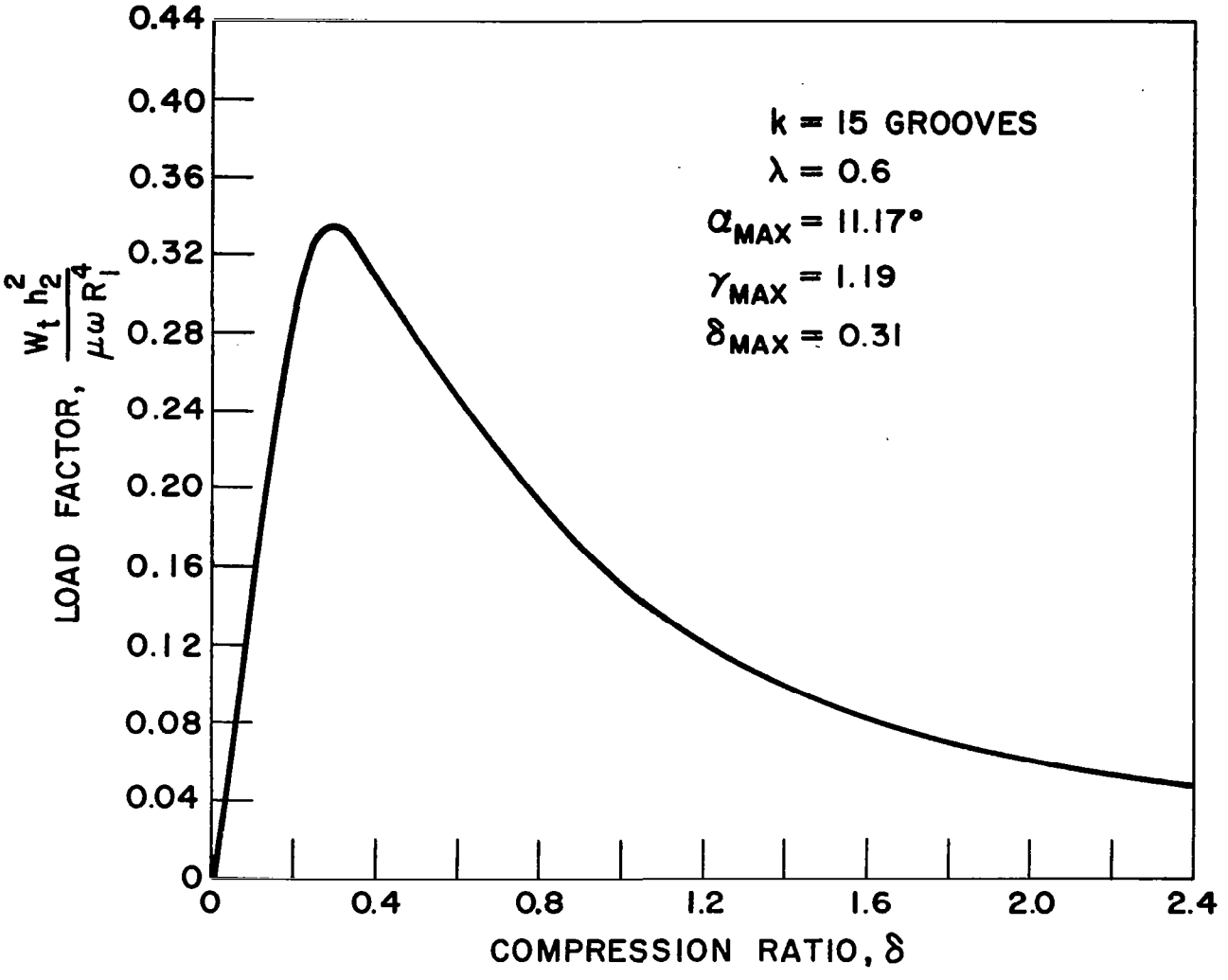

Fig. VII-1 - Load Factor vs. Compression Ratio-Spiral Groove Bearing

(3) Determine C_L from Figure VII-1

(4) Solve for W from Eq. (VII-1)

b. Friction Loss

Two separate areas contribute to the frictional drag of the thrust bearing. The first is the circular area contained inside R_2, the second is the annular area containing the spiral grooves.

For the ungrooved areas the viscous shear stresses is defined as

$$dF = \mu A \frac{dv}{dh} \tag{VII-4}$$

Considering a differential annulus

$$dF = \frac{2\pi\mu\Omega r^2}{h} dr \tag{VII-5}$$

The friction moment is thus

$$dT_f = \frac{2\pi\mu\Omega r^3}{h} dr \tag{VII-6}$$

Integrating, we obtain the total friction moment.

$$T_f = \int_o^{R_2} \frac{2\pi\mu\Omega r^3 dr}{h} = \frac{\pi}{2h} \mu\Omega R_2^4 \text{ in.-lbs} \tag{VII-7}$$

Multiplying the torque by shaft speed will yield the frictional power loss. The resulting equation in units of watts is:

$$P = \frac{.177 \mu\Omega^2 R_2^4}{h} \tag{VII-8}$$

The friction loss for the grooved portion is obtained from Figure VII-2, which was extracted from Reference 5.

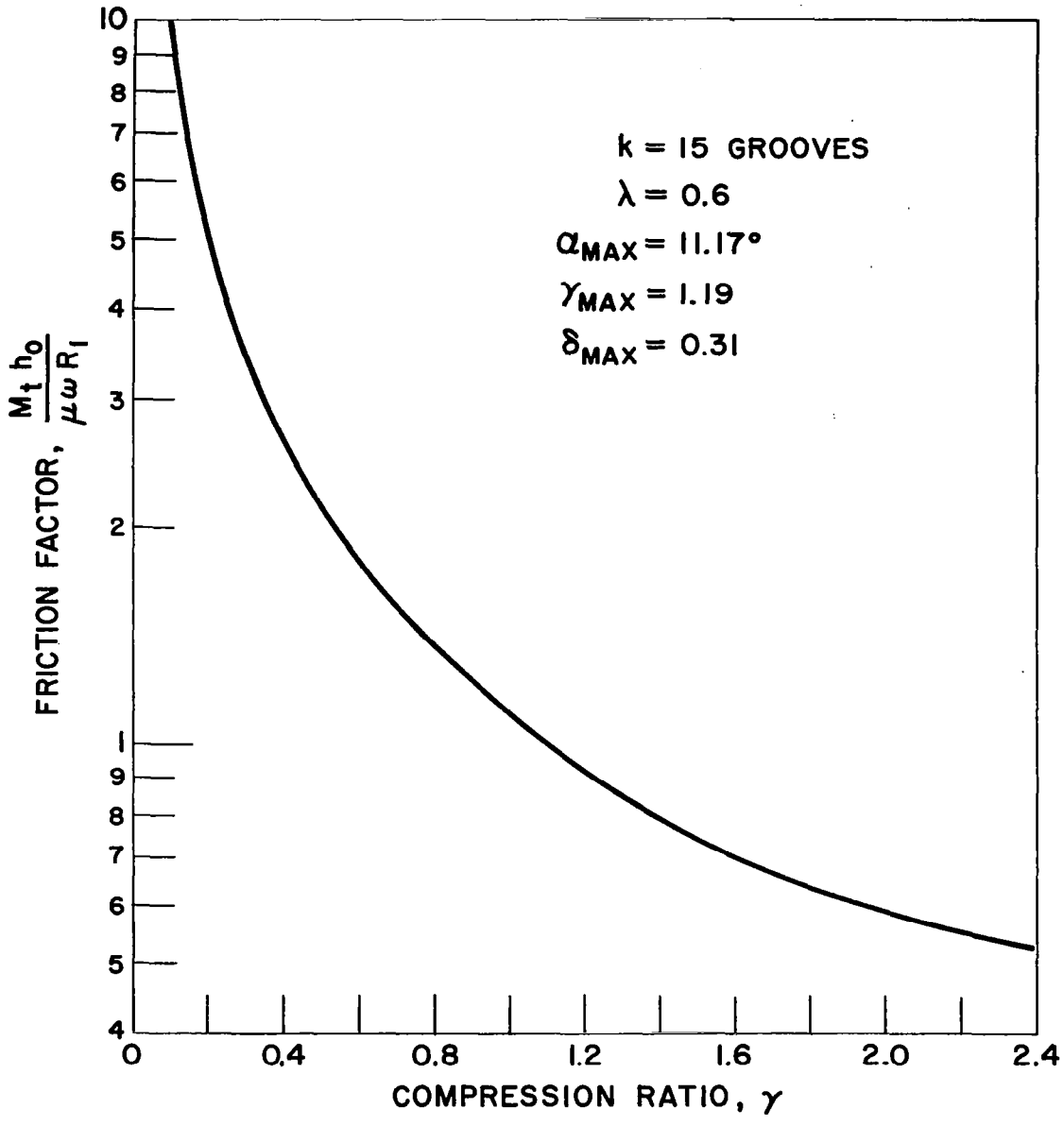

Fig. VII-2 - Friction Factor vs. Compression Ratio-Spiral Groove Bearing

c. Synchronous Vibrations of Thrust Bearing

Because the rotating collar cannot be aligned exactly perpendicular to the axis of rotation, there will be an angular swashing of the collar as it rotates. This produces a forcing function on the stationary collar and causes it to vibrate. This type of vibration has been analyzed by Whitley and Williams as described in Reference 21, and forms the basis of the analytical description following.

Referring to Figure VII-3, the rotating plate swashes through an angle $\varepsilon_o \sin \omega t$ in the plane of the paper and $\varepsilon_o \cos \omega t$ in the plane perpendicular to the paper. (ε_o is the total angular swash and ω is the speed of the rotating plate)

$$\varepsilon_1 = \varepsilon_o \sin \omega t \text{ (plane of paper)} \qquad \text{(VII-9)}$$

$$\varepsilon_2 = \varepsilon_o \cos \omega t \text{ (plane perpendicular to paper)} \qquad \text{(VII-10)}$$

Because of this motion the stationary plate will move through angles ξ and ζ according to the equations of motion

$$I_T \ddot{\xi} = -K_T (\xi - \varepsilon_o \sin \omega t) \qquad \text{(VII-11)}$$

$$I_T \ddot{\zeta} = -K_T (\zeta - \varepsilon_o \sin \omega t) \qquad \text{(VII-12)}$$

The steady-state solutions are

$$\xi = \varepsilon_o \omega_c^2 \sin \omega t / (\omega_c^2 - \omega^2) \qquad \text{(VII-13)}$$

$$\zeta = \varepsilon_o \omega_c^2 \cos \omega t / (\omega_c^2 - \omega^2) \qquad \text{(VII-14)}$$

for $\omega < \omega_c$ the stationary plate swashes in phase with the rotating plate but through a larger amplitude.

The amplitude of the relative swash ε is given by

$$\varepsilon = \xi - \varepsilon_o \sin \omega t = \varepsilon_o \sin \omega t \left(\frac{\omega^2}{\omega_c^2 - \omega^2} \right) \qquad \text{(VII-15)}$$

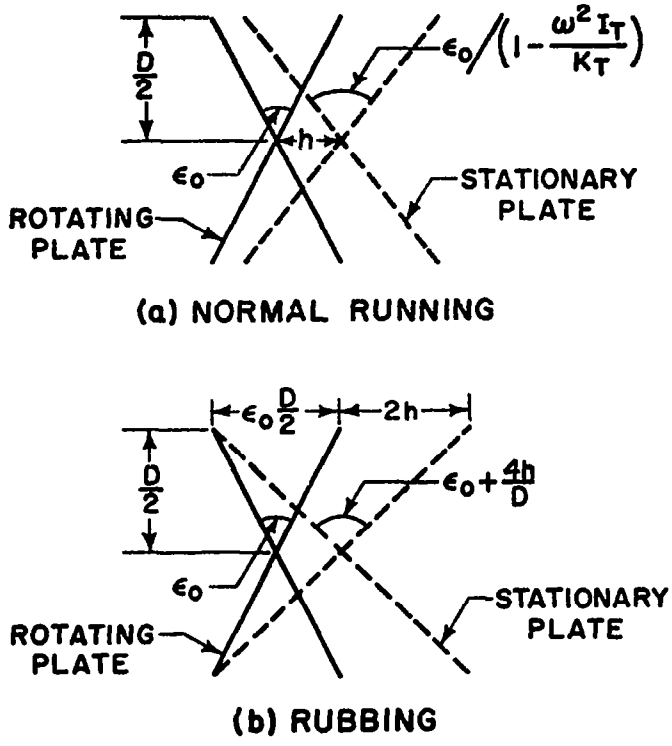

Fig. VII-3 - Synchronous Vibration of Thrust Bearing

therefore the maximum amplitude of the differential swash ε between the plates is given by

$$\varepsilon_{max} = \varepsilon_o \left(\frac{\omega^2}{\omega_c^2 - \omega^2} \right) \qquad \text{(VII-16)}$$

From the previous equation the maximum angular displacement of the stationary plate is

$$\xi_{max} = \frac{\varepsilon_o \omega_c^2}{\omega_c^2 - \omega^2} = \frac{\varepsilon_o}{1 - \omega^2 I/K_T} \qquad \text{(VII-17)}$$

At contact conditions the total displacement of the rotating plate equals $\frac{\varepsilon_o D}{2}$. The total displacement of the stationary plate is $2\frac{\varepsilon_o D}{4} + h$. Dividing by D/2 gives the total angle at the stationary plate and it equals

$$\xi_{rubbing} = \varepsilon_o + 4h/D \qquad \text{(VII-18)}$$

This shows that the maximum differential swash that the plates can sustain without rubbing is 4h/D.

d. Thermal Distortion

The analytical model for the thermal distortion problem is shown on Figure VII-4

From similar triangles

$$\frac{\Delta L}{a} = \frac{R_4}{R'} \qquad \text{(VII-19)}$$

but

$$\Delta L = \alpha' R_4 \Delta T \qquad \text{(VII-20)}$$

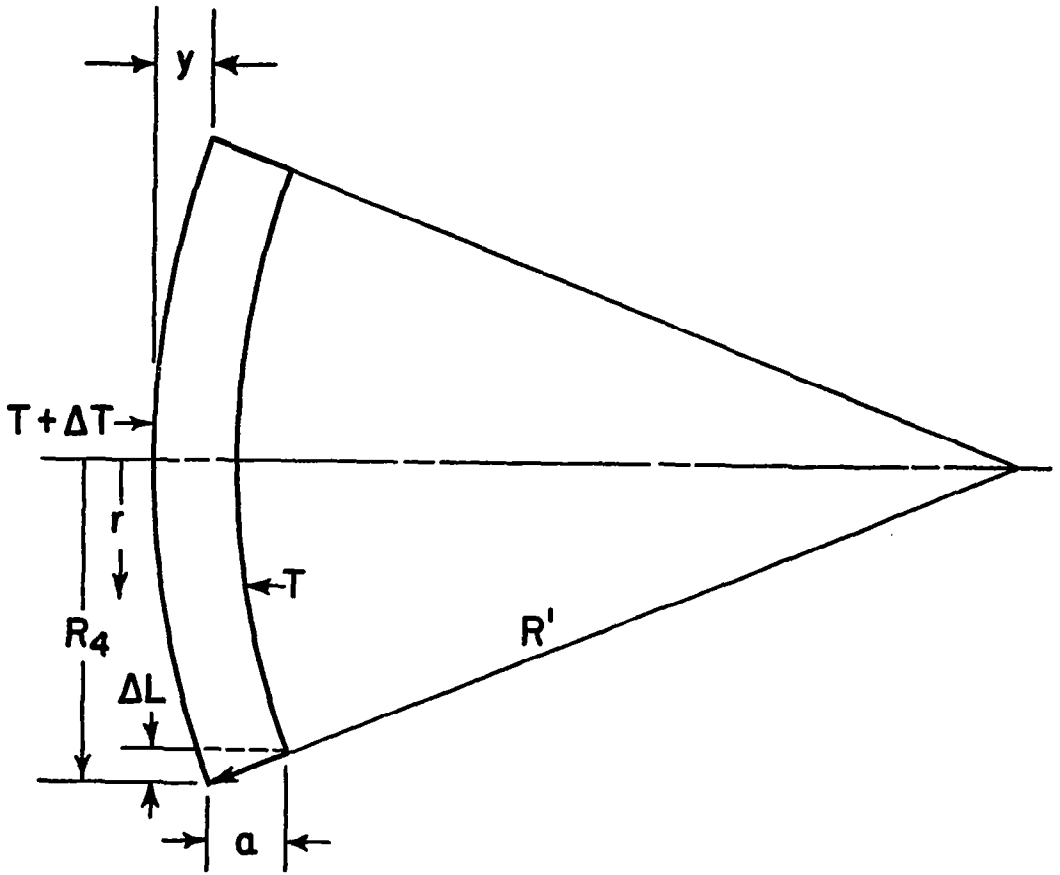

Fig. VII-4 - Thrust Bearing Thermal Distortion - Analytical Model

and

$$\Delta T = Fa/K \tag{VII-21}$$

Substituting (VII-21) into (VII-20)

$$\Delta L = \alpha' R_4 Fa/K \tag{VII-22}$$

Substituting (VII-22) into (VII-19) we obtain

$$\frac{1}{R'} = \frac{\Delta L}{R_4 a} = \frac{\alpha' F}{K} \tag{VII-23}$$

For small curvatures the reciprocal of the radius of curvature can be approximated by

$$\frac{d^2y}{dr^2} = \frac{1}{R'} = \frac{\alpha' F}{K} \tag{VII-24}$$

The heat generation F is a result of viscous friction, and is proportional to the square of the radius.

$$F = K_1 r^2 \tag{VII-25}$$

The total power generation is

$$P = \int_o^{R_4} 2\pi F r \, dr = 2\pi K_1 \int_o^{R_4} r^3 \, dr = \frac{\pi K_1 R_4^4}{2} \tag{VII-26}$$

Therefore the constant K_1 is

$$K_1 = \frac{2P}{\pi R_4^4} \tag{VII-27}$$

Substituting into (VII-25) we obtain

$$F = \frac{2P r^2}{\pi R_4^4} \tag{VII-28}$$

Now going back to Eq. (VII-24)

$$\frac{d^2y}{dr^2} = \frac{2\alpha'}{K} \frac{P_r^2}{\pi R_4^4} \qquad \text{(VII-29)}$$

The boundary conditions for this differential equation is

$$\frac{dy}{dr} = 0 \text{ at } r = 0 \qquad \text{(VII-30)}$$

$$y = 0 \text{ at } r = 0 \qquad \text{(VII-31)}$$

The solution of Eq. (VII-29) becomes

$$y = \frac{P\alpha' r^4}{6K\pi R_4^4} \qquad \text{(VII-32)}$$

With y_{max} occurring at $r = R_4$

therefore The Maximum Thermal distortion

$$y_{max} = \frac{P\alpha'}{6K\pi} \qquad \text{(VII-33)}$$

2. Externally Pressurized Opposed Pair

a. Load Capacity of Clearance and Flow

A schematic representation of the bi-directional pair is shown on Figure VII-5. For purposes of analysis the downstream orifice pressure was considered to exist inside an annulus whose width equaled the orifice diameter. Since the Rayleigh steps were incorporated in the reaction bearing, as an afterthought rather late in the program, they were not included in the reaction bearing configuration. The bearing was assumed as a smooth annulus with equally spaced orifices around the midcircumference. (See Fig. VII-6)

The method of solution is as follows: (subscript 1 refers to the reaction bearing and subscript 2 refers to the main bearing).

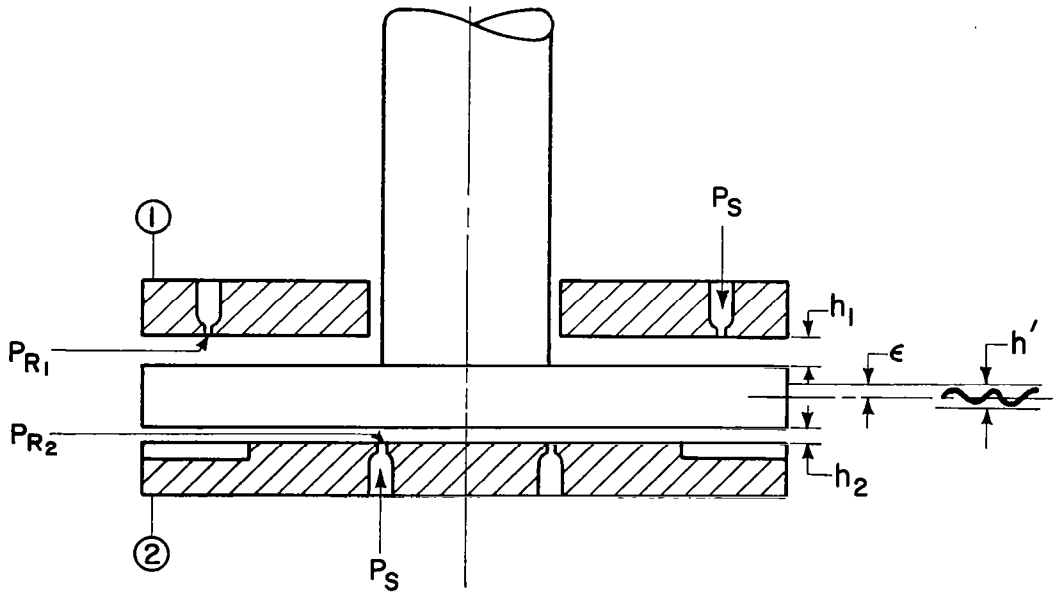

Fig. VII-5 - Bi-Directional Preloaded Pair-Schematic

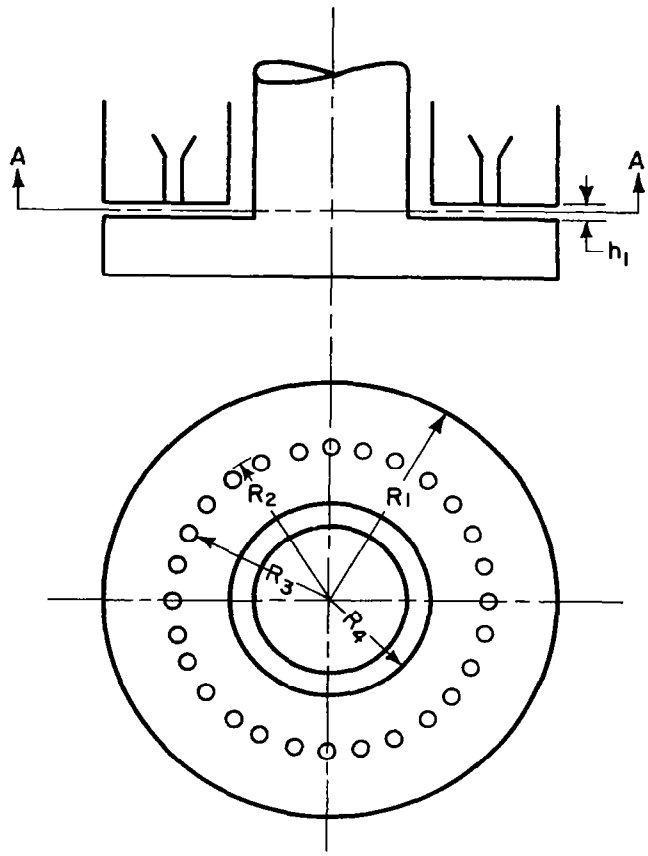

Fig. VII-6 - Schematic Representation of Reveral Thrust Bearing

Assume a given load is applied to bearing 1: then

$$P_{r1} = \frac{W_1}{A_1} + P_a \qquad \text{(VII-34)}$$

A_1 is the effective bearing area and is determined from assuming the pressure distribution. The pressure profile will vary as the ratio of recess pressure to ambient pressure (P_r/P_a) varies. This ratio changes in accordance with the load applied to the bearing. For low values of P_r/P_a compressibility affects are minimal and the shape of the pressure distribution approximates that of the incompressible case (a convex shape between the orifice circle and outer perimeter). From the data indicated in Reference 1 it was reasonable to assume an incompressible pressure distribution for $P_r/P_a < 1.8$ and a linear pressure distribution for Pr/Pa > 1.8. Using this criteria

$$A_1 = \pi \left[R_1^2 - R_4^2 - \frac{\left(R_3^3 + 2R_4^3 - 3R_3R_4^2\right)}{3\left(R_3 - R_4\right)} - \frac{\left(R_2^3 + 2R_1^3 - 3R_2R_1^2\right)}{3\left(R_1 - R_2\right)} \right] \qquad \text{(VII-35)}$$

for $P_r/P_a > 1.8$ (linear profile)

and

$$A_1 = \frac{\pi}{2} \left\{ \frac{\left(R_1^2 - R_2^2\right)}{\ln\left(R_1/R_2\right)} - \frac{\left(R_3^2 - R_4^2\right)}{\ln\left(R_3/R_4\right)} \right\} \qquad \text{(VII-36)}$$

for $P_r/P_a \leq 1.8$ (incompressible profile).

The bearing mass flow is given by

$$Q_{B1} = \frac{h_1^3 P_a^2}{R_g T_g} \left[\frac{P_{r1}^2}{P_a^2} - 1 \right] \frac{\pi}{12\mu} \left[\frac{1}{\ln\left(R_1/R_2\right)} + \frac{1}{\ln\left(R_3/R_4\right)} \right] \qquad \text{(VII-37)}$$

The expression for determining the orifice flow depends upon whether inherent compensation, is incorporated. If the orifice feeds directly into the clearance region (no recess) and the diameter of the orifice is large compared to the clearance, inherent compensation results. The

effective orifice area is then the surface area of the cylinder formed in the clearance region of diameter equal to that of the orifice and height equal to the clearance.

$$A_{o1} = \pi D_o h_1 \qquad \text{(VII-38)}$$

The flow through the orifice now becomes a function of the downstream pressure and the clearance (for constant supply pressure). For a bearing in which the orifices feed directly into recesses, the orifice area is

$$A_{o1} = \frac{\pi D_o^2}{4} \qquad \text{(VII-39)}$$

The general expression for flow through the orifice is given by

$$Q_o = N_o C_D A_o \sqrt{\frac{2\gamma}{(\gamma - 1) R_g T_g}} \; P_s \left\{ \left(\frac{P_r}{P_s}\right)^{2/\gamma} \left[1 - \left(\frac{P_r}{P_s}\right)^{\frac{\gamma-1}{\gamma}} \right] \right\}^{1/2} \qquad \text{(VII-40)}$$

when $(P_{r1}/P_s) \leq$ the critical pressure ratio, i.e.

$$(P_r/P_s)_{crit} \leq \left(\frac{2}{1+\gamma}\right)^{\frac{\gamma}{\gamma-1}} \qquad \text{(VII-41)}$$

the flow is choked and the quantity of flow is determined by replacing (P_r/P_s) in (VII-40) by $(P_r/P_s)_{crit}$. If inherent compensation is used the bearing clearance is obtained by equating Q_{o1} to Q_{B1} and solving the expression

$$h_1 = \left\{ \frac{12\mu N_{o1} D_{o1} C_D \sqrt{\frac{2\gamma R_g T_g}{(\gamma-1)}} \; P_s \left\{ \left(\frac{P_{r1}}{P_s}\right)^{2/\gamma} \left[1 - \left(\frac{P_{r1}}{P_s}\right)^{\frac{\gamma-1}{\gamma}} \right] \right\}^{1/2}}{\left(P_{r1}^2 - P_a^2\right) \left(\frac{1}{\ln (R_3/R_4)} + \frac{1}{\ln (R_1/R_2)} \right)} \right\}^{1/2} \qquad \text{(VII-42)}$$

The bearing flow is then computed from either Q_{B1}, equation (VII-37) or Q_{o1}, equation (VII-40).

If inherent compensation is not employed the orifice flow can be calculated directly, since it then is independent of the bearing clearance. Then by equating the bearing flow to the orifice flow the clearance can be obtained from

$$h_1 = \left\{ \frac{Q_o \quad 12\mu \, R_g T_g}{\pi \left(P_{r1}^2 - P_a^2\right) \left(\frac{1}{\ln (R_1/R_2)} + \frac{1}{\ln (R_3/R_4)} \right)} \right\}^{1/3} \tag{VII-43}$$

The clearance of the main bearing is constrained by the requirement that the total axial clearance must remain constant. Thus

$$h_2 = H_t - h_1 \tag{VII-44}$$

To determine the recess pressure of the main bearing the flow through the orifice is equated to the flow through the bearing. The resulting expression is

$$\frac{\pi \, h_2^3 \left(P_{r2}^2 - P_a^2\right)}{12\mu \, R_g T_g \, \ln(R_2/R_3)} = N_{o2} \, A_{o2} \, C_D \, P_s \left\{ \left(\frac{P_{r2}}{P_s}\right)^{2/\gamma} \left[1 - \left(\frac{P_{r2}}{P_s}\right)^{\frac{\gamma-1}{\gamma}} \right] \right\}^{1/2} \tag{VII-45}$$

where

$$A_{02} = \frac{\pi D_{o2}^2}{2} \quad \text{for orifice-recess compensation} \tag{VII-46}$$

or

$$A_{o2} = \pi D_{o2} h \quad \text{for inherent compensation} \tag{VII-47}$$

Determining the recess pressure from Eq. (VII-45) requires numerical methods. The roots of the transcendental equation in P_{r2}/P_s lie between 0 and 1. The equation is solved for the recess pressure by a bi-sectional routine in which successive half intervals not containing the root are eliminated until the root is straddled in an interval of the desired tolerance. The accuracy is dependent upon the number of intervals halved.

If $(P_{r2}/P_s) < (P_r/P_s)_{crit}$ the flow is determined from the orifice equation using $(P_r/P_s)_{crit}$ for (P_{r2}/P_s). Then the recess pressure must be recalculated to ensure equality of mass flows through the orifices and bearing

$$P_{r2} = \left\{ P_a^2 + \frac{Q_{o2} R_g T_g 12\mu \ln (R_2/R_3)}{\pi h_2^3} \right\}^{1/2} \qquad \text{(VII-48)}$$

for

$$P_r/P_s \leq (P_r/P_s)_{crit}$$

If $P_{r2}/P_s > (P_r/P_s)_{crit}$ the flow is determined from the orifice equation without change in the recess pressure obtained from the bi-section calculation. The total flow of both bearings is

$$Q_T = Q_{o1} + Q_{o2} \qquad \text{(VII-49)}$$

The load capacity of the main bearing from external pressurization is

$$W_2 = (P_{r2} - P_a) A_2 \qquad \text{(VII-50)}$$

where A_2 is determined from

$$A_2 = \frac{\pi}{2} \frac{(R_2^2 - R_3^2)}{\ln (R_2/R_3)} \qquad \text{(VII-51)}$$

for

$$P_{r2}/P_a \leq 1.8$$

and

$$A_2 = \frac{\pi}{3} R_3^2 \left[\left(\frac{R_2}{R_3} \right)^2 + \frac{R_2}{R_3} + 1 \right] \qquad \text{(VII-52)}$$

The net load on the bi-directional pair is the difference in load of the two separate bearings.

$$W_T = W_1 - W_2 \tag{VII-53}$$

A negative number indicates that the load is directed toward the main bearing. A positive number indicates that the load is directed toward the reaction bearing.

b. Stability Characteristics (Grooves not considered)

The procedure for determining stability characteristics of an oppossed pair of orifice-recess hydrostatic bearings is described in Reference (12). Modifications were incorporated to include inherent compensation. Stability characteristics were initially established assumming that the main hydrostatic thrust bearing was at ambient pressure at radius R_2. Modifications to another analysis for purposes of including the effects of the grooved portion are described subsequently.

The equation of motion for the shaft is

$$m \ddot{h}' = p_1' A_1 - p_2' A_2 \tag{VII-54}$$

From mass continuity the net gas inflow equals the net rate of change of mass inside the clearance regions.

For bearing 1

$$\left(\frac{\partial Q_{in(1)}}{\partial P_{r1}} - \frac{\partial Q_{out(1)}}{\partial P_{r1}} \right) p_1' + \left(\frac{\partial Q_{in(1)}}{\partial h_1} - \frac{\partial Q_{out(2)}}{\partial h_1} \right) h_1' = \frac{\partial M(1)}{\partial h} \dot{h}_1' + \frac{\partial M(2)}{\partial P_r} \dot{p}_1' \tag{VII-55}$$

For bearing 2

$$\left(\frac{\partial Q_{in(2)}}{\partial P_{r2}} - \frac{\partial Q_{out(2)}}{\partial P_{r2}} \right) p_2' + \left(\frac{\partial Q_{in(2)}}{\partial h_2} - \frac{\partial Q_{out(2)}}{\partial h_2} \right) h_2' = \frac{\partial M(2)}{\partial h} \dot{h}_2' + \frac{\partial M(2)}{\partial P_r} \dot{p}_2' \tag{VII-56}$$

h_2 can be eliminated by noting that

$$h' = h_1' = - h_2'$$

For the purpose of simplifying the notation the partial derivatives are designated as follows:

$$\lambda_1 = \frac{\partial M}{\partial h} \qquad \lambda_3 = - \frac{\partial Q_{in}}{\partial P_r} \qquad \lambda_5 = \frac{\partial Q_{out}}{\partial P_r}$$

$$\lambda_2 = \frac{\partial M}{\partial P_r} \qquad \lambda_4 = \frac{\partial Q_{out}}{\partial h} - \frac{\partial Q_{in}}{\partial h}$$

inserting these symbols and applying the Laplace transformation to equations (VII-54), (VII-55), and (VII-56) we obtain

$$\bar{h} = \frac{1}{ms^2} (\bar{p}_1 A_1 - \bar{p}_2 A_2) \qquad \text{(VII-57)}$$

$$- (\lambda_3 + \lambda_5)_1 \bar{p}_1 - (\lambda_4)_1 \bar{h} = (\lambda_1 s)_1 \bar{h} + (\lambda_2 s)_1 \bar{p}_1 \qquad \text{(VII-58)}$$

$$(\lambda_3 + \lambda_5)_2 \bar{p}_2 + (\lambda_4)_2 \bar{h} = - (\lambda_1 s)_2 \bar{h} + (\lambda_2 s)_1 \bar{p}_2 \qquad \text{(VII-59)}$$

where the bar symbol denotes the transformed quantity. Substituting Eq. (VII-57) into (VII-58) and (VII-59) and rearranging we obtain

$$\left[\frac{ms^2}{A_1} \frac{(\lambda_3 + \lambda_5 + s \lambda_2)_1}{(\lambda_4 + s \lambda_1)_1} + 1 \right] \bar{p}_1 A_1 - \bar{p}_2 A_2 = 0 \qquad \text{(VII-60)}$$

$$- \bar{p}_1 A_1 + \left[\frac{ms^2}{A_1} \frac{(\lambda_3 + \lambda_5 + s \lambda_2)_2}{(\lambda_4 + s \lambda_1)_2} \right] \bar{p}_2 A_2 = 0 \qquad \text{(VII-61)}$$

In order for a solution to exist the determinant of the coefficients must vanish. Expansion of the determinant yields the characteristic equation whose roots determine the stability threshold.

The characteristic equation is

$$S^4 + \Lambda_3 S^3 + \Lambda_2 S^2 + \Lambda_1 S + \Lambda_o = 0 \qquad \text{(VII-62)}$$

where

$$\Lambda_3 = \frac{(\lambda_3 + \lambda_5)_1 (\lambda_2)_2 + (\lambda_2)_1 (\lambda_3 + \lambda_5)_2}{(\lambda_2)_1 (\lambda_2)_2} \qquad \text{(VII-63)}$$

$$\Lambda_2 = \frac{(\lambda_3 + \lambda_5)_1 (\lambda_3 + \lambda_5)_2 + \frac{A_2}{m} (\lambda_2)_1 (\lambda_1)_2 + \frac{A_1}{m} (\lambda_2)_2 (\lambda_1)_1}{(\lambda_2)_1 (\lambda_2)_2} \qquad \text{(VII-64)}$$

$$\Lambda_1 = \frac{A_2}{m} \left[(\lambda_3 + \lambda_5)_1 (\lambda_1)_2 + (\lambda_2)_1 (\lambda_4)_2 \right] + \frac{\frac{A_1}{m} \left[(\lambda_3 + \lambda_5)_2 (\lambda_1)_1 + (\lambda_2)_2 (\lambda_4)_1 \right]}{(\lambda_2)_1 (\lambda_2)_2} \qquad \text{(VII-65)}$$

$$\Lambda_o = \frac{\frac{A_2}{m} (\lambda_3 + \lambda_5)_1 (\lambda_4)_2 + \frac{A_1}{m} (\lambda_3 + \lambda_5)_2 (\lambda_4)_1}{(\lambda_2)_1 (\lambda_2)_2} \qquad \text{(VII-66)}$$

The stability criteria is (see Reference 12)

(a) All coefficients $\Lambda > 0$

(b) $\Lambda_1 \Lambda_2 \Lambda_3 > \Lambda_1^2 + \Lambda_3^2 \Lambda_o$

The general expressions for the λ parameters are:

$$\lambda_1 = \frac{\partial M}{\partial h} = \frac{P_a A_p + (P_r - P_a)A}{R_g T_g} \qquad \text{(VII-67)}$$

$$\lambda_2 = \frac{\partial M}{\partial P_r} = \frac{Ah + A_r \Delta}{R_g T_g} \qquad \text{(VII-68)}$$

$$\lambda_3 = -\frac{\partial Q_{in}}{\partial P_r} = \frac{Q\left[\left(\frac{\gamma+1}{\gamma}\right)\left(\frac{P_r}{P_s}\right)^{\frac{\gamma-1}{\gamma}} - \frac{2}{\gamma}\right]}{2P_r\left[1 - \left(\frac{P_r}{P_s}\right)^{\frac{\gamma-1}{\gamma}}\right]} \qquad \text{(VII-69)}$$

if $\frac{P_r}{P_s} < \left(\frac{P_r}{P_s}\right)_{crit.}$ then

$$\frac{\partial Q_{in}}{\partial P_r} = 0.0 \qquad \text{(VII-70)}$$

$$\lambda_4 = \frac{\partial Q_{out}}{\partial h} - \frac{\partial Q_{in}}{\partial h}$$

$$= \frac{2Q}{h} \text{ for inherent compensation} \qquad \text{(VII-71)}$$

$$= \frac{Q}{h} \text{ for orifice compensation} \qquad \text{(VII-72)}$$

$$\lambda_5 = \frac{\partial Q_{out}}{\partial P_r} = \frac{2P_r Q}{P_r^2 - P_a^2} \qquad \text{(VII-73)}$$

c. Stability Characteristics - Grooves Considered

If the grooves are considered to restrict flow then the total bearing area will be larger. An equivalent constant clearance, and an equivalent radius can be determined that will permit the same flow as the grooved bearing.

The flow across a grooved and land is proportional to the respective widths and cube of the clearance. Therefore

$$b_L h_L^3 + b_G h_G^3 = (b_L + b_G)\, h_e^3 \qquad \text{(VII-74)}$$

rearranging terms the equivalent clearance becomes

$$h_e^3 = \frac{h_L^3 + \frac{b_G}{b_L} h_G^3}{1 + \frac{b_a}{b_L}} \qquad \text{(VII-75)}$$

We can also equate an equivalent bearing flow to the actual bearing flow and obtain an equivalent bearing radius.

$$Q_B = Q_e \qquad \text{(VII-76)}$$

$$\frac{\pi h^3 P_a^2 \left[\left(\frac{P_r}{P_a}\right)^2 - 1\right]}{12\mu R_g T_g \ln (R_2/R_3)} = \frac{\pi h_e^3 P_a^2 \left[\left(\frac{P_r}{P_a}\right)^2 - 1\right]}{12\mu R_g T_g (R_e/R_3)} \qquad \text{(VII-77)}$$

from which

$$R_e = R_3 \left(\frac{R_2}{R_3}\right)^{\left(\frac{h_e}{h}\right)^3} \qquad \text{(VII-78)}$$

The expressions for equivalent clearance and equivalent bearing radii were inserted into a computer program for analysis of the turbo-altemator thrust bearing which is described in Reference (13). There is some uncertainty with the approximations of this stability analysis, but it is believed that a reasonable indication of the stability characteristics is afforded.

It is quite obvious from the development of the governing equations and the methods of solution that hand computation is a tedious task. Consequently, digital computer programs were developed and utilized for determining performance parameters and stability information.

NOMENCLATURE

A_o = orifice area, in.

A_1, A_2 = $\frac{\alpha_1 L}{C}$, $\frac{\alpha_2 L}{C}$

a = thrust bearing thickness, in.

b_g = groove width, in.

b_L = land width, in.

C = radius of shoe minus radius of shaft, in.

C′ = radius of the pivot circle minus radius of shaft, in; pivot translation coordinate, in.

C_D = orifice discharge coefficient

C_L = $\frac{W}{p_a RL}$

D_o = orifice diameter, in.

d = distance from pivot point to shoe mass center, in.

e = shaft eccentricity, in.

e′ = pivot circle eccentricity, in.

F = heat generation, BTU/hr-ft^2

F_f = shoe friction force, lb.

F_p = perload spring force, lb; journal bearing power loss, watts

f_m = shaft friction moment, in. - lb.

H = h/C

h = local clearance, in.

h_e = equivalent clearance, in.

h_g = clearance over groove, in.

h_o = groove depth, in.

h_L = thrust land clearance, in.; shoe leading edge film thickness, in.

h_p = shoe pivot film thickness, in.

h_T = shoe trailing edge film thickness, in.

I_R = shoe roll inertia, lb. - in. - sec.^{2}

I_T = shaft transverse moment of inertia - in. - lb. - sec^2;
thrust bearing transverse inertia - in. - lb. - sec^2.

I_p = shaft polar moment of inertia - in. - lb. - sec^2;
shoe pitch inertia - in. - lb. = sec^2.

K = shoe film stiffness lb./in.; thermal conductivity
BTU/hr.-in. °F

K_T = thrust bearing tilting stiffness - in. lb./rad.

k = preload spring constant - lb./in.;
number of spiral grooves

L = length of bearing, in.

M = contained mass (thrust brg.), lb. - $sec.^2/in.$

M_f = shoe pivot friction moment, in. - lb.

M_{shoe} = mass of shoe, lb. - $sec.^2/in.$

N_o = number of orifices

P = P/P_a; power loss (spiral groove bearing), watts

P_f = spiral groove friction loss, horsepower

P_r = recess pressure, psia

P_s = supply pressure, psia

p = local pressure, psia

p_a = ambient pressure, psia

Q = P^2H^2; mass flow (thrust brg.), lb. - $sec.^2/in.^4$

R = radius of shaft, in.

R_1, R_2 = inside and outside radii of spiral groove bearing, in.

R', R = spiral groove coordinates, in.

R_g = gas constant, $in.^2/sec.^2 - °F$

R_e = equivalent radius (thrust brg.), in.

R_{e_C} = critical Reynolds number

T = dimensionless time $(t\Omega/2)$

T_g = absolute temperature - °R

t = time, sec.

u,v,w = lubricant velocities, in./sec.

W_t = total shoe load, lb.

W_x, Y_y = x,y components of shoe loads - lb.

X,Y,Z = x/c, y/c, z/c

x,y,z = cartesian coordinate system

y = thermal distortion of thrust brg., in.

α = shoe wrap angle, degrees

α' = coefficient of thermal expansion - in./in.- °F

α_1, α_2 = angular coordinate of shaft, radians

$\alpha_{max.}$ = spiral groove angle, degrees

β = pivot angle, degrees

γ = shoe roll angular coordinate, radians; groove to width ratio (spiral groove brg.)

δ = shoe pitch angular coordinate, radians; compression ratio (spiral groove brg.)

ϵ = e/C; relative angle of swash, degrees

ϵ' = (e'/C') pivot circle eccentricity ratio

ζ = z/L - 1/2

η = z/L

θ = angular coordinate for shaft rotation, degrees

Λ = $\frac{6\mu\Omega}{p_a}\left(\frac{R}{C}\right)^2$

λ = radius ratios R_2/R_1 for spiral groove bearing

μ = lubricant viscosity, lb. - sec./in.^{2}

μ_f = friction coefficient

ξ = shoe-shaft coordinate (lead angle), degrees angular displacement of stationary plate, radians

ρ = lubricant density, lb. - sec.^{2}/in.^{4}

τ = shear stress, psi

ϕ = angle from shoe leading edge to pivot point, degrees

ψ_u = angle between shaft unbalance force and moment vectors

Ω = shaft angular speed - rad./sec.

ω = angular speed radians; thrust bearing swashing frequency - radians

ω_c = swash natural frequency of thrust bearing, rad./sec.